Library Copy
R. A. 1364

AUG 1947

RESEARCH MEMORANDUM

for the

Bureau of Aeronautics, Navy Department

WIND-TUNNEL TESTS OF A $\frac{1}{8}$-SCALE POWERED MODEL OF THE XTB3F-1 AIRPLANE

TED NO. NACA 2382

By

John W. McKee and Raymond D. Vogler

Langley Memorial Aeronautical Laboratory
Langley Field, Va.

UNCLASSIFIED

CLASSIFIED DOCUMENT

This document contains classified information affecting the National Defense of the United States within the meaning of the Espionage Act, USC 50:31 and 32. Its transmission or the revelation of its contents in any manner to an unauthorized person is prohibited by law. Information so classified may be imparted only to persons in the military and naval services of the United States, appropriate civilian officers and employees of the Federal Government who have a legitimate interest therein, and to United States citizens of known loyalty and discretion who of necessity must be informed thereof.

TECHNICAL EDITING WAIVED

NATIONAL ADVISORY COMMITTEE FOR AERONAUTICS

WASHINGTON

AUG 1947

NASA Technical Library
3 1176 01437 5266

NATIONAL ADVISORY COMMITTEE FOR AERONAUTICS

RESEARCH MEMORANDUM

for the

Bureau of Aeronautics, Navy Department

WIND-TUNNEL TESTS OF A $\frac{1}{8}$-SCALE POWERED MODEL OF THE XTB3F-1 AIRPLANE

TED NO. NACA 2382

By John W. McKee and Raymond D. Vogler

CLASSIFICATION CHANGED
To UNCLASSIFIED
By Authority of
Changed by
Date

SUMMARY

A $\frac{1}{8}$-scale model of the Grumman XTB3F-1 airplane was tested in the Langley 7- by 10-foot tunnel to determine the stability and control characteristics and to provide data for estimating the airplane handling qualities. The report includes longitudinal and lateral stability and control characteristics of the complete model, the characteristics of the isolated horizontal tail, the effects of various flow conditions through the jet duct, tests with external stores attached to the underside of the wing, and tests simulating landing and take-off conditions with a ground board.

The handling characteristics of the airplane have not been computed but some conclusions were indicated by the data. An improvement in longitudinal stability was obtained by tilting the thrust line down. It is shown that if the wing flap is spring-loaded so that the flap deflection varies with airspeed, the airplane will be less stable than with the flap retracted or fully deflected. An increase in size of the vertical tail and of the dorsal fin gave more desirable yawing-moment characteristics than the original vertical tail and dorsal fin. Preventing air flow through the jet duct system or simulating jet operation with unheated air produced only small changes in the model characteristics. The external stores on the underside of the wing had only small effects on the model characteristics.

After completion of the investigation, the model was returned to the contractor for modifications indicated by the test results.

~~CONFIDENTIAL~~

UNCLASSIFIED

INTRODUCTION

At the request of the Bureau of Aeronautics, Navy Department, a $\frac{1}{8}$-scale powered model of the Grumman XTB3F-1 airplane has been tested to provide data for estimating handling qualities specified in reference 1. Sufficient data were obtained to allow for estimating the most important longitudinal, directional, and lateral static stability and control characteristics both near and away from the ground.

COEFFICIENTS AND SYMBOLS

The results of the tests are presented as standard NACA coefficients of forces and moments. Rolling-, yawing-, and pitching-moment coefficients are given about the center-of-gravity location shown in figure 1 (25 percent of the mean aerodynamic chord). The data are referred to the stability axes, which are a system of axes having their origin at the center of gravity and in which the Z-axis is in the plane of symmetry and perpendicular to the relative wind, the X-axis is in the plane of symmetry and perpendicular to the Z-axis, and the Y-axis is perpendicular to the plane of symmetry. The positive directions of the stability axes, of angular displacements of the airplane and control surfaces, and of hinge moments are shown in figure 2.

The coefficients and symbols are defined as follows:

C_L lift coefficient (Lift/qS)

C_{L_t} horizontal-tail lift coefficient (Lift/qS_t)

C_X longitudinal-force coefficient (X/qS)

C_Y lateral-force coefficient (Y/qS)

C_l rolling-moment coefficient (L/qSb)

C_m pitching-moment coefficient (M/qSc')

C_n yawing-moment coefficient (N/qSb)

C_h hinge-moment coefficient ($H/qb'\bar{c}^2$)

UNCLASSIFIED

T_c'	effective thrust coefficient based on wing area (T_{eff}/qS)
Q_c'	torque coefficient based on wing area and span (Q/qSb)
Q_c	torque coefficient $(Q/\rho V^2D^3)$
V/nD	propeller advance-diameter ratio
Lift = -Z	
X, Y, Z	forces along axes, pounds
L, M, N	moments about axes, pound-feet
H	hinge moment of control surface, pound-feet
T_{eff}	propeller or jet effective thrust, pounds
Q	propeller torque, pound-feet
q	free-stream dynamic pressure, pounds per square foot $(\rho V^2/2)$
q_t	effective dynamic pressure at tail, pounds per square foot
S	wing area (8.573 sq ft on model)
S_t	horizontal-tail area (2.14 sq ft on model)
c	airfoil section chord, feet
c'	wing mean aerodynamic chord (M.A.C.) (1.198 ft on model)
$\bar{c}$	root-mean-square chord of a control surface back of hinge line, feet
b	wing span (7.50 ft on model)
b'	control-surface span along hinge line, feet
V	air velocity, feet per second

V_{S_G} stalling speed of airplane, glide configuration

V_{S_L} stalling speed of airplane, landing configuration

D propeller diameter (1.625 ft on model)

n propeller speed, revolutions per second

and

ρ mass density of air, slugs per cubic foot

α angle of attack of original thrust line, degrees

α_t angle of attack of tail chord line

ψ angle of yaw, degrees

i_t angle of stabilizer with respect to original thrust line, positive when trailing edge is down, degrees

i_{fin} angle of the fin with respect to the plane of symmetry, positive when trailing is to the left, degrees

δ control-surface deflection, degrees

$\delta_{fantail}$ fantail deflection with respect to the stabilizer, positive when trailing edge is depressed, degrees

β propeller blade angle at 0.75 radius (22° on model, except where otherwise noted)

a.c. tail-off aerodynamic-center location, percent wing mean aerodynamic chord

n_p neutral-point location, percent wing mean aerodynamic chord (center-of-gravity location for neutral stability in trimmed flight)

Subscripts:

a aileron (a_R, a_L, right and left aileron)

e elevator

r rudder

f flap

t tab

ψ denotes partial derivatives of a coefficient with respect to yaw (example: $C_{l_\psi} = \partial C_l/\partial\psi$)

MODEL AND APPARATUS

The XTB3F-1 airplane is a two-place midwing carrier-based torpedo bomber with conventional retractable landing gear. It is powered with a reciprocating engine in the nose driving a single-rotation propeller and a jet engine with air inlets in the root of the wing and jet exit at the tail. Various sizes of engines may be installed in the airplane. In the present report the airplane is treated as having a Pratt & Whitney R3350-24 engine and a Westinghouse 24-C jet engine. The airplane is designed to carry a torpedo internally and a radar unit, a varied assortment of rockets, bombs, gas tanks, and gun packages externally under the wing. The elevator has some overhang balance, the rudder has a small shielded horn, and the ailerons have linked-plate internal balance and spring tabs. A summary of the physical characteristics of the airplane is presented in table I.

The model was furnished by the Grumman Aircraft Engineering Corporation. A three-view drawing of the $\frac{1}{8}$-scale model is shown in figure 1 and photographs of the model mounted in the tunnel are given in figure 3.

The wing of the model was equipped with a slotted trailing-edge landing flap which on the airplane is spring-loaded so that the maximum flap deflection varies with lift coefficient as shown in figure 4. Plain ailerons which could be locked at any desired deflection were provided.

The vertical tail and dorsal fin of the model as furnished (fig. 5) were modified during the course of the tests. For some tests the area of the vertical tail was increased by addition of area at the tip or root using straight-line fairing and the original dorsal fin was replaced by the large dorsal fin (fig. 6). The vertical-tail revisions compare geometrically as shown in table II. Except where otherwise noted, the vertical tail was set at an angle of of $-2^{\circ}15'$ to the airplane center line. The dorsal fins were shifted fore and aft along the fuselage with change of vertical tail so as to always meet the leading edge of the fin.

Details of the horizontal tail of the model are given in figure 7, and stabilizer and elevator ordinates are given in table III. For tests of the isolated horizontal tail, a block (fantail) was added to replace the piece between the two halves of the elevator that remains fixed to the fuselage of the model. The fantail was attached to the stabilizer and pivoted about the stabilizer pivot point (1.67 in. ahead of and 1.30 in. below the elevator hinge line).

The model was equipped with a four-blade propeller using blades A of reference 2 cut down to a diameter of 1.625 feet. The propeller was driven by a 35-horsepower electric motor, the speed of which was determined from an electric tachometer whose error is within ±0.2 percent. The original propeller thrust line is shown in figure 1; and the thrust line tilted down 3°, in figure 8.

For simulating operation of the airplane jet, the fuselage of the model was fitted with cut-outs which made it possible to duct unheated air into the model from a blower located outside the tunnel. The outside air could be used in an aspirator device to draw air through the wing inlet duct to exhaust at the model jet exit, or the outside air alone could be used to simulate the jet. Details of the setup are shown in figures 9 and 10.

Ducting the air supply onto the tunnel balance frame introduced large lift forces and rolling moments which were balanced by compensators installed on the tunnel balance system. Except for errors in compensation, the outside air contributed only a thrust force along the jet axis.

External stores to be attached to the underside of the wing of the model included two 150-gallon fuel tanks, two twin .50-caliber gun packages, and a radar unit for the right wing tip (fig. 11). The attaching support for the radar unit was a short streamlined strut. The supports for the tanks and gun packages simulated an airplane installation consisting of short pylons and sway braces.

The model configurations referred to in the text and on the figures were as follows:

Configuration	Power (piston engine only)	δ_f (deg)	Landing gear
Glide	Windmilling propeller	0	Retracted
Power-on clean	Normal rated power	0	Retracted
Landing	Windmilling propeller	50	Extended
Approach	1/2 normal rated power	50	Extended
Wave-off	Military rated power	50	Extended
Take-off	Varying T_c' at constant α	20	Extended

When the effect of the ground was required, a ground board which completely spanned the tunnel and extended about 40 inches ahead of and 80 inches behind the pivot point of the model was placed below the model (figs. 12 and 13). The ground board was positioned to give a minimum clearance of 1/4 inch at the main landing-gear wheels with the length of landing-gear strut corresponding to the static wheel position.

Without the ground board in place, the wheels were in the fully extended position when the landing gear was extended.

TESTS AND RESULTS

Test Conditions

Langley 7- by 10-foot tunnel.- The tests were made at dynamic pressure of 16.37 pounds per square foot except when the test speed was limited by the thrust available from the model propeller or jet. Tests with military rated power were made at a dynamic pressure of 9.21 pounds per square foot, tests of the jet effect at 4.09 pounds per square foot, and tests with high values of T_c' with the ground board in place at 4.09 and 2.30 pounds per square foot. The dynamic pressures correspond to airspeeds between 30 and 80 miles per hour. The test Reynolds numbers were between 300,000 and 900,000 based on the wing mean aerodynamic chord of 1.198 feet. Because of the turbulence factor of 1.6 for the tunnel, the effective Reynolds number (for maximum lift coefficients) at a dynamic pressure of 16.37 pounds per square foot was about 1,400,000.

Langley 4- by 6-foot tunnel.- The tests were made at a dynamic pressure of 13 pounds per square foot, which corresponds to an airspeed of about 71 miles per hour. The test Reynolds number was about 465,000 based on the average horizontal-tail chord of 0.708 feet. Because of the turbulence factor of 1.93 for the tunnel, the effective Reynolds number (for maximum lift coefficients) was about 900,000.

Corrections

Complete model.- The data obtained with the ground board in place were not corrected for tares caused by the model support strut because of the impracticability of obtaining tares. Jet-boundary corrections were not applied because they have been shown to be negligible for the ground-board test installation. The data obtained with jet operation simulated were not corrected for tares caused by

the model support and air-supply equipment. The model with external stores was tested inverted so that interference between the support strut and the external stores would be small, and no tare corrections were applied to the data. All other data have been corrected for tares caused by the model support strut; and jet-boundary corrections have been applied to the angles of attack, the drag coefficients, and the tail-on pitching-moment coefficients. The corrections were computed as follows by use of reference 3:

$$\Delta\alpha = 0.958C_L$$

$$\Delta C_X = -0.0142C_L^2$$

$$\Delta C_m = -7.06C_L\left(\frac{0.1853}{\sqrt{q_t/q}} - 0.1173\right)\left(\frac{\partial C_m}{\partial i_t}\right)$$

where $\Delta\alpha$ is in degrees. All jet-boundary corrections were added to the test data.

Isolated horizontal tail.- All data have been corrected for tares caused by the model support strut. A jet-boundary correction has been applied to the angle of attack as follows:

$$\Delta\alpha_t = 1.46C_{L_t}$$

The jet-boundary correction to the hinge moment was considered negligible.

Test Procedure

Propeller calibrations were made by measuring the longitudinal force of the model with flaps and landing gear retracted and tail off at an angle of attack of 0° for a range of propeller speeds. Thrust coefficients were determined from the relation

$$T_c' = C_{X_{\text{propeller operating}}} - C_{X_{\text{propeller removed}}}$$

The torque coefficients were computed by use of a calibration of motor torque as a function of minimum current. The results of the model propeller calibration are presented in figure 14.

The variation of thrust coefficient with lift coefficient for the full-scale airplane and the model is shown in figure 15. The data for the full-scale airplane were obtained from the Grumman company. The estimated thrust coefficient and model torque coefficient for take-off are presented in figure 16. The thrust coefficients of the airplane were reproduced during power-on tests by the use of figures 14 and 15 to match the propeller speed and lift coefficient of the model. The value of T_c' for the tests with propeller windmilling was about -0.03. In general, the torque coefficients for the model were nearly the same as the airplane coefficients (fig. 17).

At each angle of attack for power-on yaw tests the propeller speed was held constant throughout the yaw range. Since the lift and thrust coefficients vary with yaw when the propeller speed and angle of attack are held constant, the thrust coefficient is strictly correct only at zero yaw.

Lateral-stability derivatives were obtained from pitch tests at angles of yaw of $\pm 5^{\circ}$ by assuming a straight-line variation between these points. The large-symbol points on the plots of lateral-stability derivatives were obtained by measuring slopes through zero yaw from yaw tests. The aileron tests were made with propeller windmilling.

The model was tested with four configurations of the jet system. For the most part and except where otherwise noted, the duct system was clear from wing inlet to tail exit with no restriction placed upon the flow of air. For some tests the air-supply setup as shown in figure 9 was installed and tests were made with the following configurations:

Flow condition "P" - Tests with the jet exit and inner nozzle plugged.

Flow condition "I" - Tests made duplicating full-scale mass flow into wing inlets and also thrust of jet. The inflow corresponds to full-scale flow conditions realized with the Westinghouse 24-C jet unit operating at 12,000 rpm at sea level. Average values of mass flow obtained in the model tests compare with full-scale data as shown in figure 18.

Flow condition "S" - Tests made with a straight section replacing the inner nozzle (fig. 9) so that thrust of the jet could be simulated while flow of air into the wing inlets was zero.

The T_c' variation with C_L duplicated by jet simulation is shown in figure 15 concluded.

Presentation of Results

The results of the test are presented in the following figures:

	Figure
(1) Longitudinal:	
Glide configuration:	
Original thrust line	19(a)
Thrust line tilted down 3°	19(b)
Power-on clean configuration:	
Original thrust line	20(a)
Thrust line tilted down 3°	20(b)
Landing configuration:	
Original thrust line	21(a)
Thrust line tilted down 3°	21(b)
Approach configuration:	
Original thrust line	22(a)
Thrust line tilted down 3°	22(b)
Trim changes	23
Wing-flap deflection	24
Propeller blade angle	25
Neutral points	26, 27
(2) Lateral:	
Stability parameters	28
Characteristics in yaw:	
Glide configuration	29
Power-on clean configuration	30
Landing configuration	31
Approach configuration	32
Wave-off configuration	33
Propeller blade angle	34
Aileron characteristics	35

(3) Jet Simulation:
Longitudinal:
Propeller off, flow condition "P" . . . . . 36(a)
Propeller off, flow condition "I" . . . . . 36(b)
Propeller off, flow condition "S" . . . . . 36(c)
Power-on clean configuration, flow condition "P" . . 36(d)
Power-on clean configuration, flow condition "I" . . 36(e)
Neutral points 37
Landing configuration, duct system open and closed . . 38
Characteristics in yaw:
Glide configuration, flow conditions "P" and "I" . . . 39
Landing configuration, duct system open and closed . . 40

(4) Ground Board:
Landing configuration 41
Take-off configuration:
Elevator control 42
Rudder control, $\psi = 0^{\circ}$ 43
Rudder control, simulated crosswind 44

(5) External Stores:
Characteristics in pitch 45, 46
Lateral-stability parameters 47
Characteristics in yaw 48

(6) Isolated Horizontal Tail:
Elevator deflection . . . . . 49(a)
Tab deflection . . . . . 49(b)
Fantail deflection . . . . . 49(c)

DISCUSSION

Data are presented from which handling characteristics of the airplane can be estimated; however, this discussion will present only the more important or unusual results indicated by the data.

Longitudinal stability.- The results of the tests to determine longitudinal-stability characteristics are presented in figures 19 to 27. The data of short tests run consecutively to aid in the estimation of the most important trim changes of section D-6 of reference 1 are presented in figure 23; these data should be used in conjunction with the more complete data of figures 19 to 22 and 49 to determine the increments of elevator deflection and hinge moment required to balance the trim changes due to change of engine power and flap deflection. The model propeller was not similar to the

full-scale propeller in many respects but the proper order of side-force factor was obtained in most of the tests. An idea of the importance of blade angle can be obtained from figure 25.

The estimated neutral points summarizing the static longitudinal stability are presented in figures 26 and 27. Neutral points for the flap blow-up condition were determined from curves obtained by making cross plots of the data of figure 24. Above a lift coefficient of about 1.07, where the flap deflection reaches 50° (fig. 4), the neutral-point curves will merge with the $\delta_f = 50^\circ$ curves. The flap blow-up condition results in less stability with the tail on and greater stability with the tail off than with the flap set at either 0° or 50°. Tilting the thrust axis down 3° is shown to increase the stability for power-on conditions, but even then power has a decidedly destabilizing influence upon the neutral-point location.

A positive static margin is required (reference 1) for speeds above $1.4V_{S_G}$ in the power-on clean configuration; with the tilted thrust line, this requirement is met. The flap blow-up approach configuration shows a small measure of instability for the rearmost center-of-gravity position at a lift coefficient of 1.0, but the beneficial effects gained by tilting the thrust line should result in about neutral stability. It should be noted that the power for the approach configuration is slightly too low for level flight at $1.15V_{S_L}$ (class IV airplane, reference 1).

Lateral stability.- The lateral-stability parameters of figure 28 (original vertical tail, original dorsal fin) seem to be satisfactory, with power having relatively small effect on the slope of yawing- and rolling-moment coefficients. Tests through the yaw range (figs. 29 to 33) show somewhat different results. Power markedly reduces the effective dihedral at large angles of yaw when the flap is deflected 50°, and the yawing-moment curves are nonlinear so that for the power-on clean configuration the directional stability near $\psi = 0^\circ$ is very low. It can be seen that increasing the size of the vertical tail greatly improved the directional stability near $\psi = 0^\circ$ and that increasing the size of the vertical tail or the dorsal fin improved the yawing-moment characteristics at large angles of yaw.

Tests with maximum up and down deflection of the right aileron (fig. 35) indicate that the ailerons remain effective up to the stall angle, power off.

Jet simulation.- Except for the change of longitudinal-force coefficient, the operation of the jet or free air flow through the jet produced only small changes in the model characteristics. (See figs. 36 to 40.) Some of the changes of pitching-moment characteristics

with change of jet operation that appear in the data seem to be due to inaccurate test data, partly due to the low tunnel test speed and partly due to inexact compensation of the loads introduced by ducting the air supply onto the balance frame. Elevator hinge-moment coefficients were not appreciably affected by operation of the jet, indicating that the jet did not change the flow conditions at the tail surfaces.

Ground board.- The pitching-moment data of figure 41 indicate a rather sharp decrease in effectiveness of the elevator control at deflections higher than 20° of up-elevator. Sufficient control is available, however, to provide trim at a lift coefficient of about 1.8 (three-point attitude) for center-of-gravity positions as far forward as the 19 percent mean aerodynamic chord position.

The data simulating take-off (figs. 42 to 44) do not, of course, include the ground reactions on the wheels which must be considered when estimating the control deflections for trim during the take-off run. The propeller-torque coefficients, which strongly influence the rolling-moment coefficients, are presented in figure 16. The rolling moment is nearly zero for the crosswind take-off data (fig. 44) but would have large negative values for a crosswind from the right.

External stores.- For these tests (figs. 45 to 48) the model was mounted inverted with no tare corrections applied. The absolute values of the data are therefore somewhat in error but the increments due to the external stores should be reliable. The presence of the external stores had very little effect on the stability characteristics of the model. An increase in the drag for the windmilling propeller condition and an increase in the lateral force due to yaw can be noted; all other effects are small or indeterminate.

Isolated horizontal tail.- The data of the isolated horizontal tail (fig. 49) can be used to supplement data of the complete model when only limited elevator characteristics were obtained. Proper account should be taken of the dynamic pressure ratio and downwash angle at the tail of the model when using the isolated horizontal tail to estimate flying qualities.

CONCLUDING REMARKS

Data are presented from which handling characteristics of the Grumman XTB3F-1 airplane can be estimated.

The results of the longitudinal-stability investigation show that an improvement in power-on stability can be obtained by tilting the thrust line down and that a spring-loaded flap whose deflection decreases with increasing airspeed will cause the airplane to be less stable than with the flap retracted or fully deflected.

Lateral-stability tests indicated that an increase in size of the vertical tail and of the dorsal fin gave more desirable yawing-moment characteristics than the original vertical tail and dorsal fin. Aileron effectiveness was maintained up to the stall angle, power off.

Preventing air flow through the jet duct system or simulating jet operation with unheated air produced only small changes in the model characteristics.

Sufficient elevator control was shown for landing in the three-point attitude.

The presence of external stores on the underside of the wing has little effect on the stability characteristics of the model.

Langley Memorial Aeronautical Laboratory
National Advisory Committee for Aeronautics
Langley Field, Va.

John W. McKee
John W. McKee
Aeronautical Engineer

Raymond D Vogler by J. McK
Raymond D. Vogler
Engineering Aide

Approved: Hartley A. Soulé
Hartley A. Soulé
Chief of Stability Research Division

CJB

REFERENCES

1. Anon.: Specification for Stability and Control Characteristics of Airplanes. SR-199A, Bur. Aero., April 7, 1945.

2. Lesley, E. P., and Reid, Elliott G.: Tests of Five Metal Model Propellers with Various Pitch Distributions in a Free Wind Stream and in Combination with a Model VE-7 Fuselage. NACA Rep. No. 326, 1929.

3. Gillis, Clarence L., Polhamus, Edward C., and Gray, Joseph L., Jr.: Charts for Determining Jet-Boundary Corrections for Complete Models in 7- by 10-Foot Closed Rectangular Wind Tunnels. NACA ARR No. L5G31, 1945.

TABLE I

PHYSICAL CHARACTERISTICS OF GRUMMAN XTB3F-1 AIRPLANE

Weight and balance:	
Design gross weight, lb	19,470
Wing loading, lb/sq ft	35.5
Most forward center of gravity, percent M.A.C.	20.9
Normal center of gravity, percent M.A.C.	26.1
Most rearward center of gravity, percent M.A.C.	27.9
Vertical range, above untilted thrust line, in.	1.7 to 8.0
Wing:	
Span, ft	60.0
Area, sq ft	548.7
Mean aerodynamic chord, ft	9.59
Airfoil section at side of fuselage	NACA 23018 (Modified T. E.)
Tip section	NACA 23012 (Modified T. E.)
Incidence, deg	2
Dihedral, deg	5
Aspect ratio	6.56
Taper ratio	2:1
Sweepback, 30 percent chord line, deg	0
High-lift devices:	
Center section of wing	0.25 to 0.30c slotted flap
	Full flap deflection is 50° above a lift coefficient of 1.07 and varies with lift coefficient as shown in figure 4. Flap deflection for take-off is 20°.
Aileron	
Area (one aileron) behind hinge line, sq ft	16.7
Span, ft	10.69
Vertical tail (original, fig. 5)	
Area, sq ft	45.31
Fin area to rudder hinge, sq ft	31.58
Rudder area aft of hinge, sq ft	13.73
Root-mean-square chord, rudder, ft	1.847
Angle to airplane center line, deg	-2.0

NATIONAL ADVISORY
COMMITTEE FOR AERONAUTICS

TABLE I - Concluded

PHYSICAL CHARACTERISTICS OF GRUMMAN XTB3F-1 AIRPLANE - Concluded

Horizontal tail:	
Area, sq ft	136.84
Span, ft	24.17
Aspect ratio	4.27
Elevator span, ft	21.80
Elevator area aft of hinge, sq ft	41.84
Root-mean-square chord, elevator, ft	1.942
Incidence, deg	2.0
Control movement:	
Stick length, ft	1.42
Elevator, deg	30 up, 15 down
Degree elevator/degree stick travel	0.895
Elevator tab, deg	15 up, 20 down
Rudder pedal arm, ft	0.917
Rudder, deg	29.5
Degree rudder/degree pedal travel	1.74
Rudder tab, deg	±20
Aileron, deg	±17
Aileron spring tab, deg	17 up, 15 down
Aileron trim tab, deg	±5
Power plant:	
Engine	P. & W. R3350-24
Propeller gear ratio	0.4375 to 1
Take-off power (engine alone)	2500 hp at 2800 rpm (S.L.)
Jet unit	Westinghouse 24-C unit (Static thrust = 3000 lb)
Propeller:	
Type	Curtiss Electric, Model 732-0
Diameter, ft	13
Number of blades	4
Landing gear:	
Conventional (tail wheel)	Retractable type, with arresting hook

NATIONAL ADVISORY
COMMITTEE FOR AERONAUTICS

TABLE II

GEOMETRIC CHARACTERISTICS OF ORIGINAL AND MODIFIED VERTICAL TAILS

	Original tail	Tip extended 2.5 in.	Base extended 2.0 in.	Base extended 1.5 in.
Rudder span along hinge line, ft	1.040	1.260	1.207	1.165
Rudder root-mean-square chord, ft	0.231	--------	--------	0.236
[a]Vertical-tail span along hinge line, ft	1.055	1.263	1.222	1.180
[a]Vertical-tail area, sq ft	0.688	0.774	0.856	0.813
[a]Vertical-tail aspect ratio	1.62	2.06	1.74	1.71

[a]Above horizontal tail.

NATIONAL ADVISORY
COMMITTEE FOR AERONAUTICS

TABLE III

HORIZONTAL-TAIL ORDINATES XTB3F-1 AIRPLANE

(a) Station, 0; chord length, 83 in.; elevator chord, 26 in.

Station (percent chord)	Station (in.)	Ordinate (in.)
1.25	1.038	1.38
2.5	2.075	1.93
5	4.150	2.70
7.5	6.225	3.26
10	8.30	3.68
20	16.60	4.85
30	21.90	5.26
40	33.20	5.60
50	41.50	5.44
60	49.80	4.90
68.67 (hinge line)	57.00	4.00
68.67	57.00	Straight line
100	83.00	
L.E. radius: 1.17 in.		

Elevator Nose

Station (in.)	Ordinate (in.)
51.3	0
52.6	2.88
53.9	3.80
55.2	4.24
57.0	4.34
57.0	Straight line
83.0	
Nose radius: 3.54 in.	

NATIONAL ADVISORY
COMMITTEE FOR AERONAUTICS

TABLE III - Concluded

HORIZONTAL-TAIL ORDINATES XTB3F-1 AIRPLANE - Concluded

(b) Station, $134\frac{3}{4}$ in.; chord length, 52.24 in.; elevator chord, 22.19 in.

Station (percent chord)	Station (in.)	Ordinate (in.)
1.25	0.653	0.56
2.5	1.306	.79
5	2.612	1.07
7.5	3.918	1.28
10	5.224	1.45
20	10.448	1.88
30	15.672	2.04
40	20.896	2.06
50	26.120	1.95
57.52 (hinge line)	30.05	1.74
57.52	30.05	Straight line
100	52.24	
L.E. radius: 0.32 in.		

Elevator Nose

Station (in.)	Ordinate (in.)
26.19	0
27.30	1.56
28.41	1.86
29.52	1.92
30.05	1.91
30.05	Straight line
52.24	
Nose radius: 1.6 in.	

NATIONAL ADVISORY
COMMITTEE FOR AERONAUTICS

FIGURE LEGENDS

Figure 1.- Three-view drawing of the $\frac{1}{8}$-scale model of the XTB3F-1 airplane.

Figure 2.- System of axes and control-surface hinge moments and deflections. Positive values of forces, moments, and angles are indicated by arrows. Positive values of tab hinge moments and deflections are in the same directions as the positive values for the control surfaces to which the tabs are attached.

Figure 3.- The $\frac{1}{8}$-scale model of the Grumman XTB3F-1 airplane mounted in the Langley 7- by 10-foot tunnel.

(a) Three-quarter front view, flaps up.

Figure 3.- Concluded.

(b) Three-quarter rear view, flaps down.

Figure 4.- Variation of maximum flap deflection with lift coefficient for the Grumman XTB3F-1 airplane.

Figure 5.- Drawing of the original vertical tail of the $\frac{1}{8}$-scale model of the Grumman XTB3F-1 airplane.

Figure 6.- Modifications to vertical tail of the $\frac{1}{8}$-scale model of Grumman XTB3F-1 airplane.

Figure 7.- Horizontal tail of the $\frac{1}{8}$-scale model of the Grumman XTB3F-1 airplane.

Figure 8.- Schematic diagram of thrust line revision made on the $\frac{1}{8}$-scale model of the Grumman XTB3F-1 airplane.

Figure 9.- Details of setup for jet-simulation tests. Grumman XTB3F-1 airplane model ($\frac{1}{8}$-scale).

Figure 10.- Setup used for jet-simulation tests on Grumman XTB3F-1 model ($\frac{1}{8}$-scale).

Figure 10.- Continued.

Figure 10.- Concluded.

FIGURE LEGENDS - Continued

Figure 11.- General arrangement of external stores tested on $\frac{1}{8}$-scale model of Grumman XTB3F-1 airplane.

(a) Front view.

Figure 11.- Continued.

(b) Three-quarter front view.

Figure 11.- Concluded.

(c) Detail of gun package.

Figure 12.- Location of model with respect to ground board; $\alpha = 0^{\circ}$.

Figure 13.- The $\frac{1}{8}$-scale model of the Grumman XTB3F-1 airplane mounted in the tunnel with ground board in place.

Figure 14.- Calibration of propeller used on $\frac{1}{8}$-scale model of the Grumman XTB3F-1 airplane. D = 1.625 ft.

Figure 15.- Variation of effective thrust coefficient with lift coefficient for the Grumman XTB3F-1 airplane.

Figure 15.- Concluded.

Figure 16.- Model torque coefficient and estimated variation of effective thrust coefficient with airplane velocity during take-off for the Grumman XTB3F-1 airplane. Military rated power.

Figure 17.- Variation of torque coefficient with lift coefficient for the $\frac{1}{8}$-scale model of the Grumman XTB3F-1 airplane and the prototype airplane with R3350-24 engine and Curtiss electric propeller.

Figure 18.- Comparison of mass flow of air into wing ducts obtained in model tests with full-scale Grumman XTB3F-1 airplane data.

Figure 19.- Aerodynamic characteristics in pitch of a $\frac{1}{8}$-scale model of the Grumman XTB3F-1 airplane. Glide configuration.

(a) Original thrust line.

FIGURE LEGENDS - Continued

Figure 19.- Continued.

(b) Thrust line tilted down 3°.

Figure 19.- Continued.

(b) Continued.

Figure 19.- Concluded.

(b) Concluded.

Figure 20.- Aerodynamic characteristics in pitch of a $\frac{1}{8}$-scale model of the Grumman XTB3F-1 airplane. Power-on clean configuration.

(a) Original thrust line.

Figure 20.- Continued.

(b) Thrust line tilted down 3°.

Figure 20.- Continued.

(b) Continued.

Figure 20.- Concluded.

(b) Concluded.

Figure 21.- Aerodynamic characteristics in pitch of a $\frac{1}{8}$-scale model of the Grumman XTB3F-1 airplane. Landing configuration.

(a) Original thrust line.

Figure 21.- Continued.

(b) Thrust line tilted down 3°; $i_t = 2.25°$.

Figure 21.- Concluded.

(b) Concluded.

FIGURE LEGENDS - Continued

Figure 22.- Aerodynamic characteristics in pitch of a $\frac{1}{8}$-scale model of the Grumman XTB3F-1 airplane. Approach configuration.

(a) Original thrust line.

Figure 22.- Continued.

(b) Thrust line tilted down 3°.

Figure 22.- Continued.

(b) Continued.

Figure 22.- Concluded.

(b) Concluded.

Figure 23.- Longitudinal trim changes due to power and flap deflection of a $\frac{1}{8}$-scale model of the Grumman XTB3F-1 airplane. Thrust line tilted down 3°, $i_t = 2^{\circ}15'$.

Part A

Figure 23.- Continued.

Part B

Figure 23.- Continued.

Part C

Figure 23.- Concluded.

Part D

Figure 24.- Effect of various wing-flap deflections on the aerodynamic characteristics in pitch of a $\frac{1}{8}$-scale model of the Grumman XTB3F-1 airplane. Thrust line tilted down 3°.

(a) Tail off; windmilling propeller.

FIGURE LEGENDS - Continued

Figure 24.- Continued.

(b) $i_t = 2.0^\circ$; windmilling propeller.

Figure 24.- Continued.

(c) $i_t = 4.8^\circ$; windmilling propeller.

Figure 24.- Continued.

(d) Tail off; half normal rated power.

Figure 24.- Continued.

(e) $i_t = 2.0^\circ$; half normal rated power.

Figure 24.- Concluded.

(f) $i_t = 4.8^\circ$; half normal rated power.

Figure 25.- Effect of propeller blade angle on aerodynamic characteristics in pitch of a $\frac{1}{8}$-scale model of the Grumman XTB3F-1 airplane. $T_c' = 0$; $\delta_f = 0^\circ$; $q = 16.37$ pounds per square foot.

Figure 26.- Effect of flap deflection on neutral point location of the $\frac{1}{8}$-scale model of the Grumman XTB3F-1 airplane. Thrust line tilted down 3°.

(a) Windmilling propeller.

Figure 26.- Concluded.

(b) Half normal rated power.

Figure 27.- Effect of thrust line tilt on neutral point location of the $\frac{1}{8}$-scale model of the Grumman XTB3F-1 airplane.

(a) $\delta_f = 0^\circ$

Figure 27.- Concluded.

(b) $\delta_f = 50^\circ$

FIGURE LEGENDS - Continued

Figure 28.- Lateral stability parameters of a $\frac{1}{8}$-scale model of the Grumman XTB3F-1 airplane. Original vertical tail; original dorsal fin.

(a) $\delta_r = 0^\circ$

Figure 28.- Concluded.

(b) $\delta_r = 50^\circ$

Figure 29.- Aerodynamic characteristics in yaw of a $\frac{1}{8}$-scale model of the Grumman XTB3F-1 airplane. Glide configuration.

(a) $\alpha = -.9^\circ$; $i_{fin} = -2^\circ 15'$; original vertical tail; original dorsal fin.

Figure 29.- Continued.

(a) Concluded; $\delta_r = 0^\circ$

Figure 29.- Continued.

(b) $\alpha = 8.9^\circ$; $i_{fin} = -2^\circ 15'$; original vertical tail; original dorsal fin.

Figure 29.- Continued.

(b) Concluded; $\delta_r = 0^\circ$

Figure 29.- Continued.

(c) $\alpha = 8.9^\circ$; original vertical tail; no dorsal fin.

Figure 29.- Continued.

(d) $\alpha = 1.3^\circ$; 1.5-inch base extension on vertical tail; original dorsal fin.

Figure 29.- Continued.

(d) Continued.

FIGURE LEGENDS - Continued

Figure 29.- Concluded.

(d) Concluded; $\delta_r = 0^\circ$

Figure 30.- Aerodynamic characteristics in yaw of a $\frac{1}{8}$-scale model of the Grumman XTB3F-1 airplane. Power-on clean configuration.

(a) $\alpha = 7.9^\circ$; $i_{fin} = -2^\circ 15'$; original vertical tail; original dorsal fin.

Figure 30.- Continued.

(a) Concluded; $\delta_r = 0^\circ$

Figure 30.- Continued.

(b) $\alpha = 7.9^\circ$; original vertical tail; no dorsal fin.

Figure 30.- Continued.

(c) $\alpha = 8.2^\circ$; original vertical tail.

Figure 30.- Continued.

(d) $\alpha = 9.2^\circ$; 2.5-inch tip extension on vertical tail.

Figure 30.- Continued.

(d) Continued.

Figure 30.- Continued.

(d) Concluded; original dorsal fin; $i_{fin} = -2^\circ 15'$.

Figure 30.- Continued.

(e) $\alpha = 9.2^\circ$; 2-inch base extension on vertical tail.

Figure 30.- Continued.

(e) Concluded.

Figure 30.- Continued.

(f) $\alpha = 8.5^\circ$; 1.5-inch base extension on vertical tail; original dorsal fin.

FIGURE LEGENDS - Continued

Figure 30.- Concluded.

(f) Concluded.

Figure 31.- Aerodynamic characteristics in yaw of a $\frac{1}{8}$-scale model of the Grumman XTB3F-1 airplane. Landing configuration; original dorsal fin.

(a) $\alpha = 11.8^{\circ}$; $i_{fin} = -2^{\circ}15'$; original vertical tail.

Figure 31.- Continued.

(a) Concluded.

Figure 31.- Continued.

(b) $\alpha = 9.6^{\circ}$; 1.5-inch base extension on vertical tail.

Figure 31.- Continued.

(b) Continued.

Figure 31.- Concluded.

(b) Concluded.

Figure 32.- Aerodynamic characteristics in yaw of a $\frac{1}{8}$-scale model of the Grumman XTB3F-1 airplane. Approach configuration.

(a) $\alpha = 5.6^{\circ}$; $i_{fin} = -2^{\circ}15'$; original vertical tail; original dorsal fin.

Figure 32.- Continued.

(a) Continued.

Figure 32.- Continued.

(a) Continued.

Figure 32.- Continued.

(a) Concluded.

FIGURE LEGENDS - Continued

Figure 32.- Continued.

(b) $\alpha = 7.3^{\circ}$; $i_{fin} = -2^{\circ}15'$; 2-inch base extension on vertical tail.

Figure 32.- Continued.

(b) Continued.

Figure 32.- Continued.

(b) Concluded.

Figure 32.- Continued.

(c) $\alpha = 6.7^{\circ}$; 1.5-inch base extension on vertical tail; original dorsal fin.

Figure 32.- Concluded.

(c) Concluded.

Figure 33.- Aerodynamic characteristics in yaw of a $\frac{1}{8}$-scale model of the Grumman XTB3F-1 airplane. Wave-off configuration.

(a) $\alpha = 10.1^{\circ}$; 2-inch base extension on vertical tail.

Figure 33.- Continued.

(a) Continued.

Figure 33.- Continued.

(a) Concluded; original dorsal fin.

Figure 33.- Continued.

(b) $\alpha = 8.7^{\circ}$; 1.5-inch base extension on vertical tail.

Figure 33.- Continued.

(b) Continued.

Figure 33.- Concluded.

(b) Concluded; $\delta_r = 0^{\circ}$.

FIGURE LEGENDS - Continued

Figure 34.- Effect of propeller blade angle on aerodynamic characteristics in yaw of a $\frac{1}{8}$-scale model of the Grumman XTB3F-1 airplane. $T_c' = 0$; $\delta_f = 0^\circ$; $q = 16.37$ pounds per square foot.

(a) $\alpha = .89^\circ$.

Figure 34.- Concluded.

(b) $\alpha = 8.86^\circ$.

Figure 35.- Aileron characteristics of a $\frac{1}{8}$-scale model of the Grumman XTB3F-1 airplane. Windmilling propeller; $\delta_{a_L} = 0^\circ$.

(a) Glide configuration.

Figure 35.- Concluded.

(b) Landing configuration.

Figure 36.- Effect of jet simulation on the aerodynamic characteristics in pitch of a $\frac{1}{8}$-scale model of the Grumman XTB3F-1 airplane. $\delta_f = 0^\circ$.

(a) Propeller off; flow condition "P".

Figure 36.- Continued.

(a) Concluded.

Figure 36.- Continued.

(b) Propeller off; flow condition "I".

Figure 36.- Continued.

(b) Concluded.

Figure 36.- Continued.

(c) Propeller off; flow condition "S".

Figure 36.- Continued.

(c) Concluded.

FIGURE LEGENDS - Continued

Figure 36.- Continued.

(d) Power-on clean; flow condition "P".

Figure 36.- Continued.

(d) Concluded.

Figure 36.- Continued.

(d) Power-on clean; flow condition "I".

Figure 36.- Concluded.

(e) Concluded.

Figure 37.- Effect of jet simulation on neutral point location of the $\frac{1}{8}$-scale model of the Grumman XTB3F-1 airplane. $\delta_f = 0^\circ$

Figure 38.- Effect of airflow through the duct system on the aerodynamic characteristics in pitch of the $\frac{1}{8}$-scale model of the Grumman XTB3F-1 airplane. $i_t = 2.16^\circ$; landing configuration.

Figure 39.- Effect of jet simulation on the aerodynamic characteristics in yaw of a $\frac{1}{8}$-scale model of the Grumman XTB3F-1 airplane. Glide configuration; $C_L = .97$; $\alpha = 9.8^\circ$; propeller off.

Figure 39.- Concluded

Figure 40.- Effect of airflow through the duct system on the aerodynamic characteristics in yaw of the $\frac{1}{8}$-scale model of the Grumman XTB3F-1 airplane. Landing configuration; $\alpha = 11.8^\circ$.

Figure 41.- Aerodynamic characteristics in pitch of a $\frac{1}{8}$-scale model of the Grumman XTB3F-1 airplane with ground board in place. Landing configuration; $\beta = 25^\circ$; original thrust line.

(a) $\delta_e = 0^\circ$.

Figure 41.- Continued.

(b) $i_t = 2.25^\circ$.

FIGURE LEGENDS - Continued

Figure 41.- Continued.

(b) Continued.

Figure 41.- Concluded.

(b) Concluded.

Figure 42.- Aerodynamic characteristics of a $\frac{1}{8}$-scale model of the Grumman XTB3F-1 airplane with ground board in place. Take-off configuration; $\beta = 25^{\circ}$; $\psi = 0^{\circ}$.

(a) $\alpha = 0^{\circ}$; original thrust line.

Figure 42.- Continued.

(a) Continued.

Figure 42.- Continued.

(a) Concluded.

Figure 42.- Continued.

(b) $\alpha = 11.5^{\circ}$; original thrust line.

Figure 42.- Continued.

(b) Continued.

Figure 42.- Continued.

(b) Concluded.

Figure 42.- Continued.

(c) $\alpha = -.1^{\circ}$; thrust line tilted down 3°.

Figure 42.- Continued.

(c) Concluded.

Figure 42.- Continued.

(d) $\alpha = 11.3^{\circ}$; thrust line tilted down 3°; $i_t = 2.25^{\circ}$.

FIGURE LEGENDS - Continued

Figure 42.- Concluded.

(d) Concluded.

Figure 43.- Effect of rudder deflection on the aerodynamic characteristics of a $\frac{1}{8}$-scale model of the Grumman XTB3F-1 airplane with the ground board in place. Take-off configuration; $\beta = 15^{\circ}$; $\psi = 0^{\circ}$; original dorsal fin; $i_{fin} = -2^{\circ}15'$.

(a) $\alpha = 0^{\circ}$; original thrust line; original vertical tail.

Figure 43.- Continued.

(a) Continued.

Figure 43.- Continued.

(a) Concluded.

Figure 43.- Continued.

(b) $\alpha = 11.5^{\circ}$; original thrust line; original vertical tail.

Figure 43.- Continued.

(b) Continued.

Figure 43.- Continued.

(b) Concluded.

Figure 43.- Continued.

(c) $\alpha = 11.4^{\circ}$; 1.5-inch base extension on vertical tail; thrust line tilted down 3°.

Figure 43.- Continued.

(c) Continued.

Figure 43.- Concluded.

(c) Concluded.

FIGURE LEGENDS - Continued

Figure 44.- Effect of rudder deflection on the aerodynamic characteristics of a $\frac{1}{8}$-scale model of the Grumman XTB3F-1 airplane with the ground board in place. Simulated take-off in a 17.6 m.p.h. crosswind, from the left, at 90° to the flight path; take-off configuration; $\alpha = 11.4^{\circ}$; $\beta = 15^{\circ}$; 1.5-inch base extension on vertical tail; original dorsal fin; thrust line tilted down 3°; $i_{fin} = -2^{\circ}15'$.

Figure 44.- Continued.

Figure 44.- Concluded.

Figure 45.- Effect of external stores on the aerodynamic characteristics in pitch of a $\frac{1}{8}$-scale model of the Grumman XTB3F-1 airplane. Thrust line tilted down 3°.

(a) Glide configuration.

Figure 45.- Concluded.

(b) Power-on clean configuration.

Figure 46.- Increment in neutral-point location due to external stores for a $\frac{1}{8}$-scale model of the Grumman XTB3F-1 airplane.

Figure 47.- Effect of external stores on the lateral stability parameters of a $\frac{1}{8}$-scale model of the Grumman XTB3F-1 airplane. Large dorsal fin; 1.5-inch base extension on vertical tail.

(a) Glide configuration.

Figure 47.- Concluded.

(b) Power-on clean configuration.

Figure 48.- Effect of external stores on the aerodynamic characteristics in yaw of a $\frac{1}{8}$-scale model of the Grumman XTB3F-1 airplane. Large dorsal fin; 1.5-inch base extension on vertical tail.

(a) Glide configuration; $\alpha = -1.1^{\circ}$, $C_L = 0.11$.

FIGURE LEGENDS - Concluded

Figure 48.- Concluded.

(b) Power-on clean configuration; $\alpha = 9.8^{\circ}$, $C_L = 1.05$.

Figure 49.- Aerodynamic characteristics of the isolated horizontal tail of a $\frac{1}{8}$-scale model of the Grumman XTB3F-1 airplane.

(a) $\delta_{e_t} = 0^{\circ}$, $\delta_{fantail} = 0^{\circ}$.

Figure 49.- Continued.

(a) Concluded.

Figure 49.- Continued.

(b) $\delta_e = 0^{\circ}$; $\delta_{fantail} = 0^{\circ}$.

Figure 49.- Continued.

(b) Concluded.

Figure 49.- Continued.

(c) $\delta_e = 0^{\circ}$; $\delta_{e_t} = 0^{\circ}$.

Figure 49.- Concluded.

(c) Concluded.

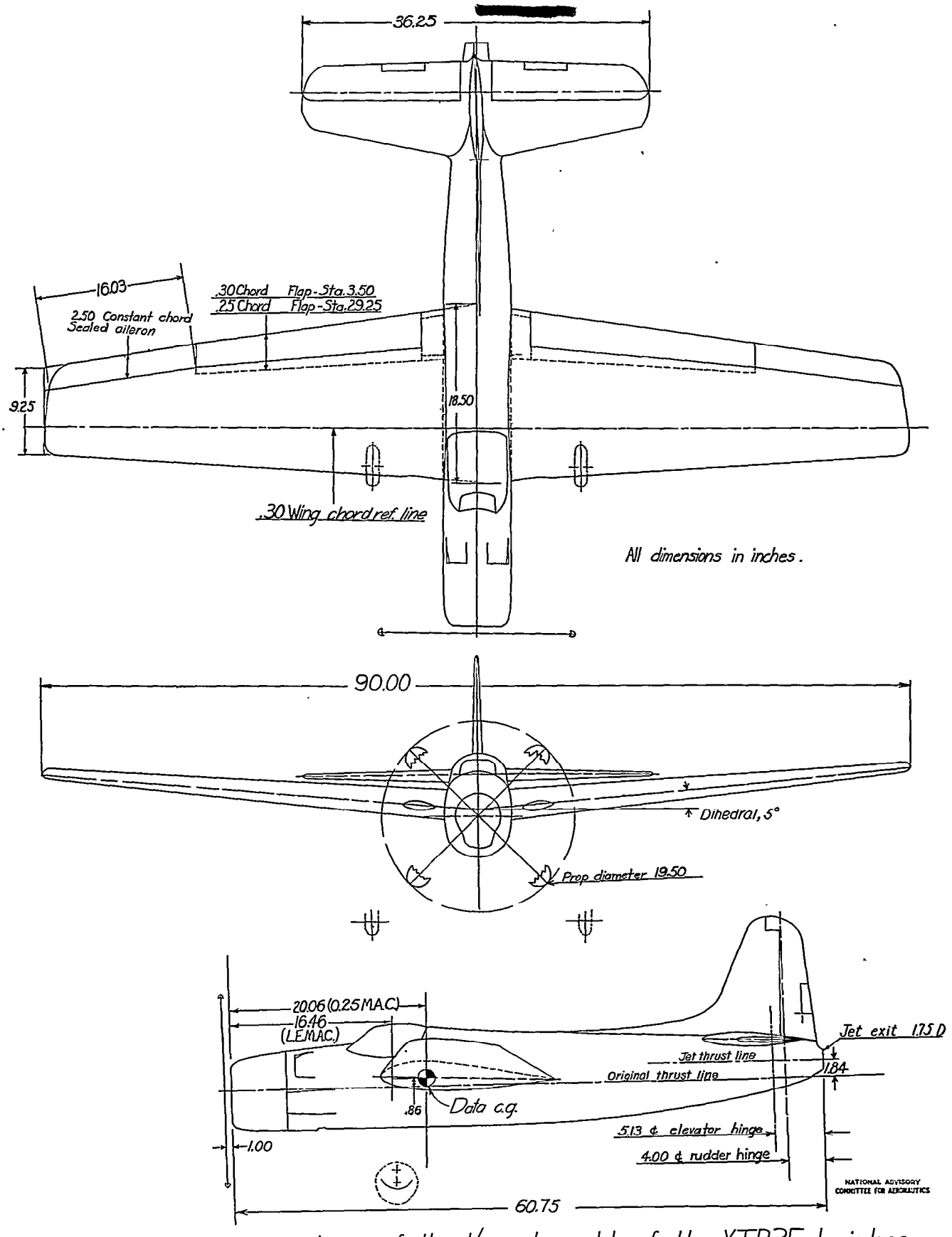

Figure 1. – Three-view drawing of the 1/8-scale model of the XTB3F-1 airplane.

[redacted]

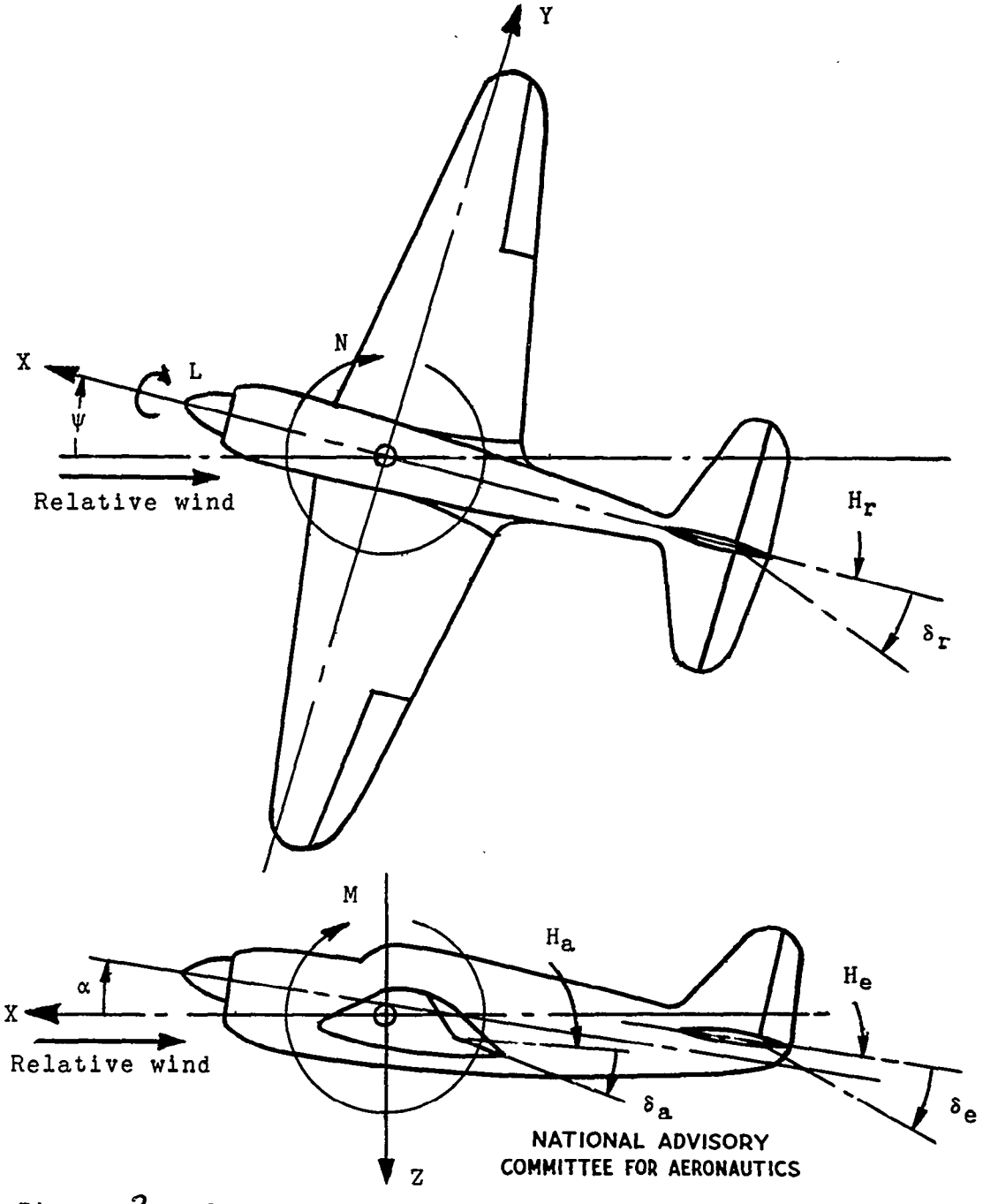

Figure 2.- System of axes and control-surface hinge moments and deflections. Positive values of forces, moments, and angles are indicated by arrows. Positive values of tab hinge moments and deflections are in the same directions as the positive values for the control surfaces to which the tabs are attached.

[redacted]

[redacted]

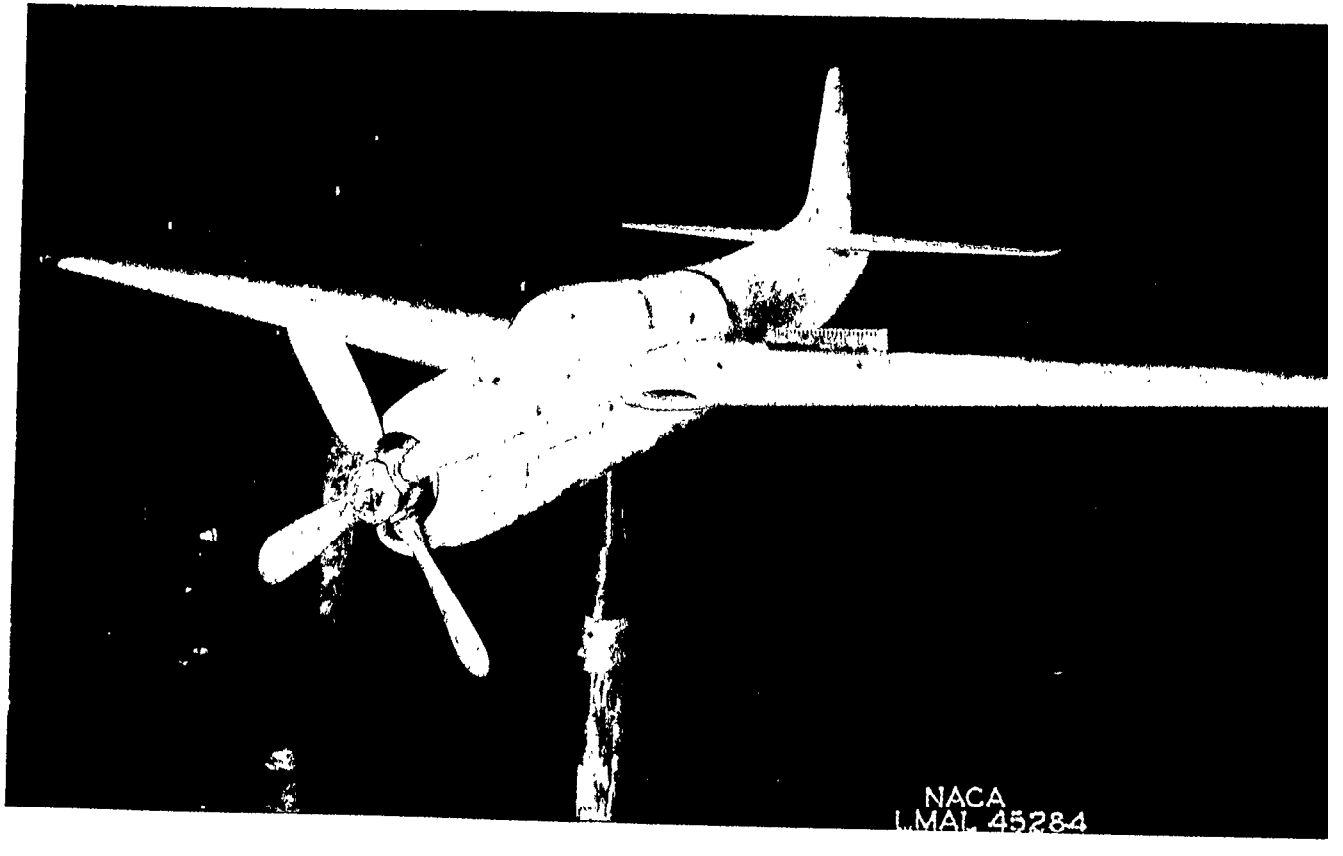

(a) Three-quarter front view, flaps up.

Figure 3.- The $\frac{1}{8}$-scale model of the Grumman XTB3F-1 airplane mounted in t
Langley 7- by 10-foot tunnel.

[redacted]

NATIONAL ADVISORY COMMITTEE FOR AERONAUTICS
LANGLEY MEMORIAL AERONAUTICAL LABORATORY LANGLEY FIELD, VA

[redacted]

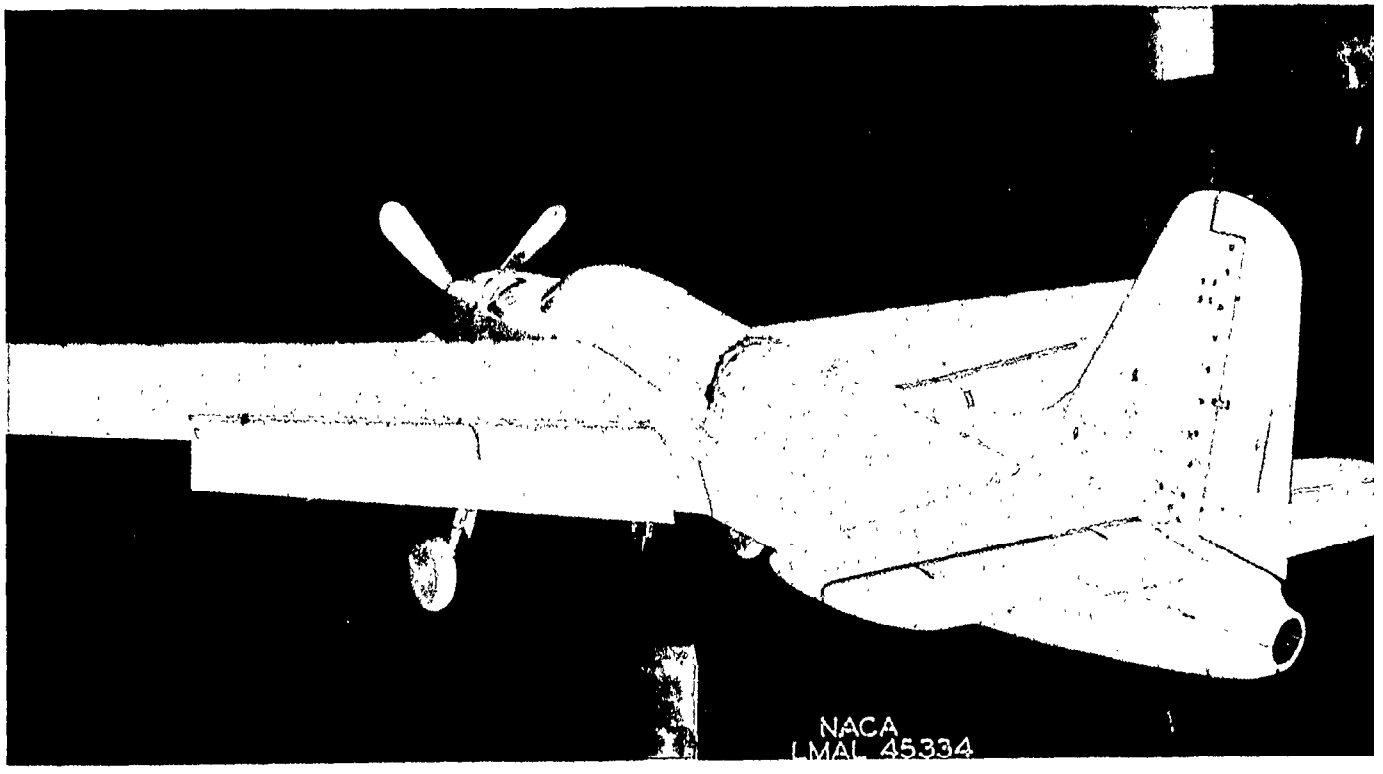

(b) Three-quarter rear view, flaps down.

Figure 3.- Concluded.

[redacted]

NATIONAL ADVISORY COMMITTEE FOR AERONAUTICS
LANGLEY MEMORIAL AERONAUTICAL LABORATORY LANGLEY FIELD VA

[redacted]

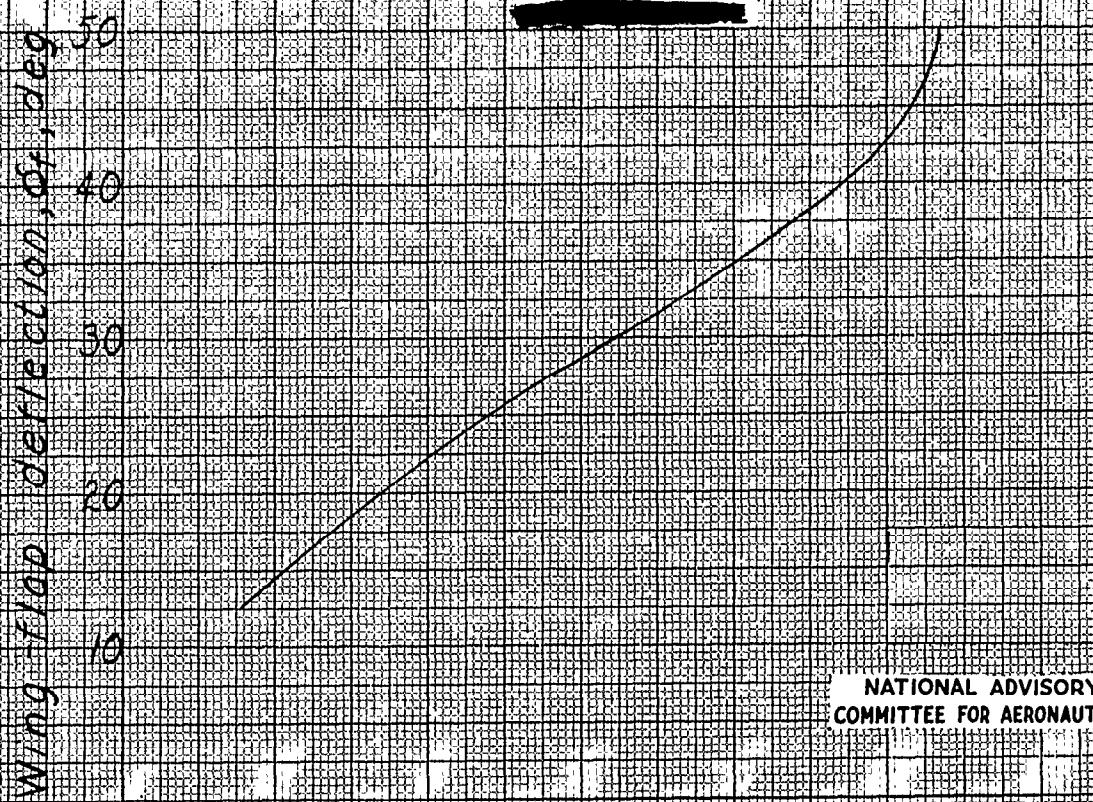

NATIONAL ADVISORY COMMITTEE FOR AERONAUTICS

Figure 4.- Variation of maximum flap deflection with lift coefficient for the Grumman XTB3F-1 airplane.

[redacted]

[redacted]

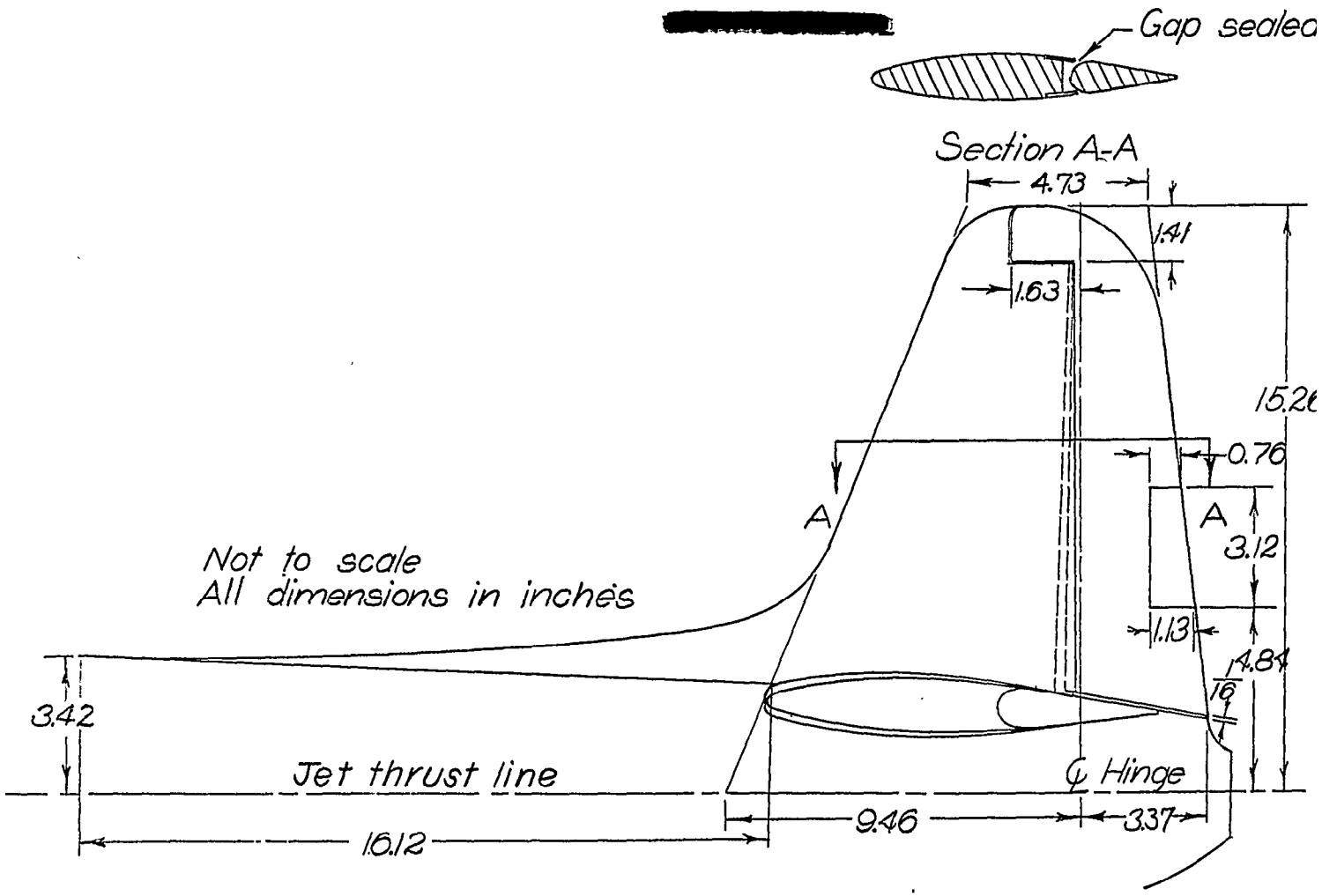

NATIONAL ADVISORY
COMMITTEE FOR AERONAUTICS

Figure 5.-Drawing of the original vertical tail of the 1/8-scale r
of the Grumman XTB3F-1 airplane.

[redacted]

[redacted]

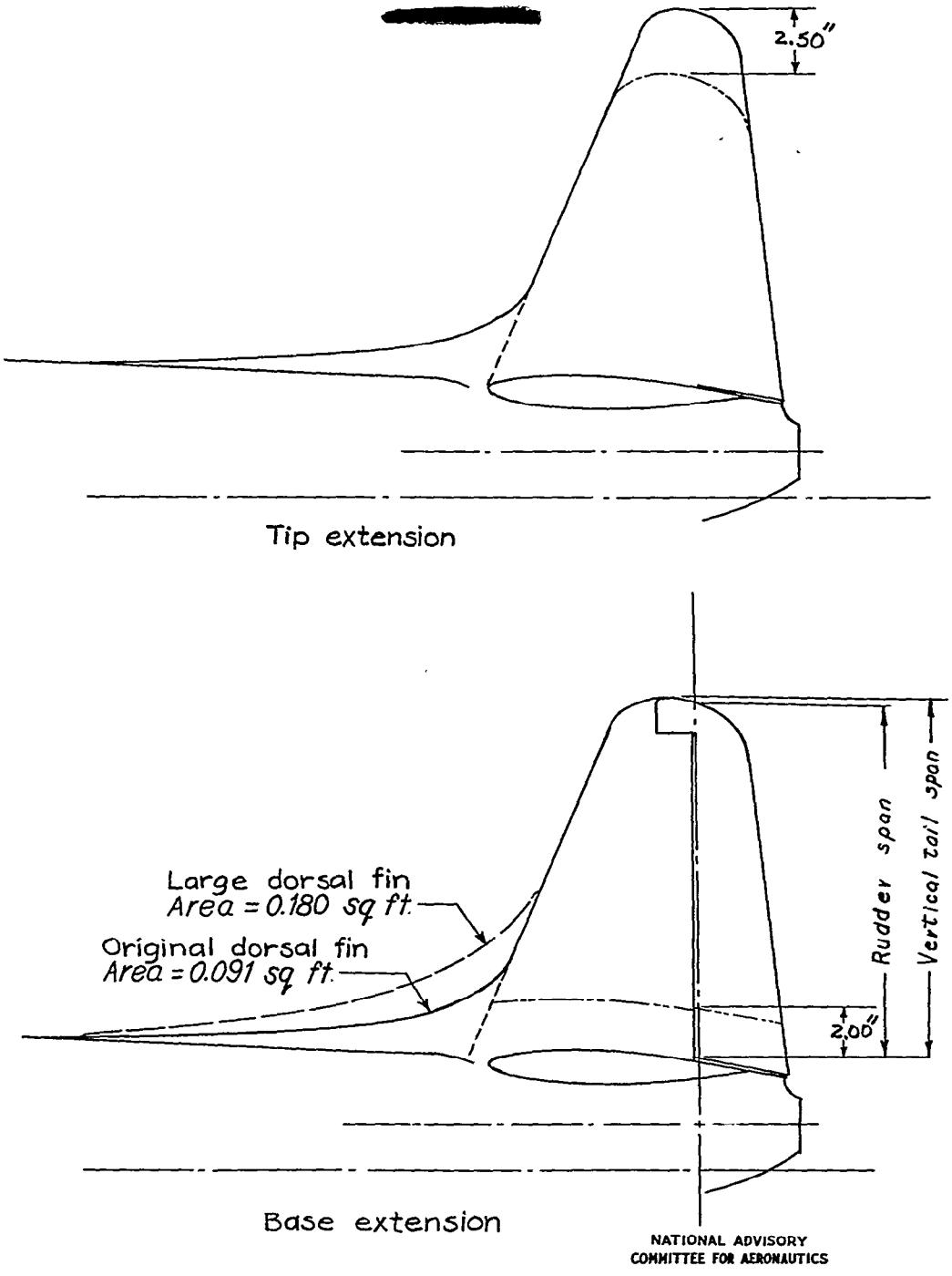

Figure 6.—Modifications to vertical tail of the 1/8-scale model of Grumman XTB3F-1 airplane.

[redacted]

[redacted]

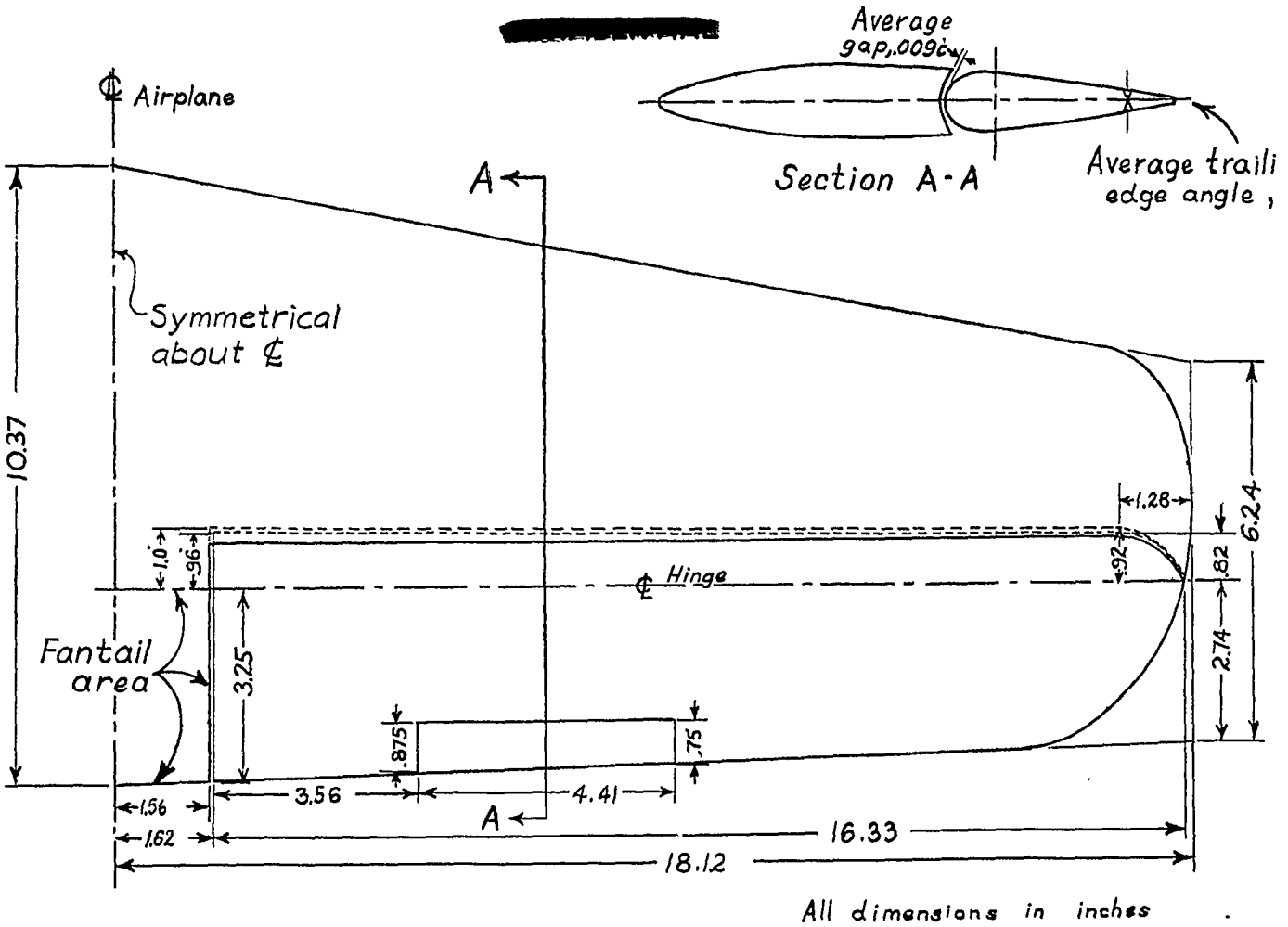

Figure 7 .— Horizontal tail of the $\frac{1}{8}$-scale model of the Grumman XTB3F-1 airplane.

NATIONAL ADVISORY COMMITTEE FOR AERONAUTICS

[redacted]

[redacted]

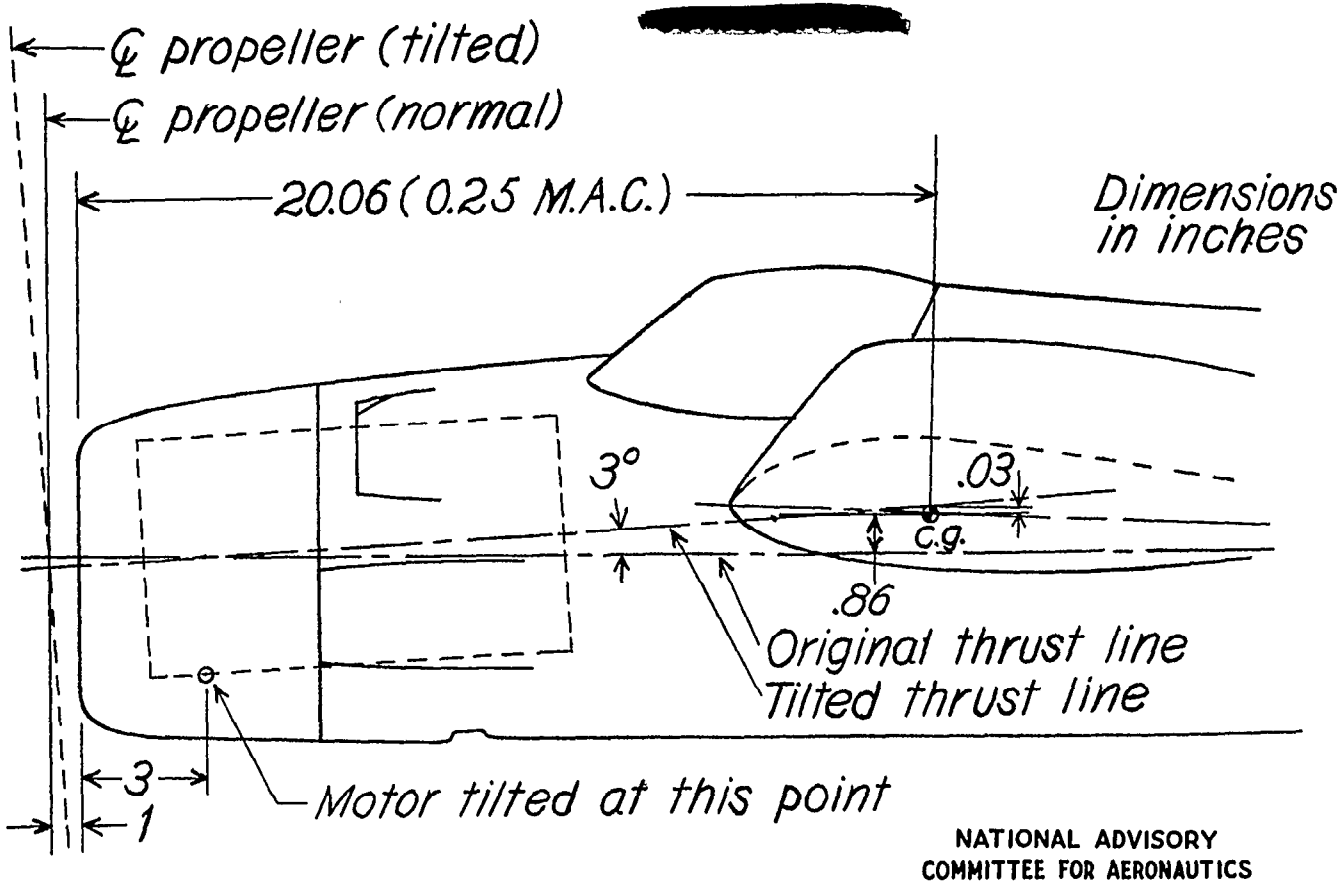

Figure 8.- Schematic diagram of thrust line revision ma
on the 1/8-scale model of the Grumman XTB3F-1 air

[redacted]

[redacted]

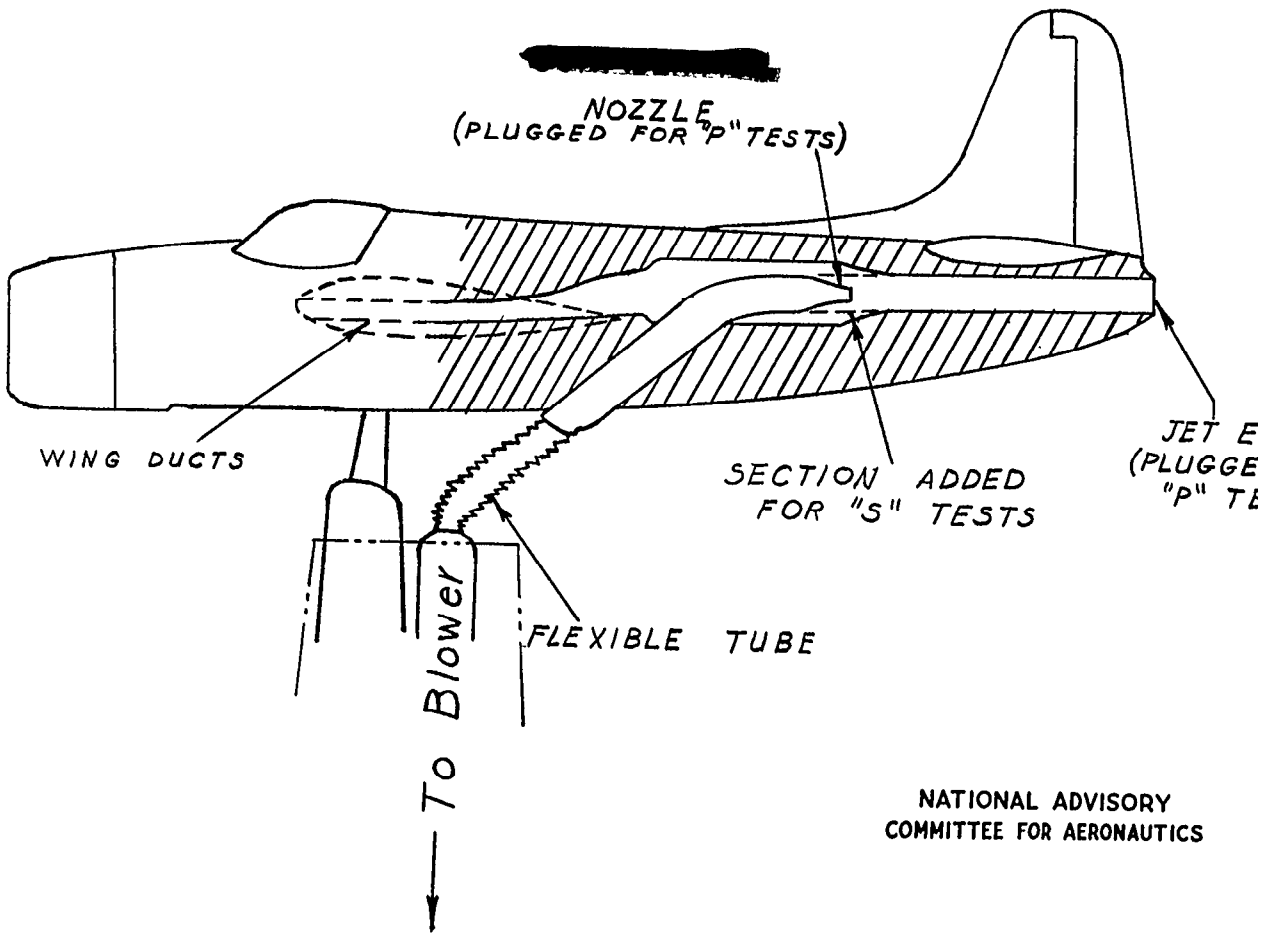

NATIONAL ADVISORY
COMMITTEE FOR AERONAUTICS

Figure 9.- Details of setup for jet-simulation tests. Grumman XTB3F-1 airplane mode (1/8-scale).

[redacted]

[redacted]

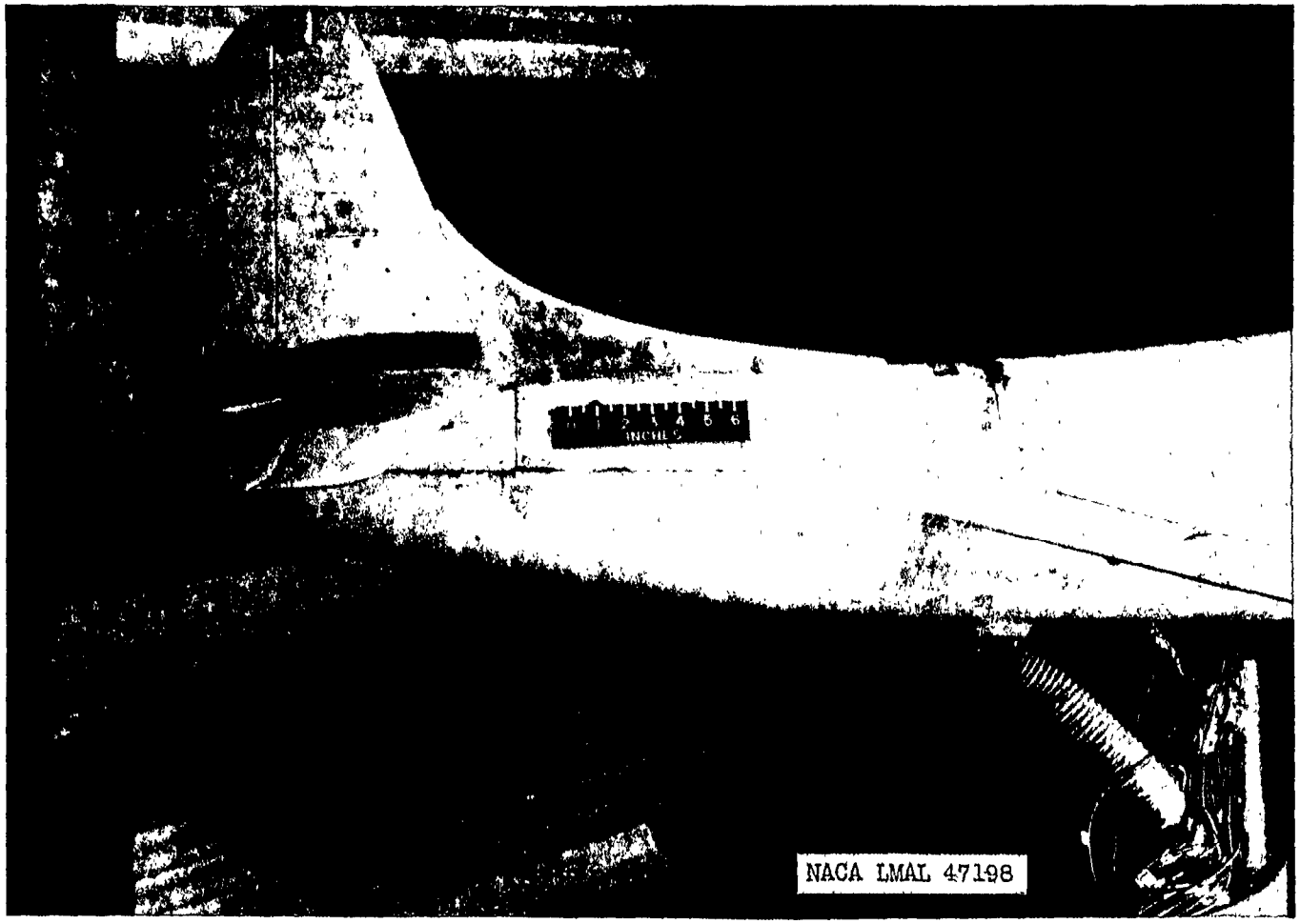

Figure 10.- Setup used for jet-simulation tests on Grumman XTB3F-1 model ($\frac{1}{8}$-scale).

[redacted]

NATIONAL ADVISORY COMMITTEE FOR AERONAUTICS
LANGLEY MEMORIAL AERONAUTICAL LABORATORY - LANGLEY FIELD, VA

[redacted]

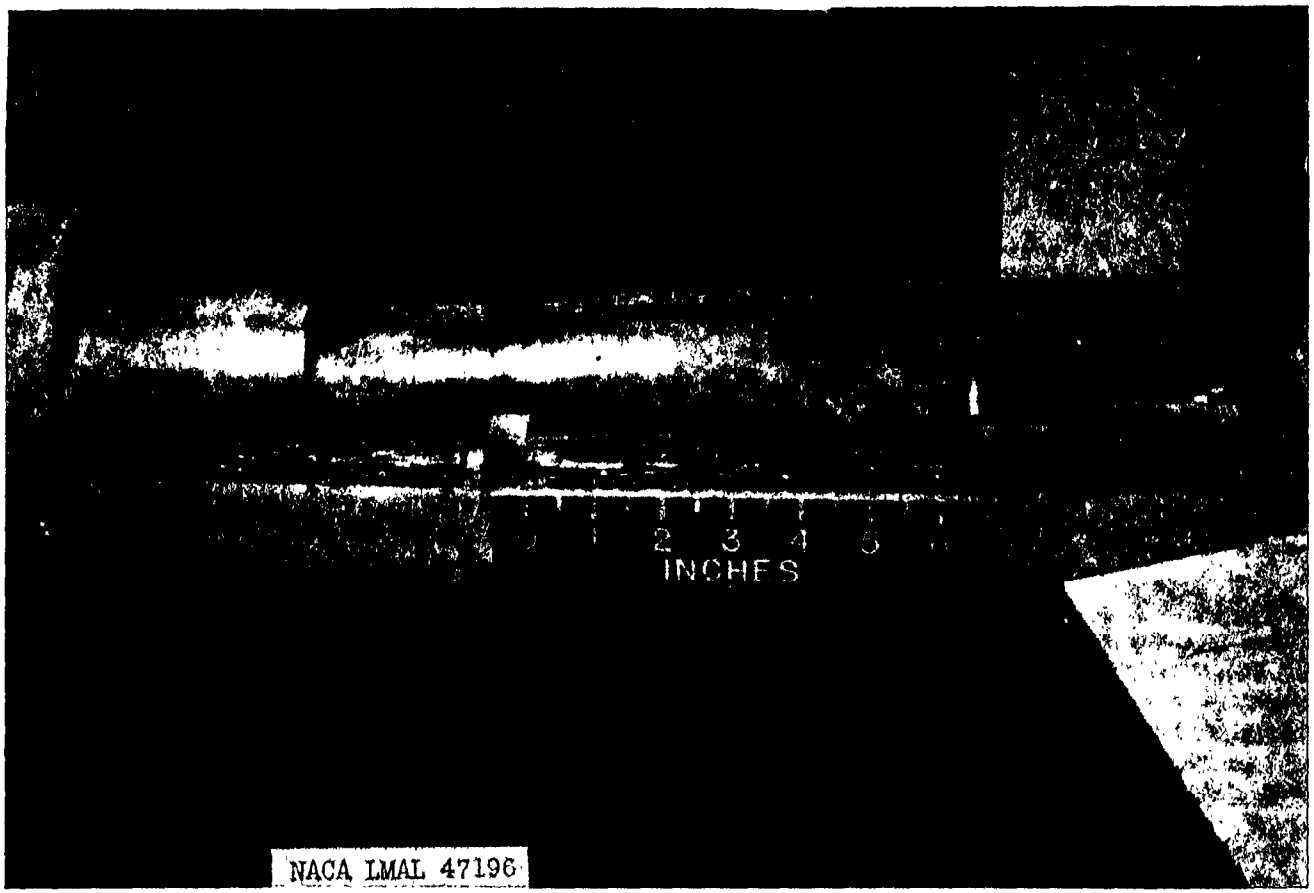

[redacted] Figure 10.- Continued.

NATIONAL ADVISORY COMMITTEE FOR AERONAUTICS
LANGLEY MEMORIAL AERONAUTICAL LABORATORY - LANGLEY FIELD VA

[redacted]

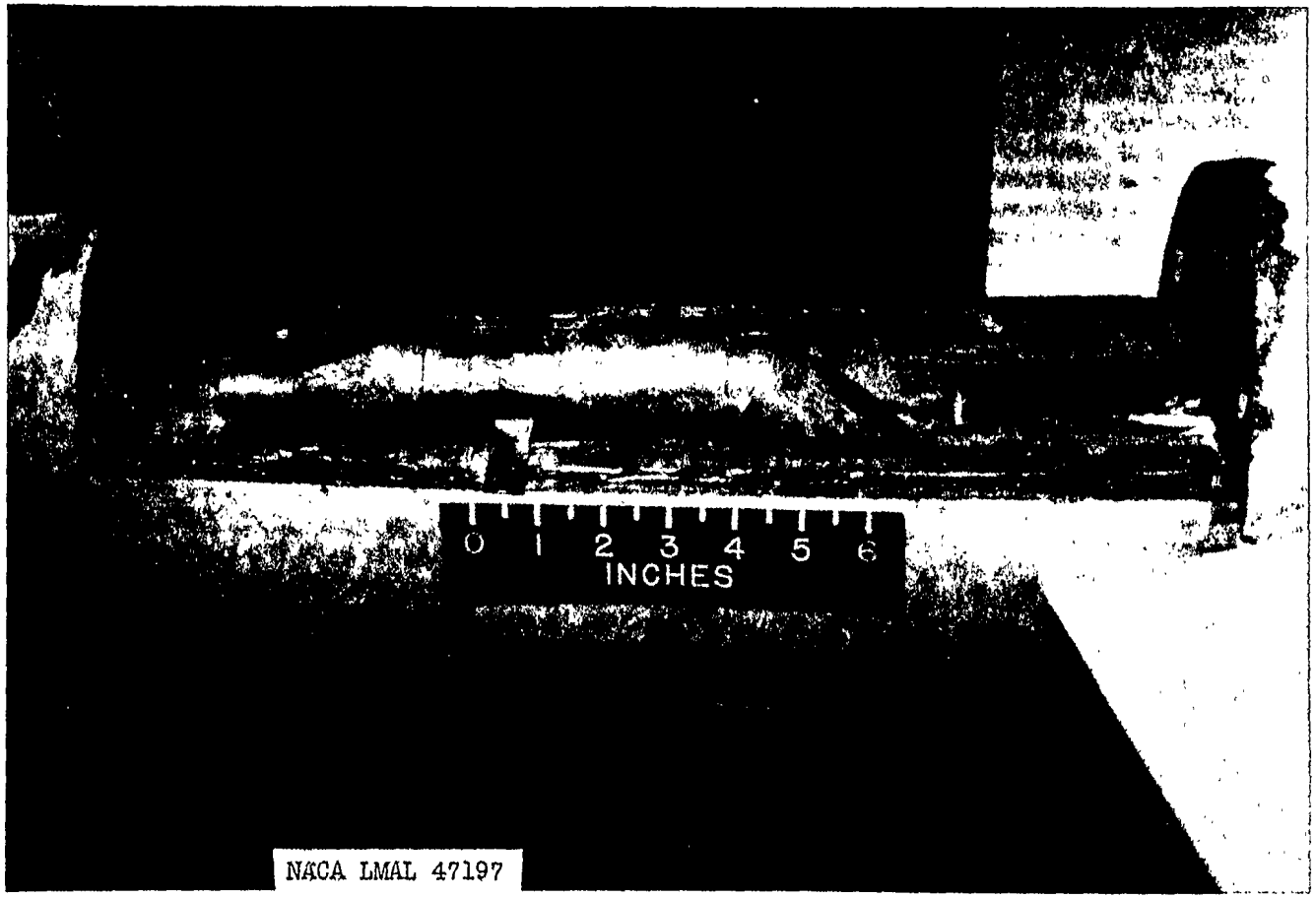

Figure 10.- Concluded.

[redacted]

NATIONAL ADVISORY COMMITTEE FOR AERONAUTICS
LANGLEY MEMORIAL AERONAUTICAL LABORATORY · LANGLEY FIELD, VA

[redacted]

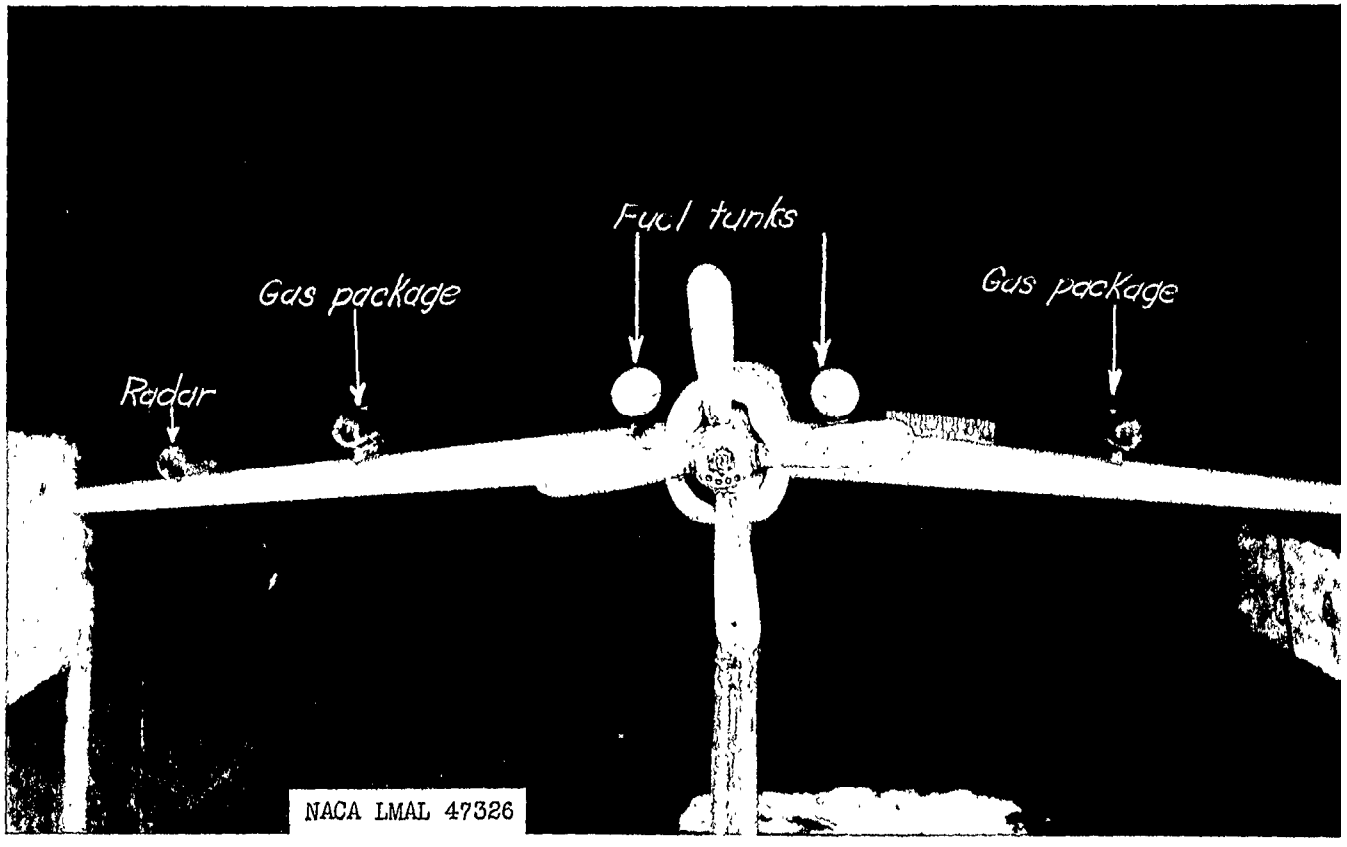

(a) Front view.

Figure 11.- General arrangement of external stores tested on $\frac{1}{8}$-scale model Grumman XTB3F-1 airplane.

[redacted]

NATIONAL ADVISORY COMMITTEE FOR AERONAUTICS
LANGLEY MEMORIAL AERONAUTICAL LABORATORY LANGLEY FIELD VA

[redacted]

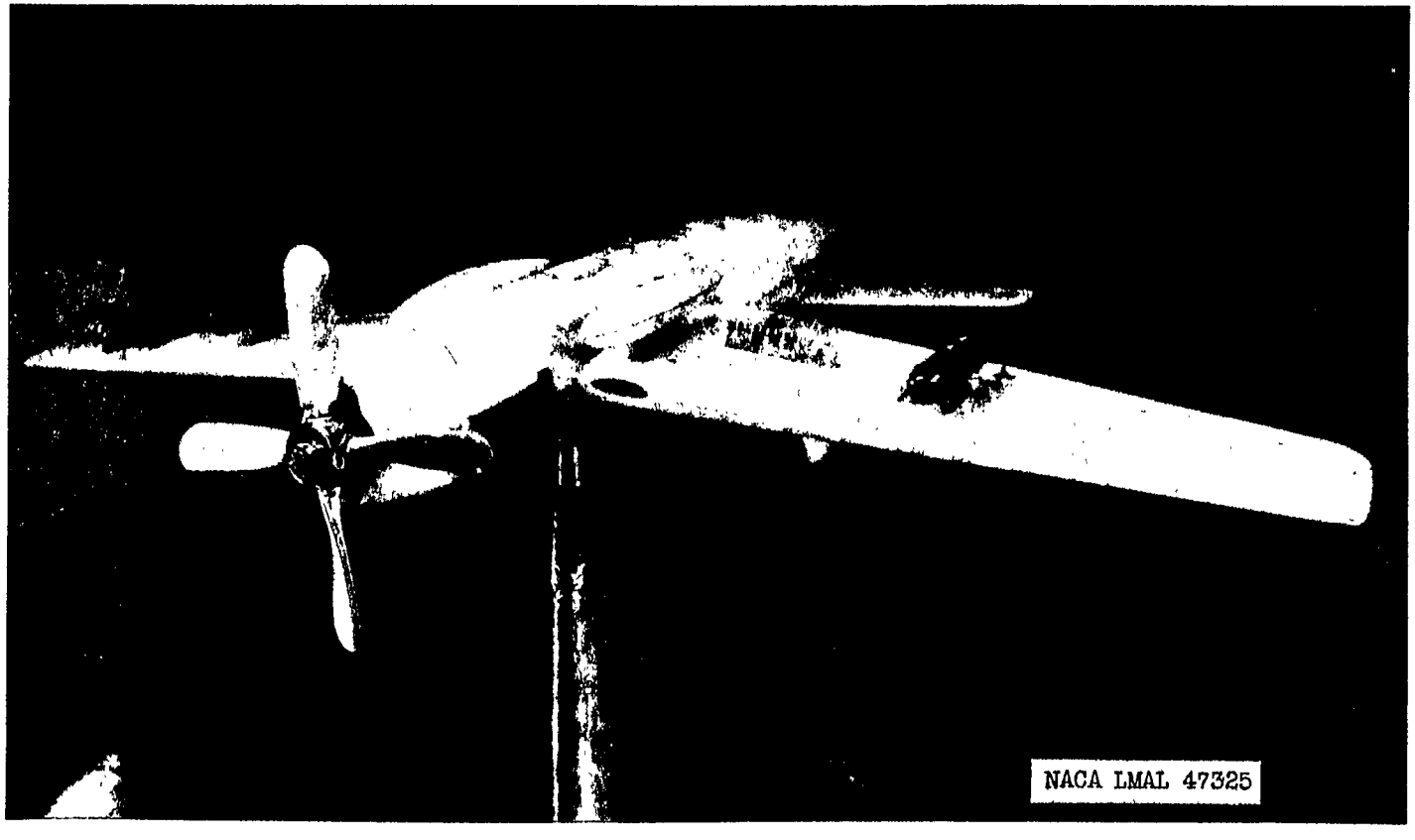

(b) Three-quarter front view.

Figure 11.- Continued.

[redacted]

NATIONAL ADVISORY COMMITTEE FOR AERONAUTICS
LANGLEY MEMORIAL AERONAUTICAL LABORATORY LANGLEY FIELD VA

[redacted]

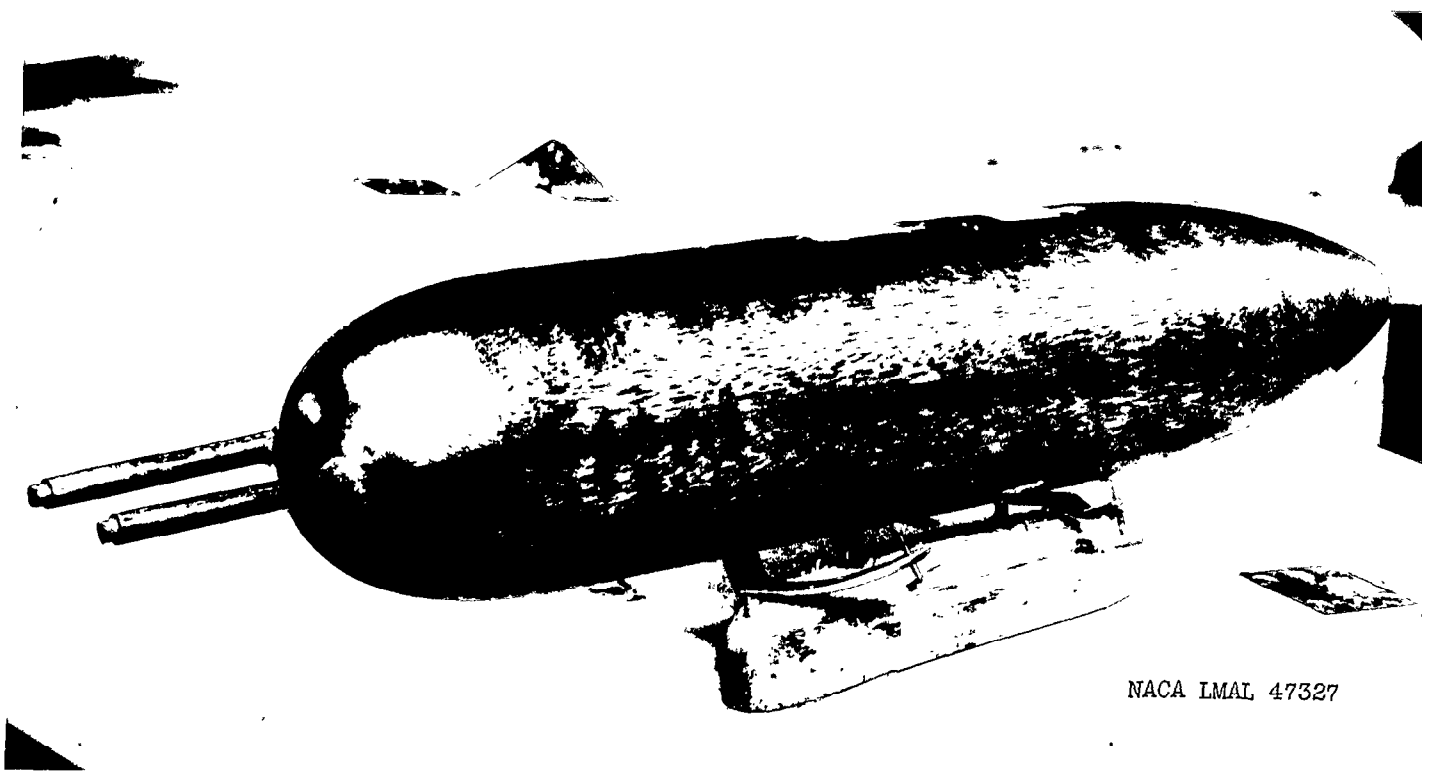

(c) Detail of gun package.

Figure 11.- Concluded.

[redacted]

NATIONAL ADVISORY COMMITTEE FOR AERONAUTICS
LANGLEY MEMORIAL AERONAUTICAL LABORATORY - LANGLEY FIELD VA

[redacted]

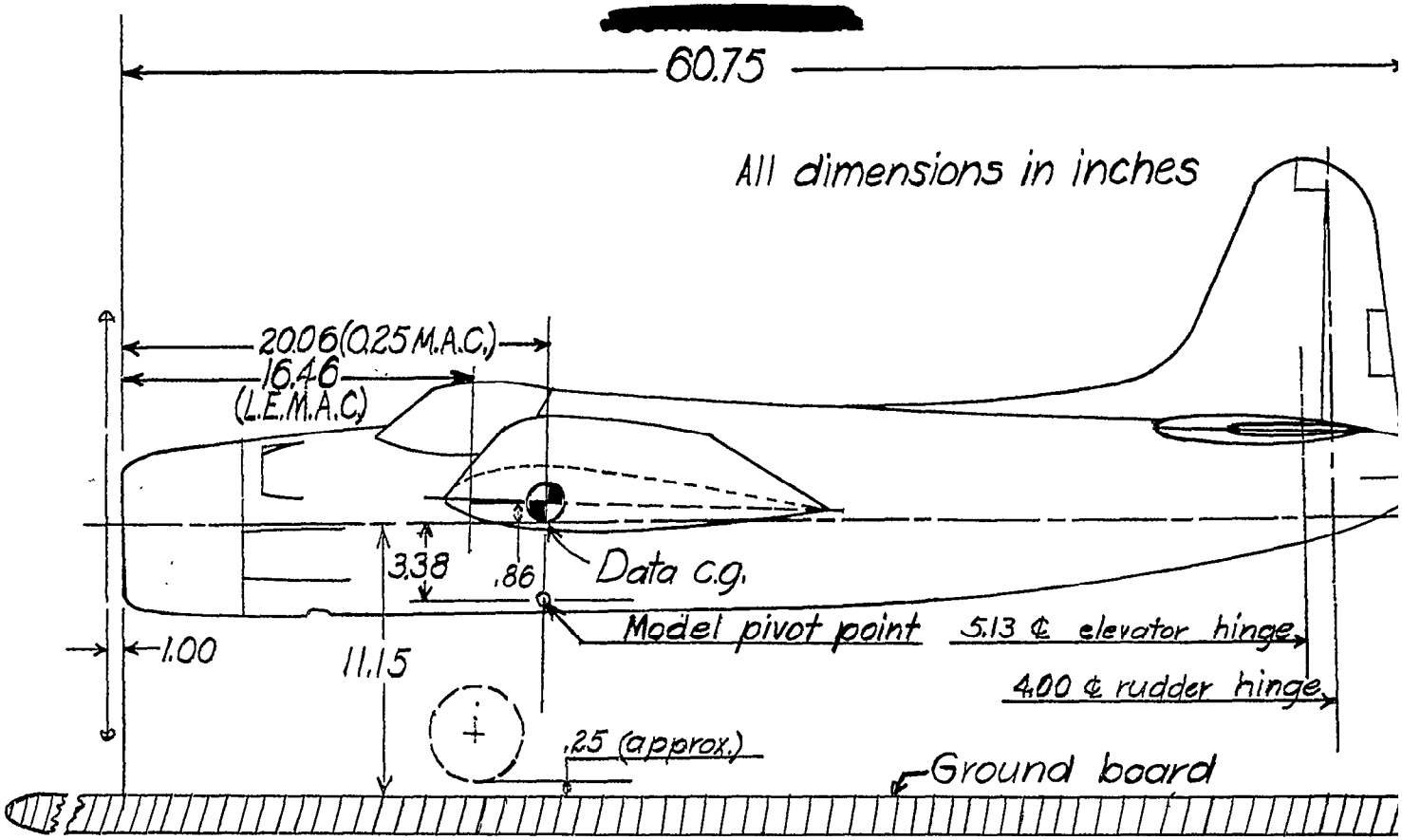

[redacted]

Figure 12.- Location of model with respect to gr
board; $\alpha = 0°$.

NATIONAL ADVISORY
COMMITTEE FOR AERONAUTICS

[redacted]

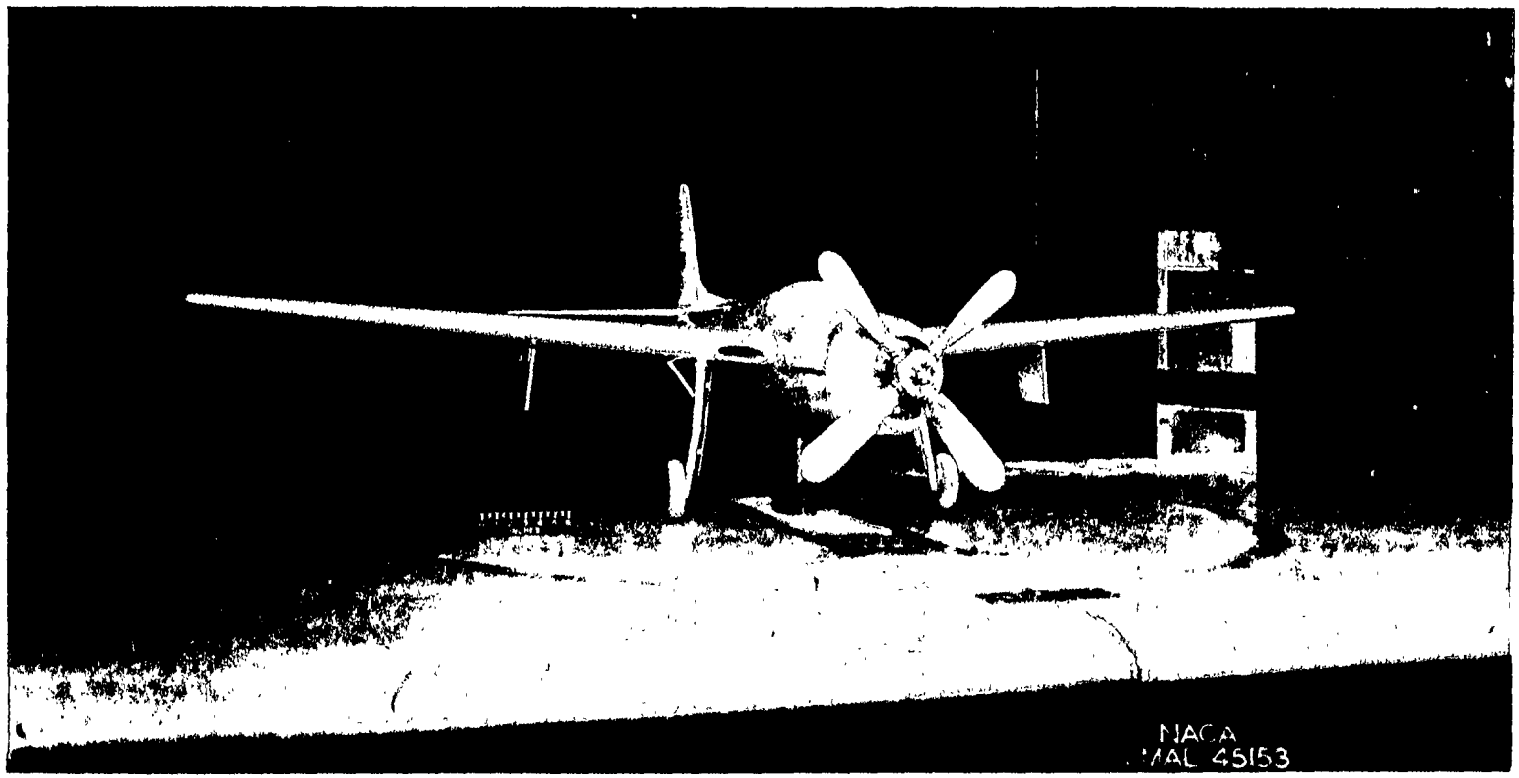

Figure 13.- The $\frac{1}{8}$-scale model of the Grumman XTB3F-1 airplane mounted in the tunnel with ground board in place.

[redacted]

NATIONAL ADVISORY COMMITTEE FOR AERONAUTICS
LANGLEY MEMORIAL AERONAUTICAL LABORATORY LANGLEY FIELD VA

[redacted]

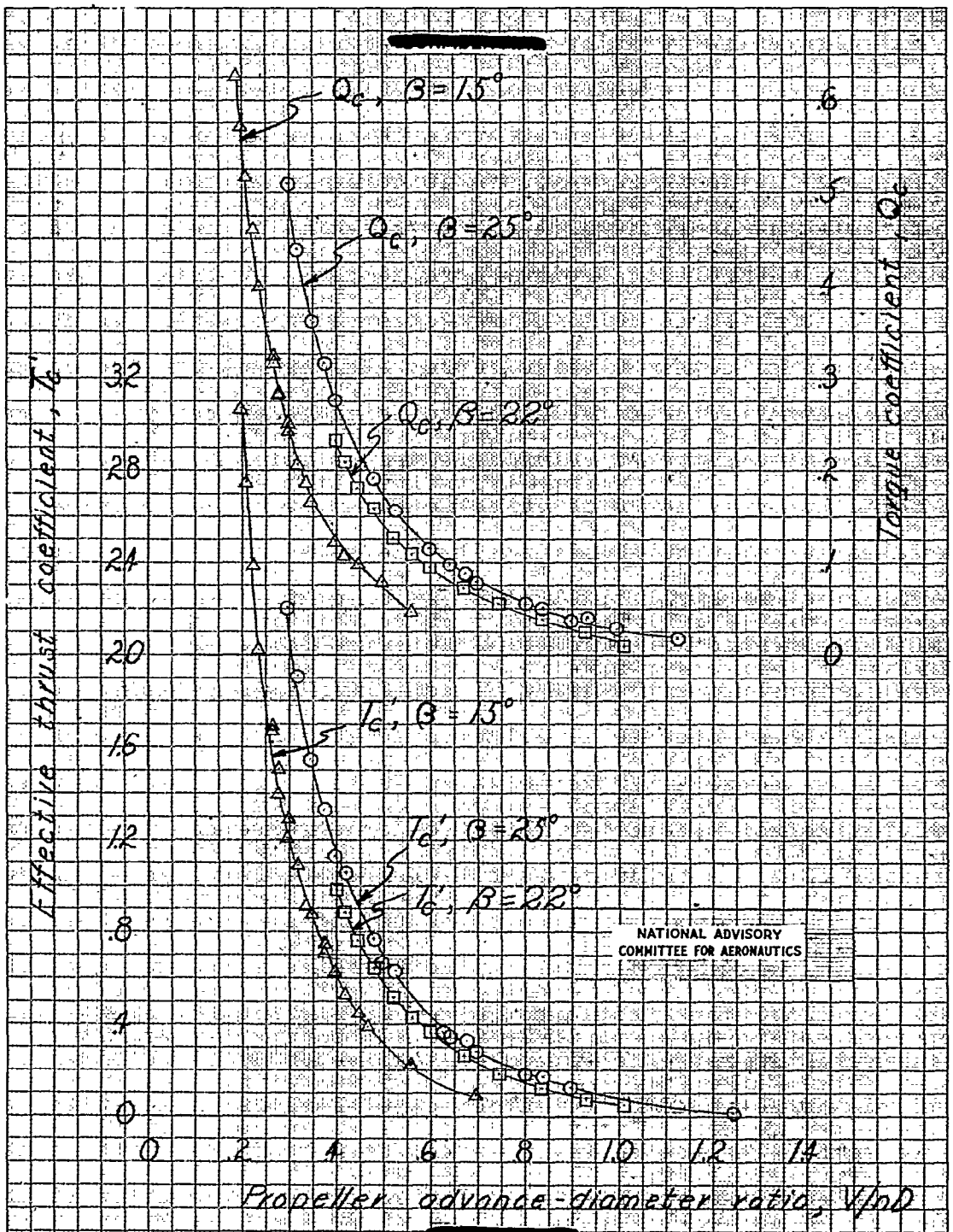

[redacted]

Figure 14.- Calibration of propeller used on 1/8-scale model of the Grumman XTBF-1 airplane. D = 16.25 ft.

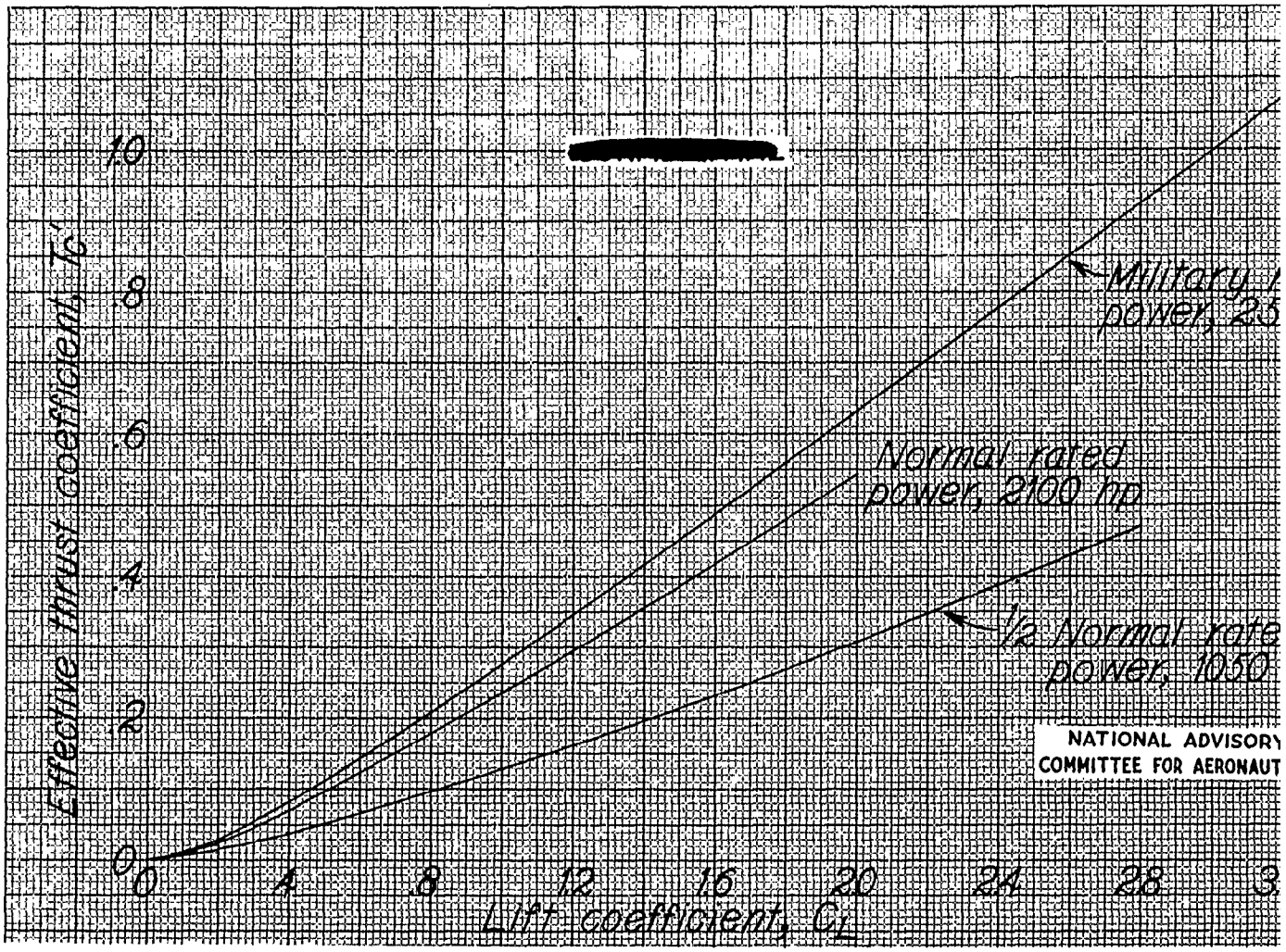

Figure 15.- Variation of effective thrust coefficient with lift coefficient for the Grumman XTB3F-1 airplane.

[redacted]

[redacted]

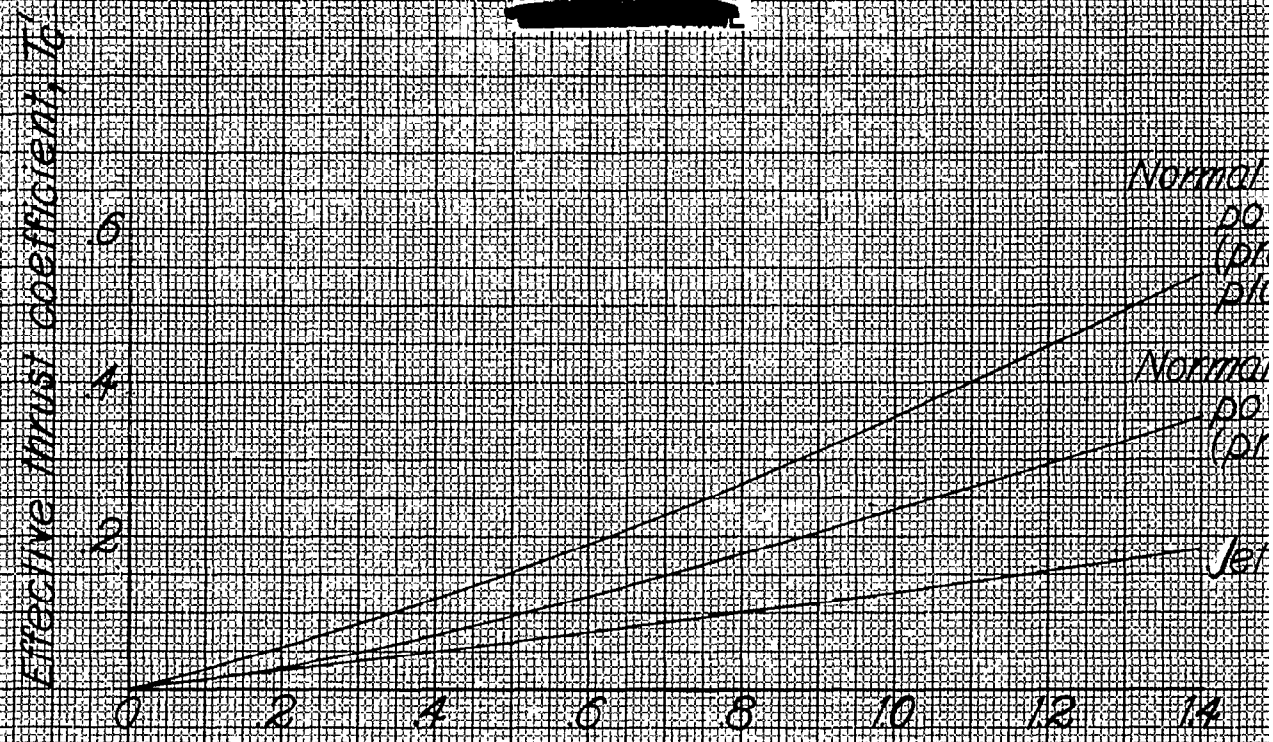

NATIONAL ADVISORY COMMITTEE FOR AERONAUTICS

Figure 15.- Concluded.

[redacted]

[redacted]

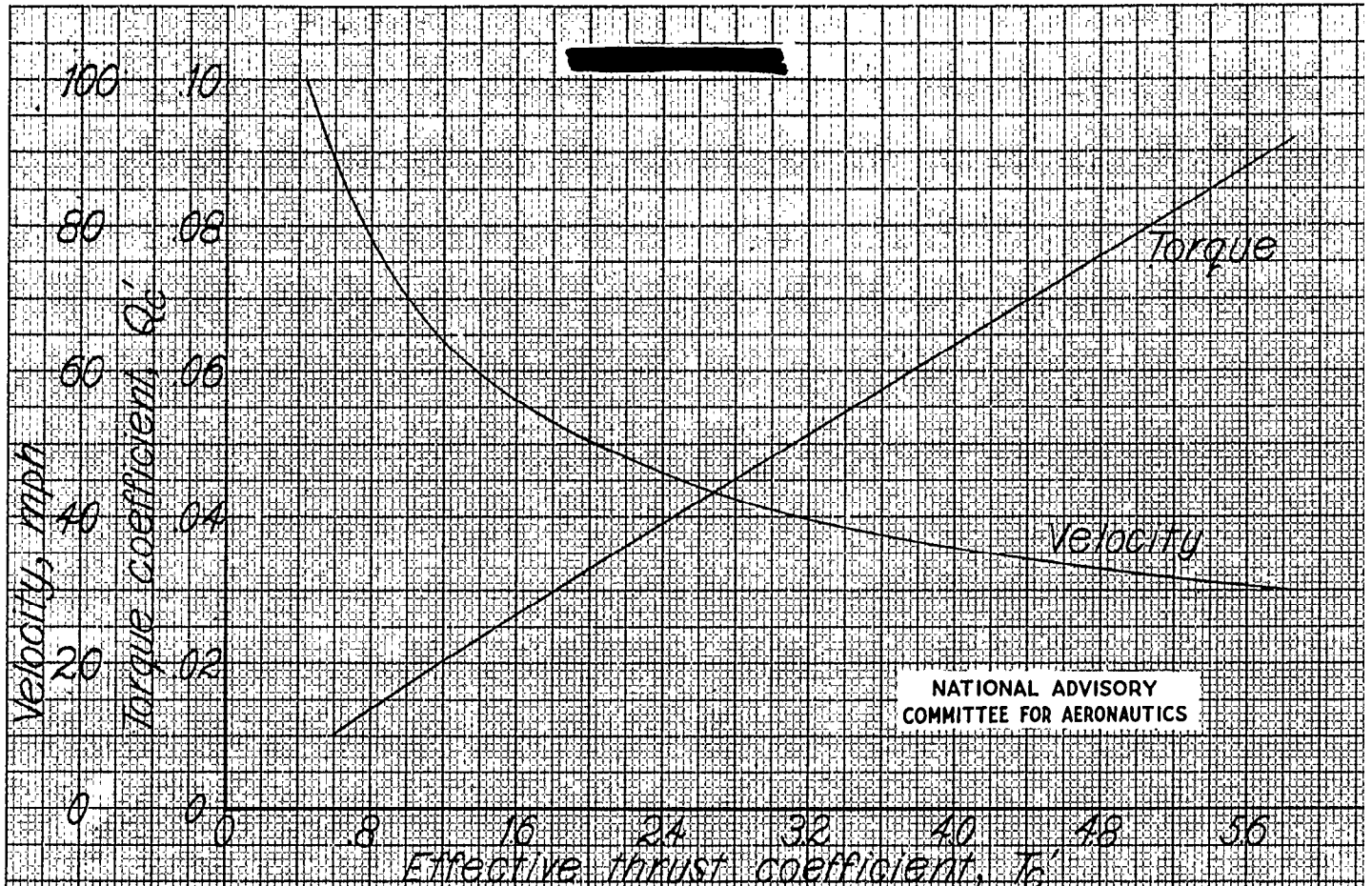

Figure 16.- Model torque coefficient and estimated variation of effective thrust coefficient with airplane velocity during take-off for the Grumman XTB3F-1 airplane. Military rated power.

[redacted]

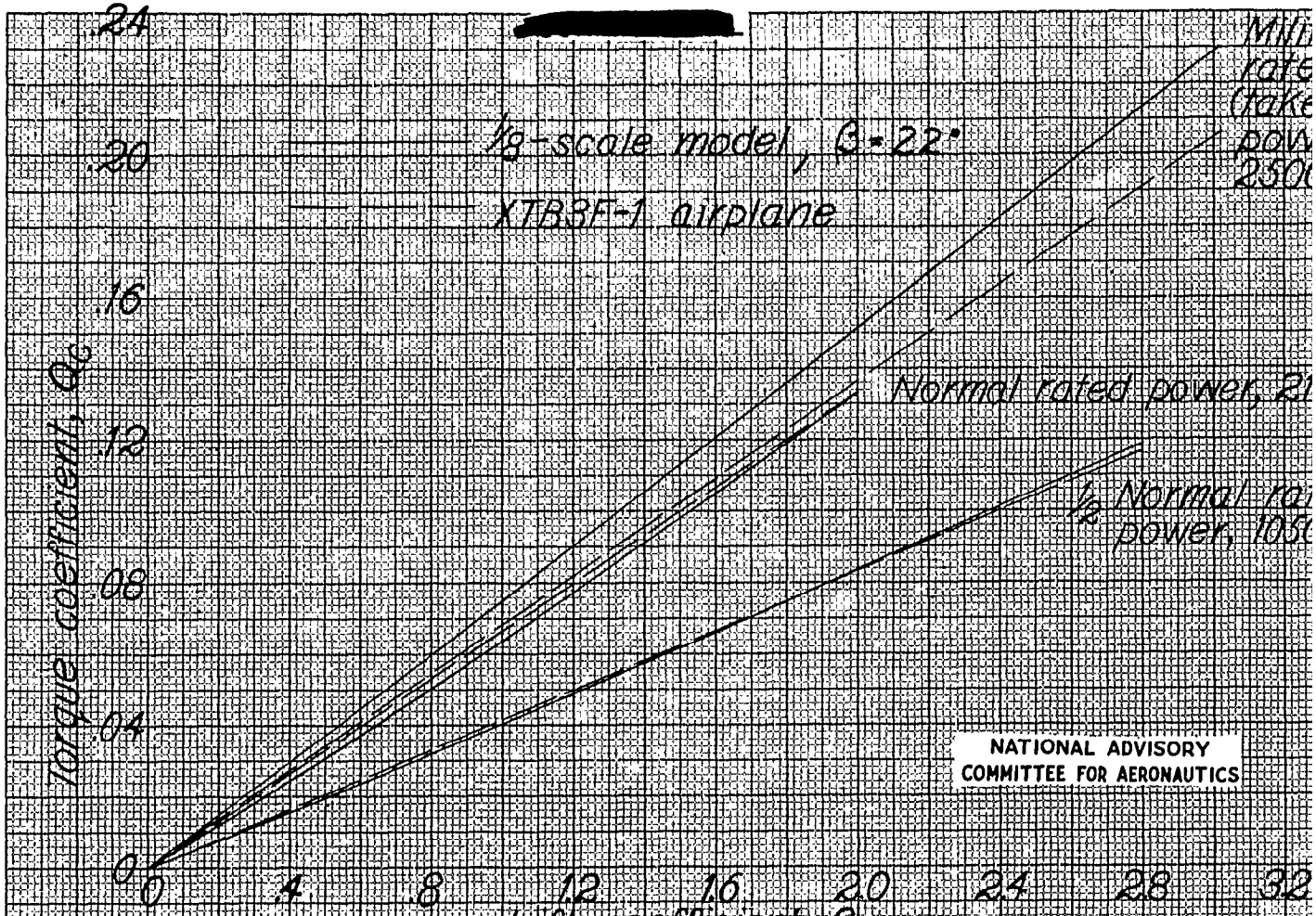

Figure 17.- Variation of torque coefficient with lift coefficient fo the 1/8-scale model of the Grumman XTB3F-1 airplane and the prototype airplane with R3350-24 engine and Curt electric propeller.

[redacted]

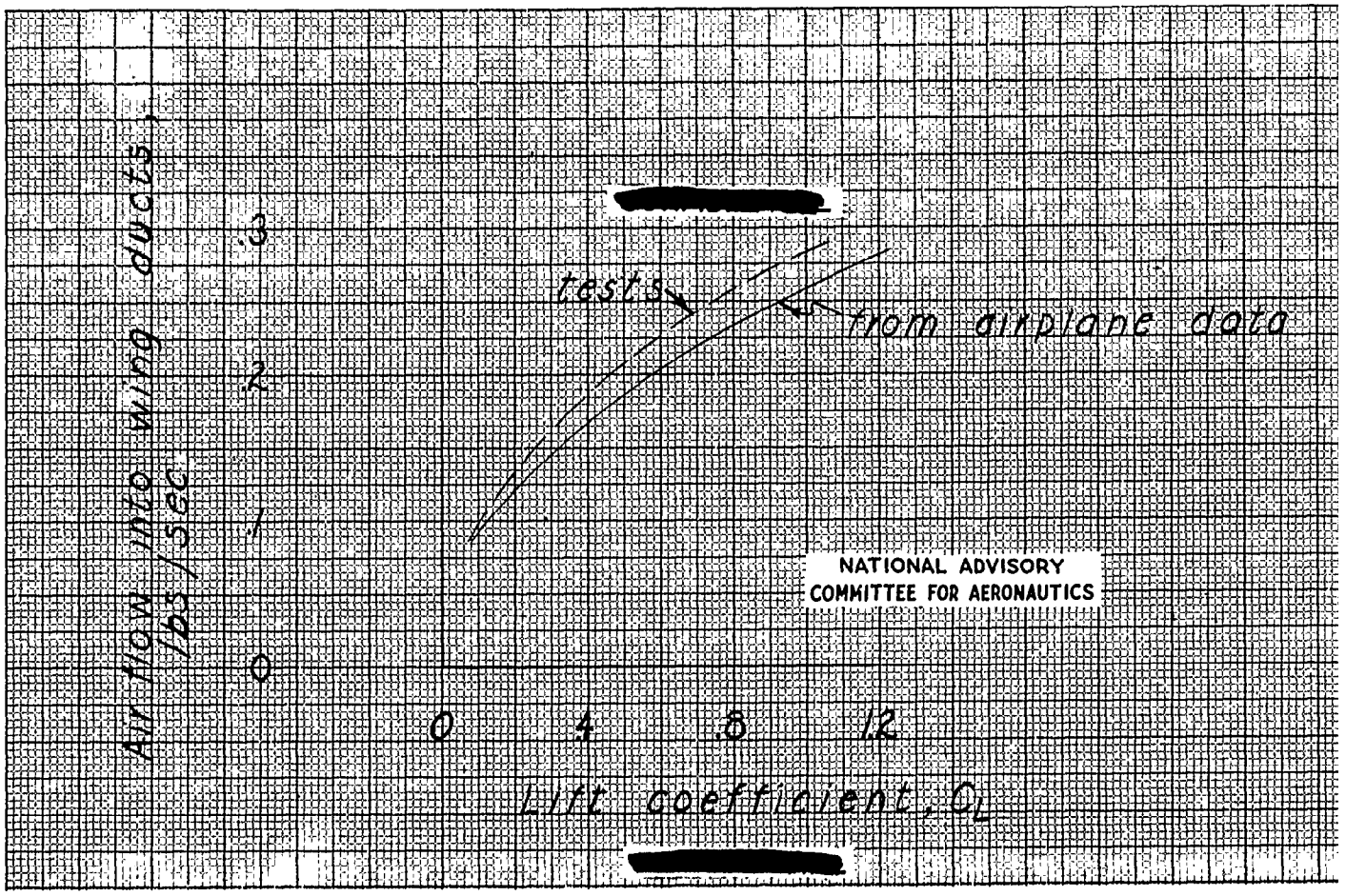

Figure 18.- Comparison of mass flow of air into wing ducts obtained in model tests with full-s
Grumman XTB3F-1 airplane data.

[redacted]

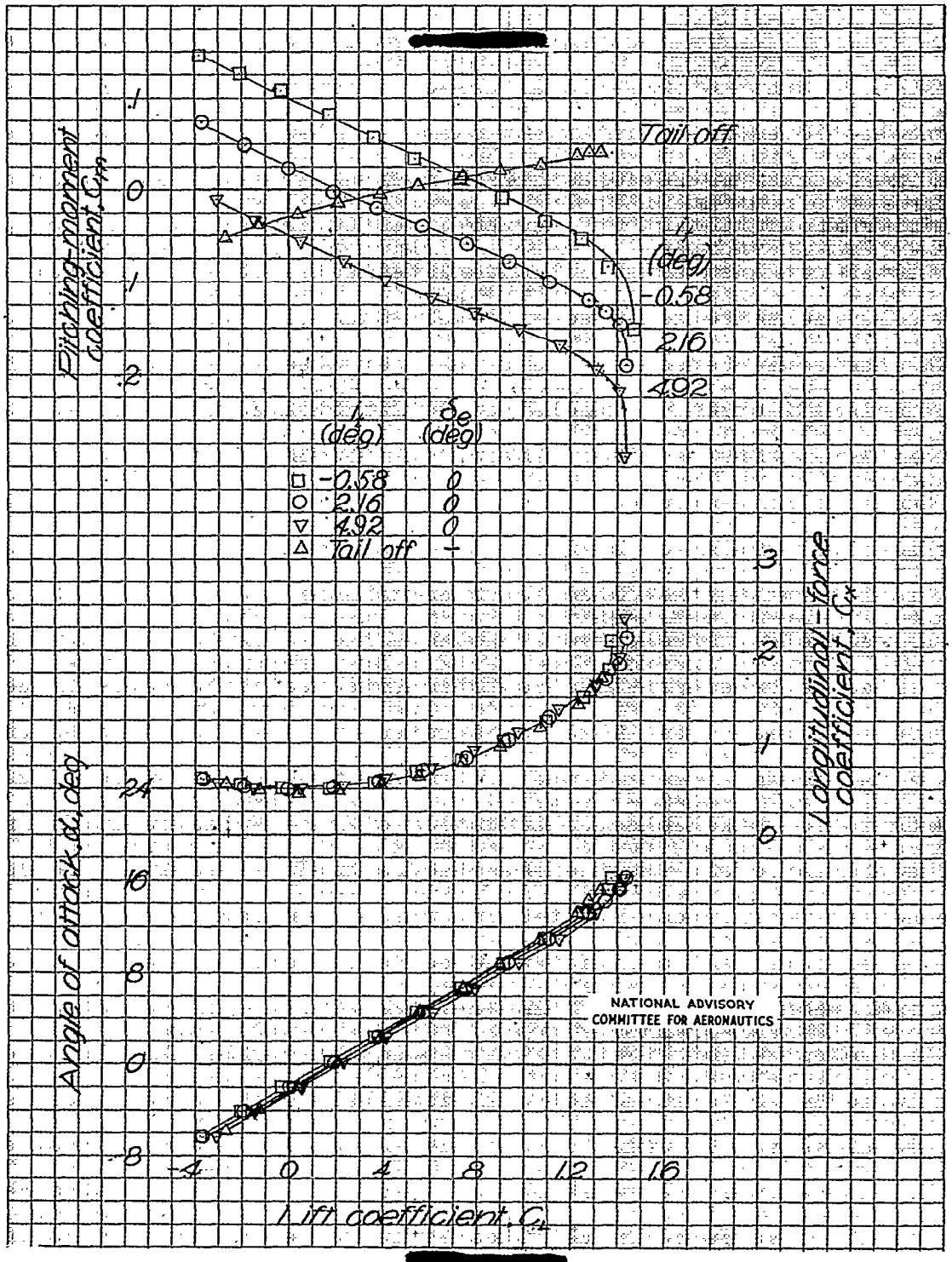

[redacted]

(a) Original thrust line.

Figure 19.- Aerodynamic characteristics in pitch of a 1/8-scale model of the Grumman XTB3F-1 airplane. Glide configuration.

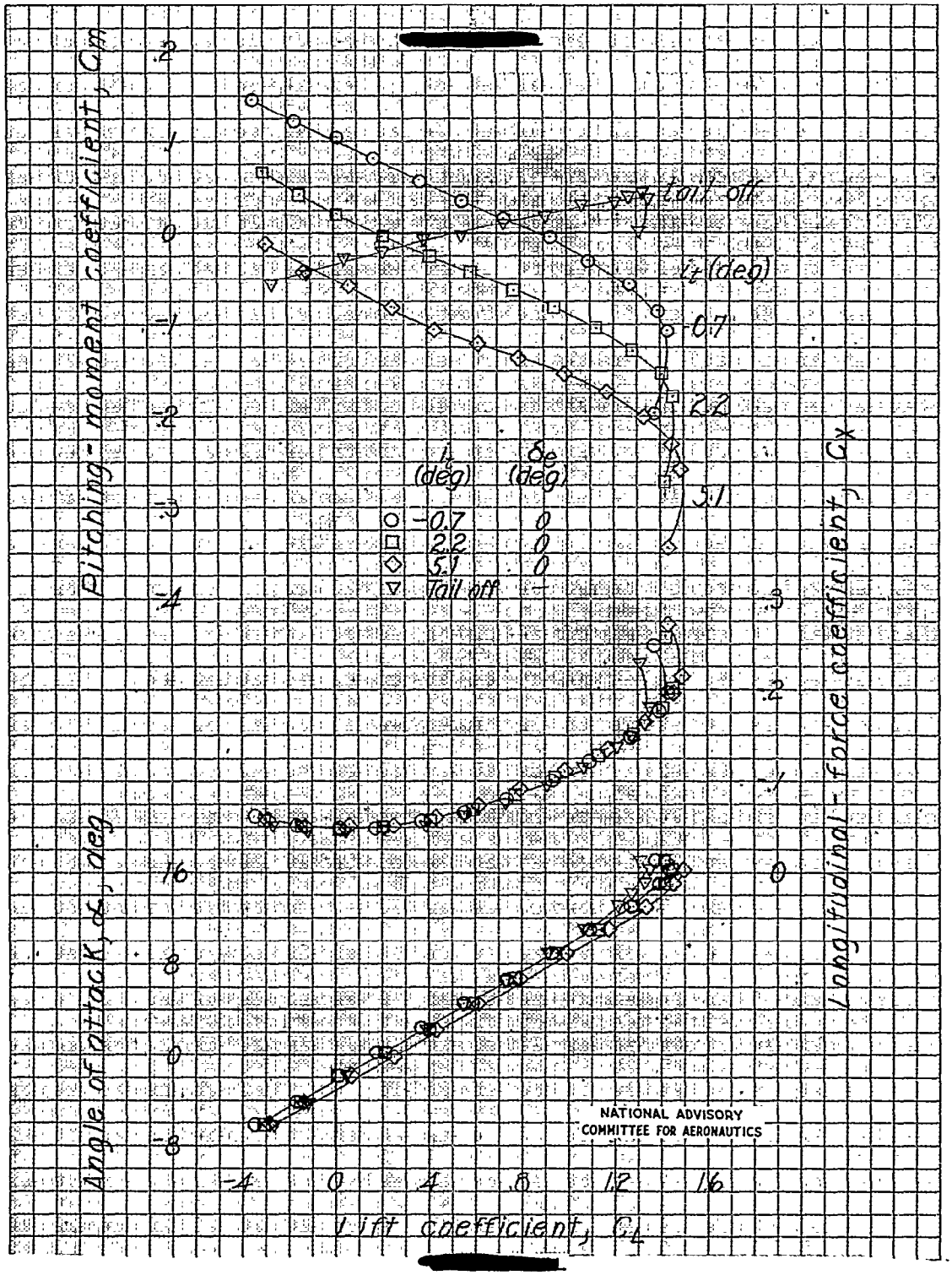

(b) Thrust line tilted down 3°.

Figure 19.- Continued.

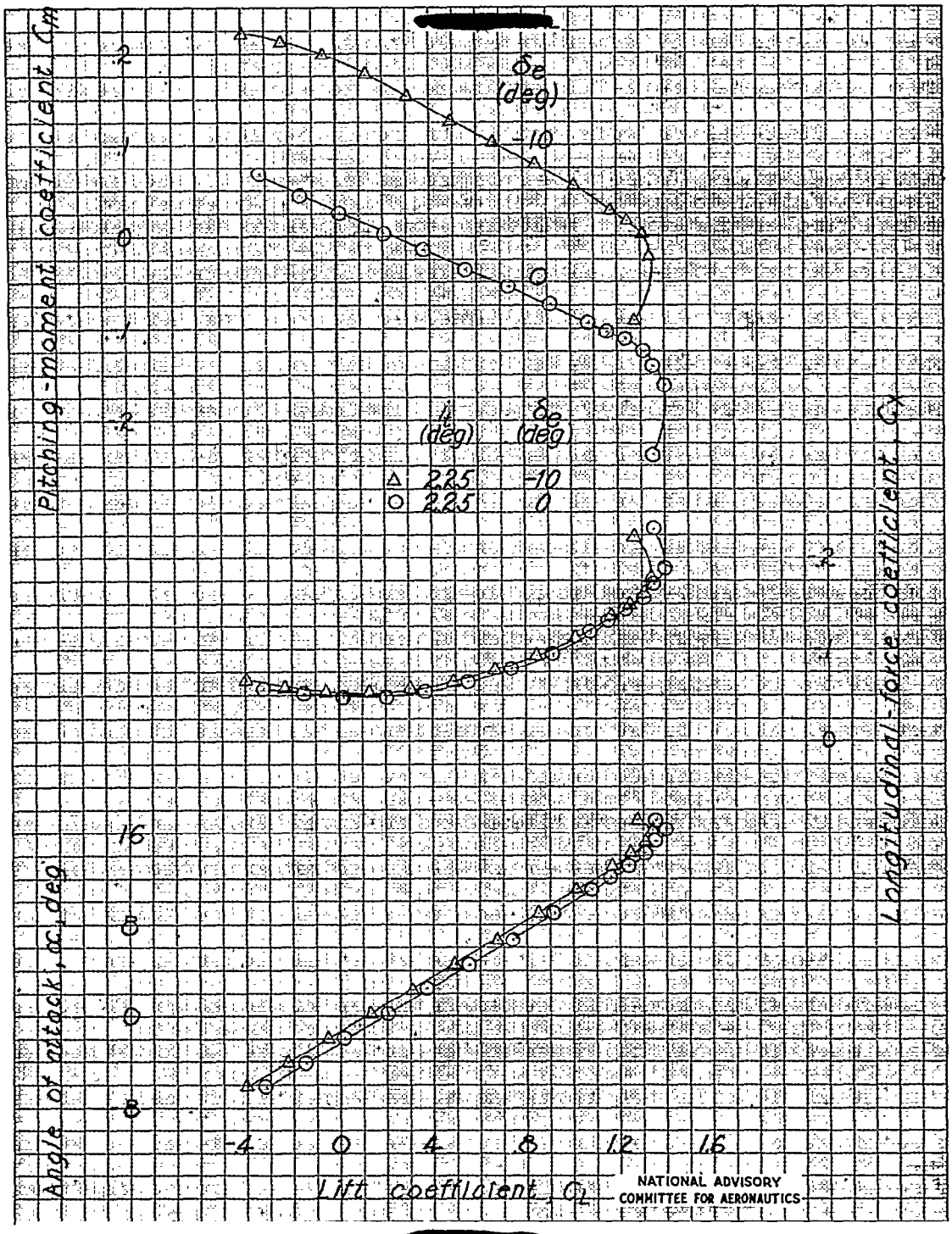

(b) Continued.

Figure 19.- Continued.

[redacted]

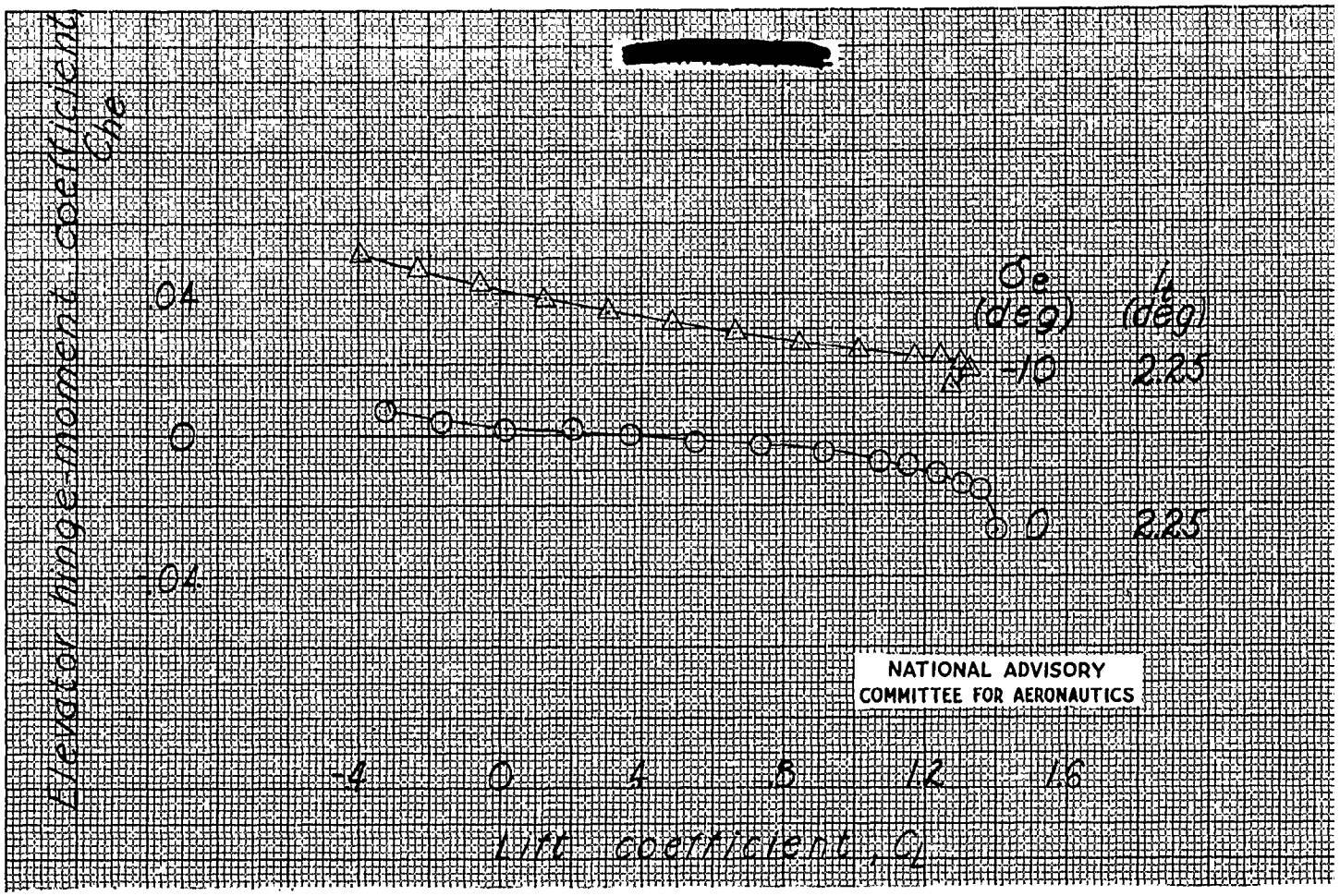

[redacted]

(b) Concluded.

Figure 19.- Concluded.

[redacted]

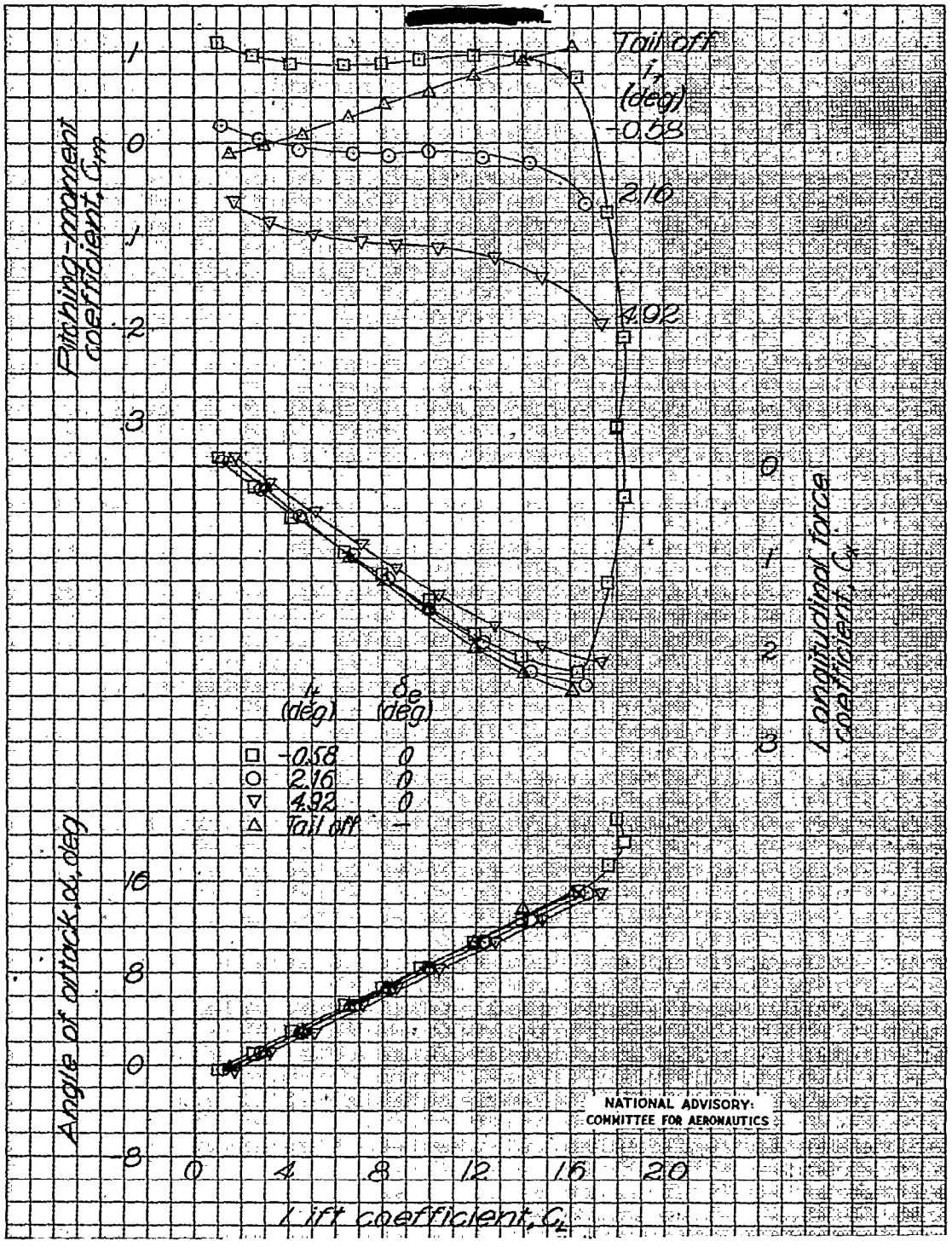

[redacted]

(a) Original thrust line.

Figure 20.- Aerodynamic characteristics in pitch of a 1/8-scale model of the Grumman XTB3F-1 airplane. Power-on clean configuration.

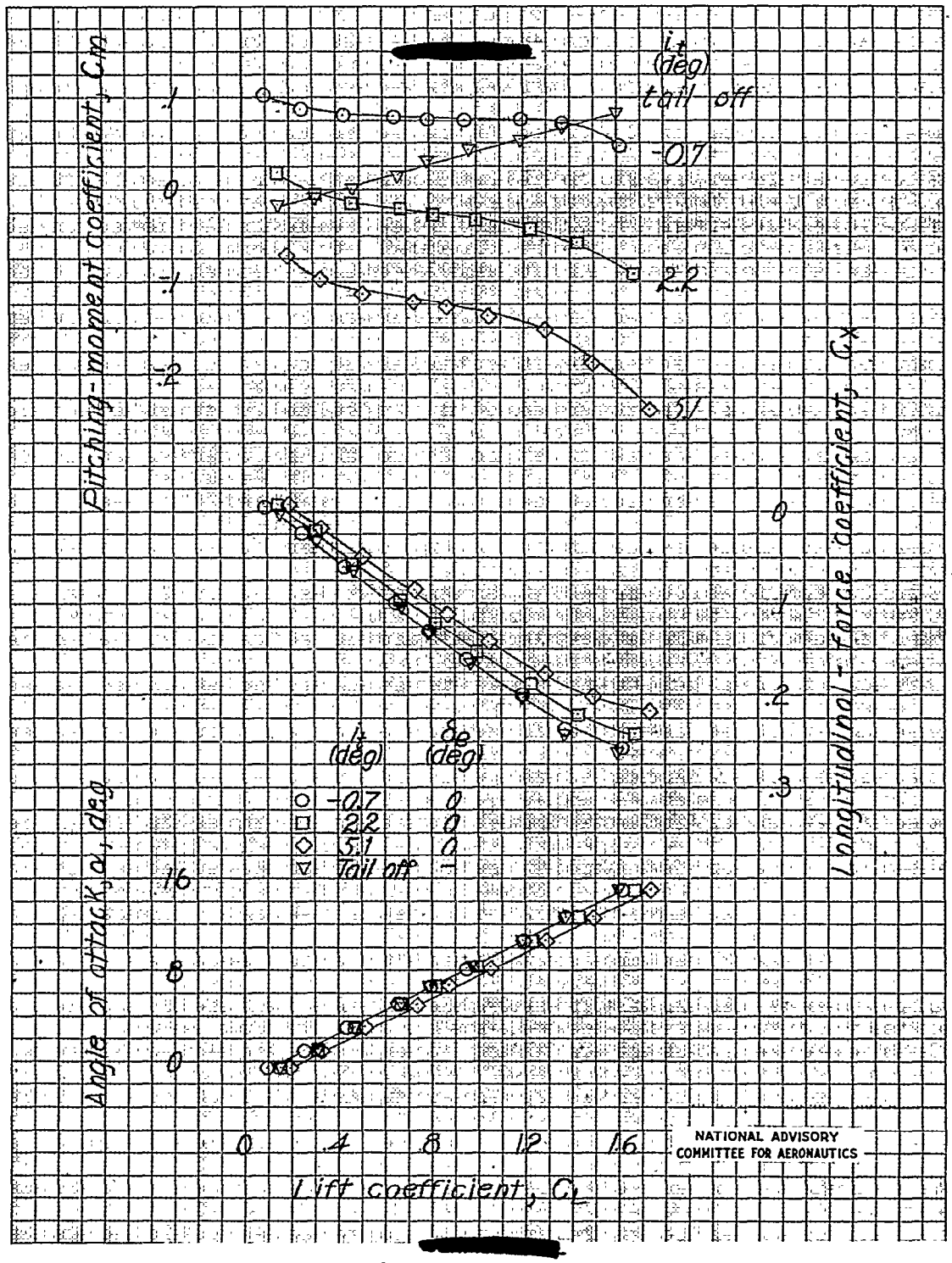

(b) Thrust line tilted down 3°

Figure 20.- Continued.

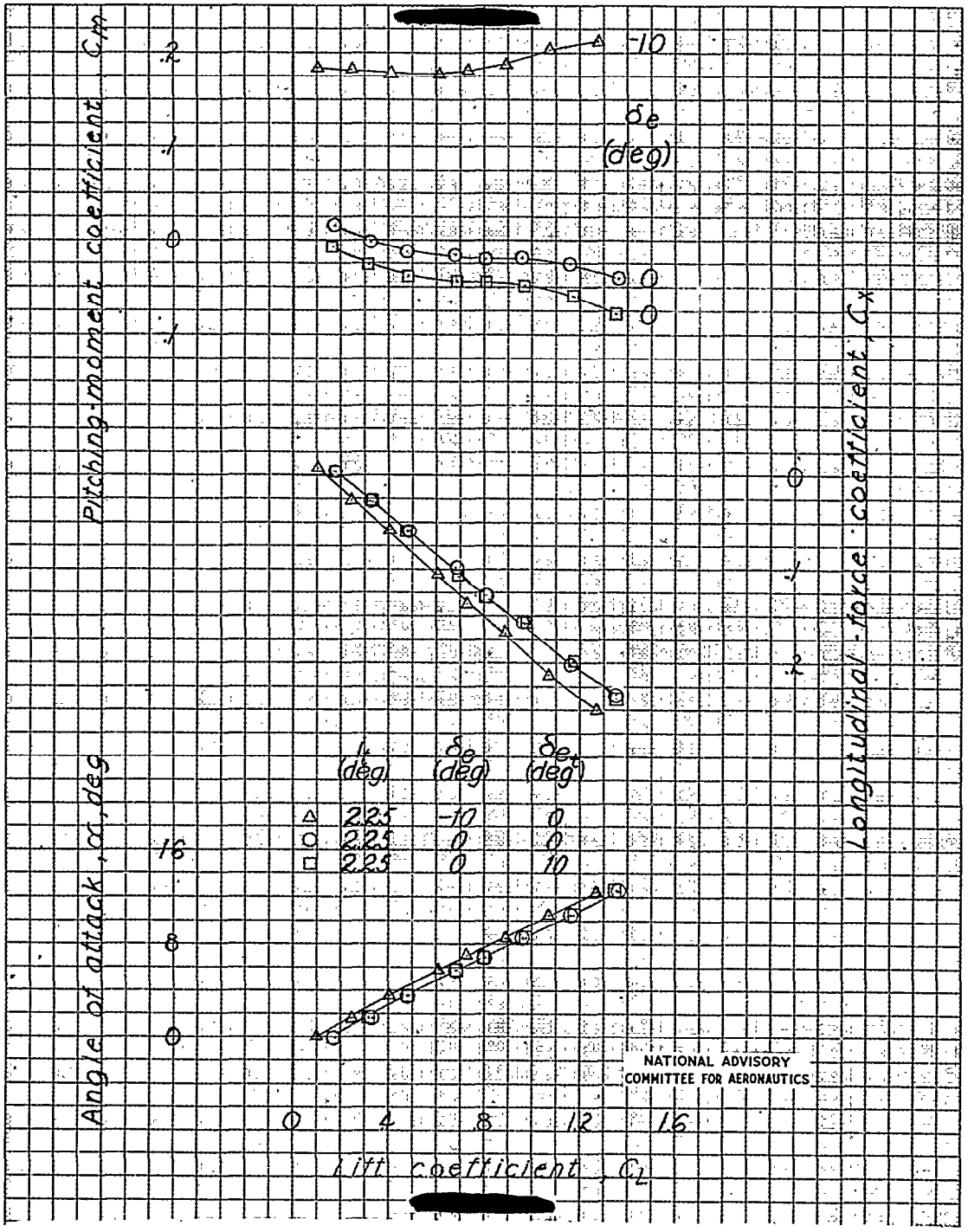

(b) Continued.

Figure 20.- Continued.

[redacted]

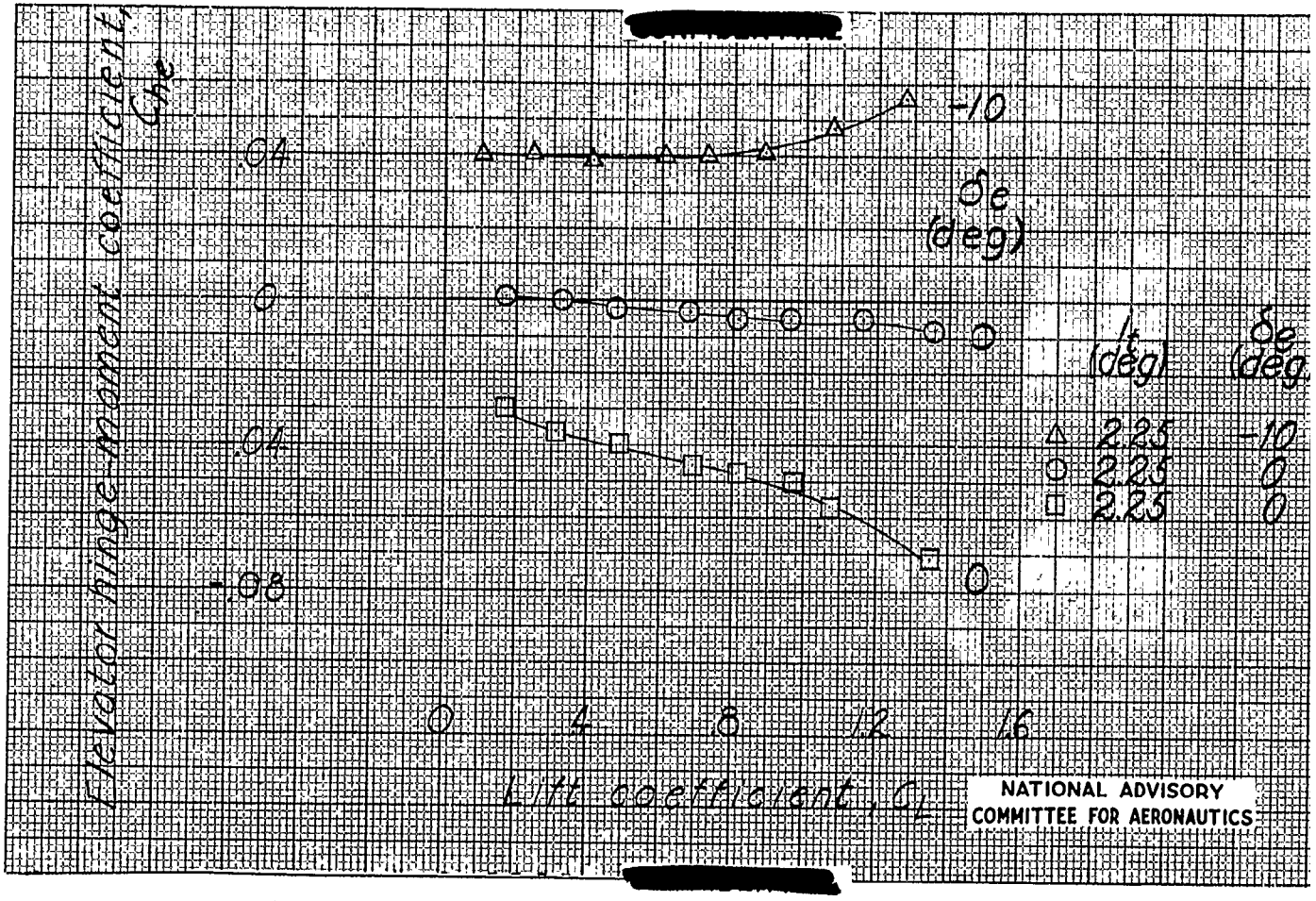

[redacted]

(b) Concluded.

Figure 20.- Concluded.

[redacted]

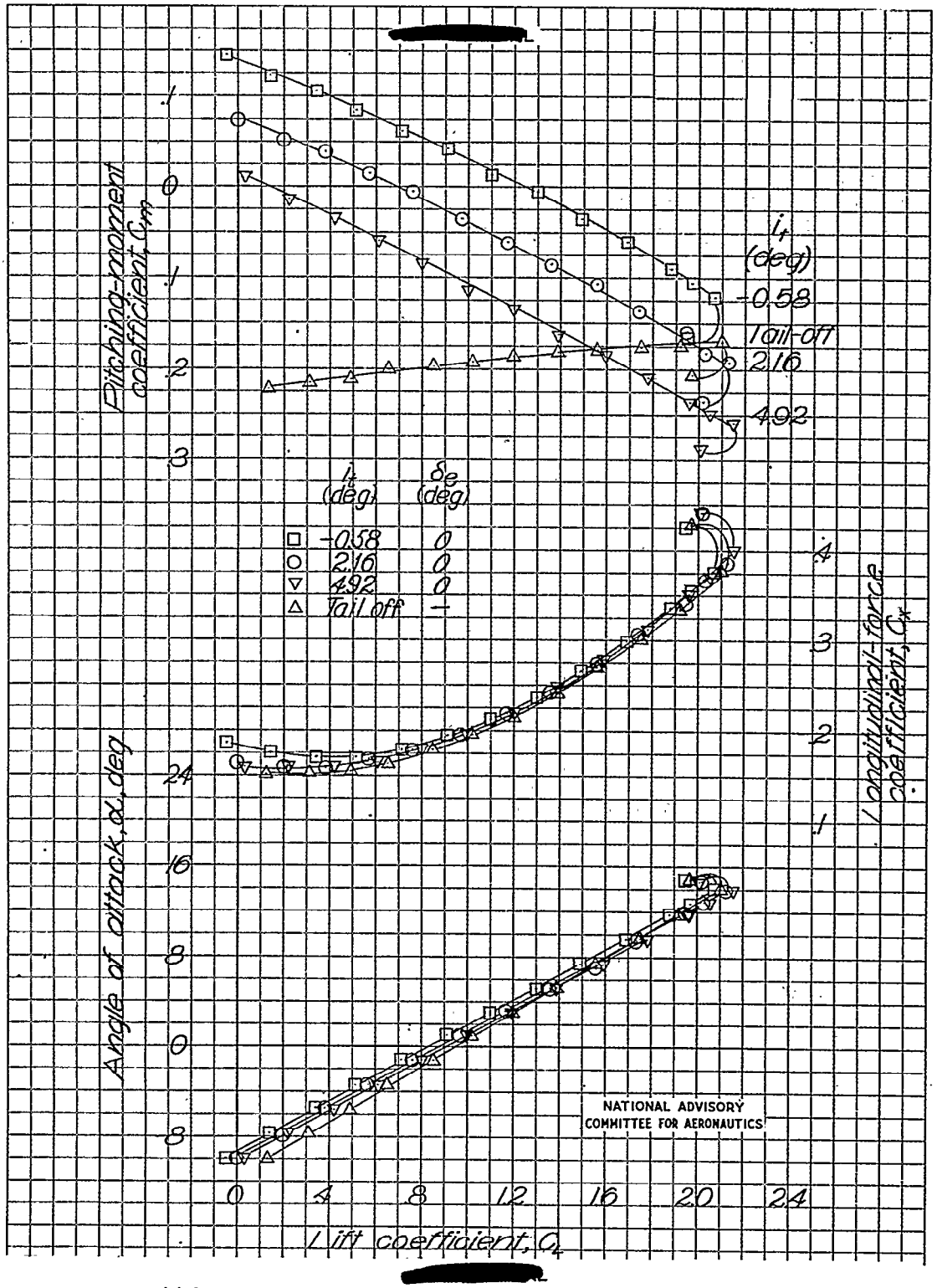

[redacted]

(a) Original thrust line.

Figure 21.- Aerodynamic characteristics in pitch of a 1/8-scale model of the Grumman XTB3F-1 airplane. Landing configuration.

[redacted]

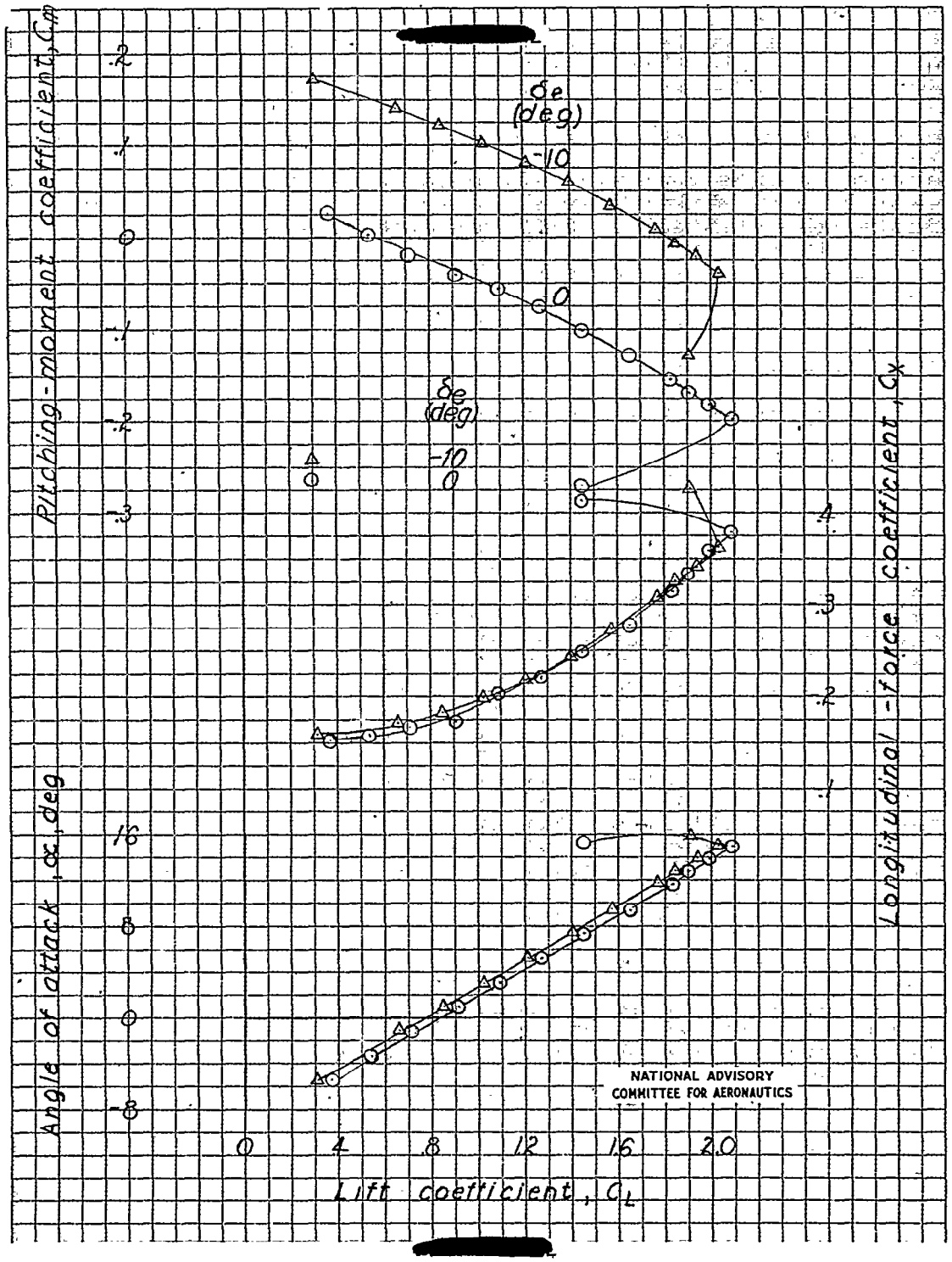

[redacted]

(b) Thrust line tilted down 3°; $i_t = 2.25°$.

Figure 21.- Continued.

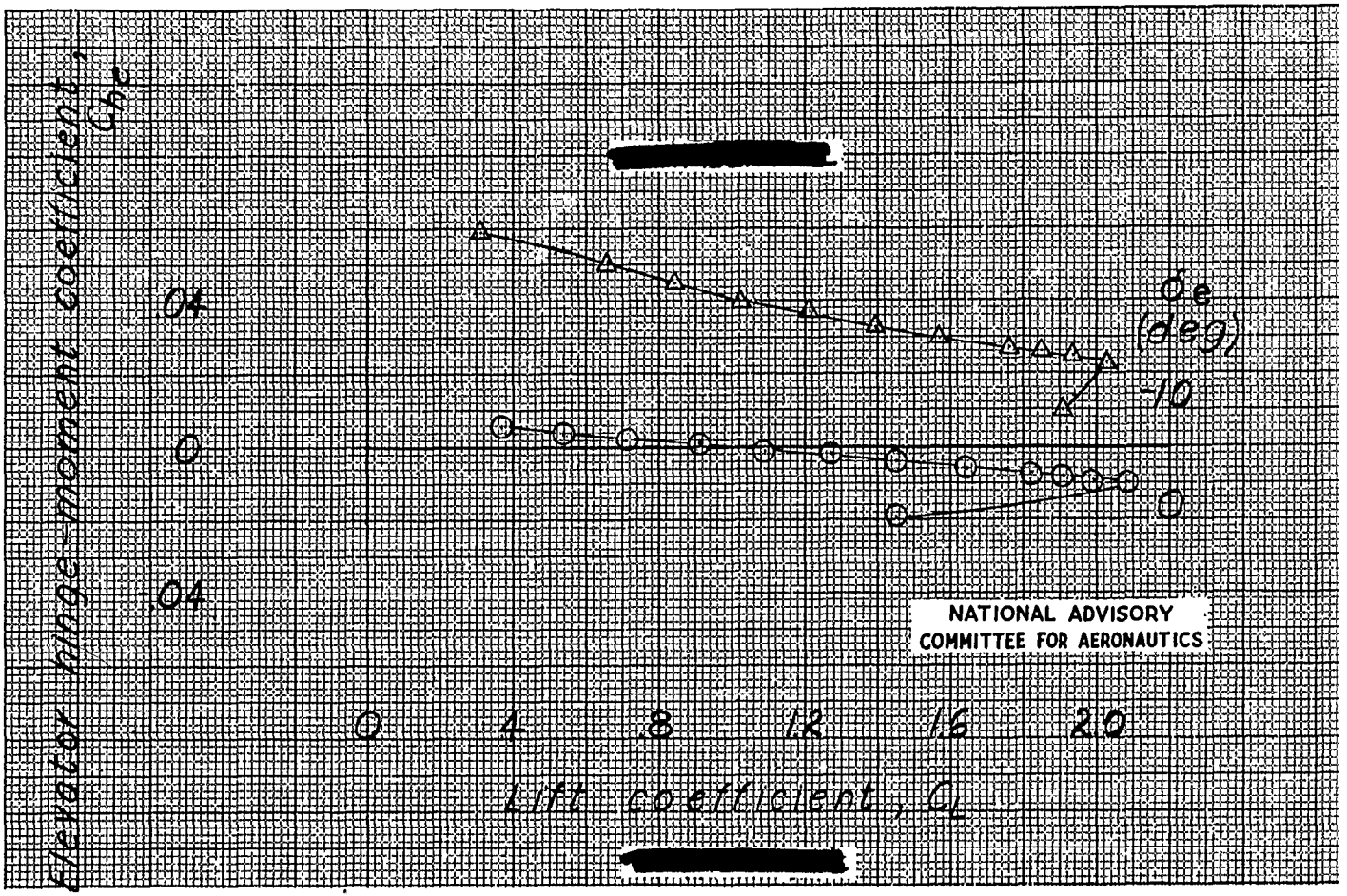

(b) Concluded.

Figure 21.- Concluded.

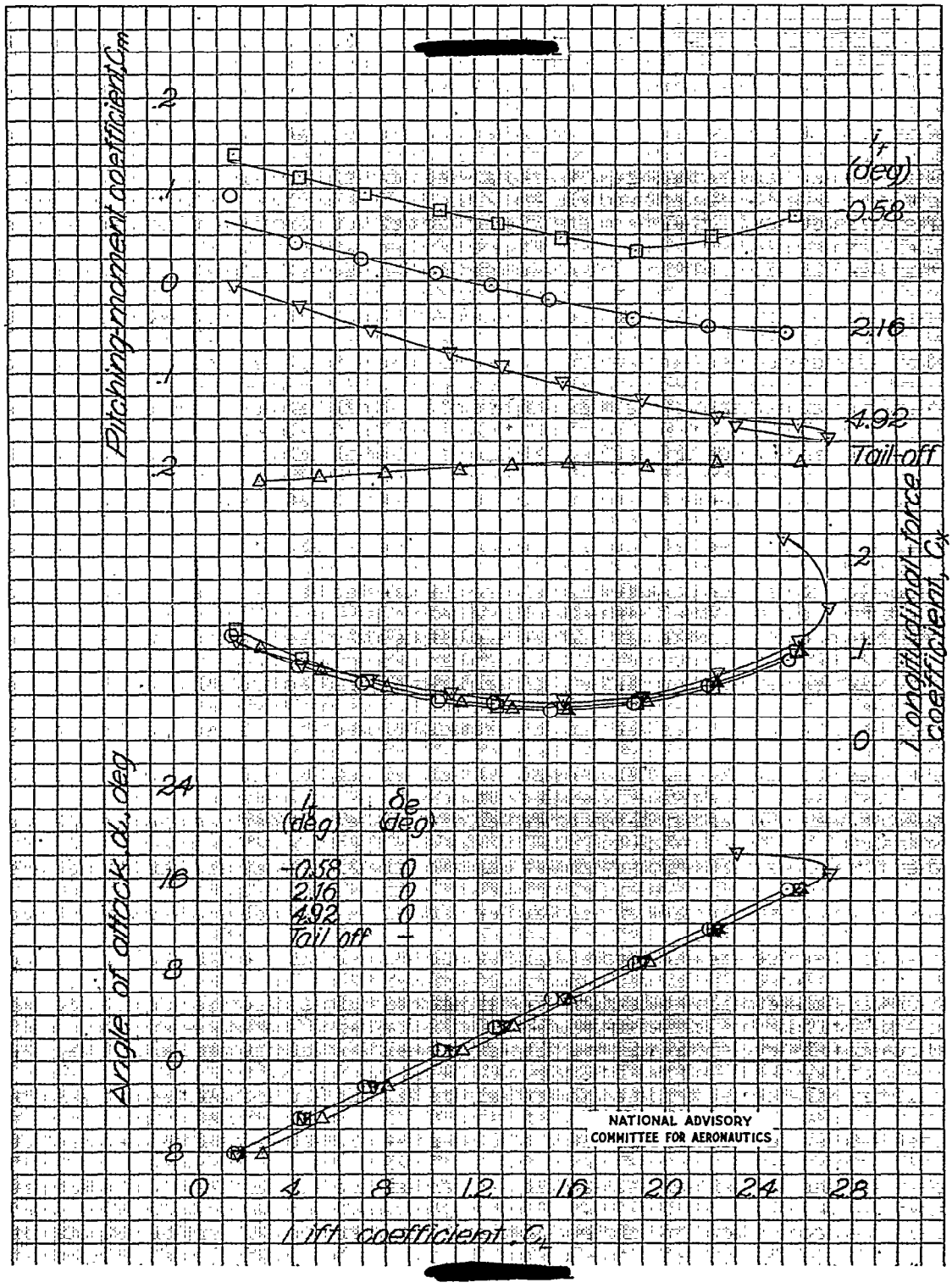

(a) Original thrust line.

Figure 22.- Aerodynamic characteristics in pitch of a 1/8-scale model of the Grumman XTB3F-1 airplane. Approach configuration.

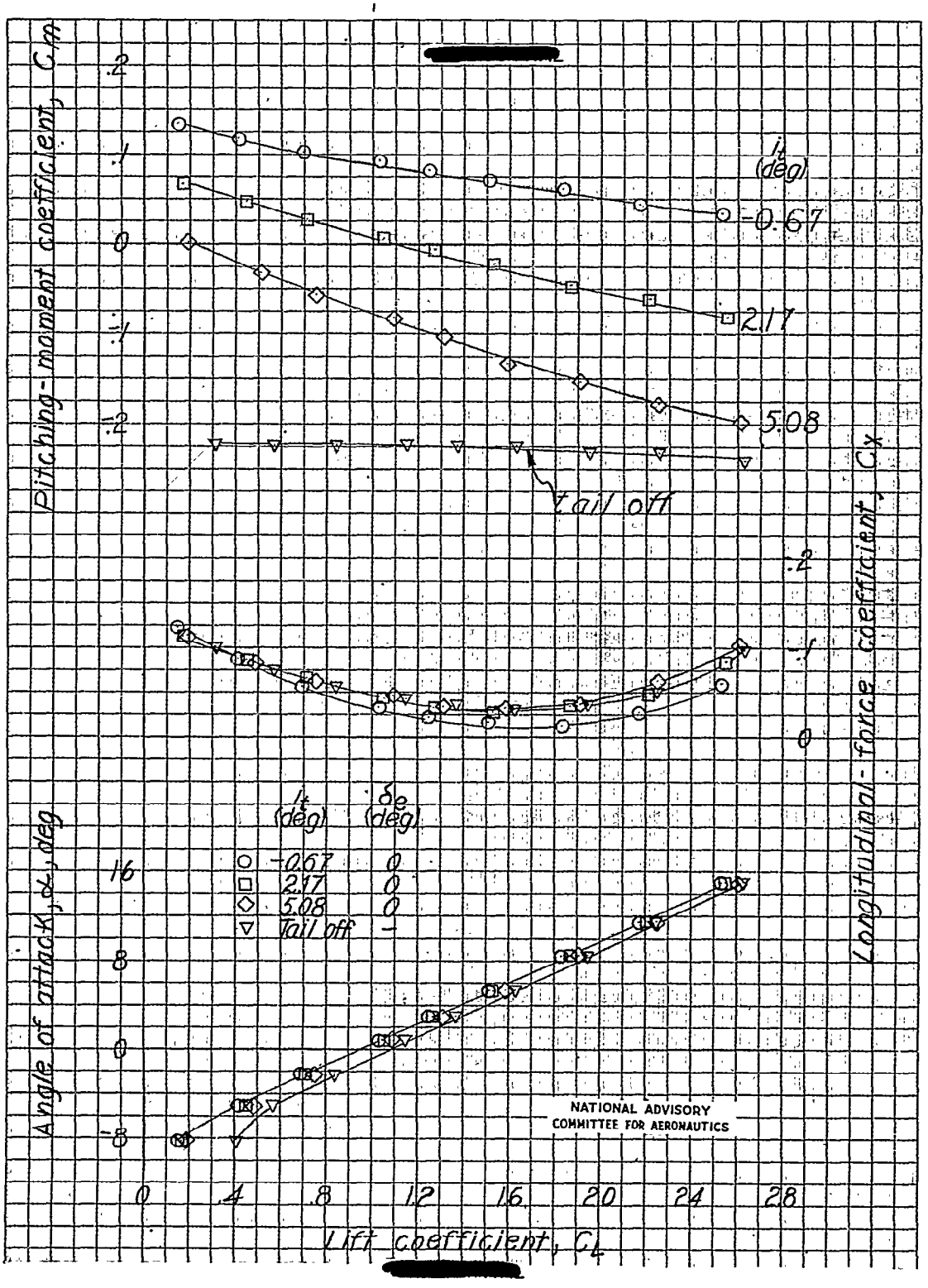

(b) Thrust line tilted down 3°.

Figure 22.- Continued .

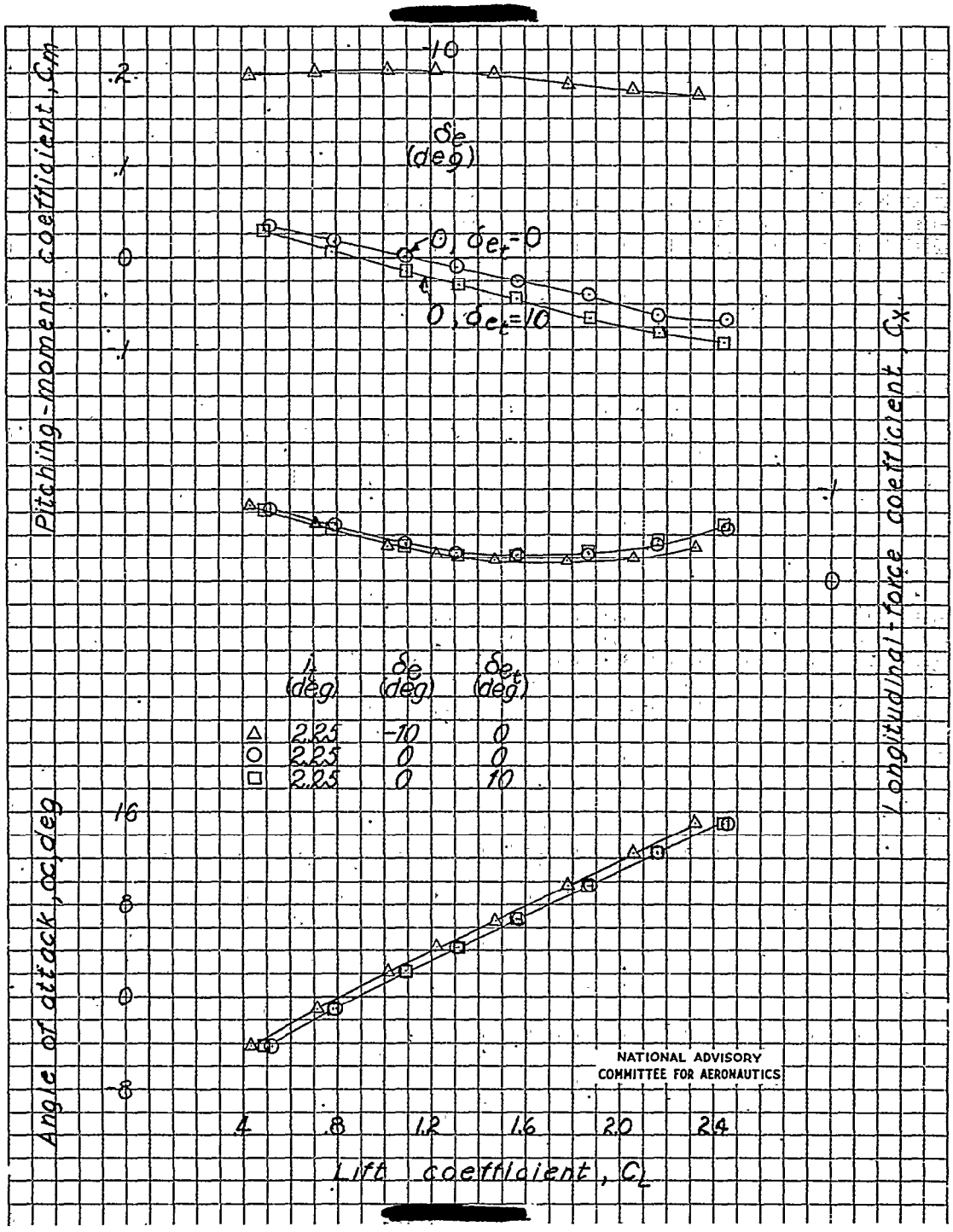

(b) Continued.

Figure 22.- Continued.

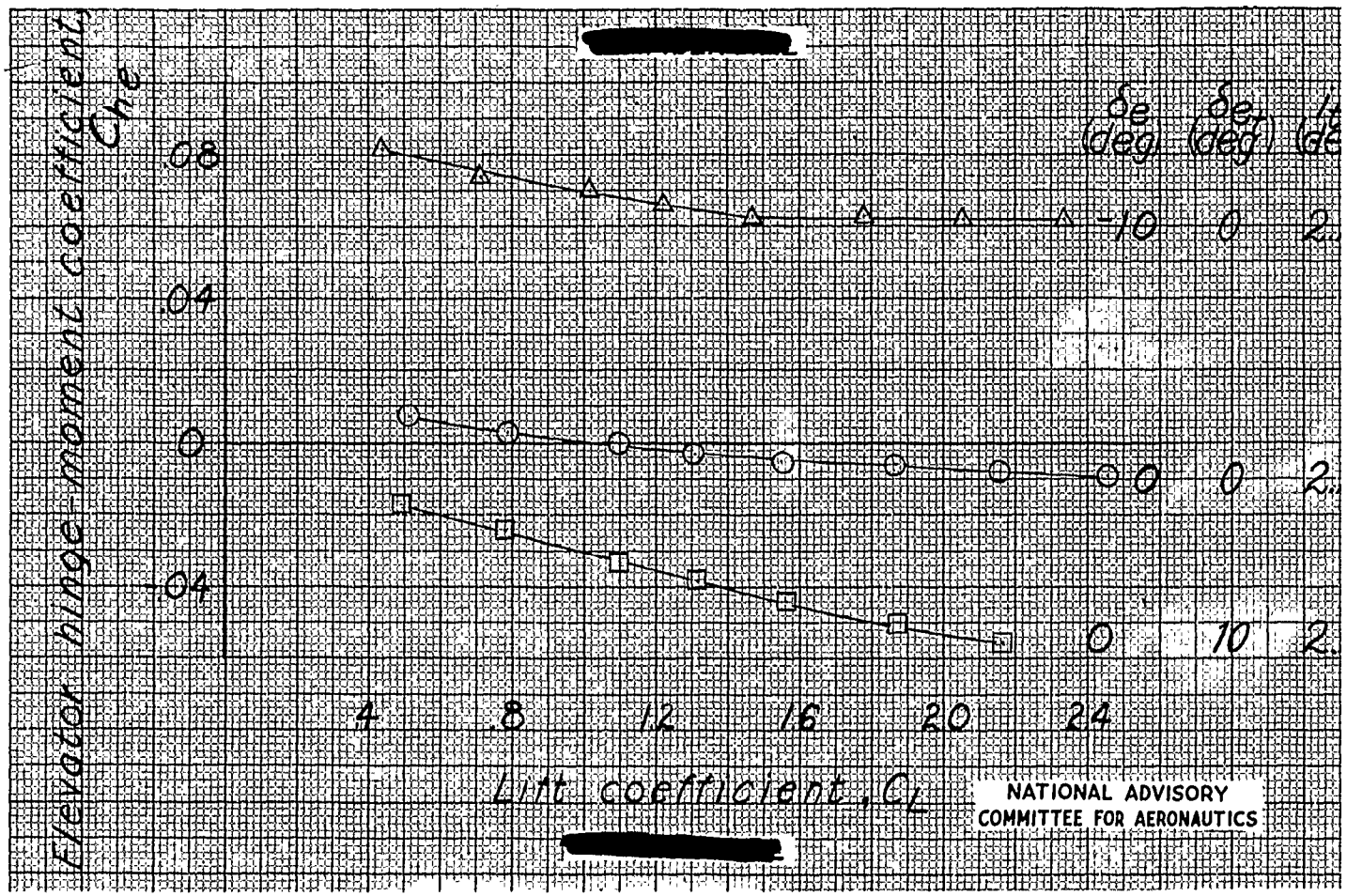

(b) Concluded.

Figure 22.- Concluded.

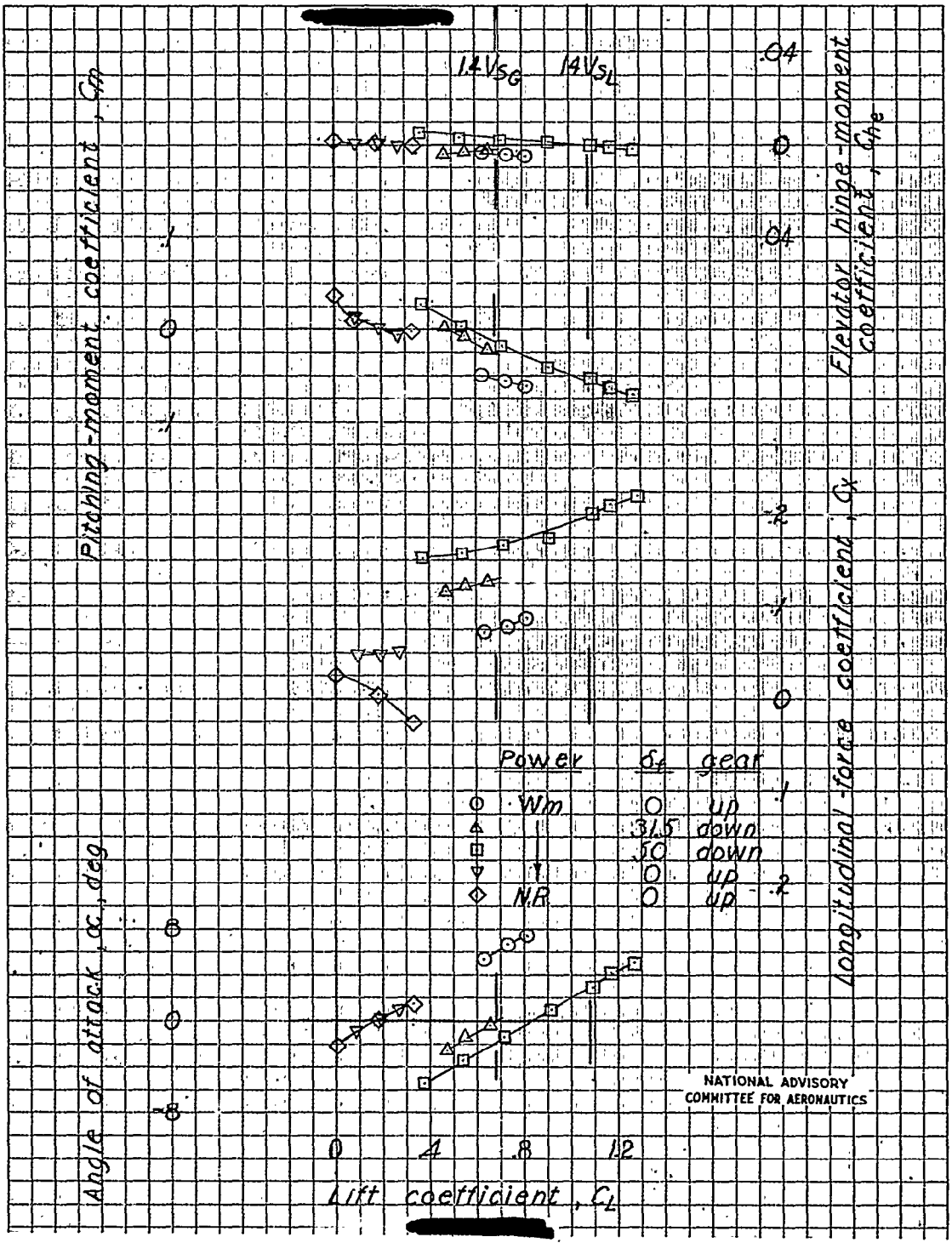

Part A

Figure 23.- Longitudinal trim changes due to power and flap deflection of a 1/8-scale model of the Grumman XTB3F-1 airplane. Thrust line tilted down 3°, $i_t = 2°15'$.

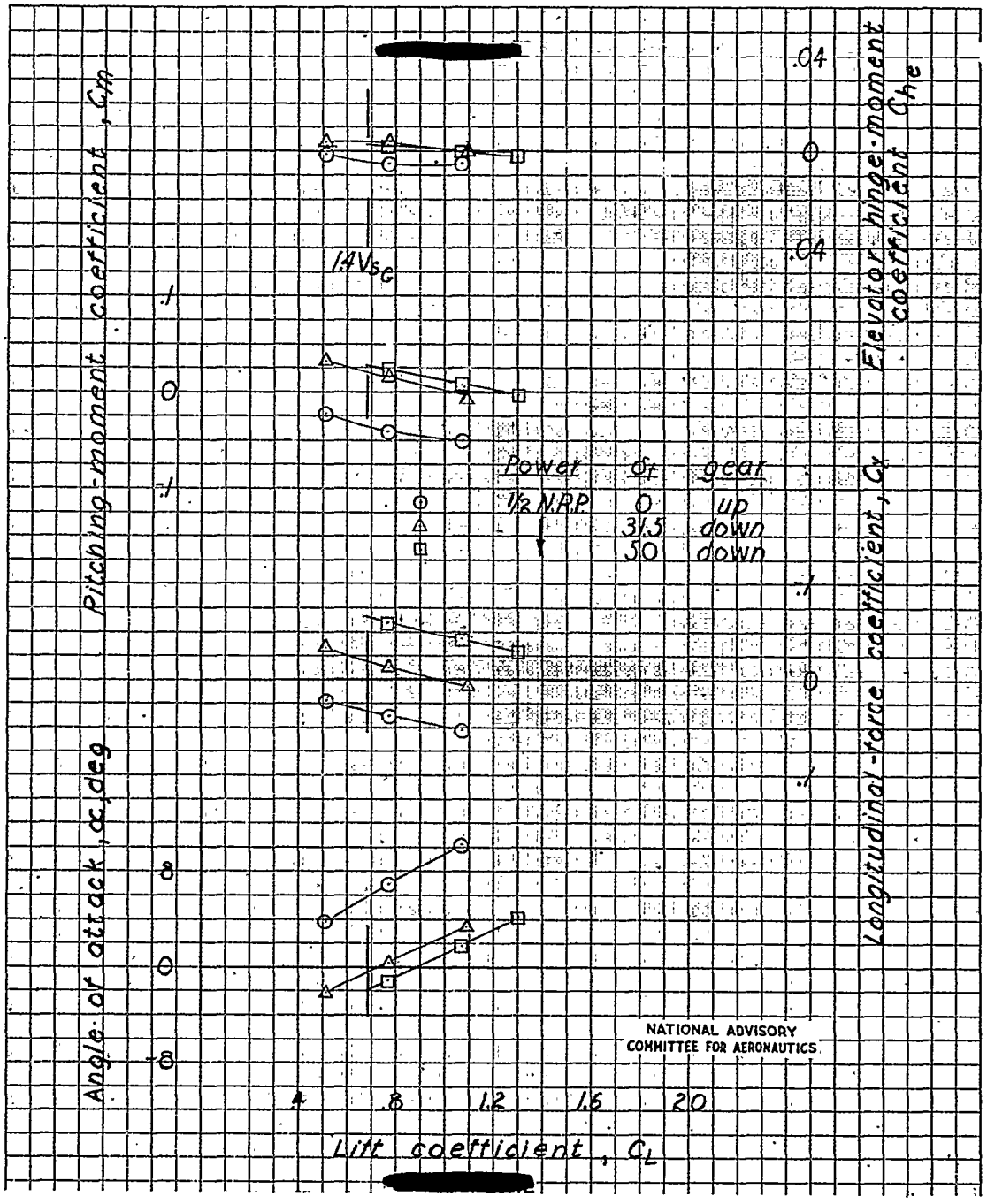

Part B

Figure 23.- Continued.

[redacted]

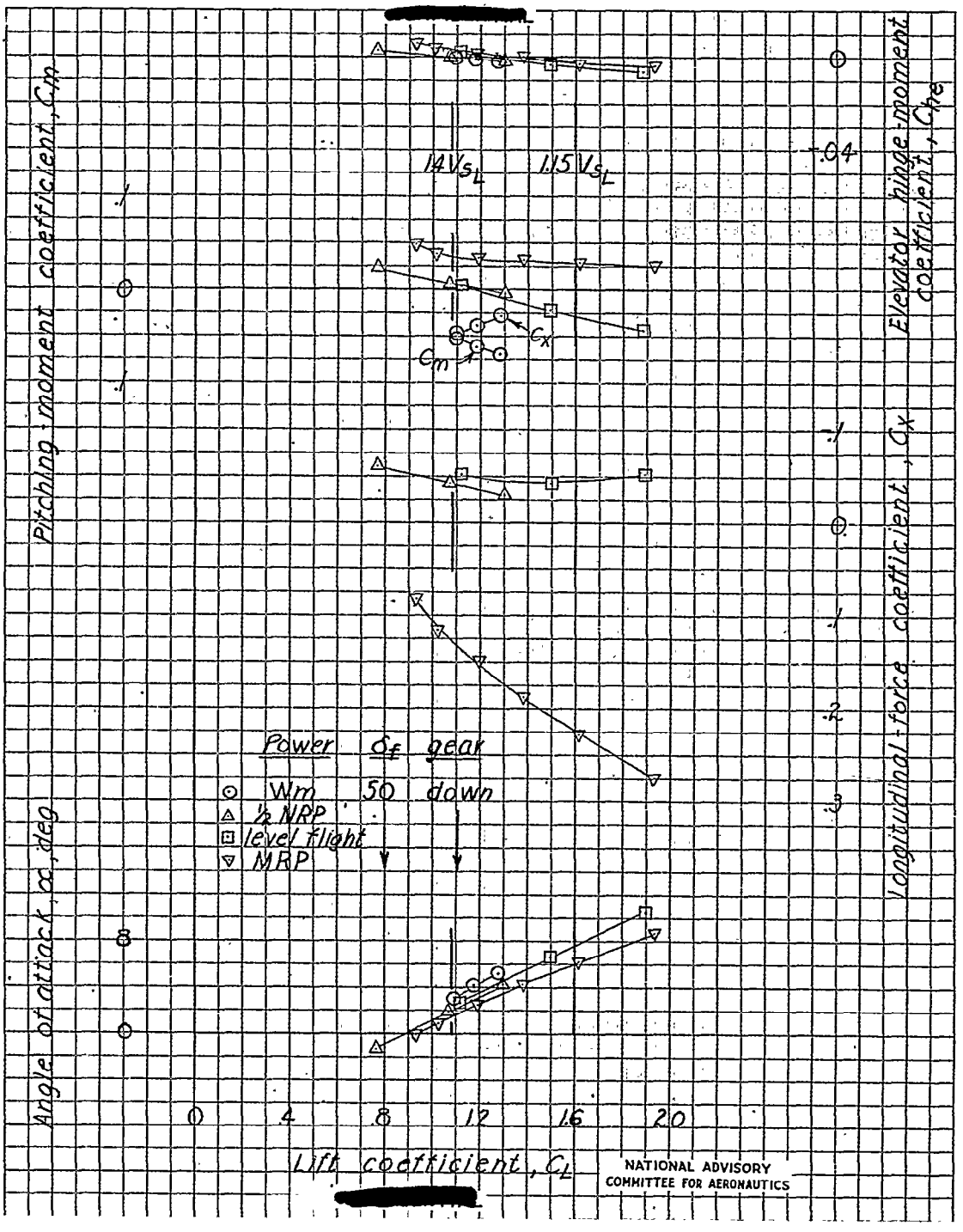

NATIONAL ADVISORY COMMITTEE FOR AERONAUTICS

[redacted]

Part C

Figure 23.- Continued.

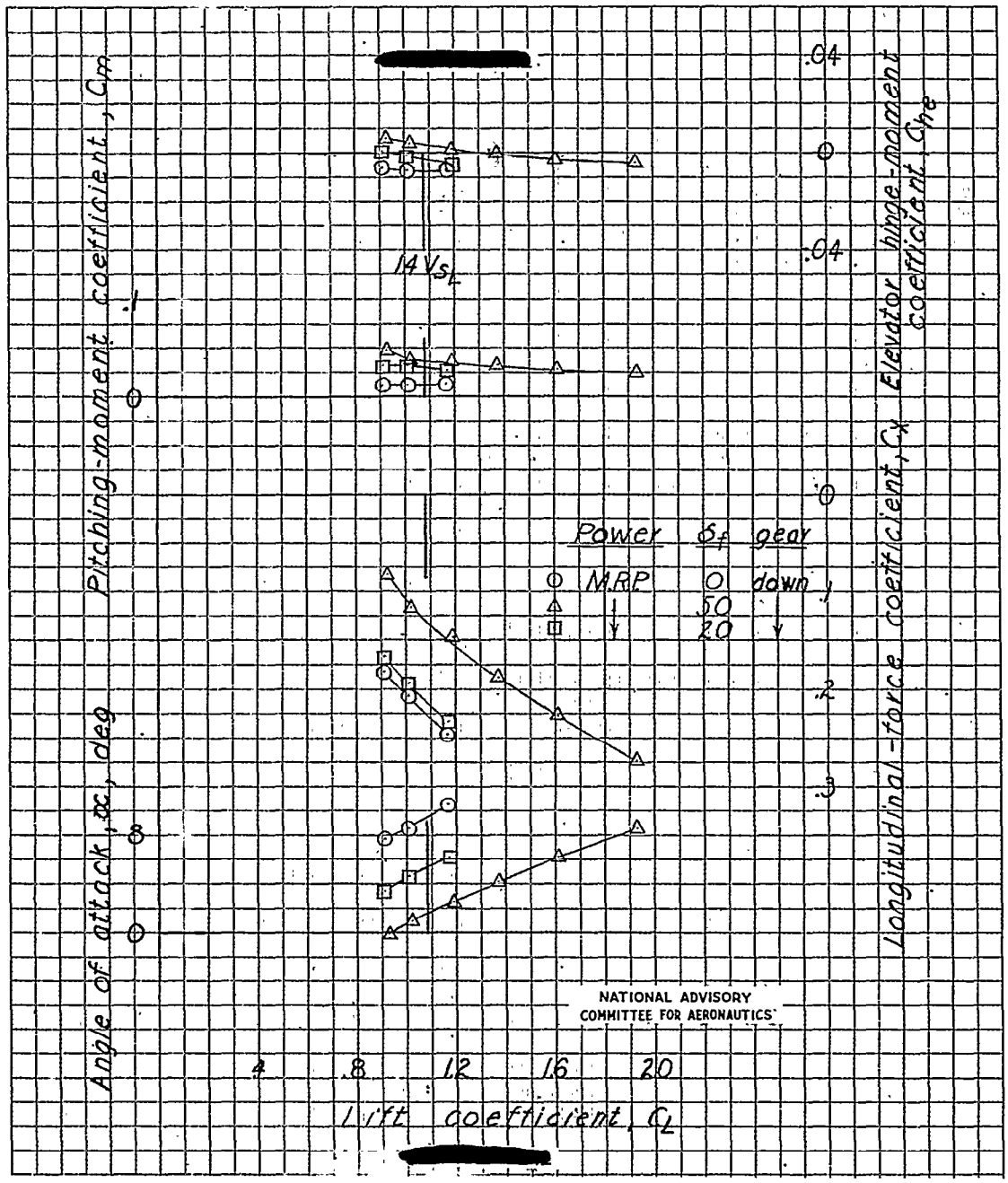

Part D

Figure 23.- Concluded.

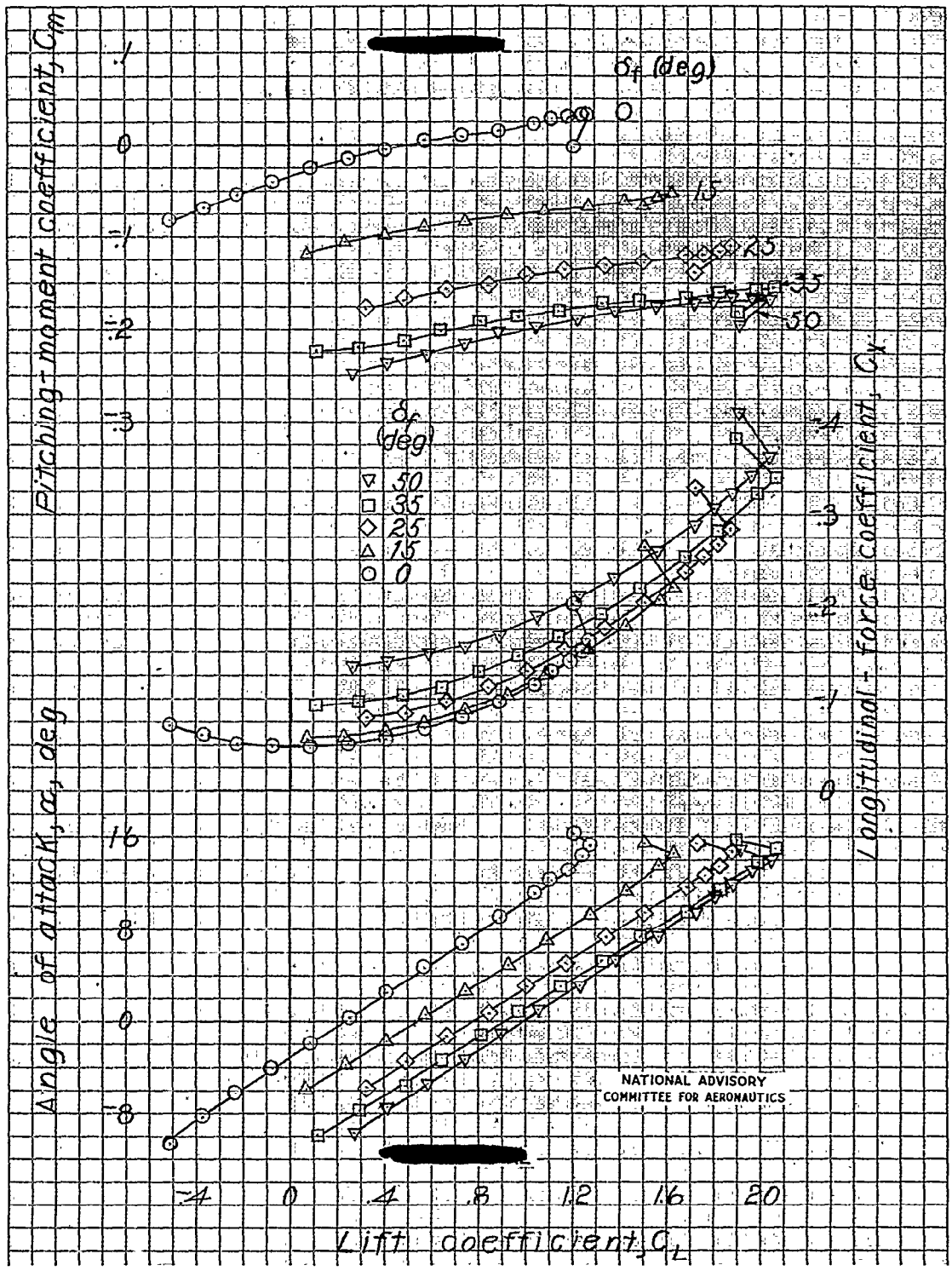

(a) Tail off; windmilling propeller.

Figure 24.- Effect of various wing-flap deflections on the aerodynamic characteristics in pitch of a 1/8-scale model of the Grumman XTB3F-1 airplane. Thrust line tilted down 3°.

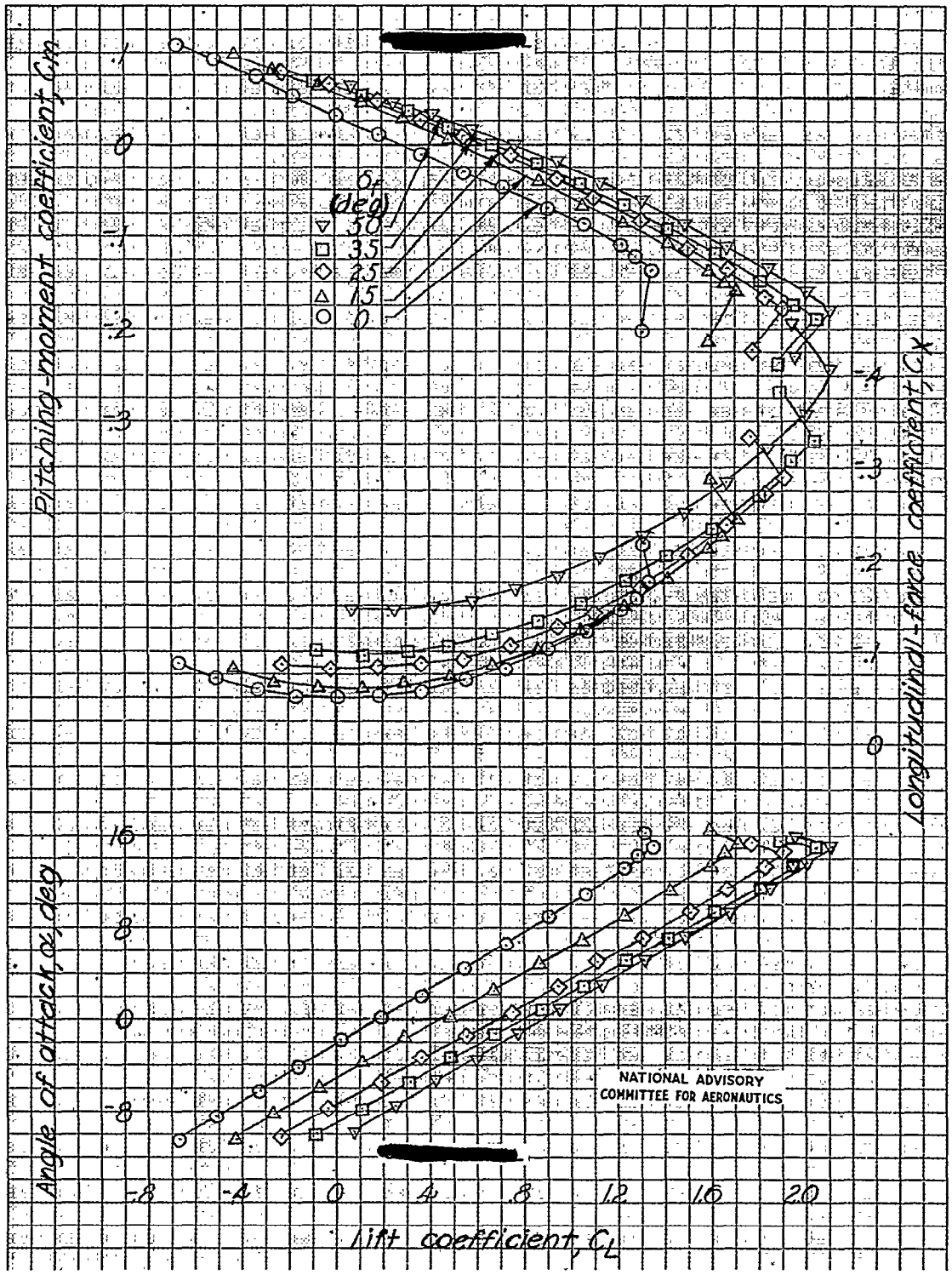

(b) $i_t = 2.0^\circ$; windmilling propeller.

Figure 24.- Continued.

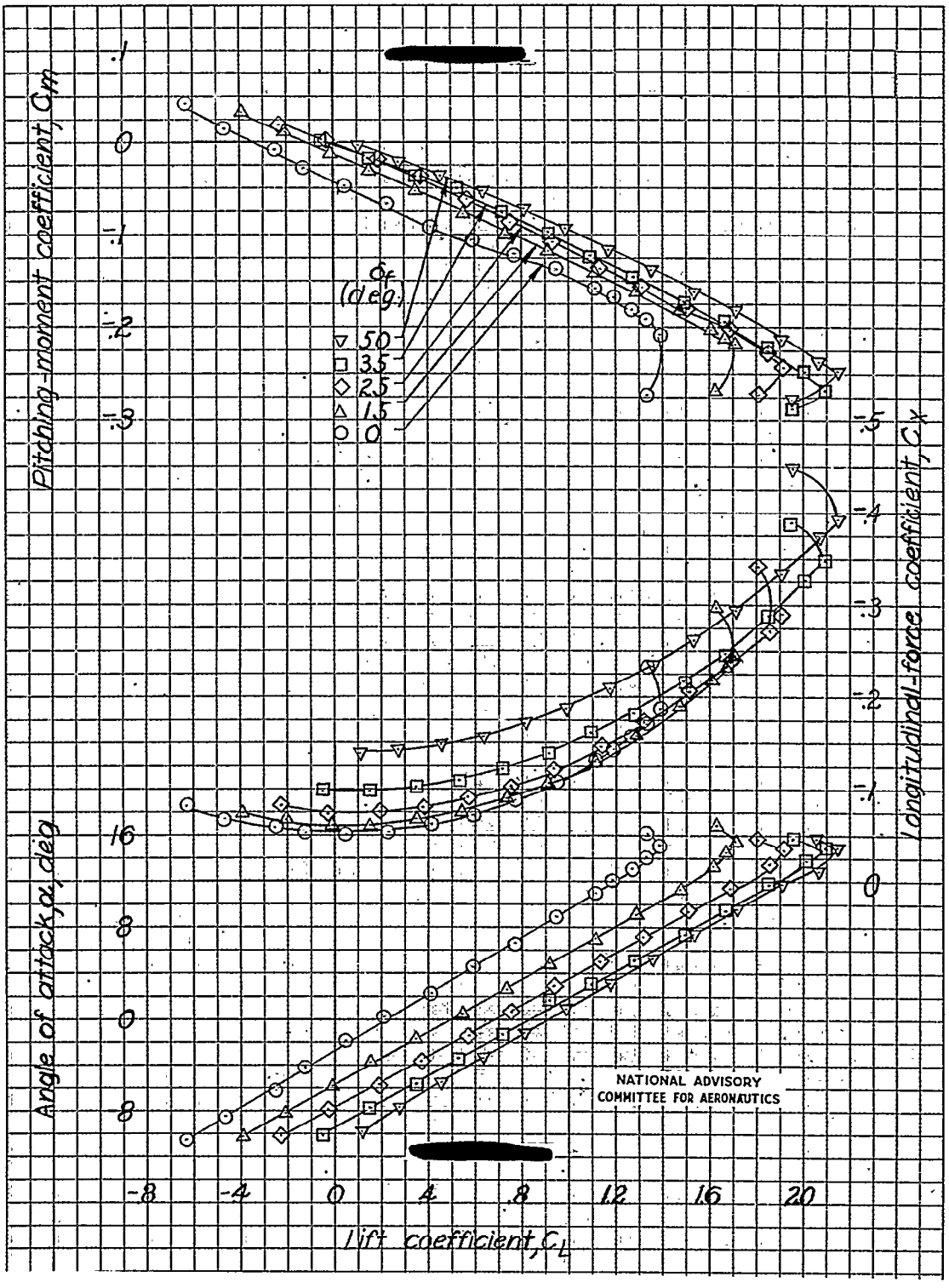

(c) $i_t = 4.8^\circ$; windmilling propeller.

Figure 24.- Continued.

[redacted]

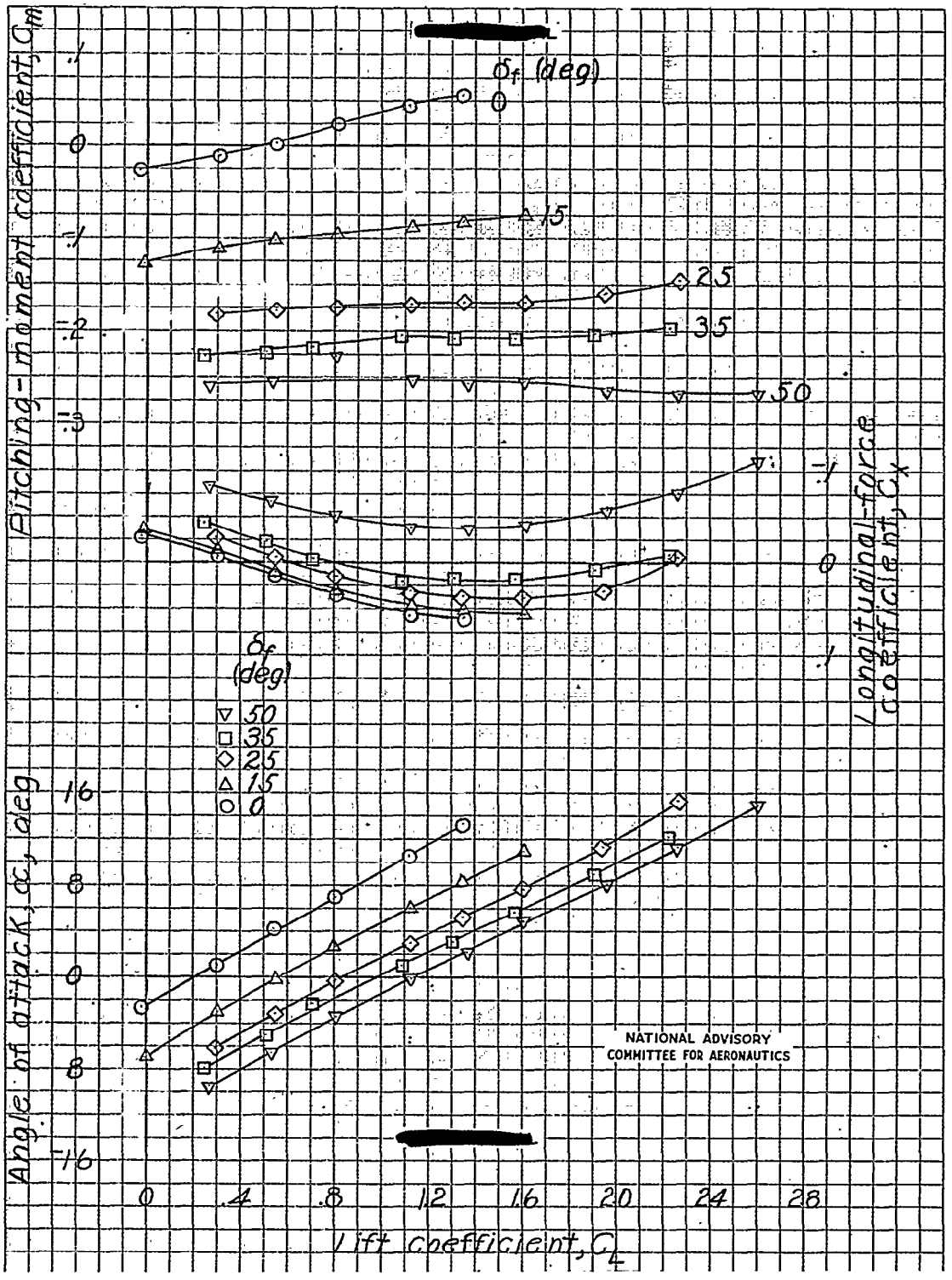

[redacted]

(d) Tail off; half normal rated power.

Figure 24.- Continued.

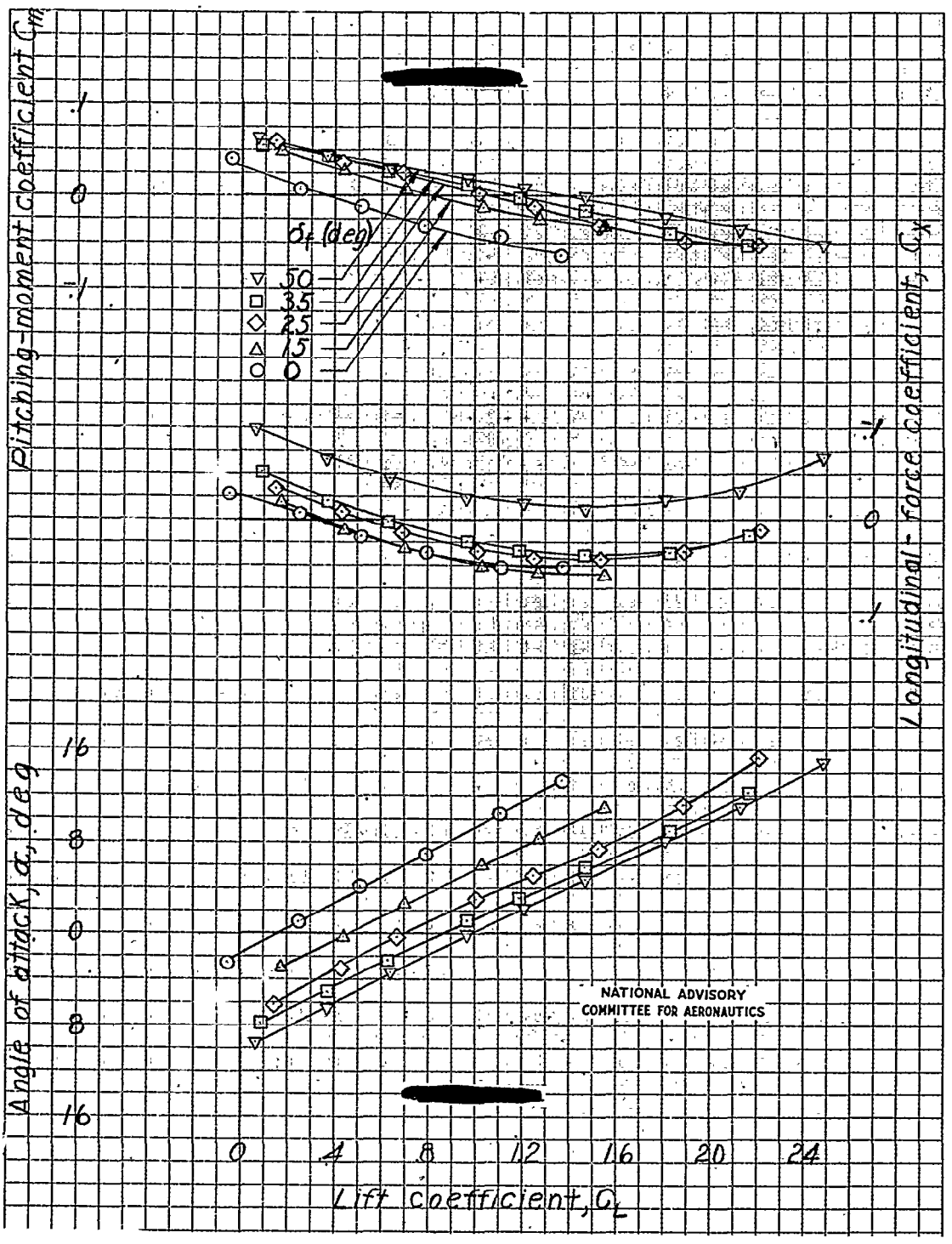

(e) $i_t = 2.0^\circ$; half normal rated power

Figure 24.- Continued.

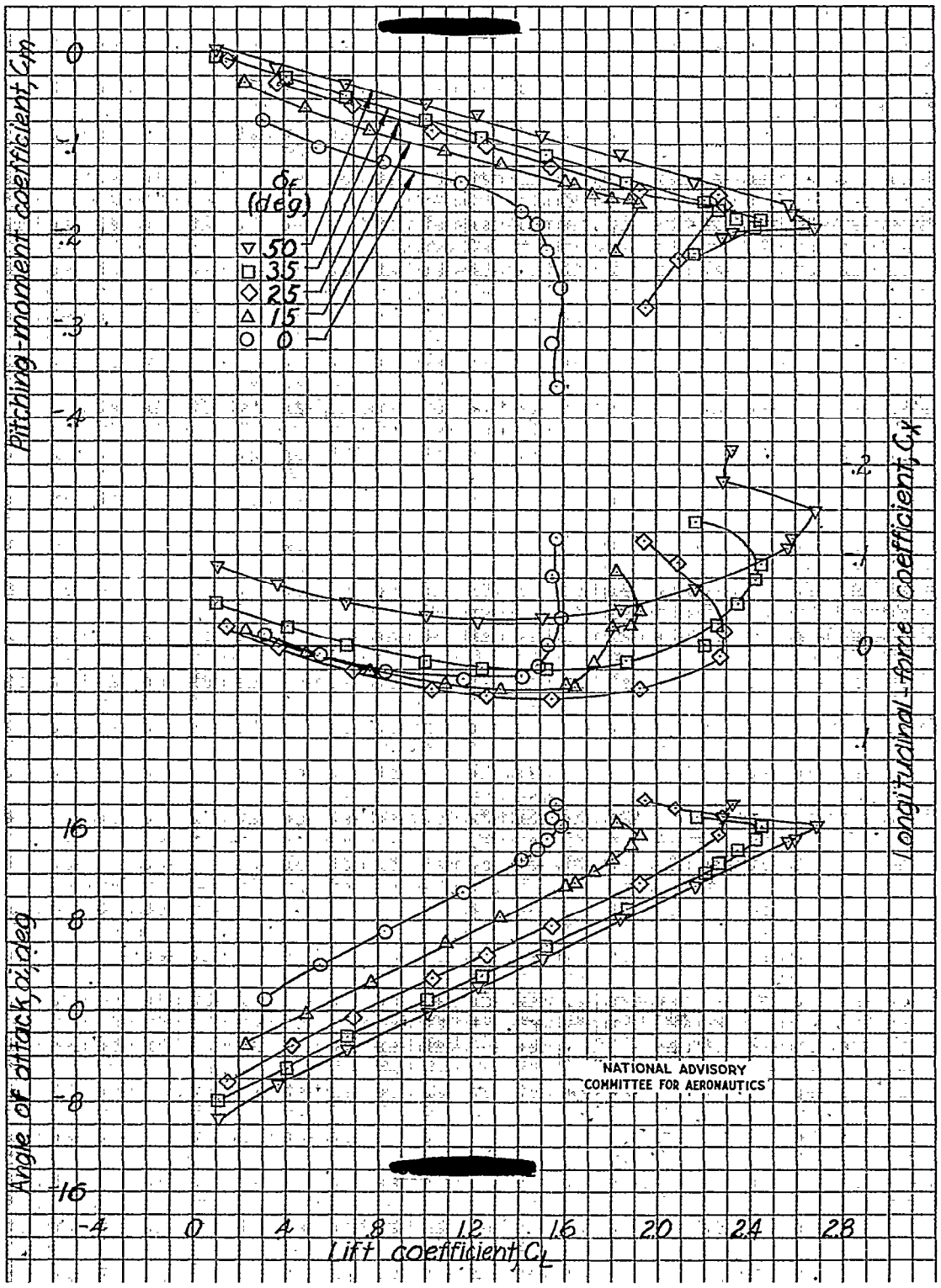

(f) $i_t = 4.8^\circ$; half normal rated power.

Figure 24.- Concluded.

[redacted]

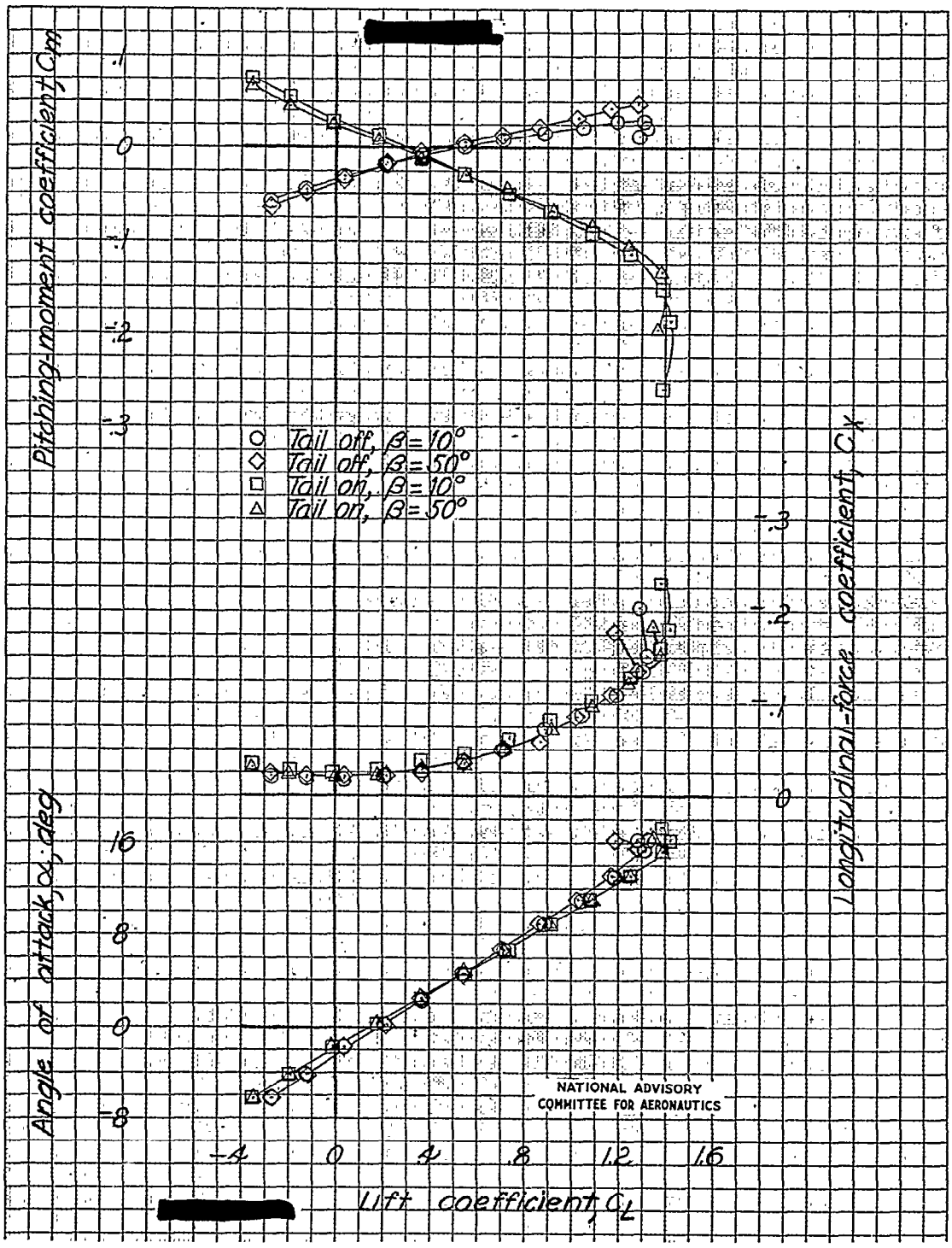

[redacted]

Figure 25.- Effect of propeller blade angle on aerodynamic characteristics in pitch of a 1/8-scale model of the Grumman XTB3F-1 airplane. $T_c' = 0$; $\delta_f = 0°$; $q = 16.37$ pounds per square foot.

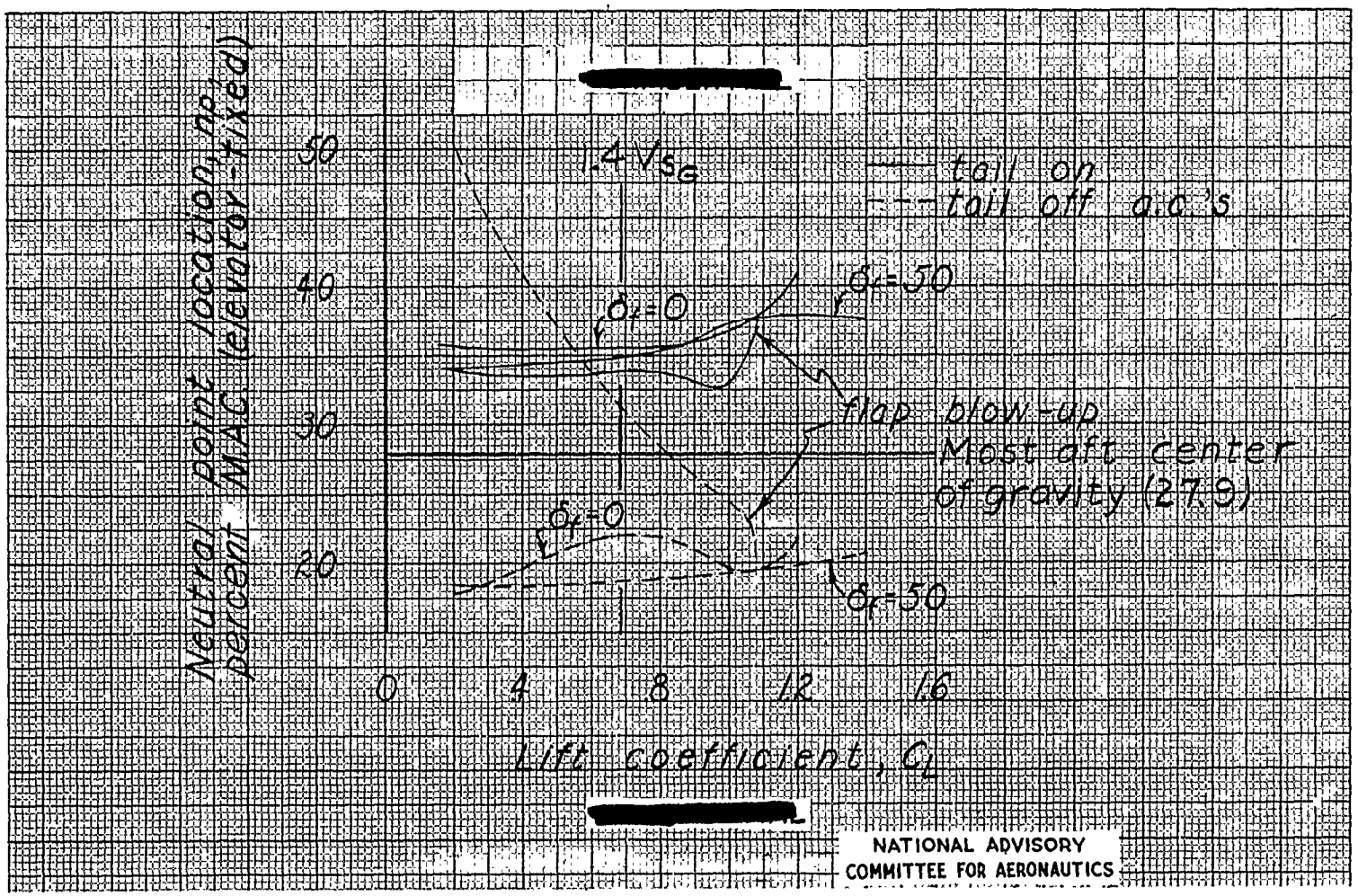

(a) Windmilling propeller.

Figure 26.- Effect of flap deflection on neutral point location of the 1/8-scale model of the Grumman XTB3F-1 airplane. Thrust line tilted down 3°.

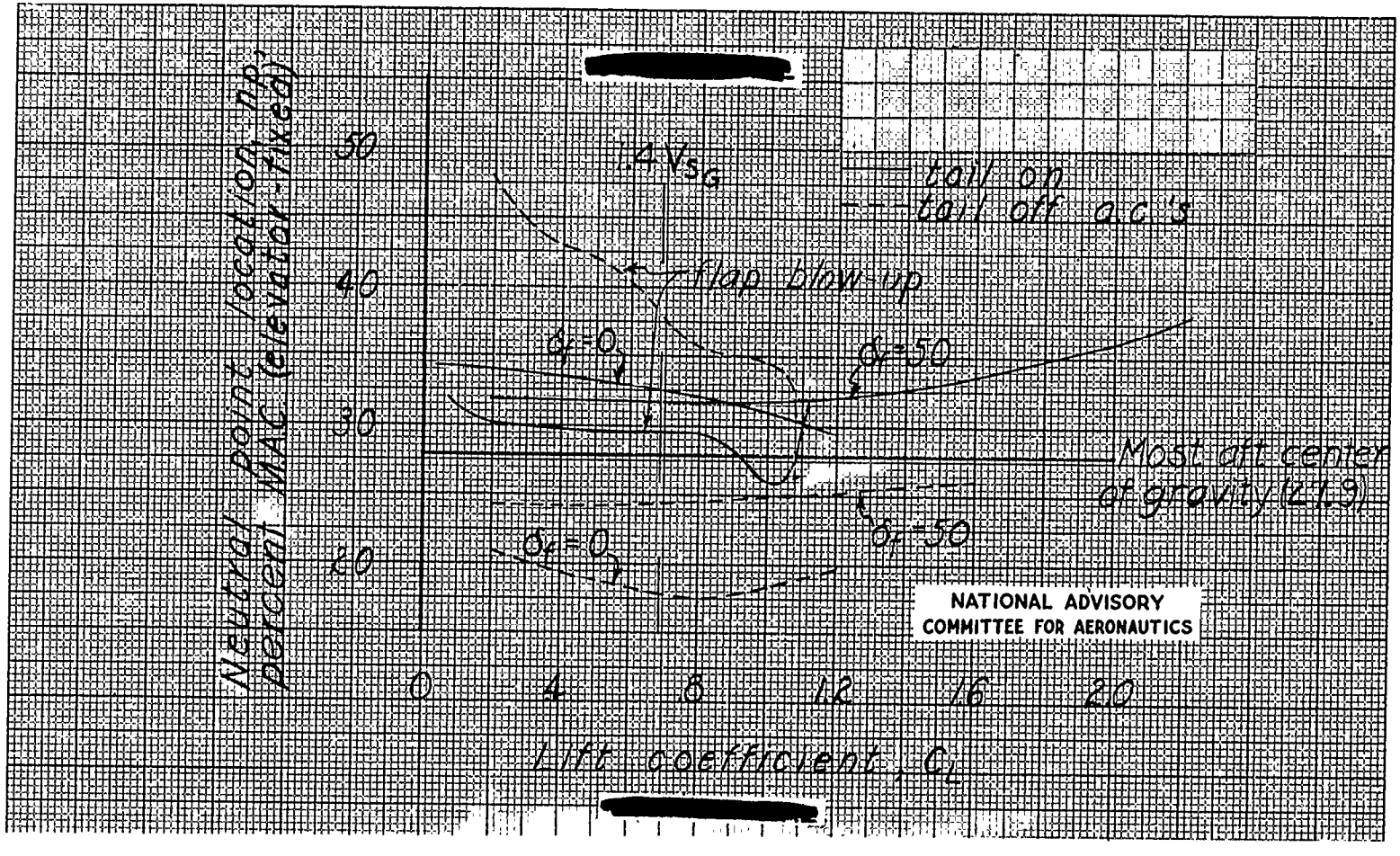

(b) Half normal rated power.

Figure 26.- Concluded.

[redacted]

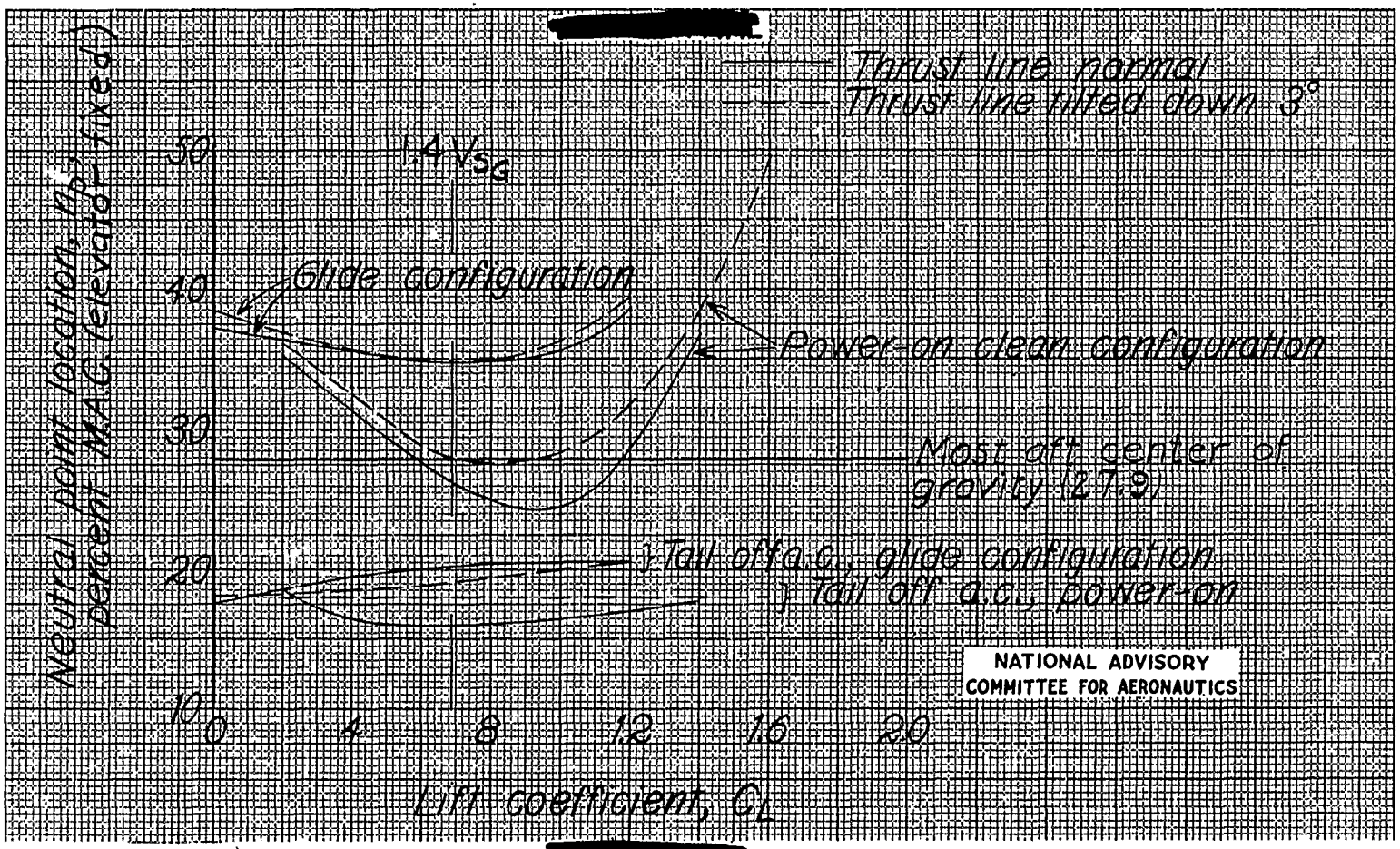

[redacted]

(a) $\delta_f = 0^\circ$

Figure 27.- Effect of thrust line tilt on neutral point location of the 1/8-scale model of the Grumman XTB3F-1 airplane.

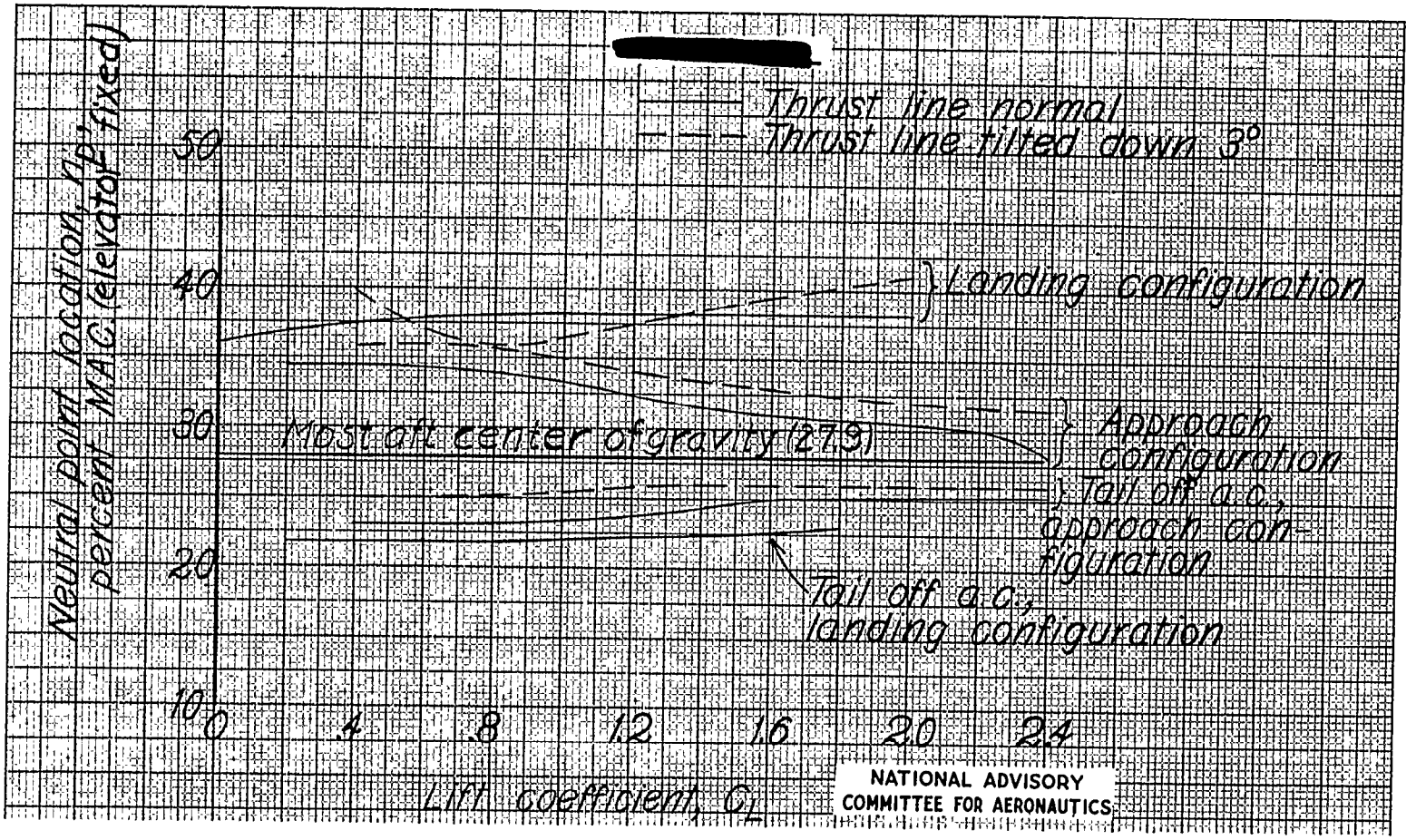

(b) $\delta_f = 50^\circ$

Figure 27.- Concluded

[redacted]

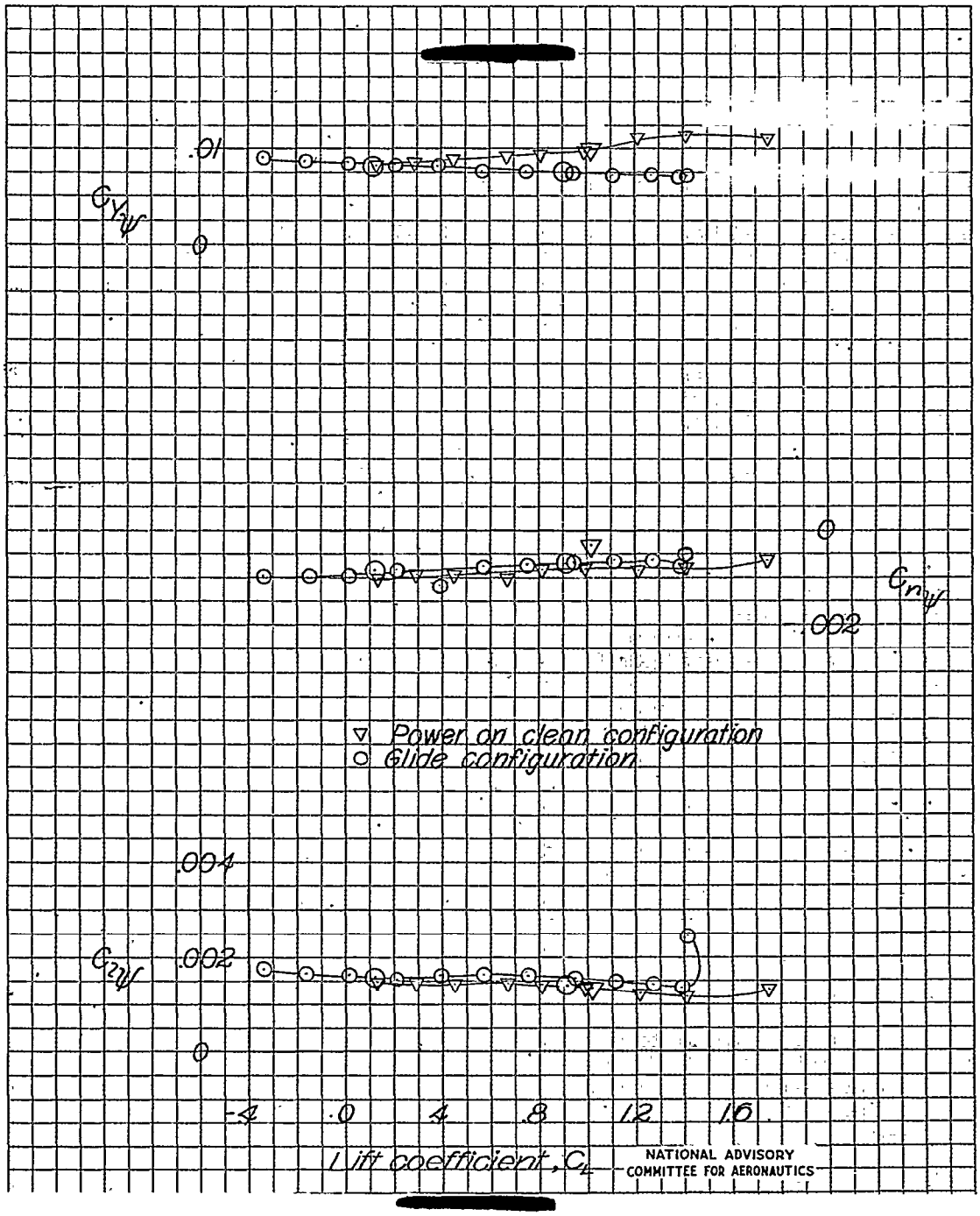

[redacted]

(a) $\delta_f = 0^\circ$

Figure 28.- Lateral stability parameters of a 1/8-scale model of the Grumman XTB3F-1 airplane. Original vertical tail; original dorsal fin.

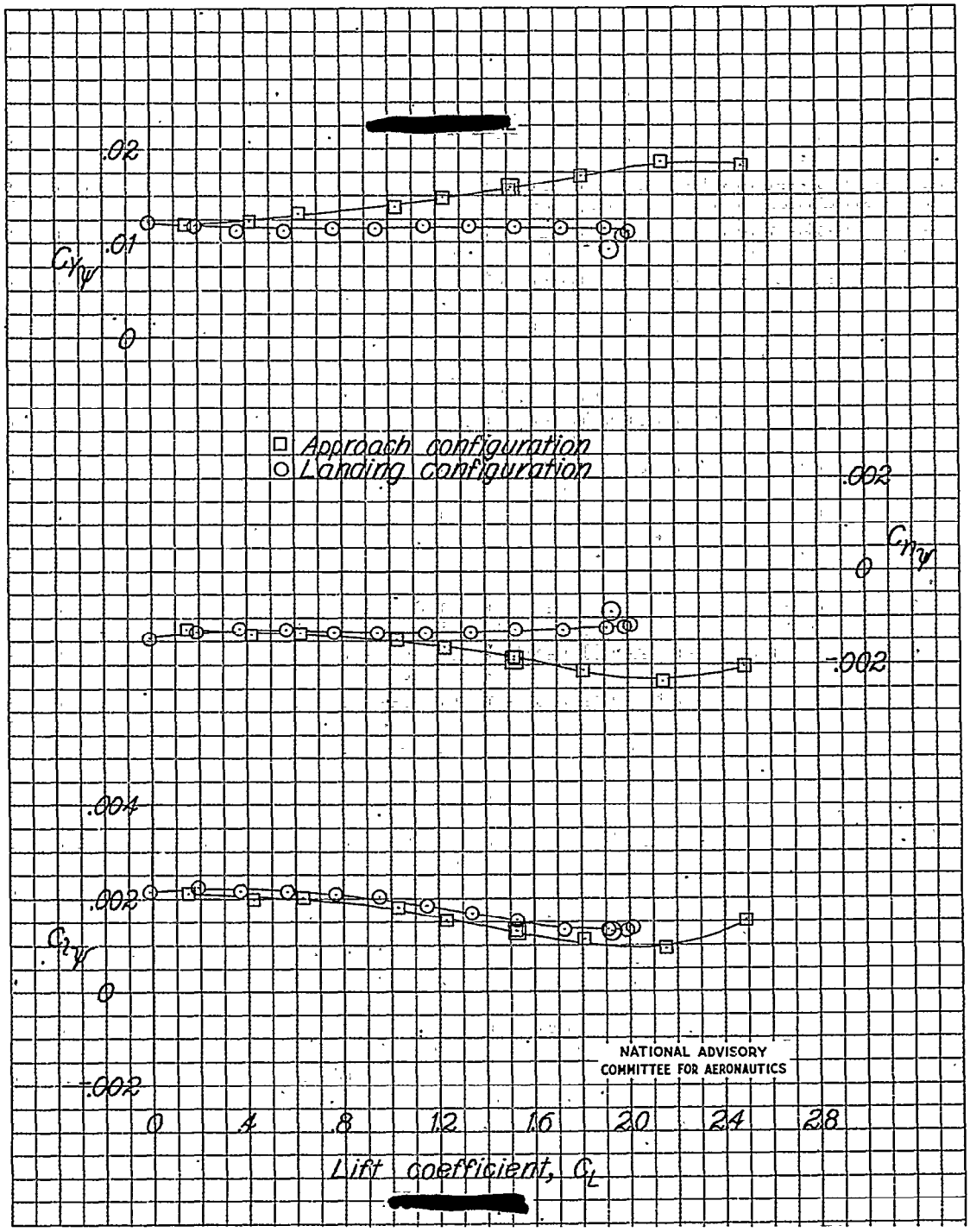

(b) $\delta_f = 50^\circ$

Figure 28.- Concluded.

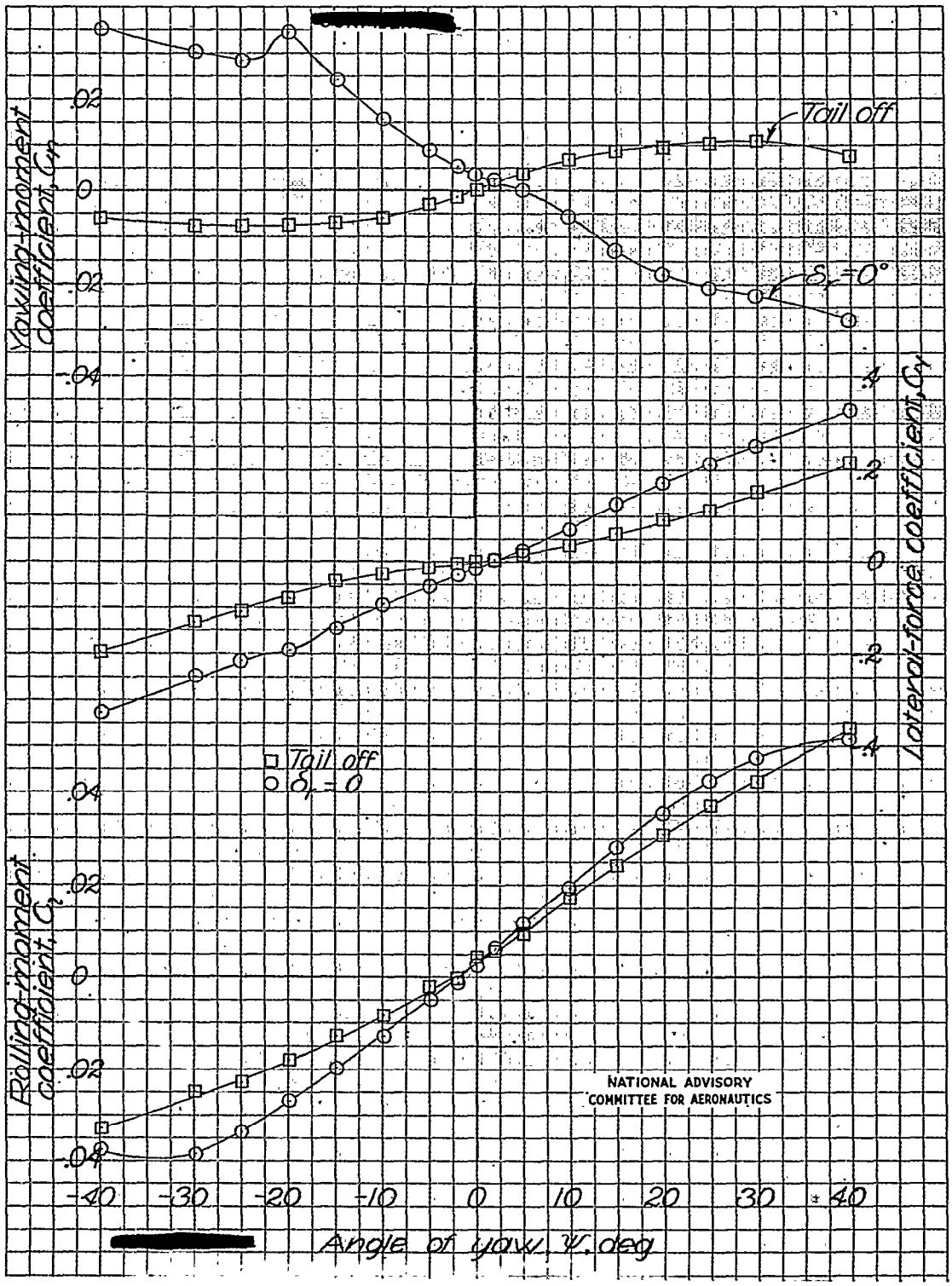

(a) $\alpha = -.9°$; $i_{fin} = -2°15'$; original vertical tail; original dorsal fin.

Figure 29.- Aerodynamic characteristics in yaw of a 1/8-scale model of the Grumman XTB3F-1 airplane. Glide configuration.

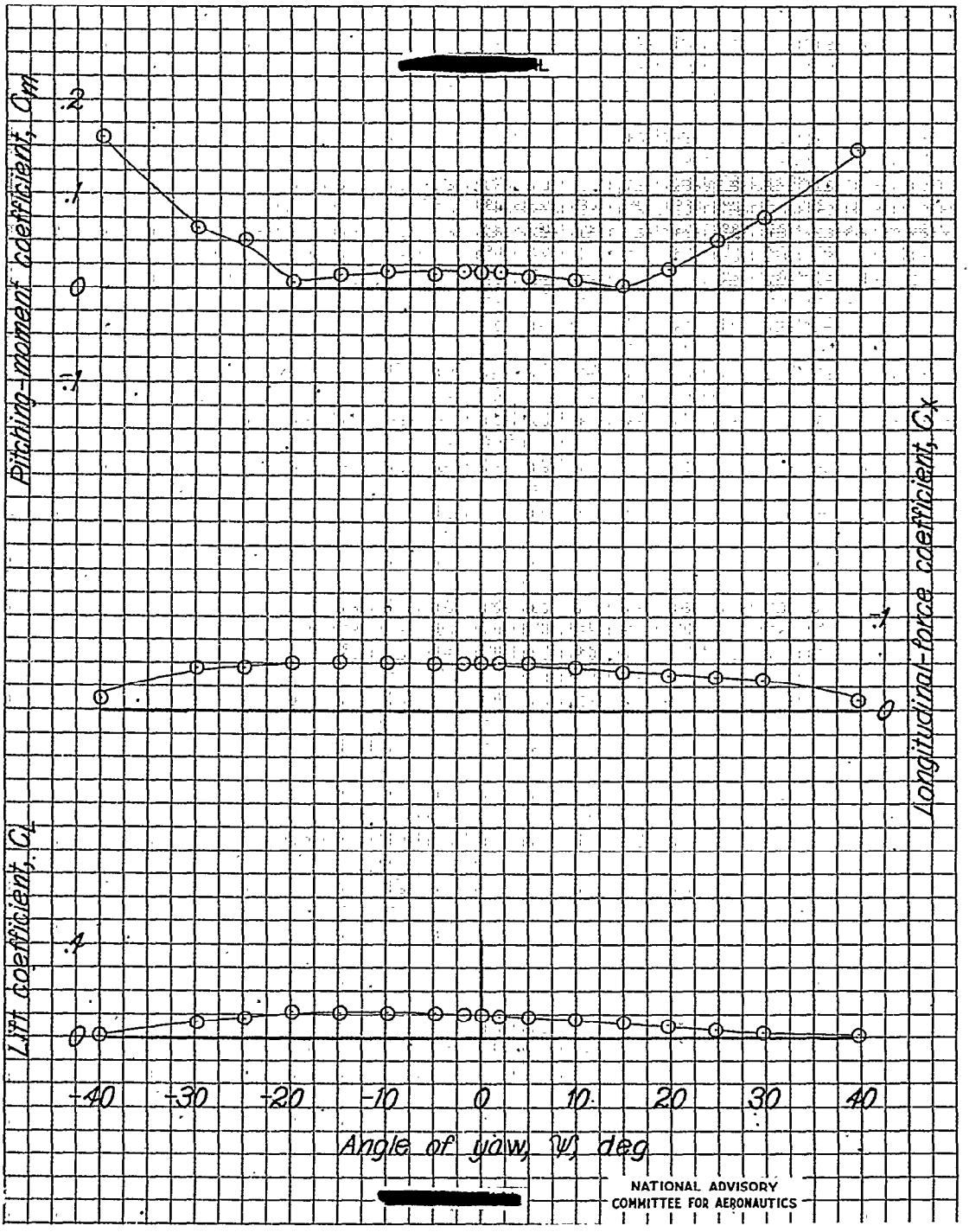

(a) Concluded; $\delta_r = 0^\circ$

Figure 29.- Continued.

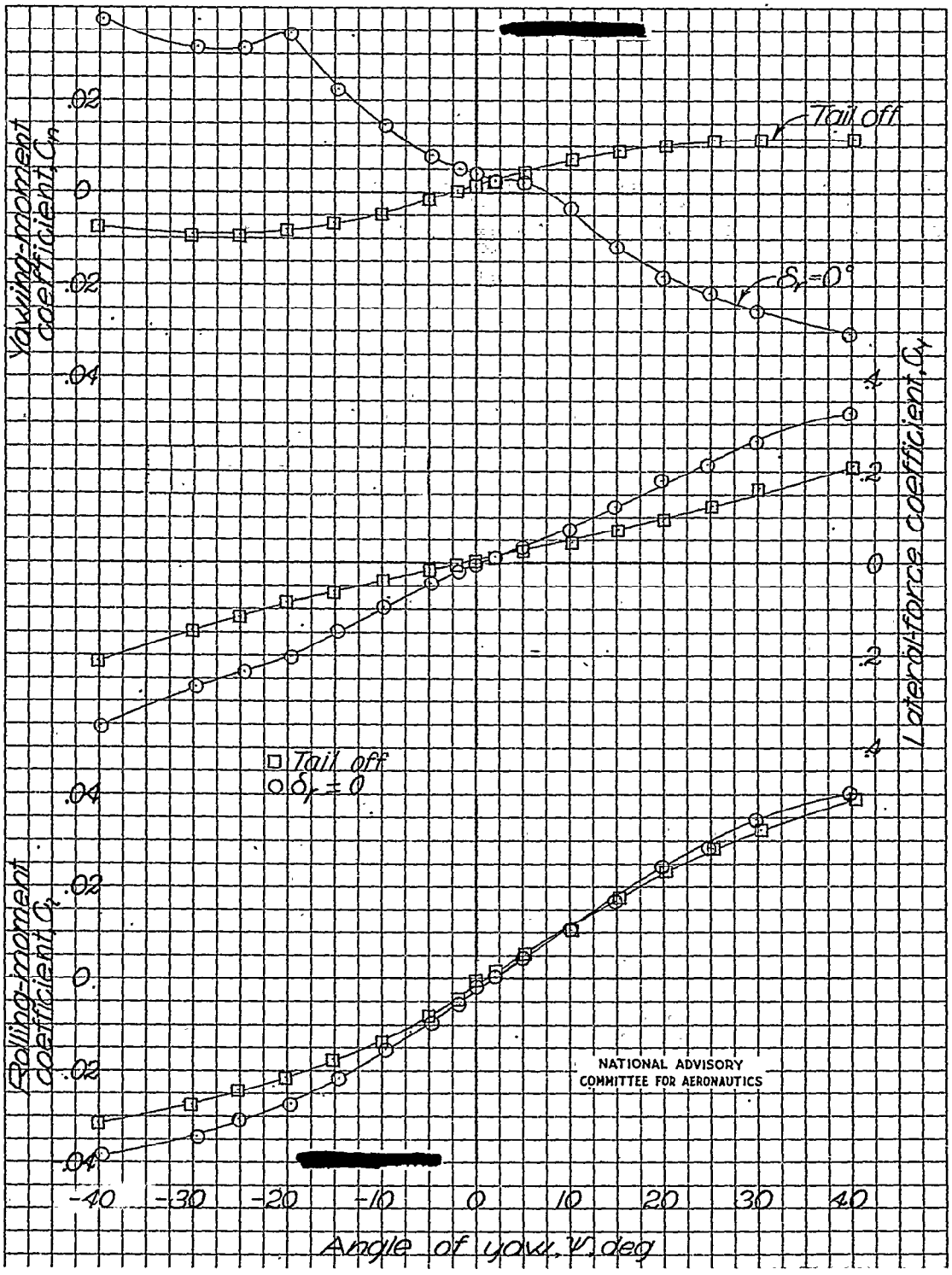

(b) $\alpha = 8.9^\circ$; $i_{fin} = -2^\circ 15'$; original vertical tail; original dorsal fin.

Figure 29.- Continued.

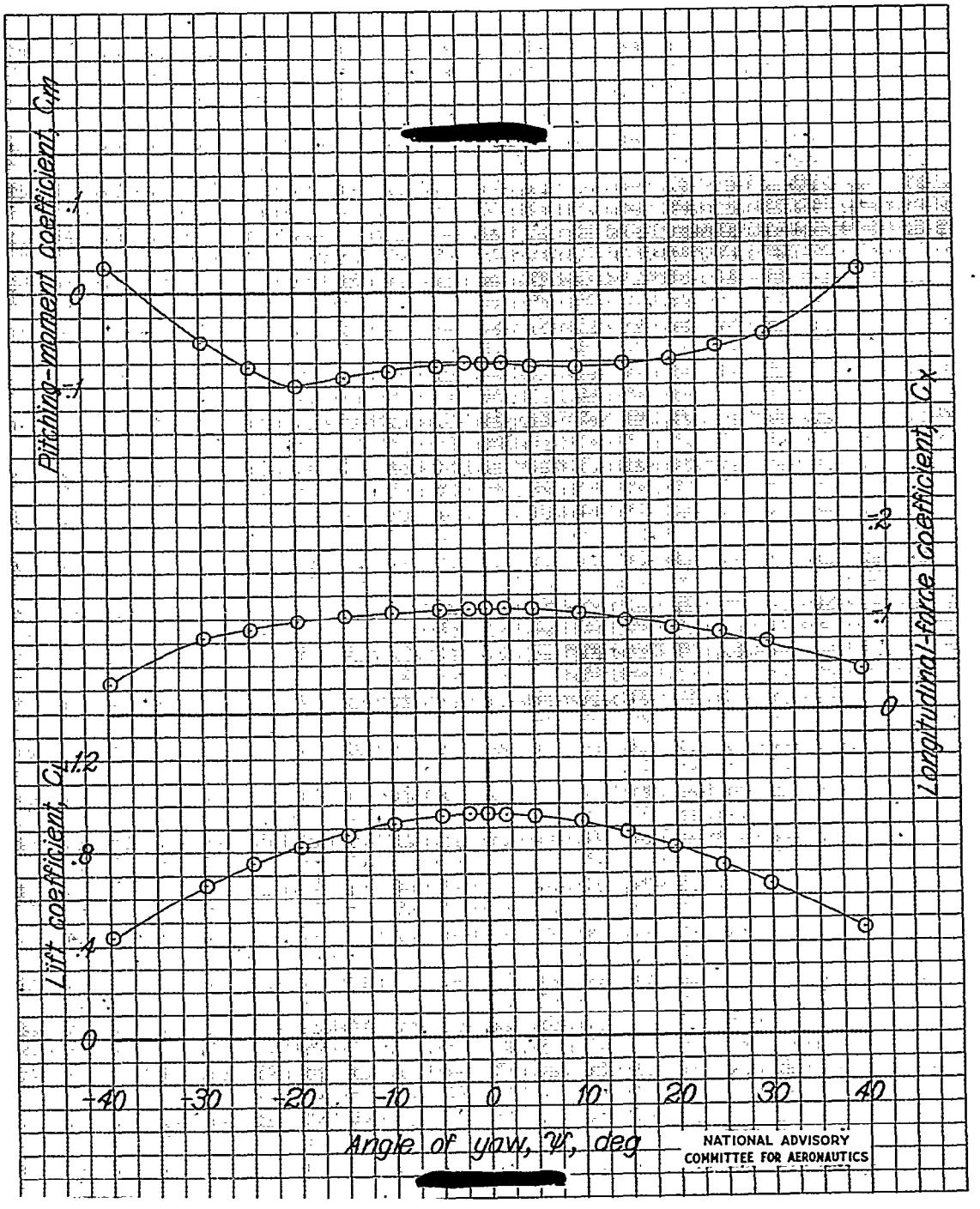

(b) Concluded; $\delta_r = 0^\circ$

Figure 29.- Continued.

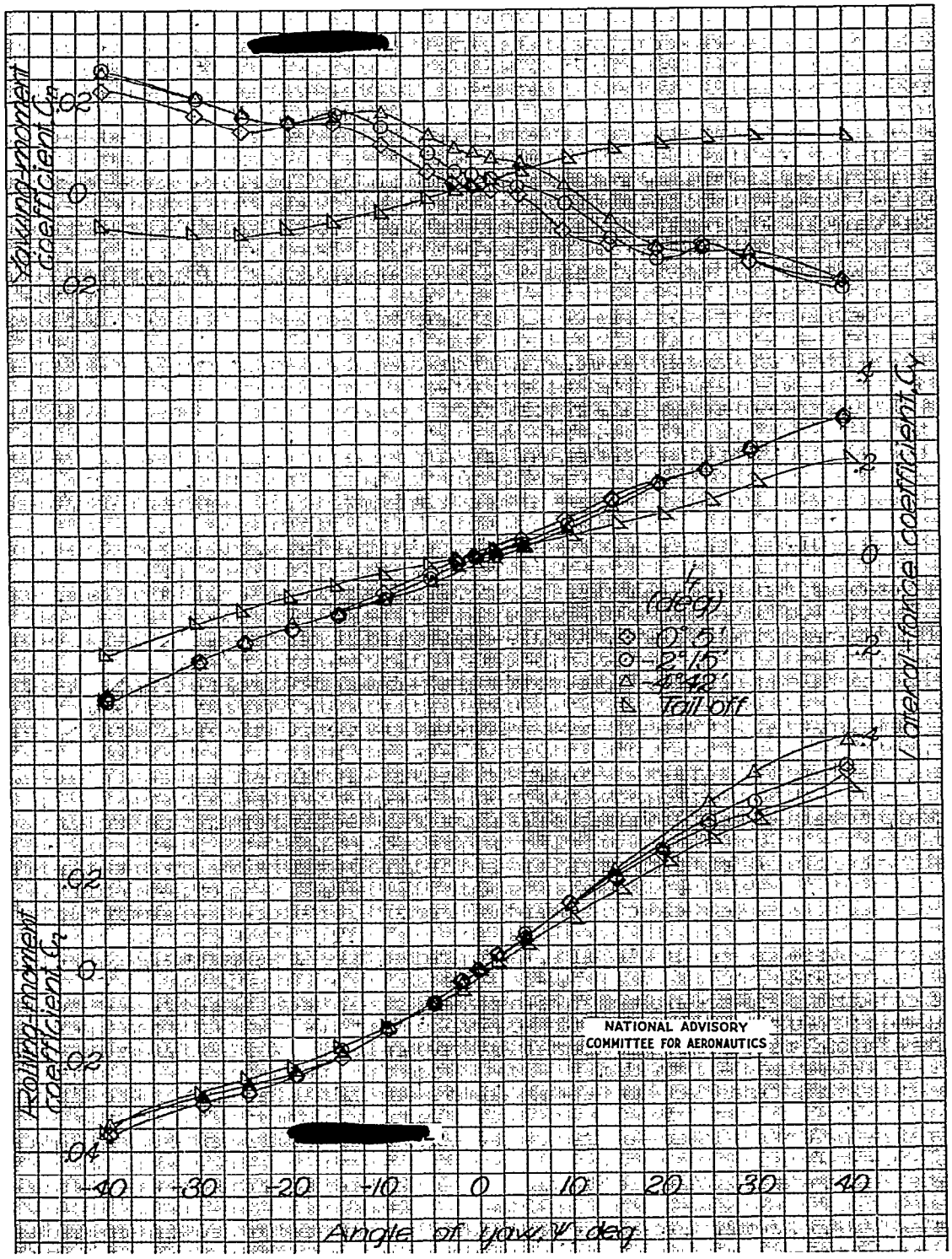

(c) $\alpha = 8.9^{\circ}$; original vertical tail; no dorsal fin.

Figure 29.- Continued.

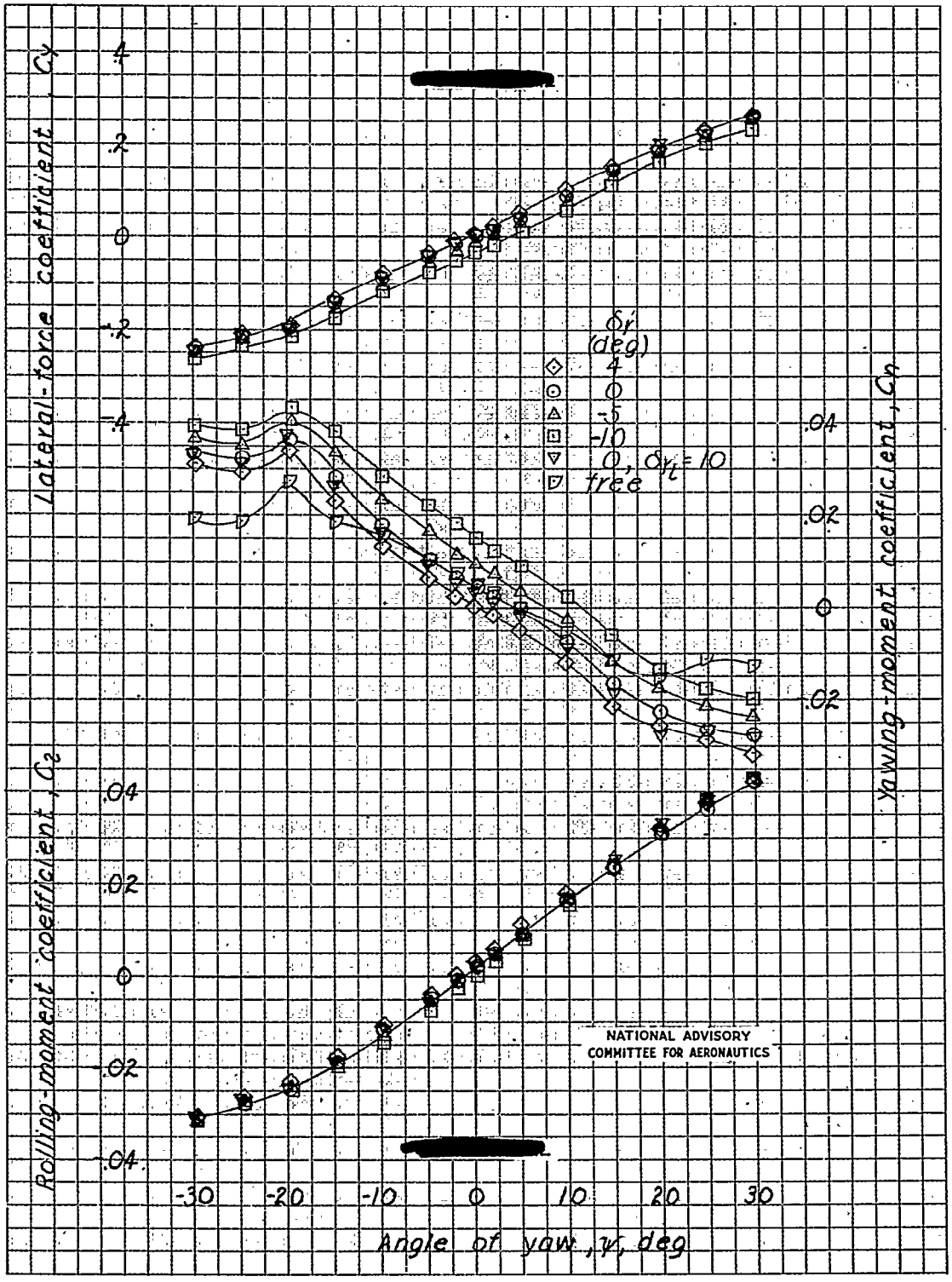

(d) $\alpha = 1.3^{\circ}$; 1.5-inch base extension on vertical tail; original dorsal fin.

Figure 29.- Continued.

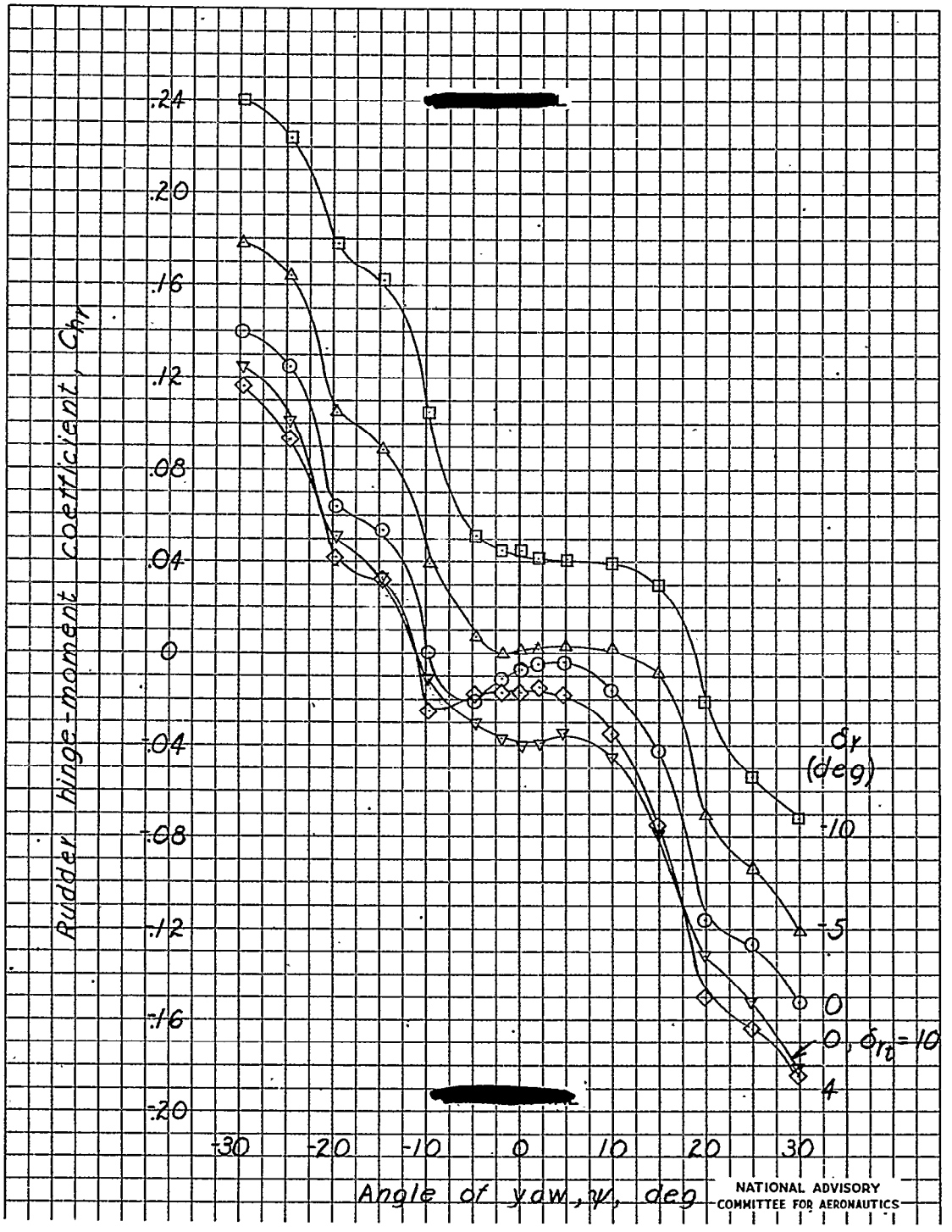

(d) Continued.

Figure 29 .- Continued.

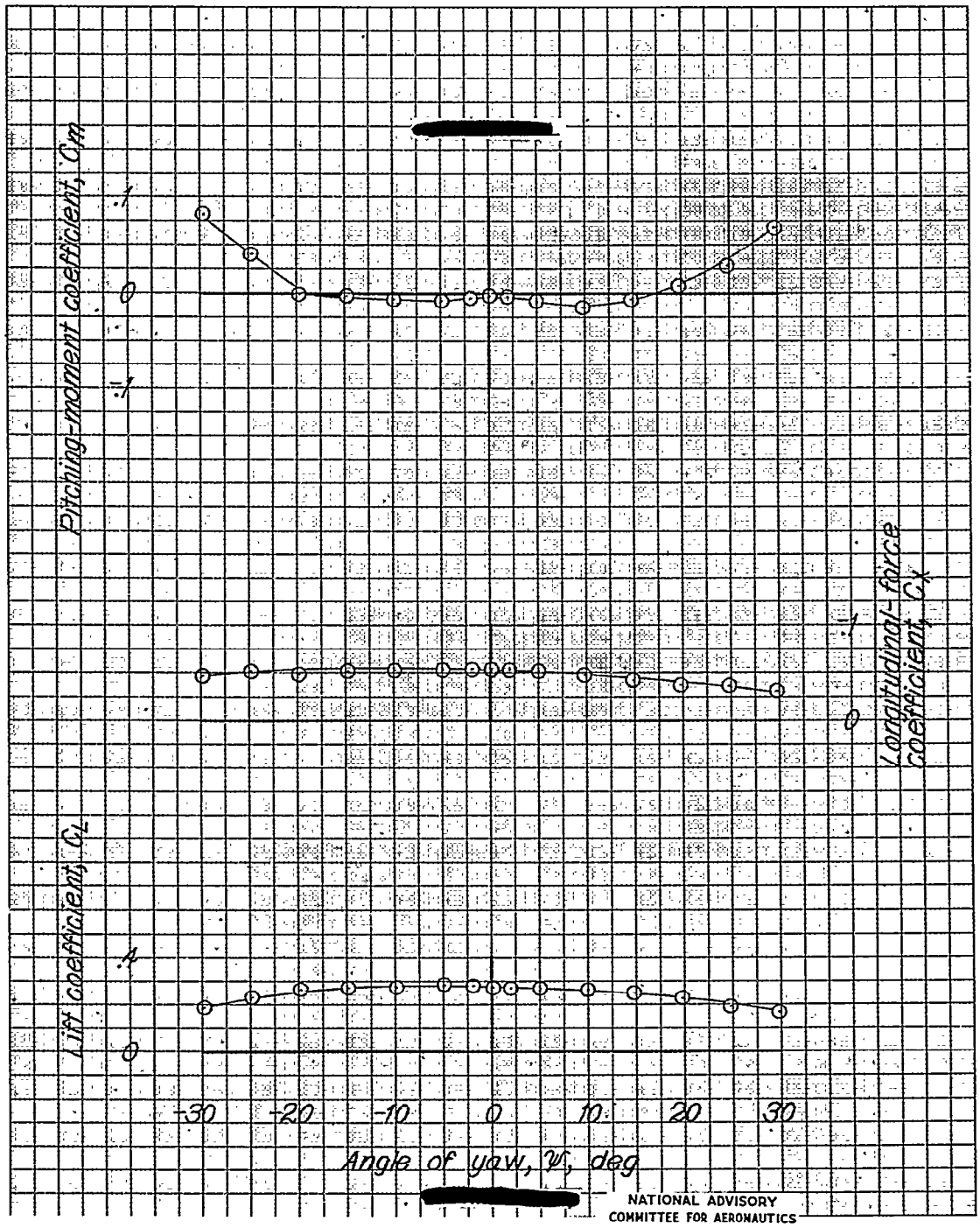

(d) Concluded; $\delta_r = 0^\circ$.

Figure 29.- Concluded.

[redacted]

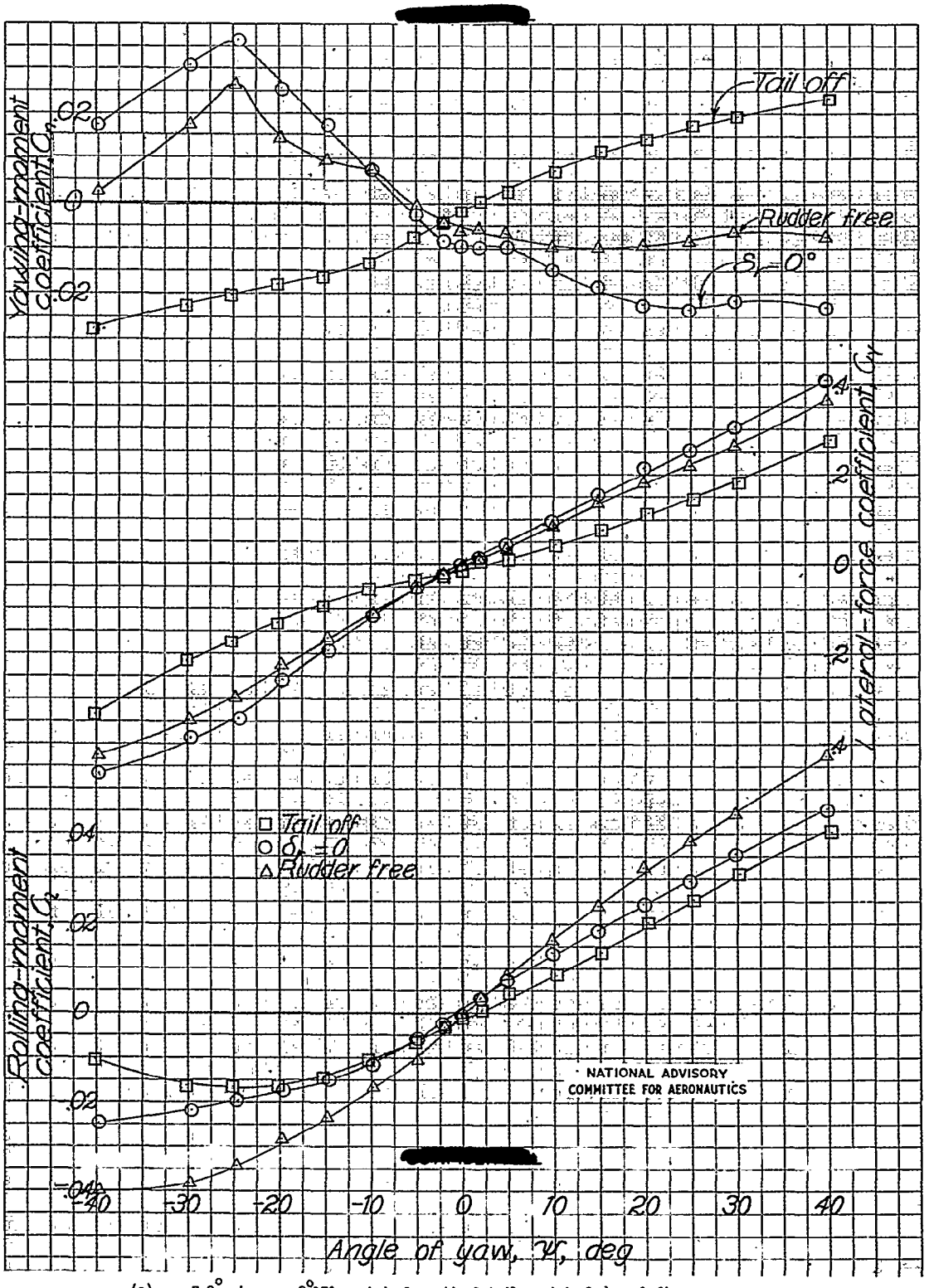

[redacted]

(a) $\alpha = 7.9°$; $i_{fin} = -2°15'$; original vertical tail; original dorsal fin.

Figure 30.- Aerodynamic characteristics in yaw of a 1/8-scale model of the Grumman XTB3F-1 airplane. Power-on clean configuration.

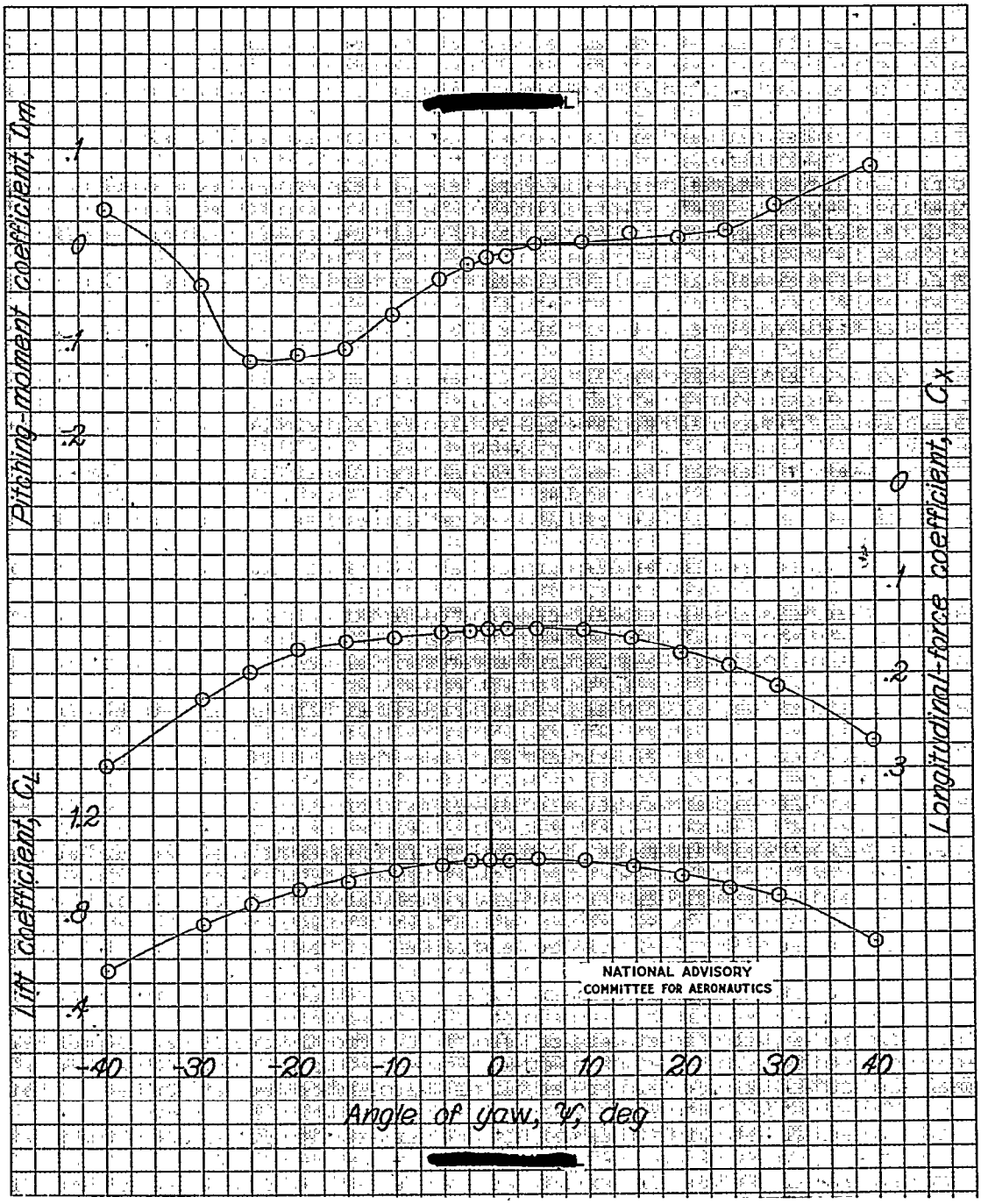

(a) Concluded; $\delta_r = 0^\circ$

Figure 30.- Continued.

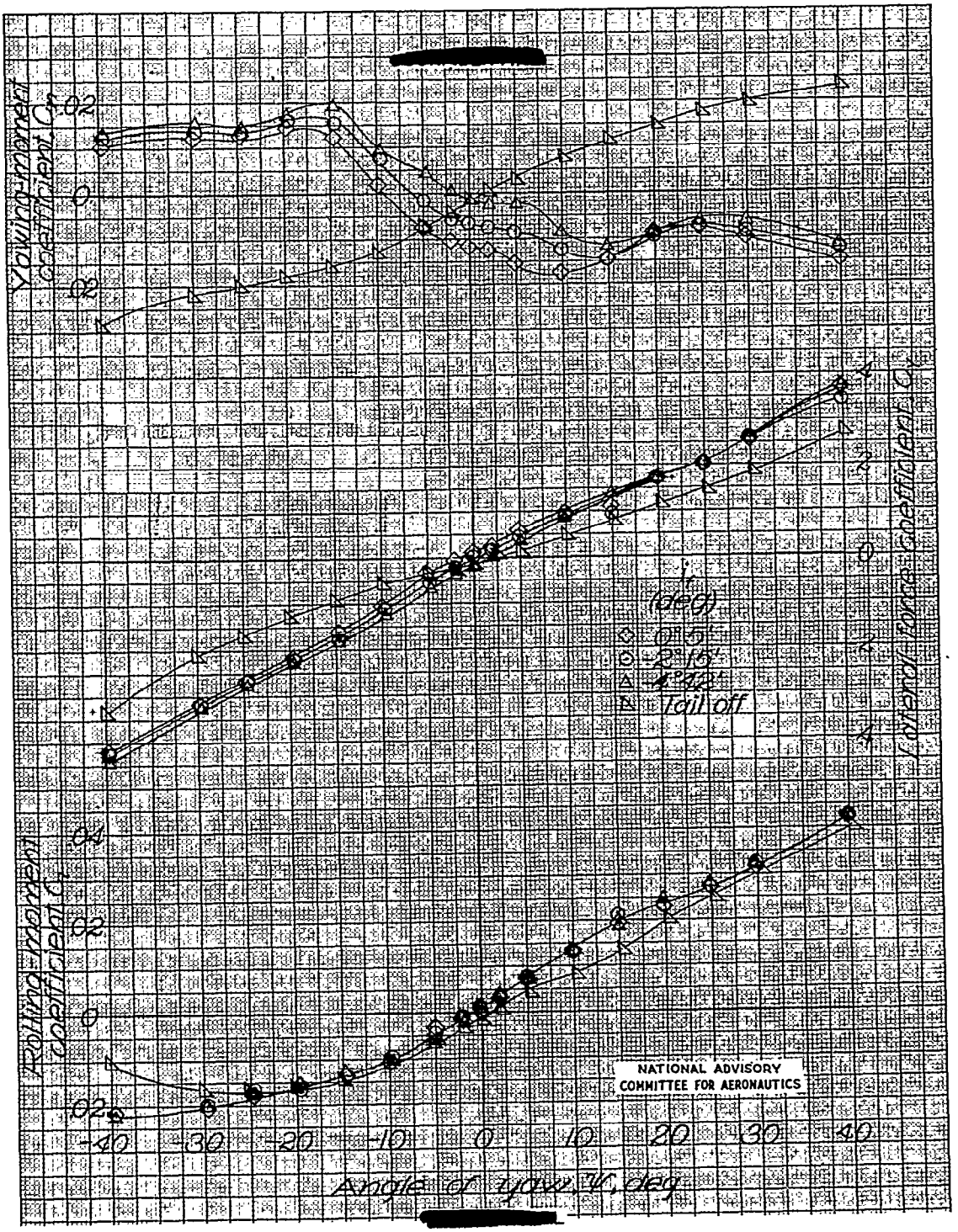

(b) $\alpha = 7.9^{\circ}$; original vertical tail; no dorsal fin.

Figure 30.- Continued.

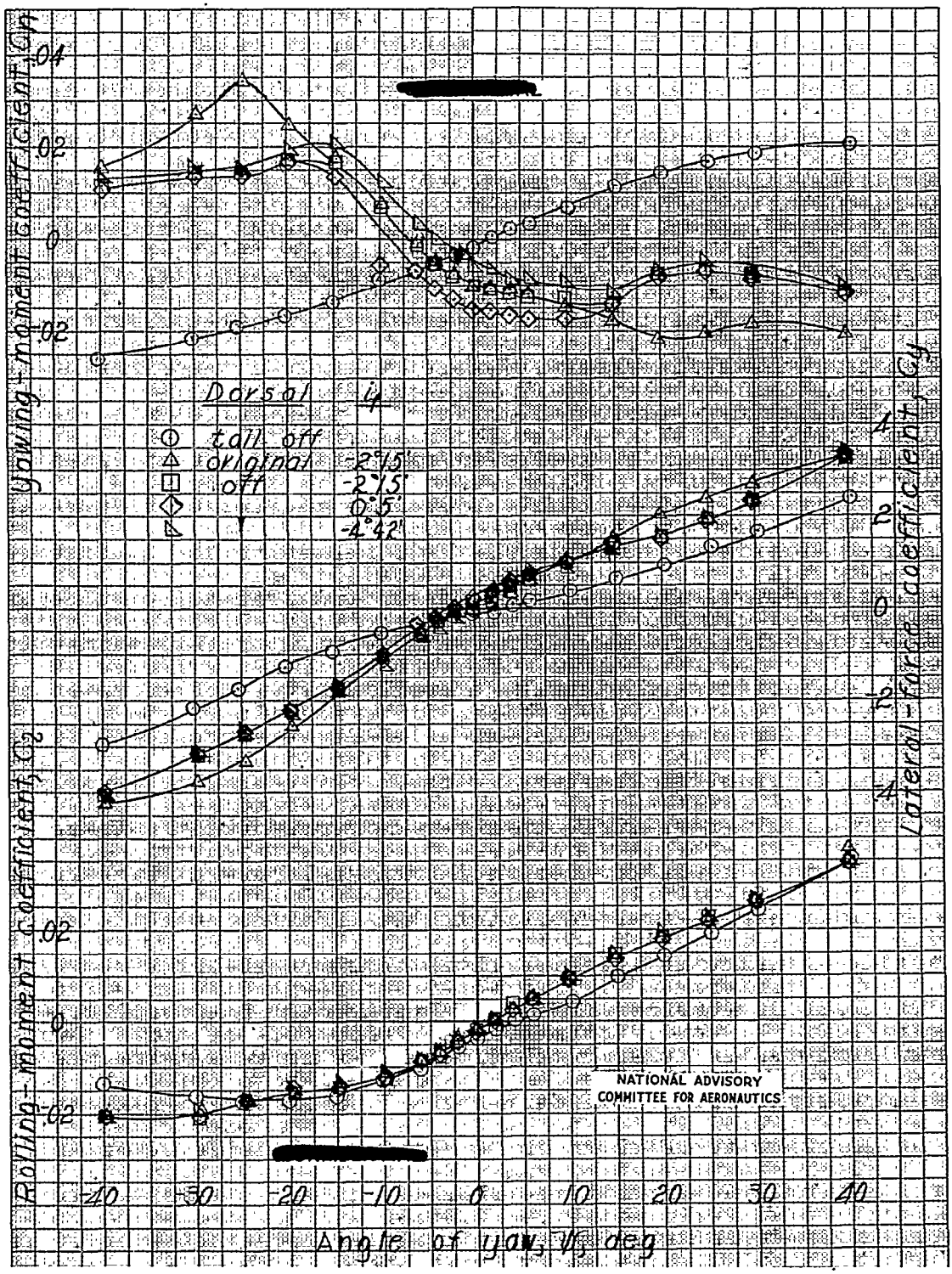

(c) $\alpha = 8.2^{\circ}$; original vertical tail.

Figure 30.- Continued.

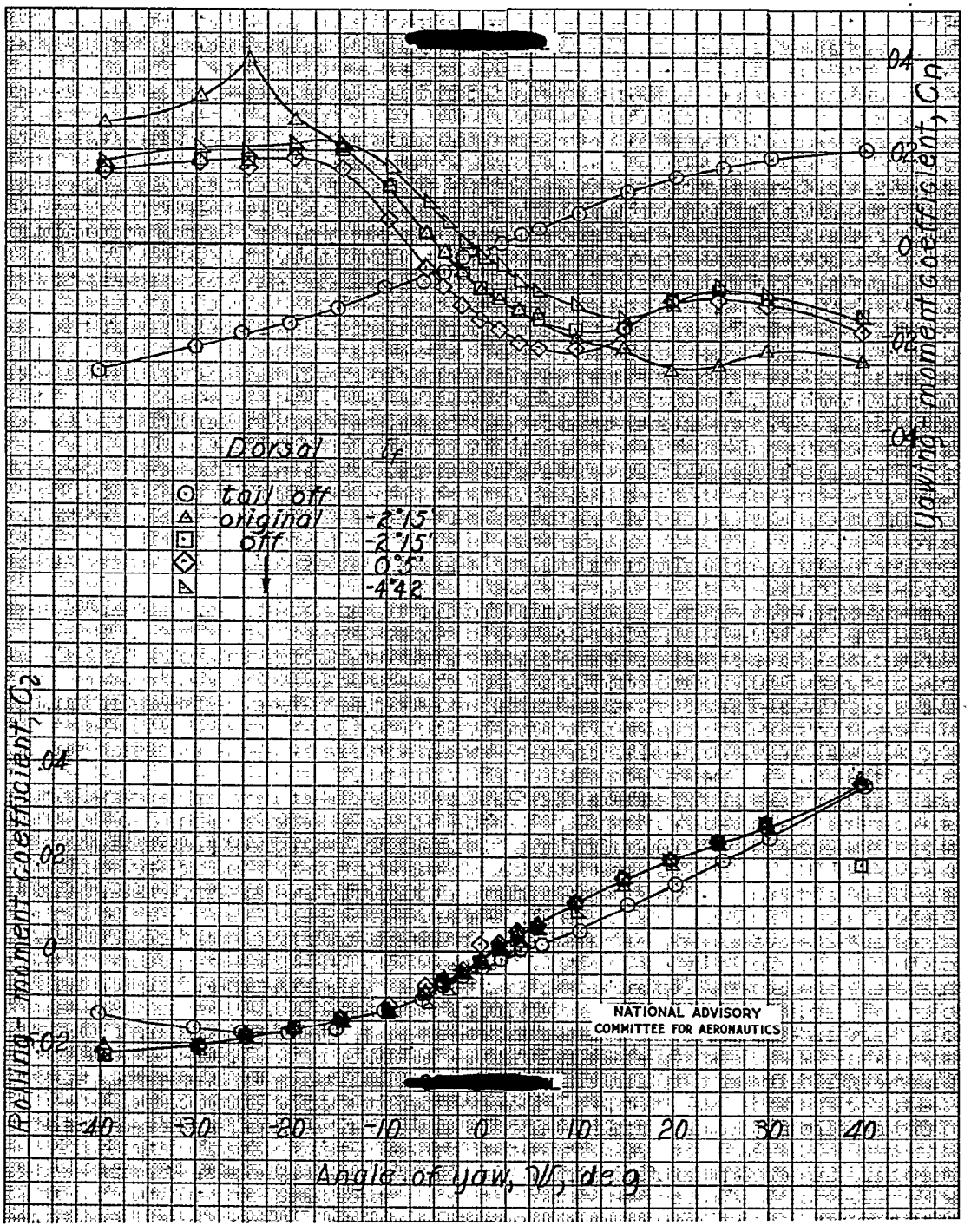

(d) $\alpha = 9.2^{\circ}$; 2.5-inch tip extension on vertical tail.

Figure 30.- Continued.

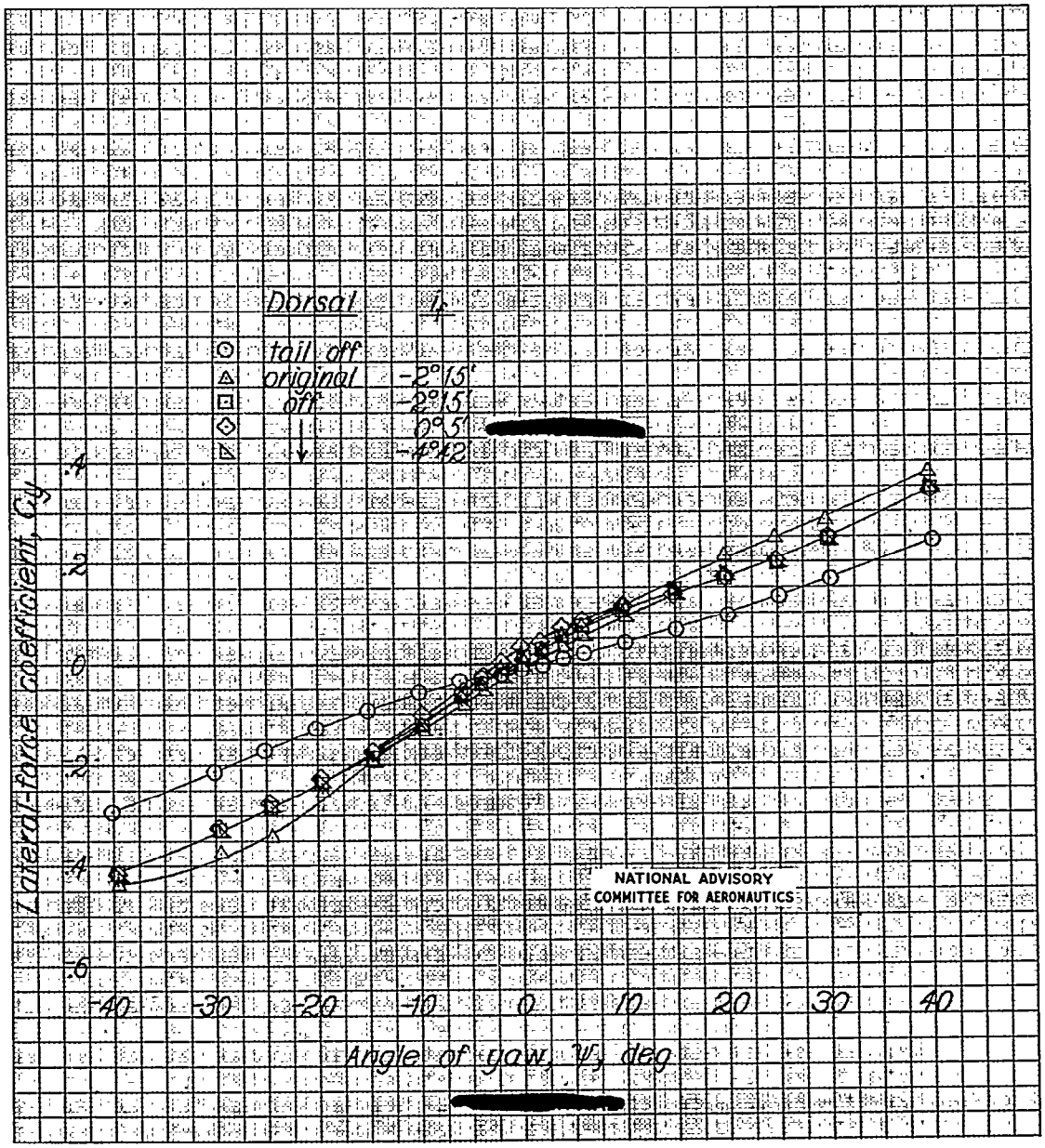

(d) Continued.

Figure 30.- Continued.

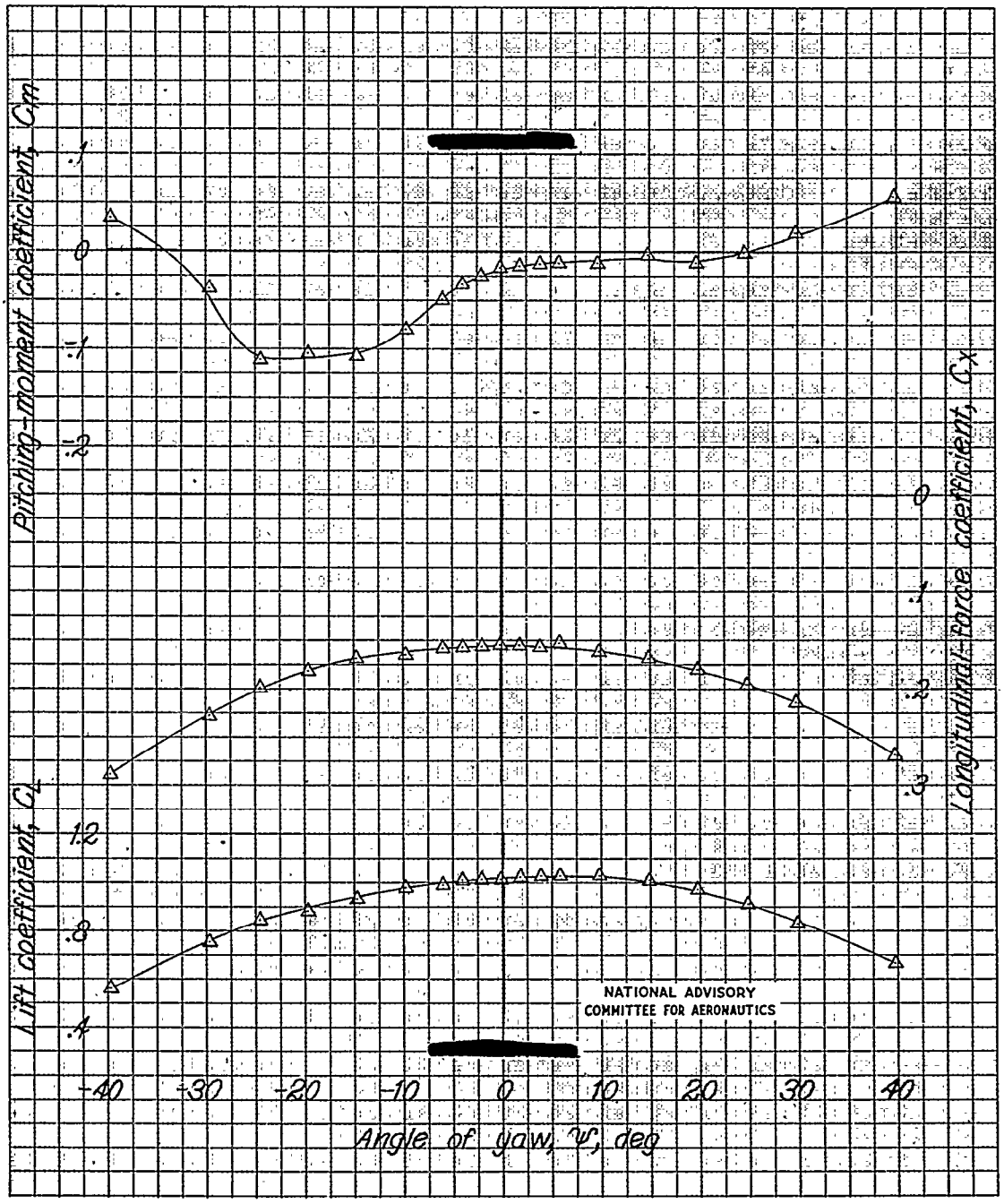

(d) Concluded; original dorsal fin; $i_{fin} = -2^{\circ}15'$.

Figure 30.- Continued.

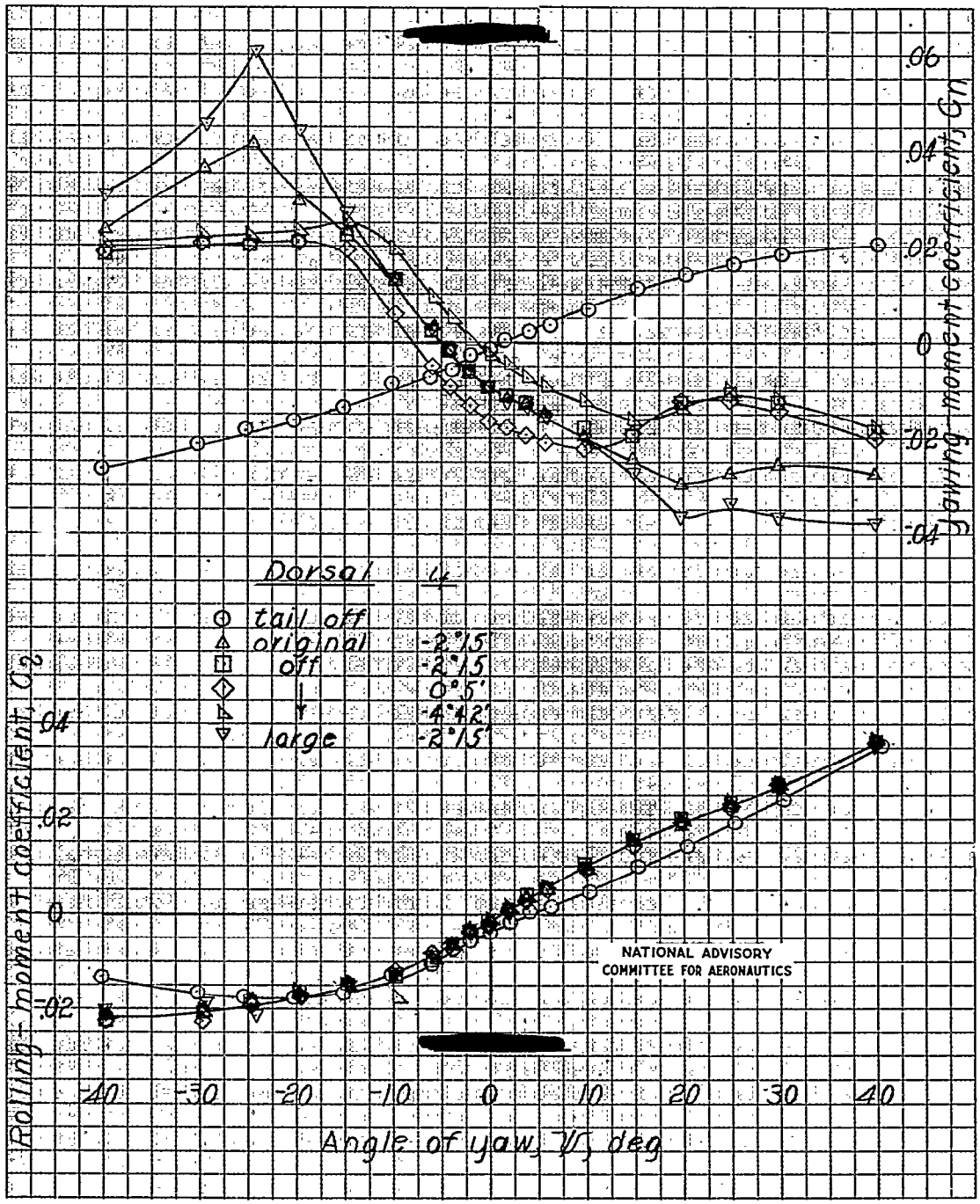

(e) α = 9.2°; 2-inch base extension on vertical tail.

Figure 30.- Continued.

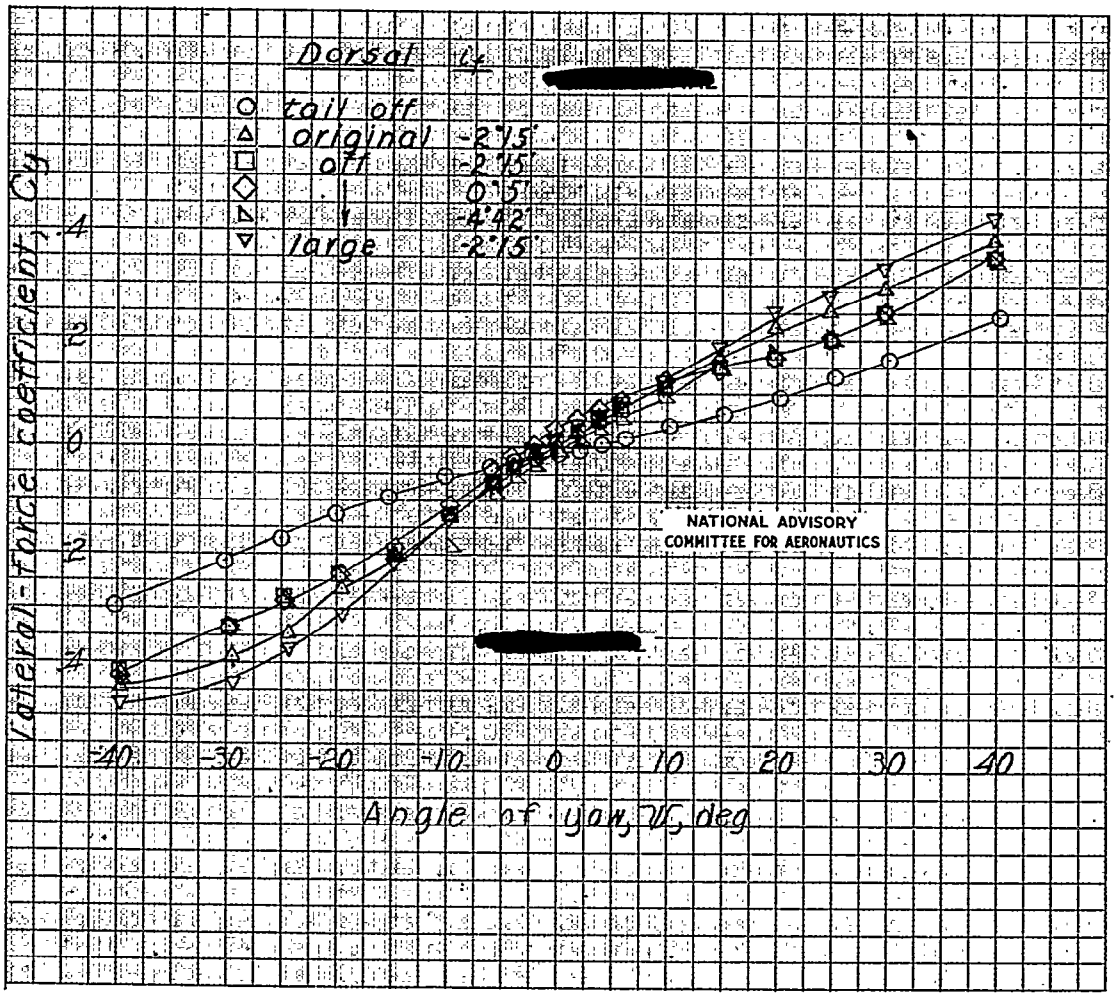

(e) Concluded.

Figure 30.- Continued.

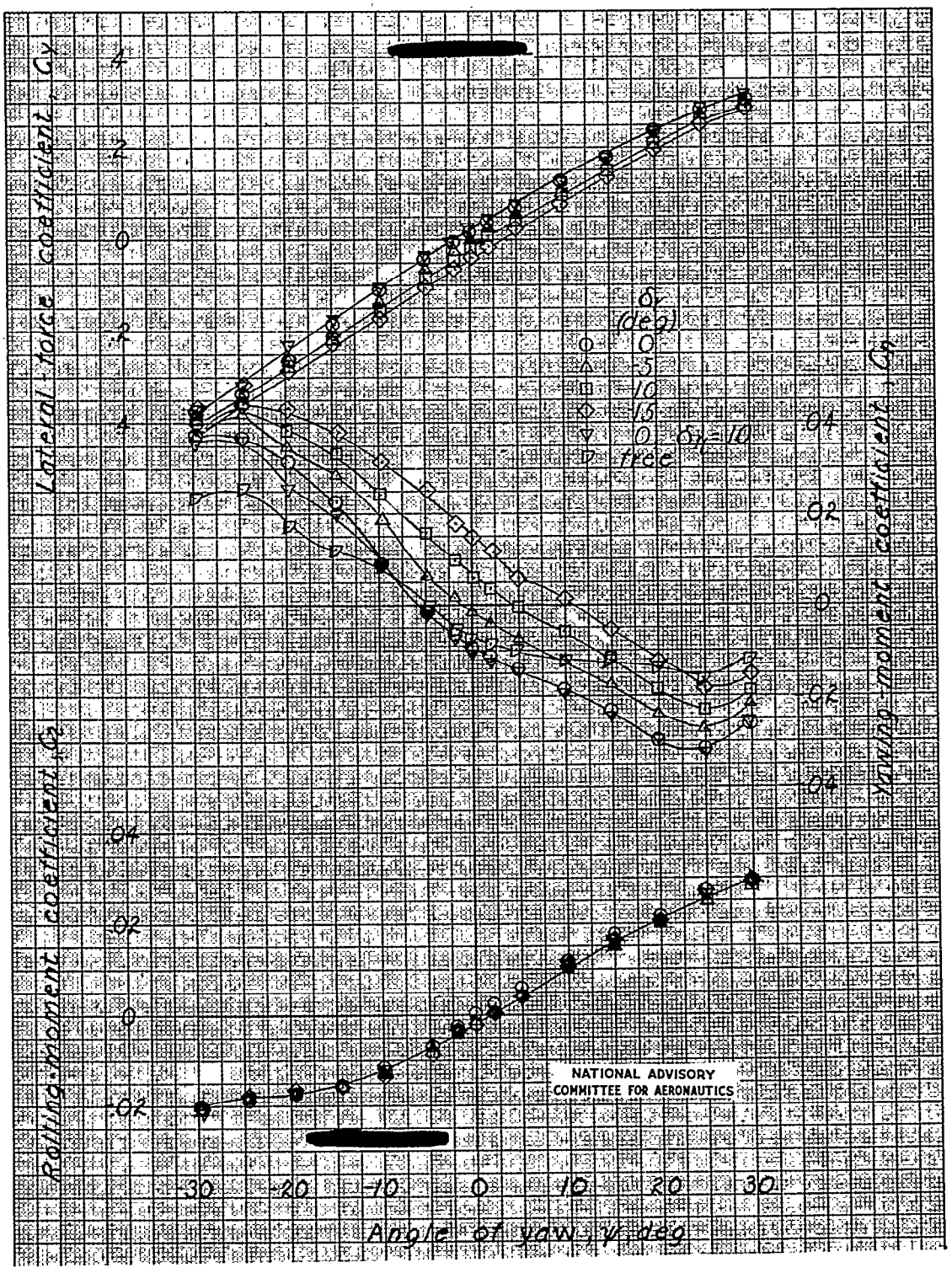

(f) $\alpha = 8.5^{\circ}$; 1.5-inch base extension on vertical tail; original dorsal fin.

Figure 30.- Continued.

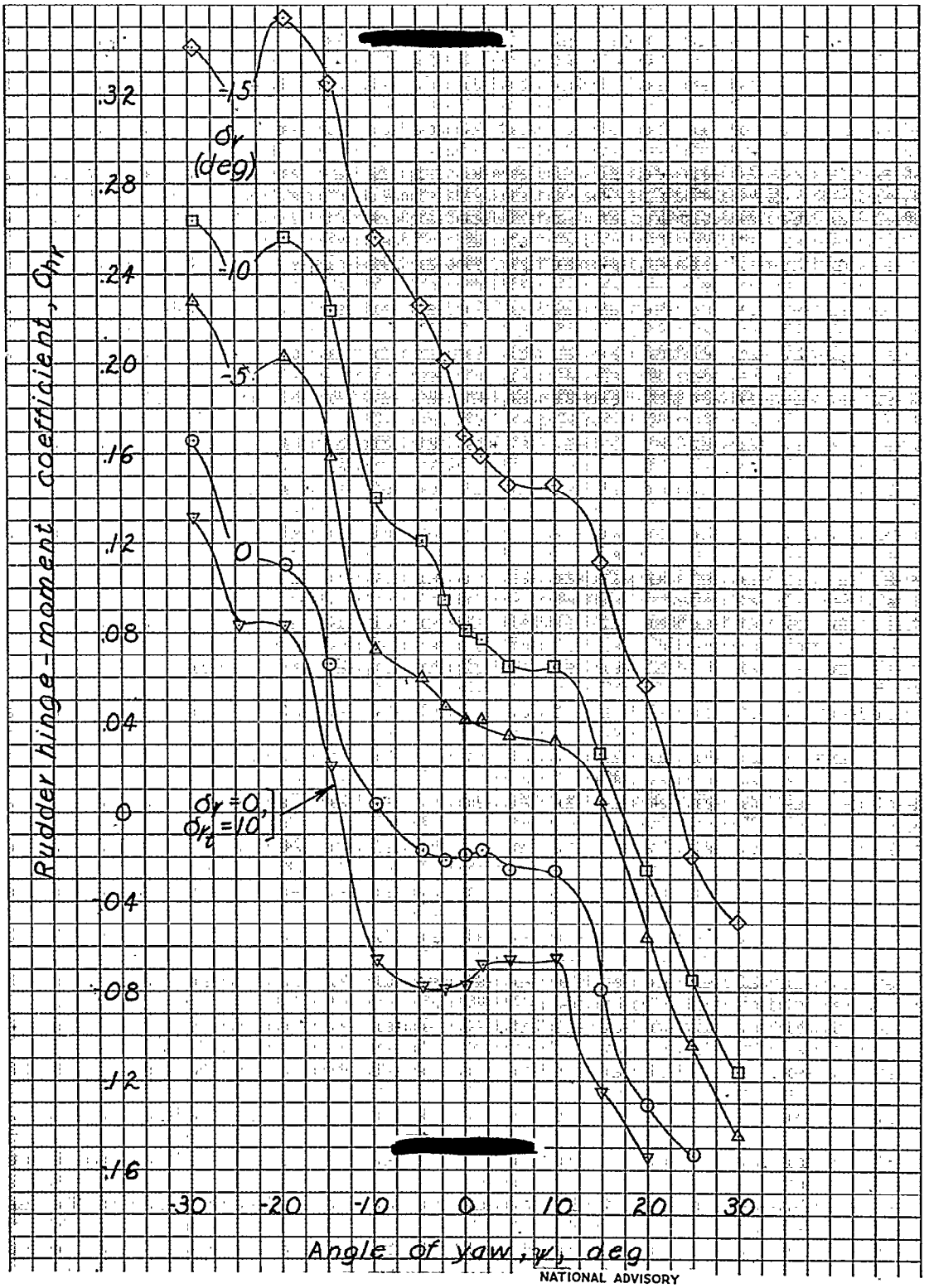

NATIONAL ADVISORY COMMITTEE FOR AERONAUTICS

(f) Concluded.

Figure 30.- Concluded.

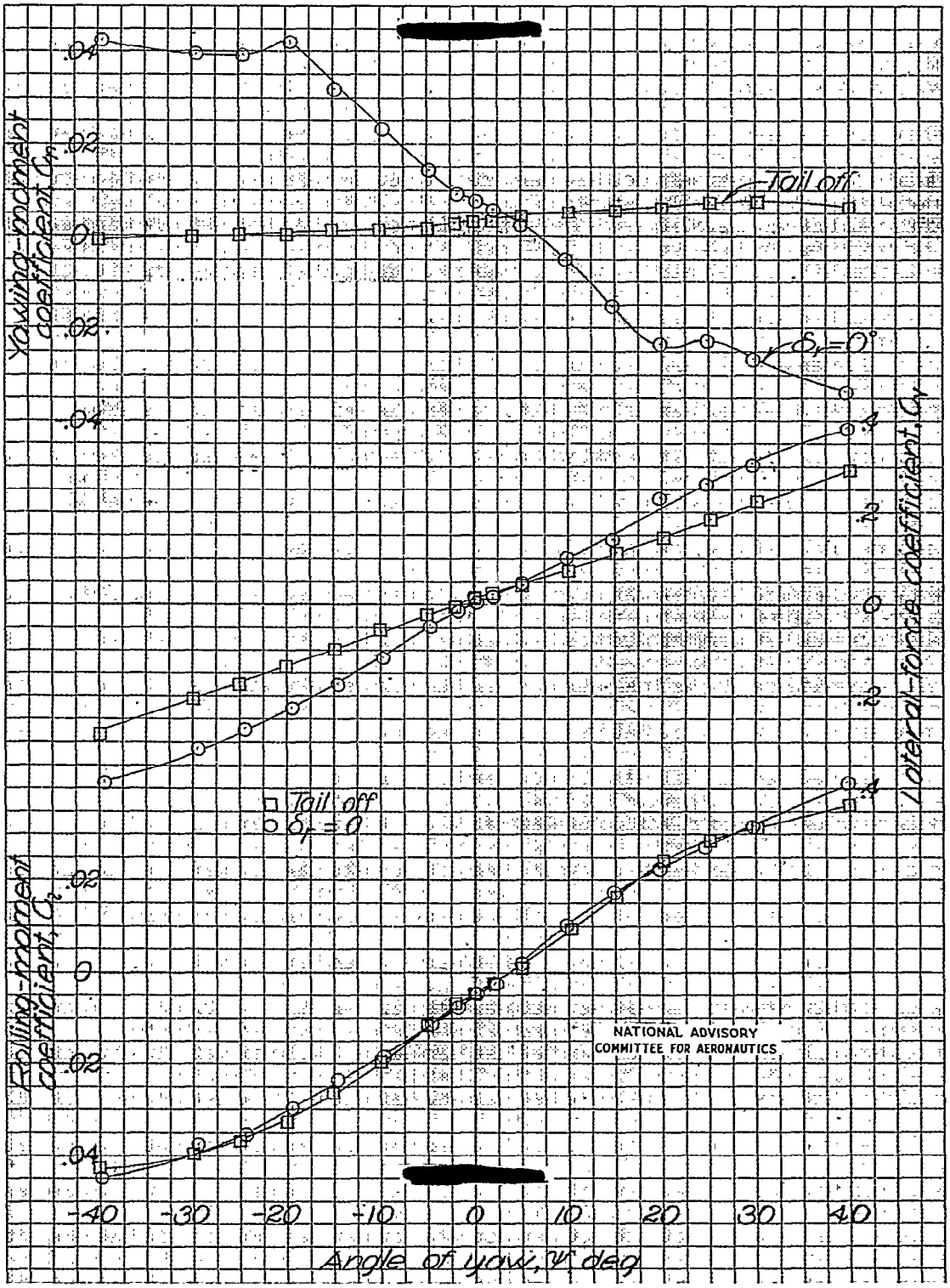

(a) $\alpha = 11.8°$; $i_{fin} = -2°15'$; original vertical tail.

Figure 31.- Aerodynamic characteristics in yaw of a 1/8-scale model of the Grumman XTB3F-1 airplane. Landing configuration; original dorsal fin.

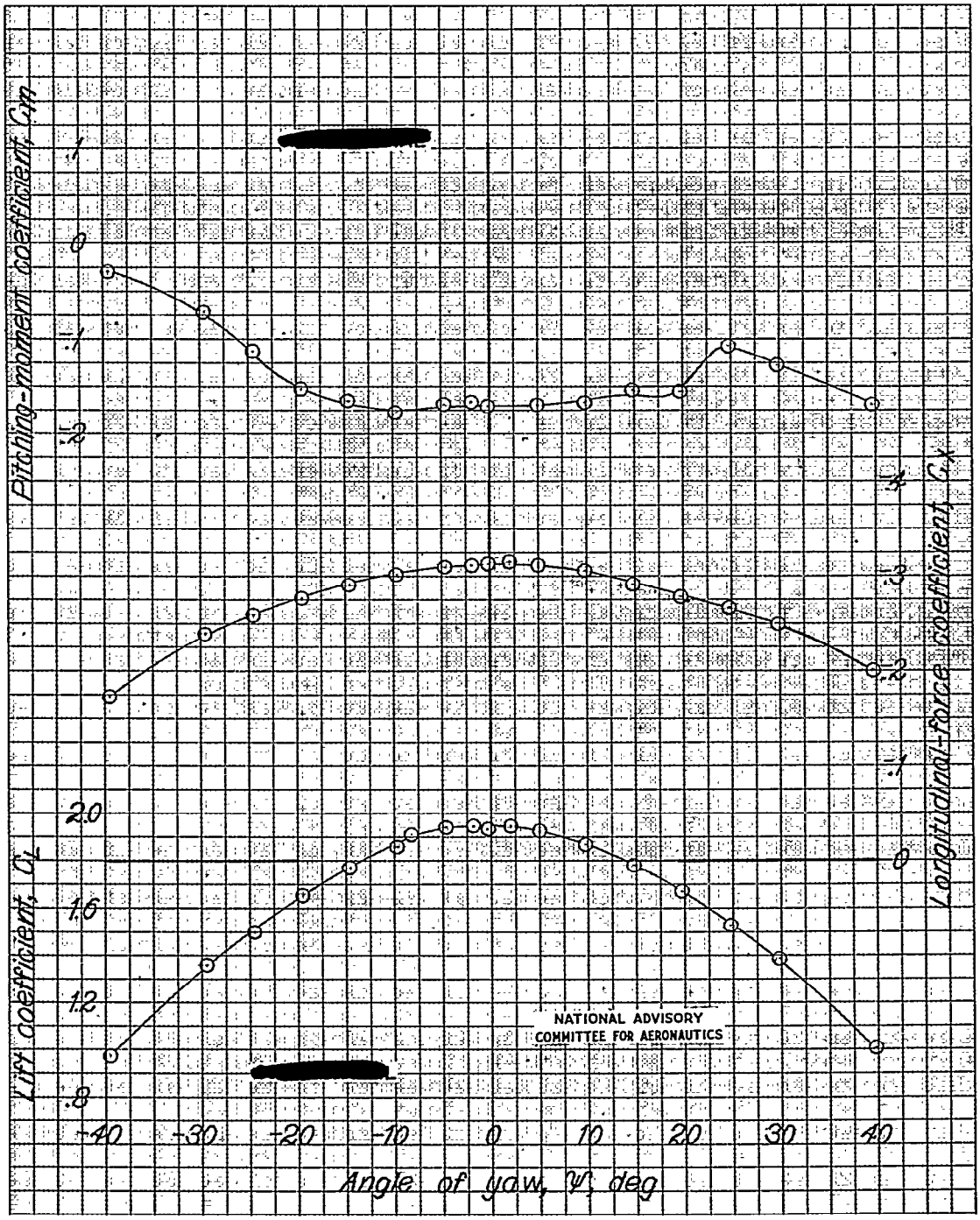

(a) Concluded.

Figure 31.- Continued.

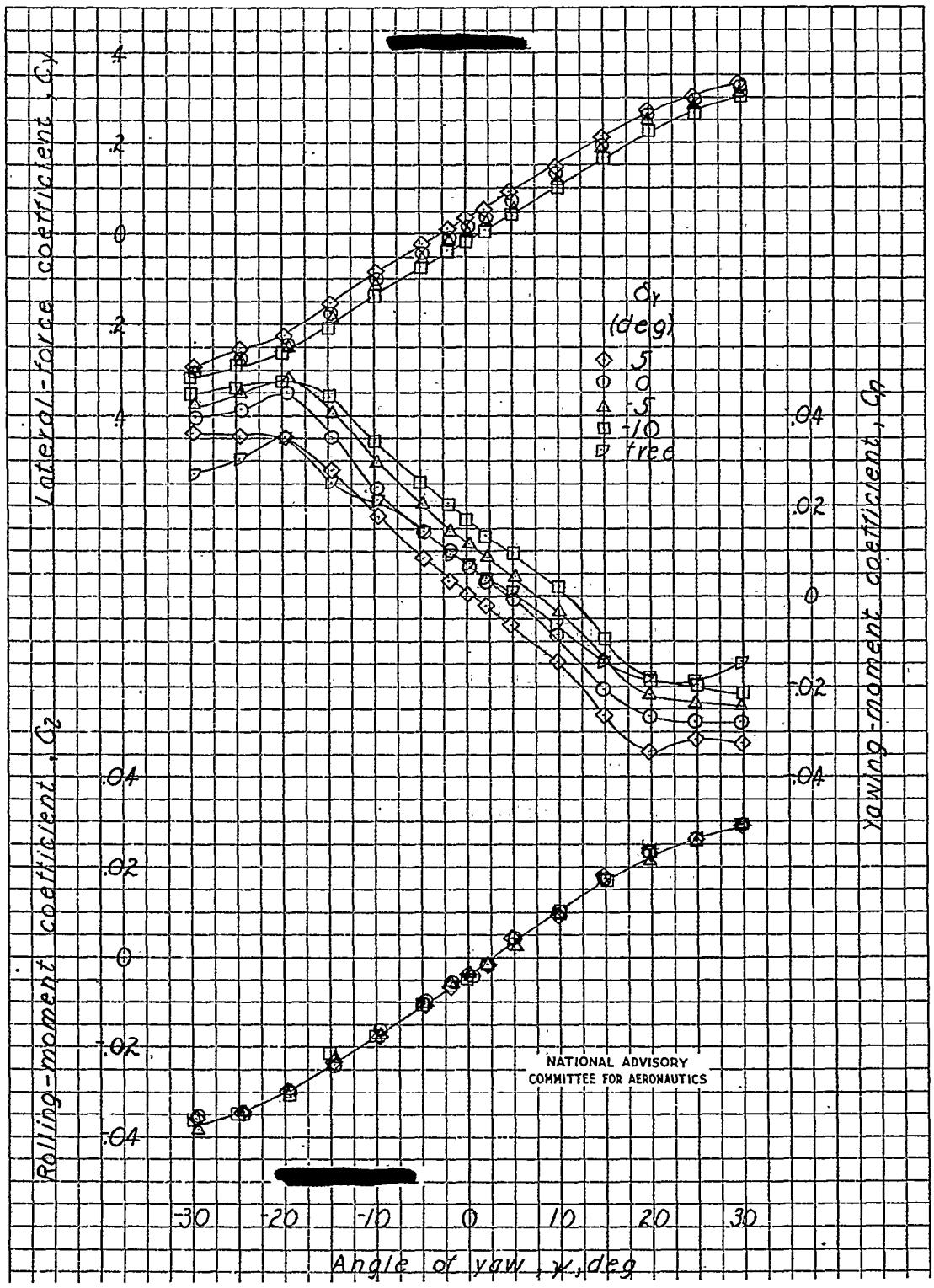

(b) $\alpha = 9.6^{\circ}$; 1.5-inch base extension on vertical tail.

Figure 31.- Continued.

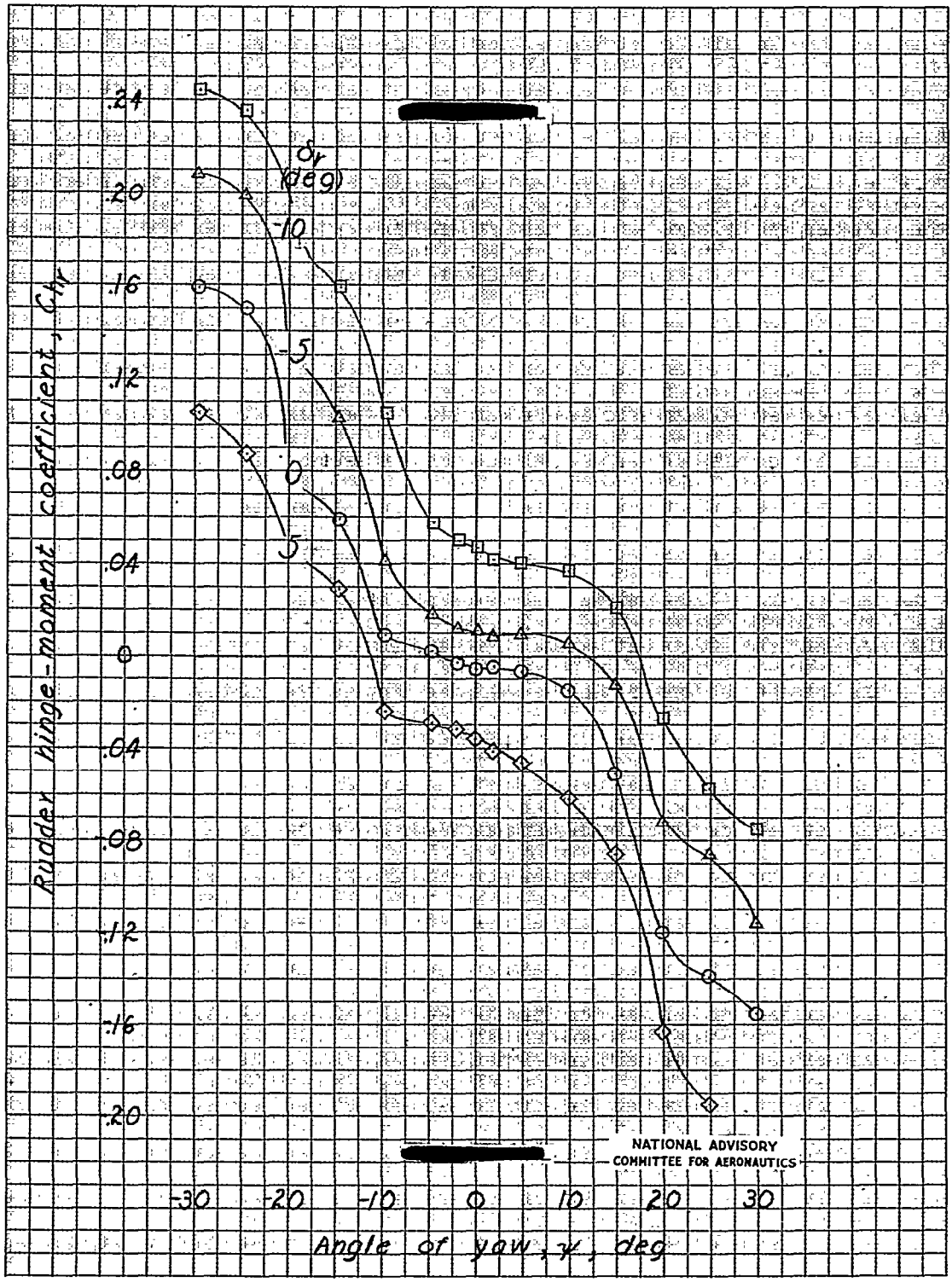

(b) Continued.

Figure 31.- Continued.

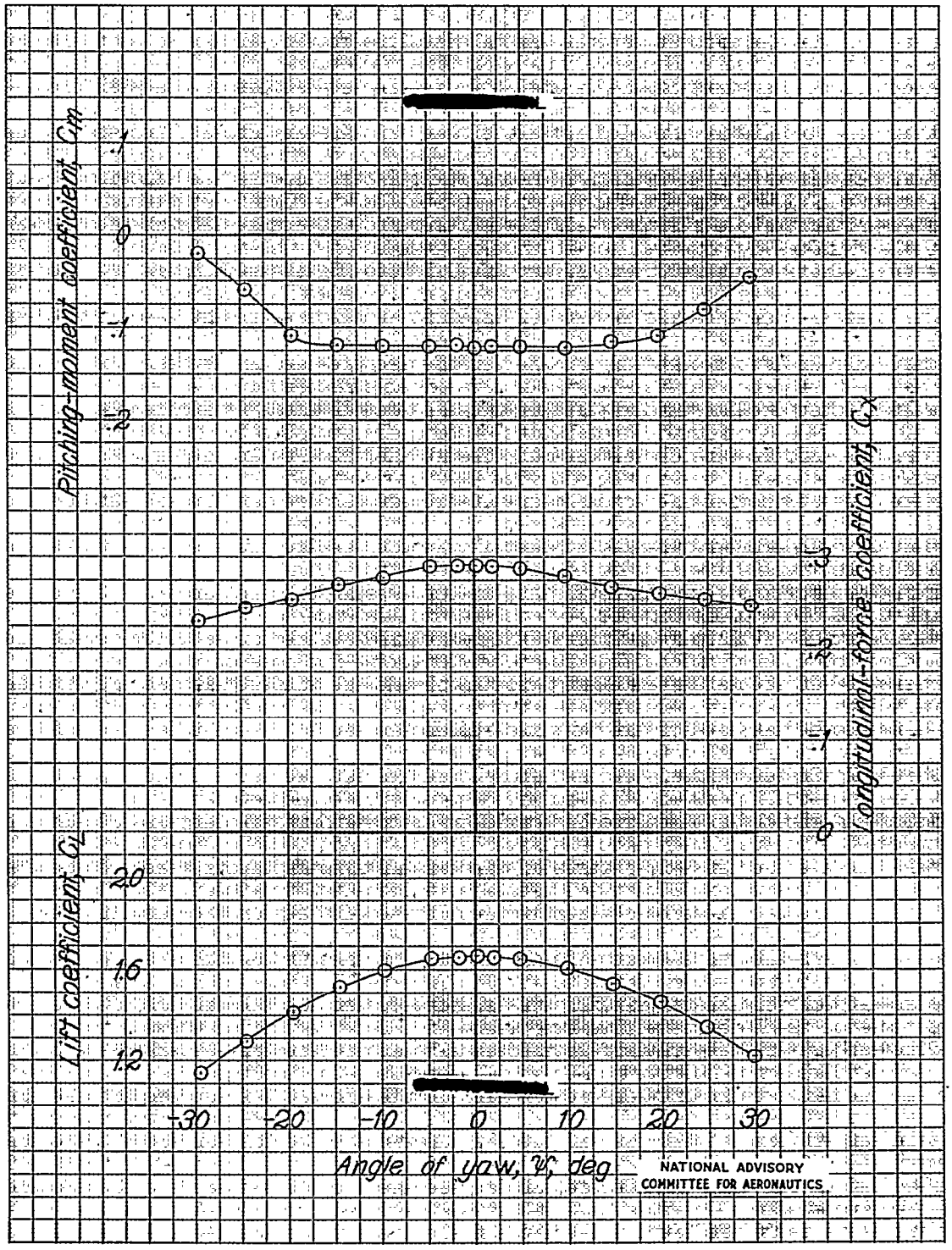

(b) Concluded.

Figure 31.- Concluded.

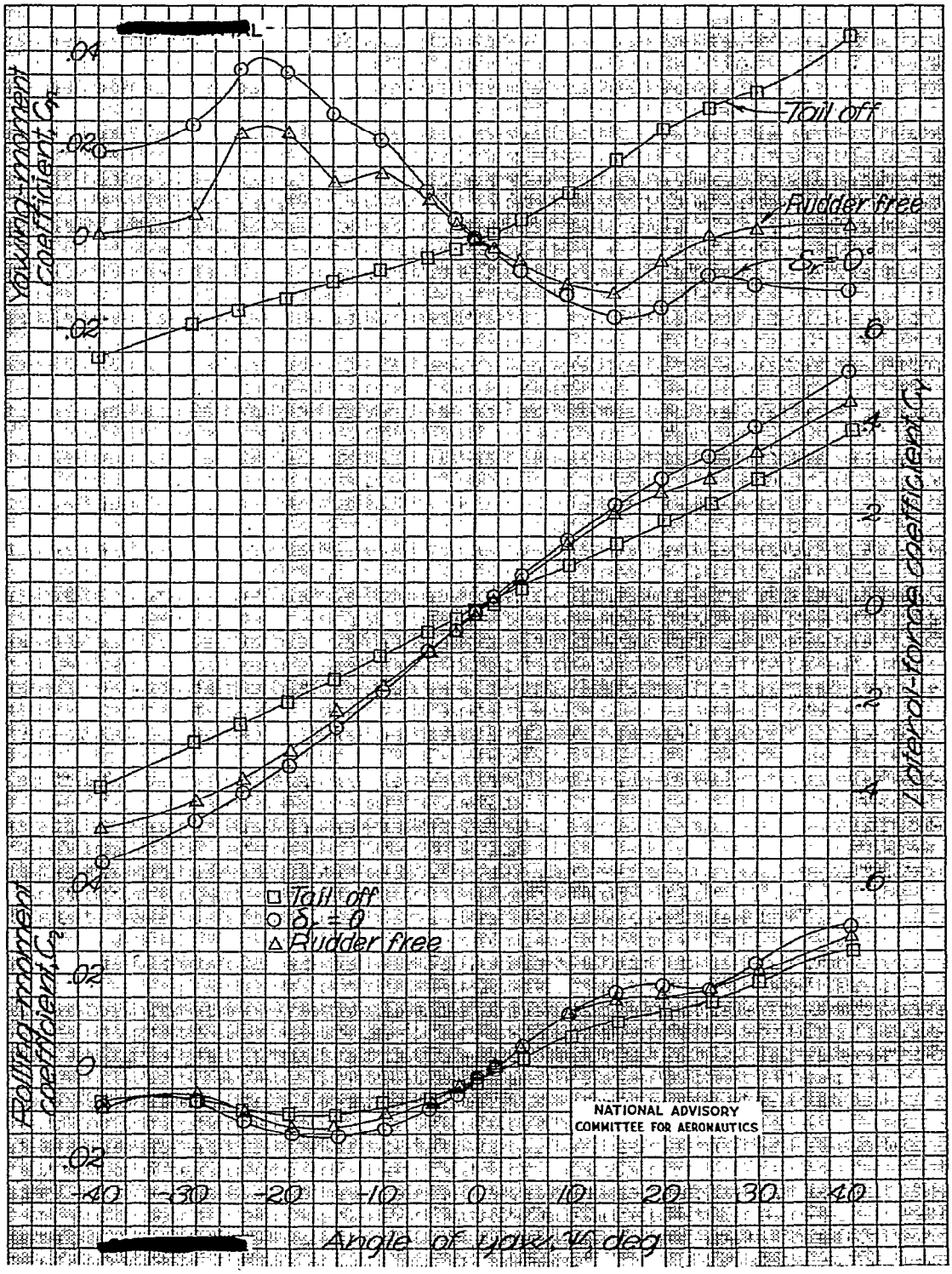

(a) $\alpha = 5.6^{\circ}$; $i_{fin} = -2^{\circ}15'$; original vertical tail; original dorsal fin.

Figure 32.- Aerodynamic characteristics in yaw of a 1/8-scale model of the Grumman XTB3F-1 airplane. Approach configuration.

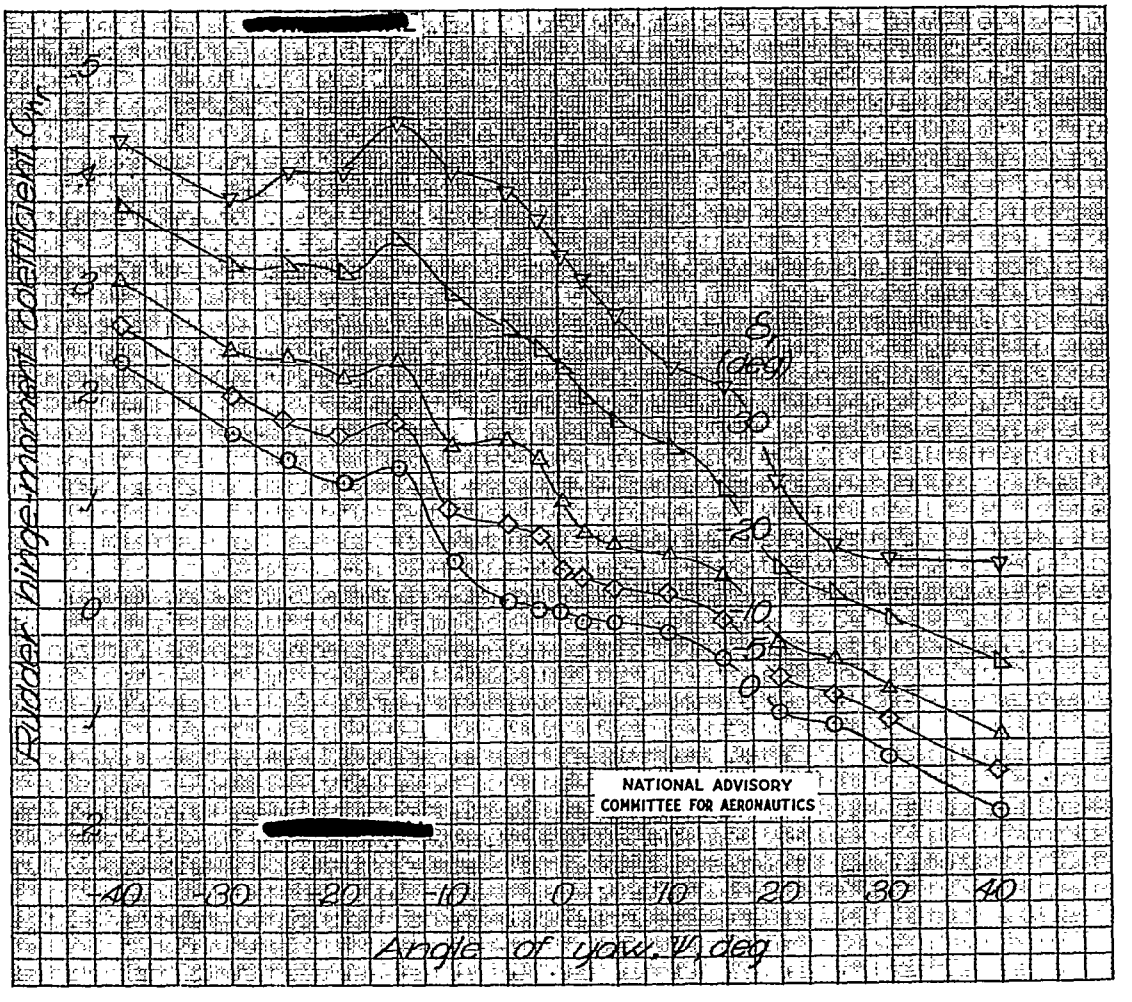

(a) Continued.

Figure 32.- Continued.

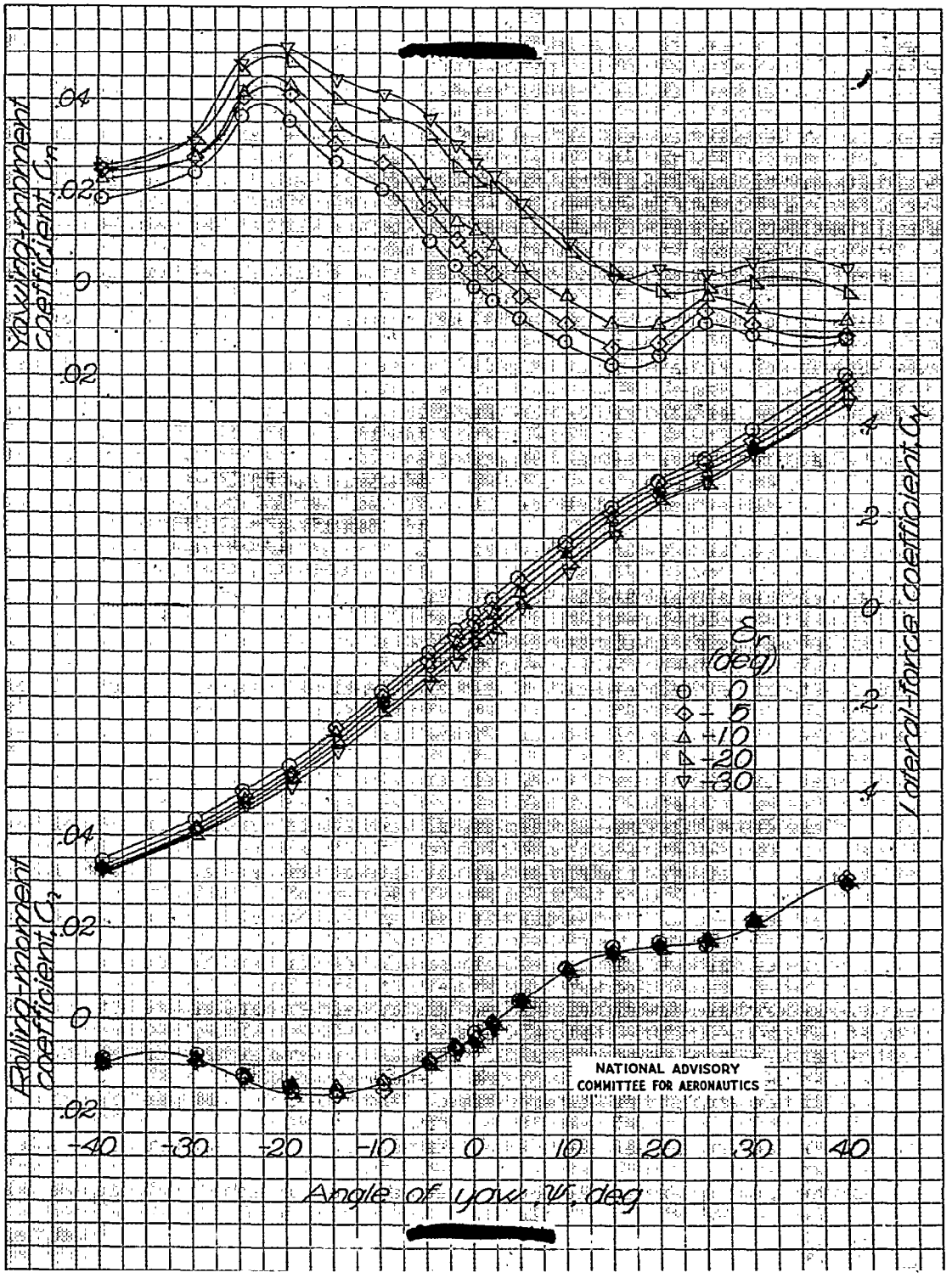

(a) Continued.

Figure 32.- Continued.

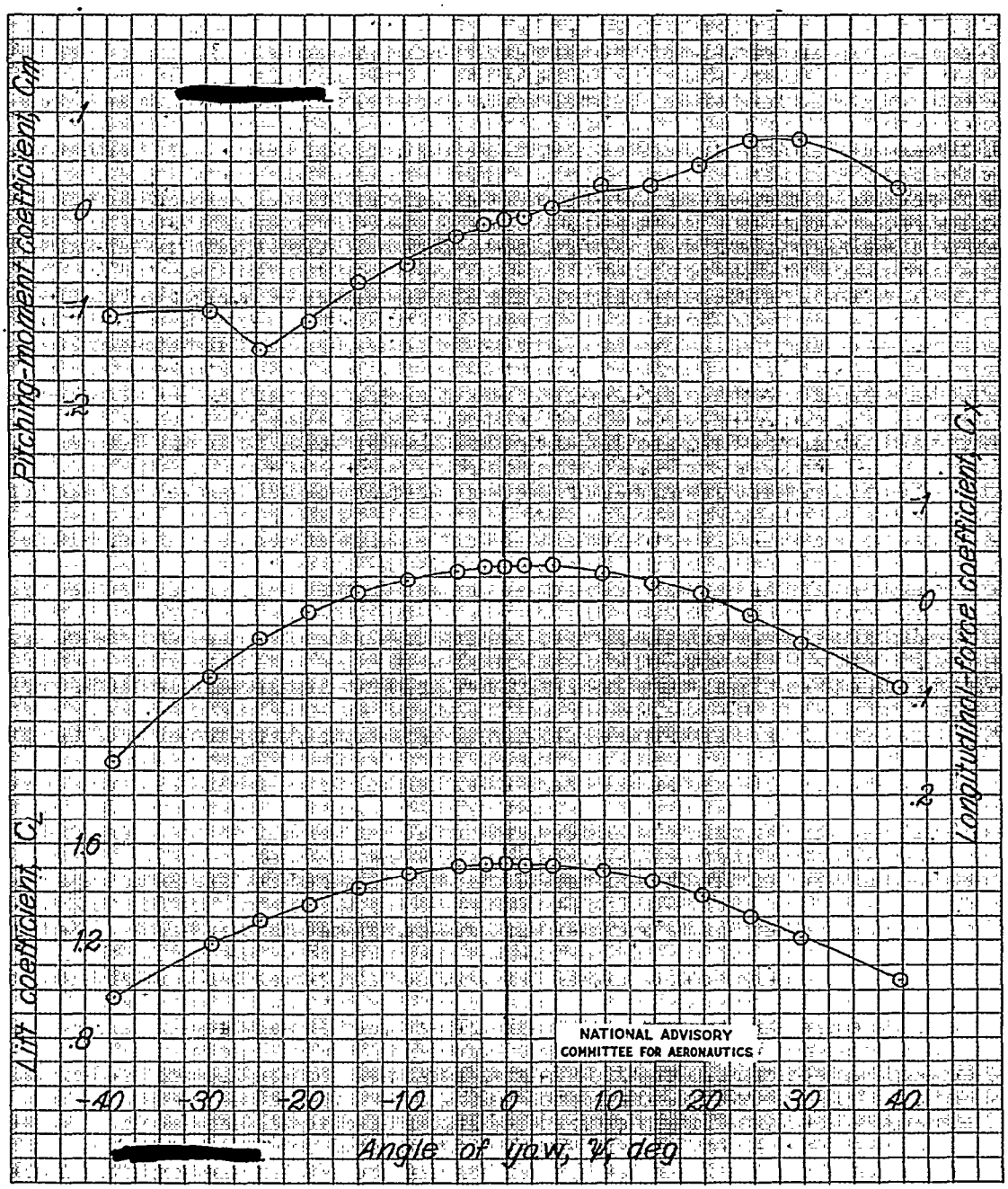

(a) Concluded.

Figure 32.- Continued.

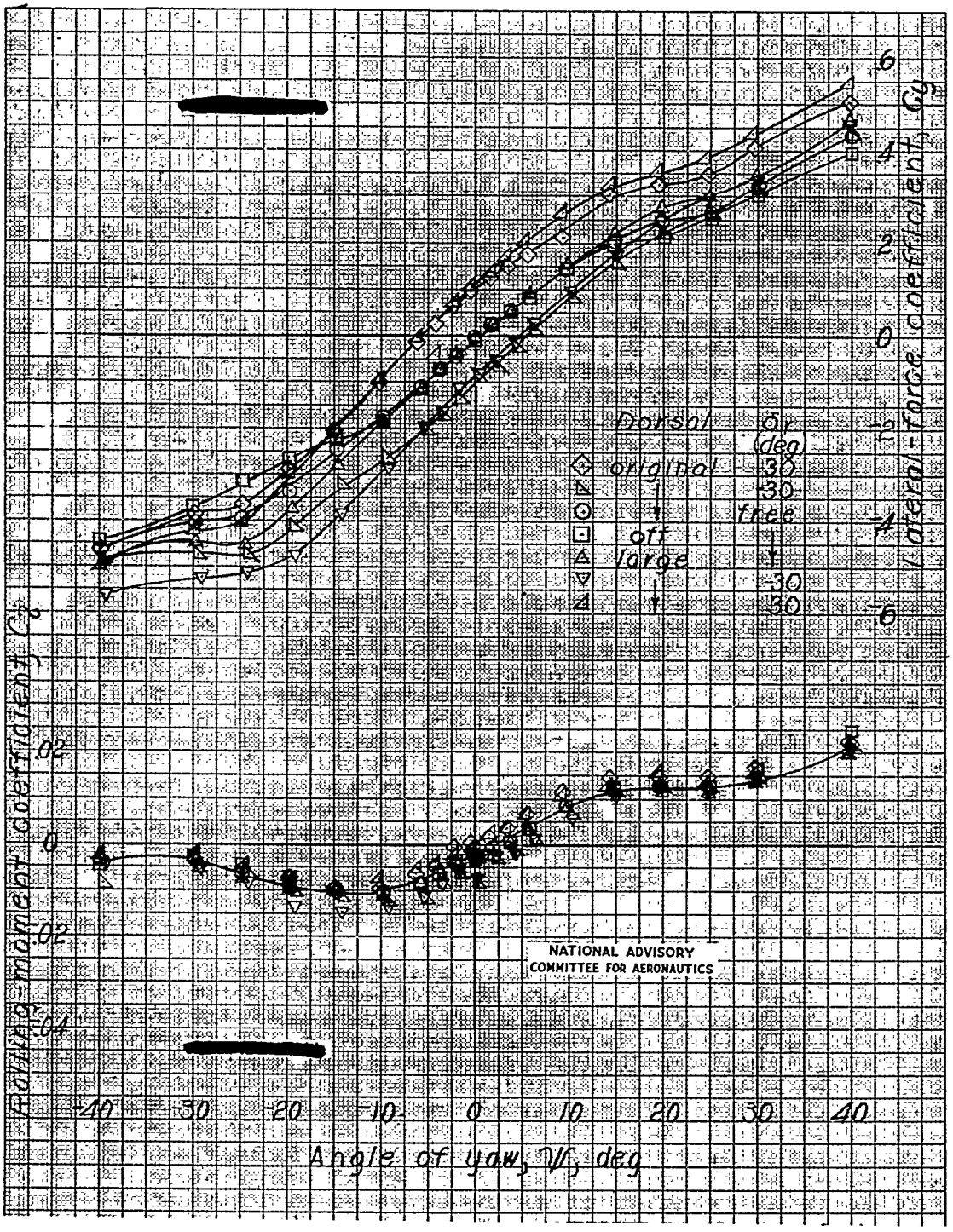

(b) $\alpha = 7.3^{\circ}$; $i_{fin} = -2^{\circ}15'$; 2-inch base extension on vertical tail.

Figure 32.- Continued.

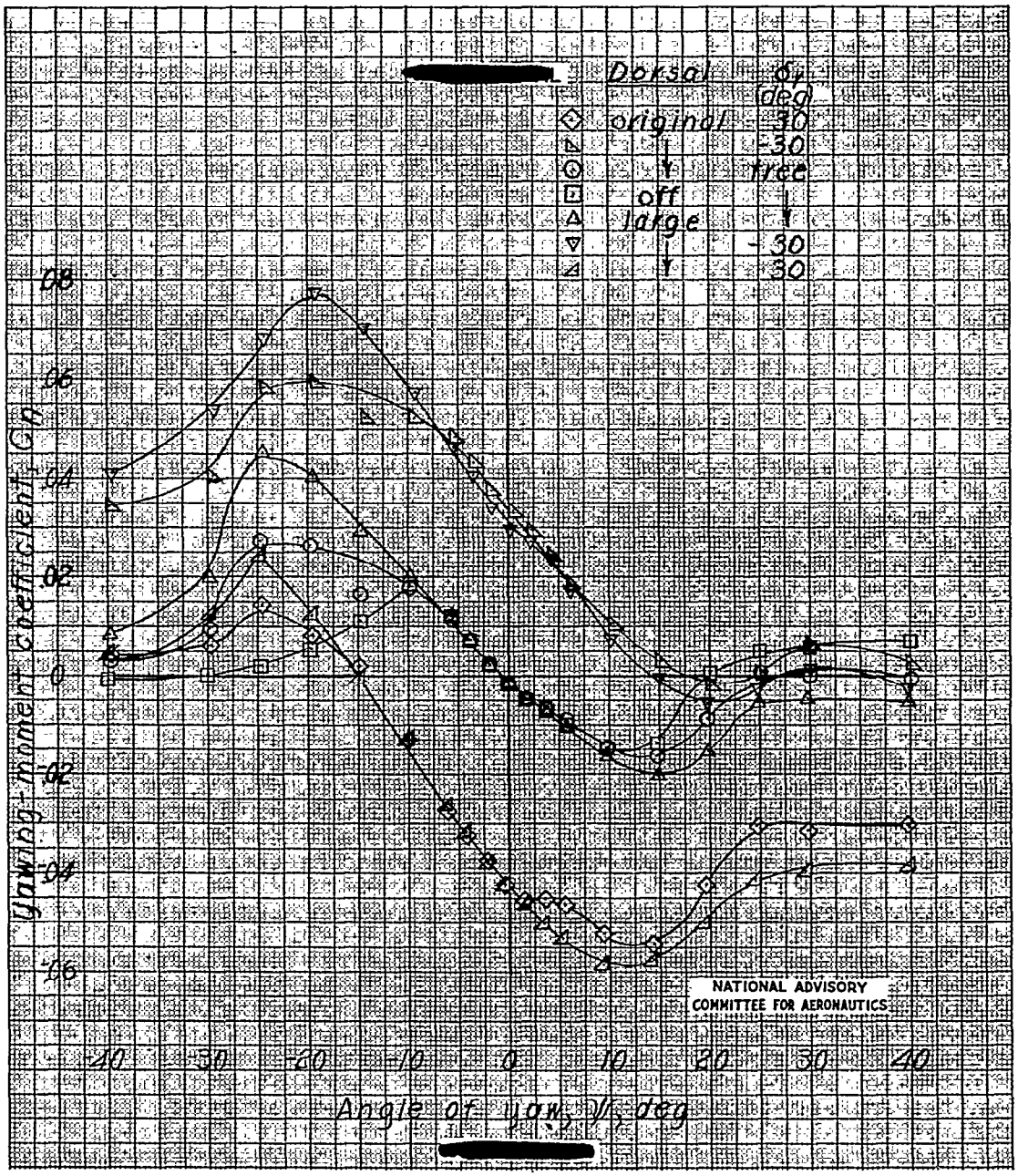

(b) Continued.

Figure 32.- Continued.

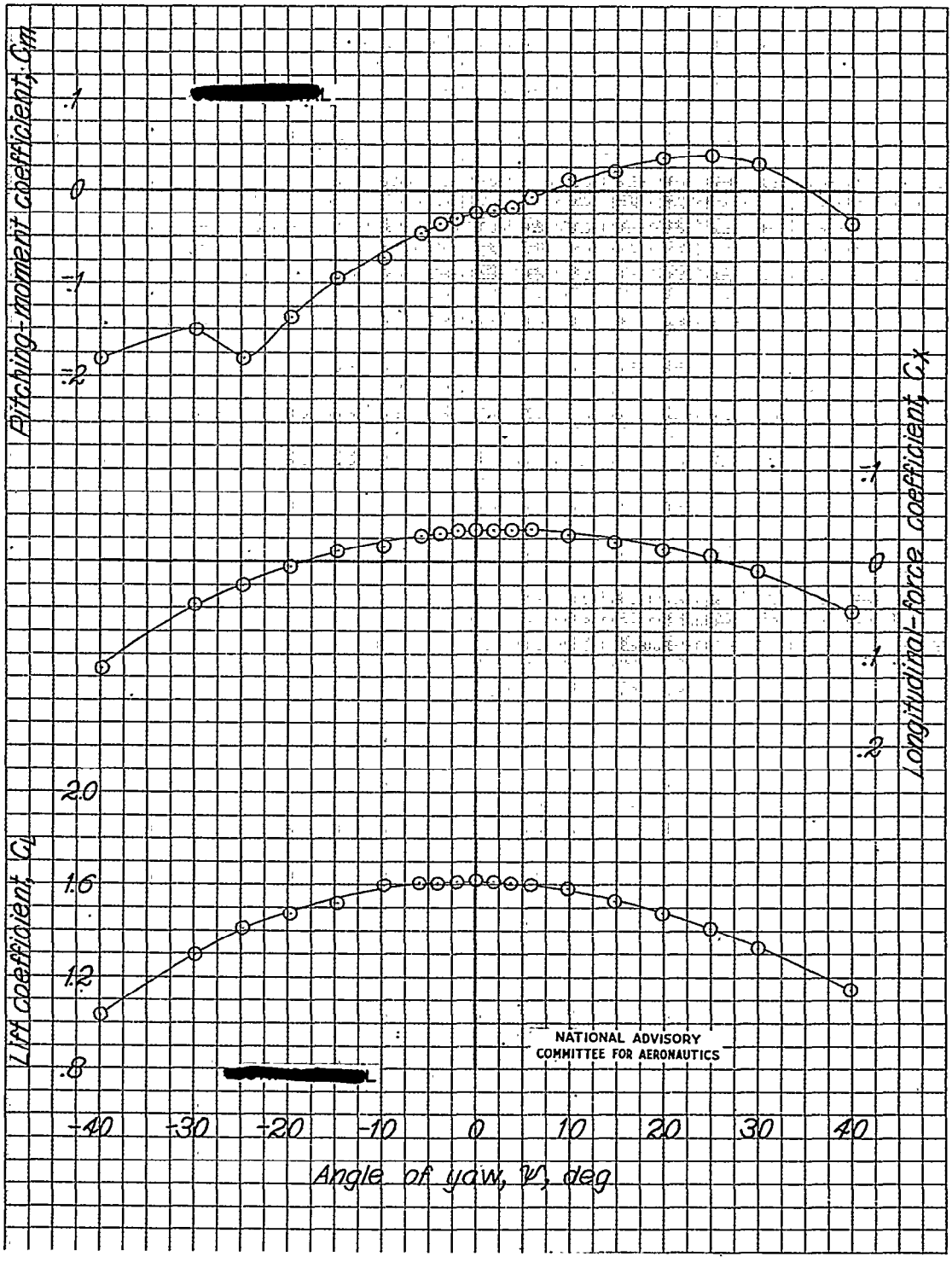

(b) Concluded.

Figure 32.- Continued.

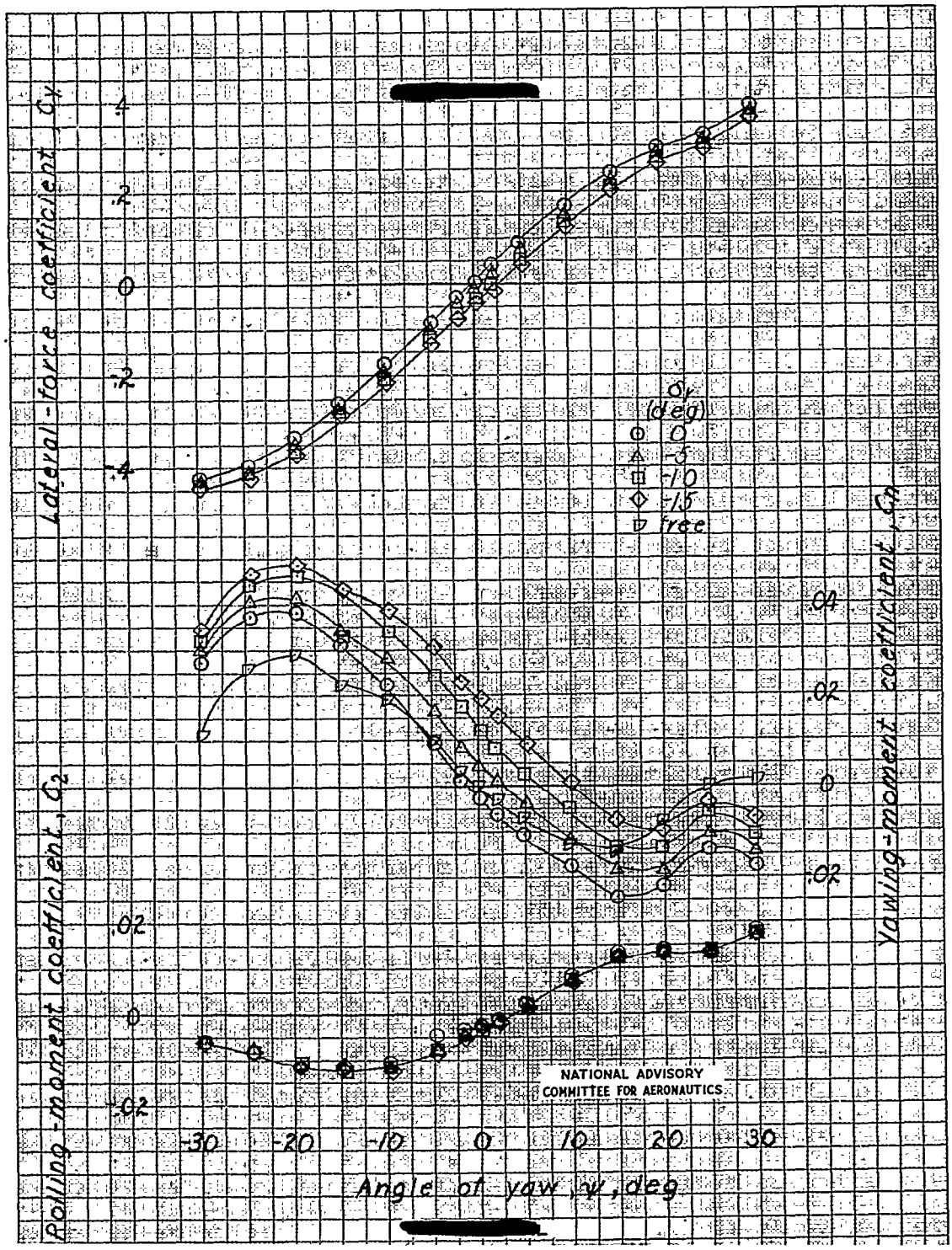

(c) $\alpha = 6.7^{\circ}$; 1.5-inch base extension on vertical tail; original dorsal fin.

Figure 32.- Continued.

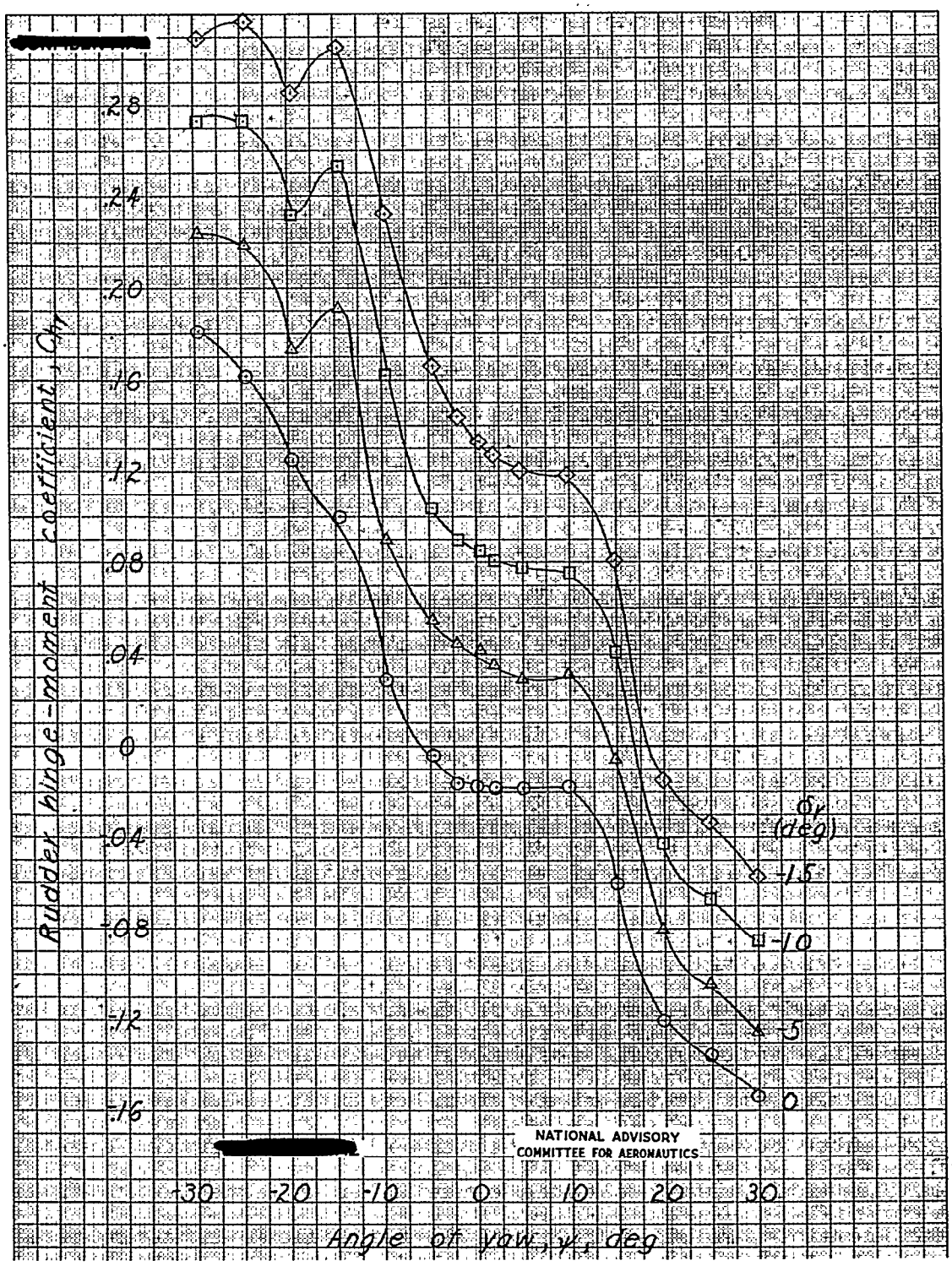

(c) Concluded.

Figure 32.- Concluded.

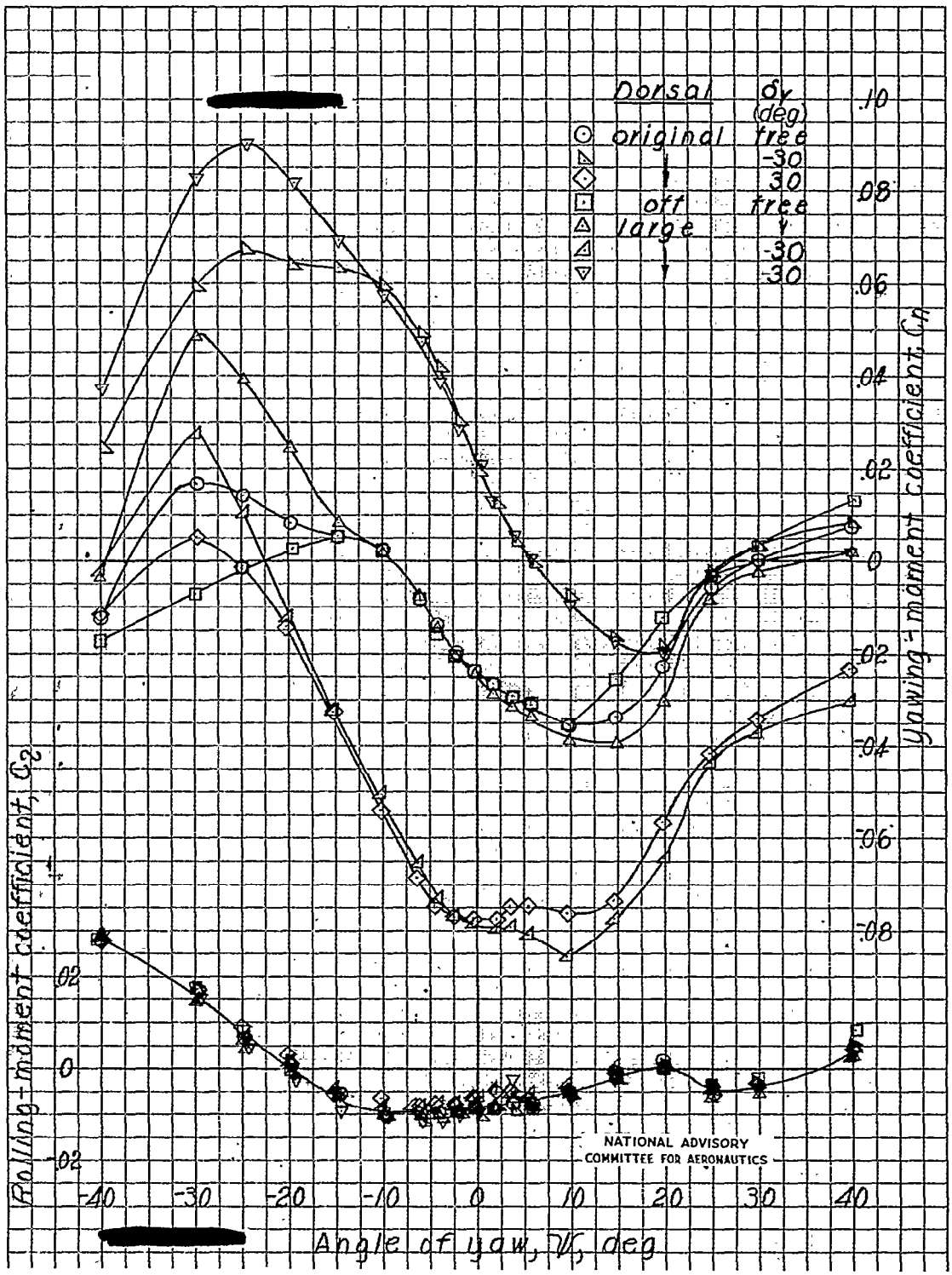

(a) $\alpha = 10.1^{\circ}$; 2-inch base extension on vertical tail.

Figure 33.- Aerodynamic characteristics in yaw of a 1/8-scale model of the Grumman XF3F-1 airplane. Wave-off configuration.

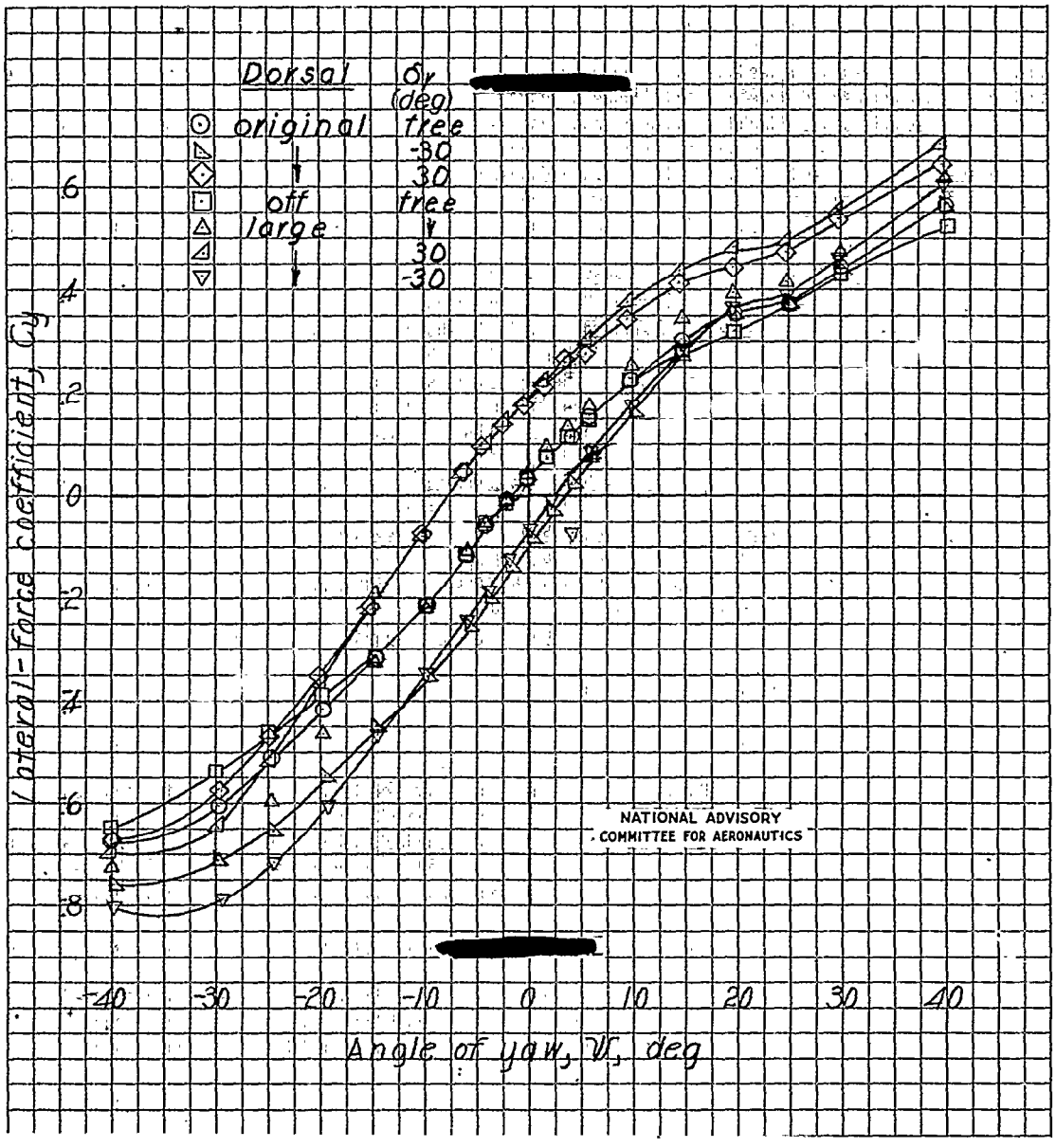

(a) Continued.

Figure 33.- Continued.

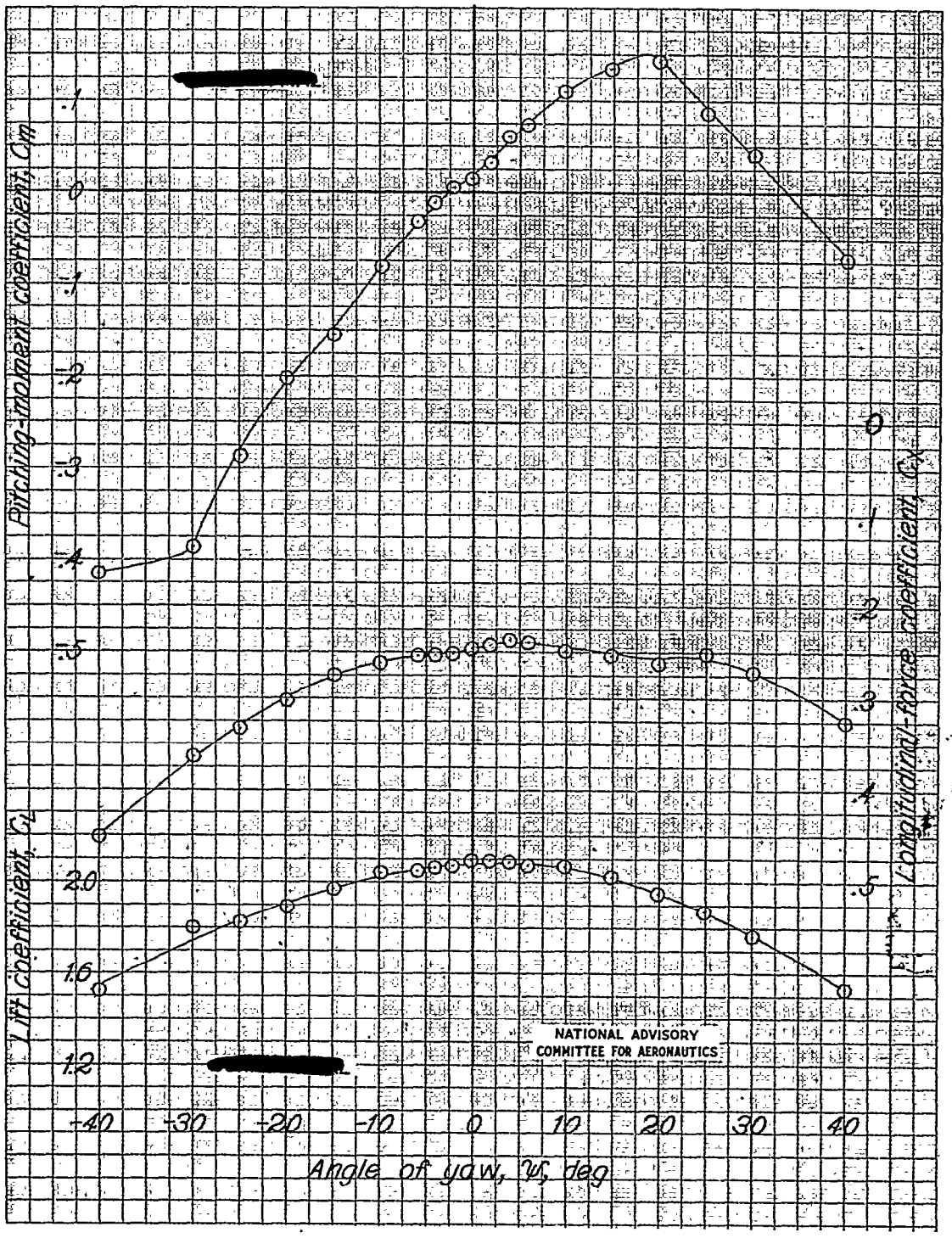

(a) Concluded; original dorsal fin.

Figure 33.- Continued.

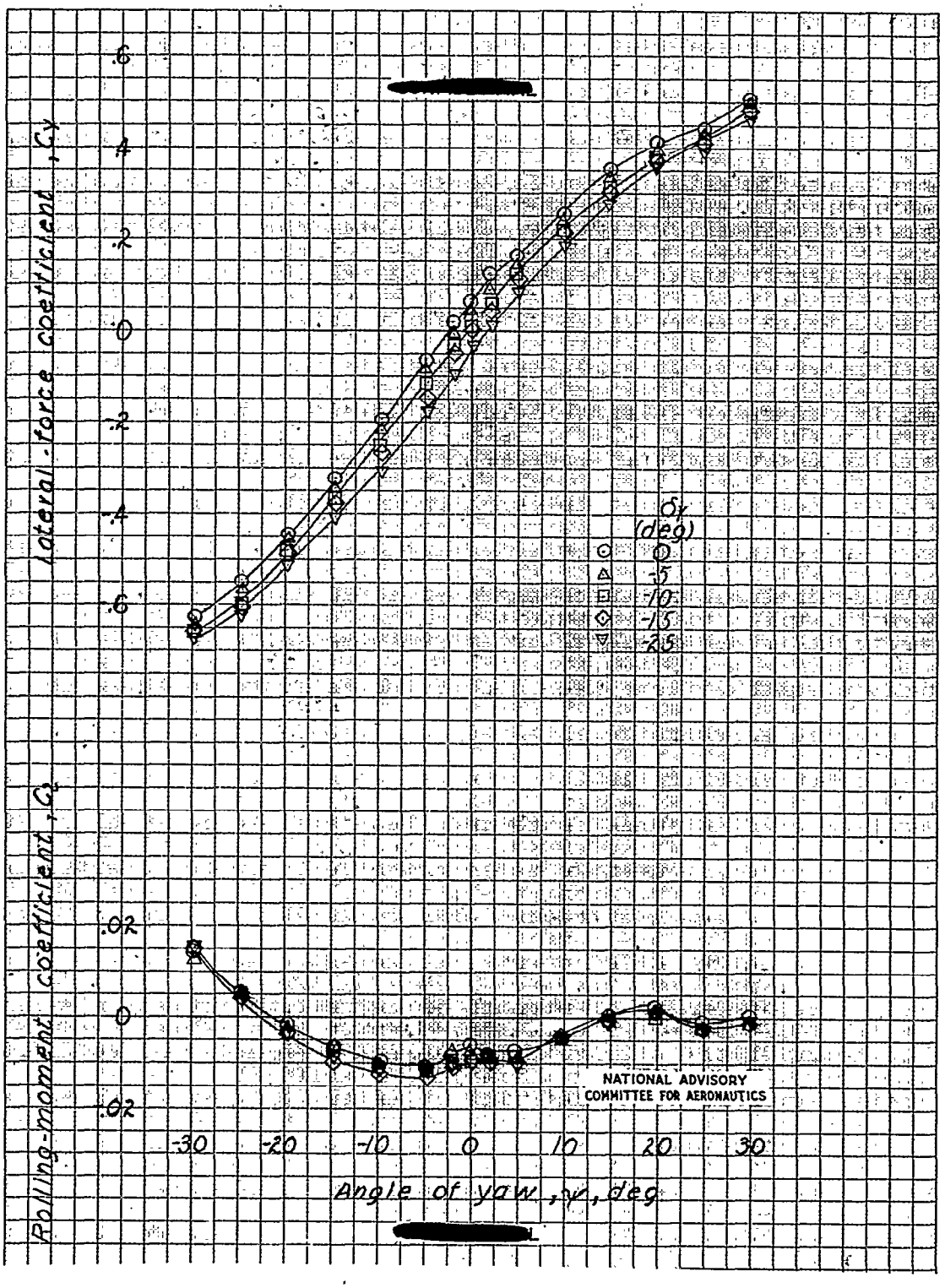

(b) $\alpha = 8.7^{\circ}$; 1.5-inch base extension on vertical tail.

Figure 33.- Continued.

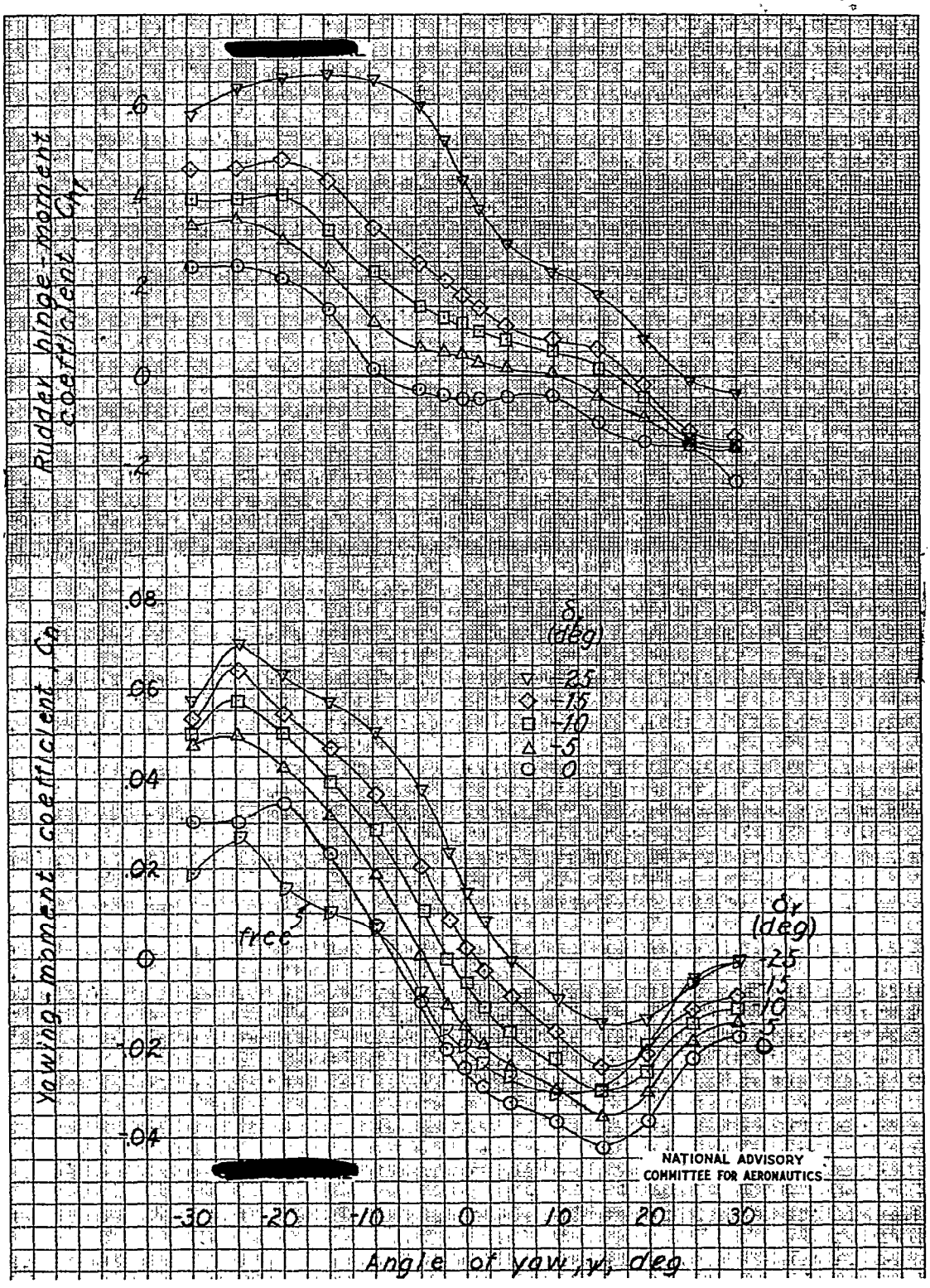

(b) Continued.

Figure 33.- Continued.

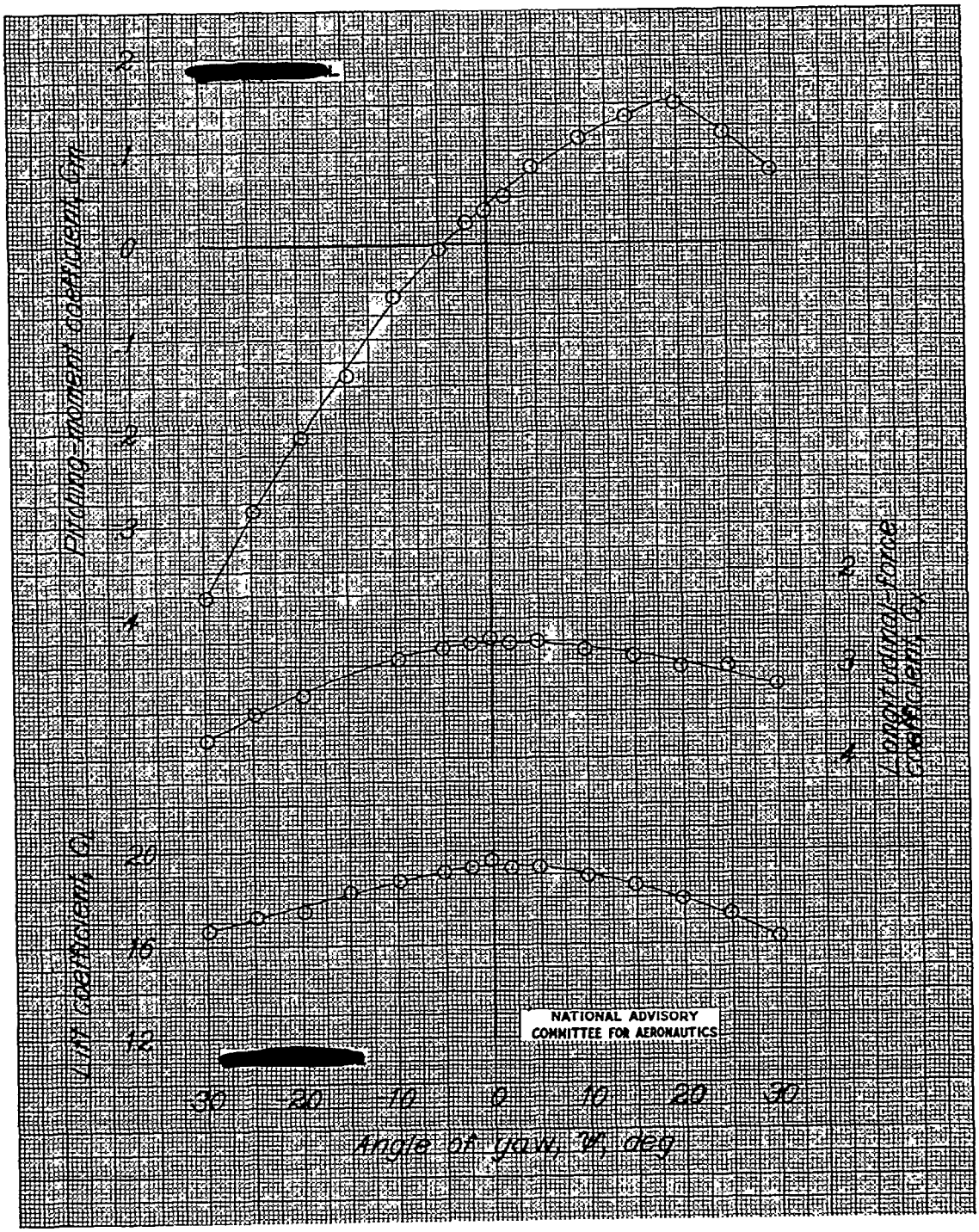

(b) Concluded; $\delta_r = 0^\circ$.

Figure 33.- Concluded.

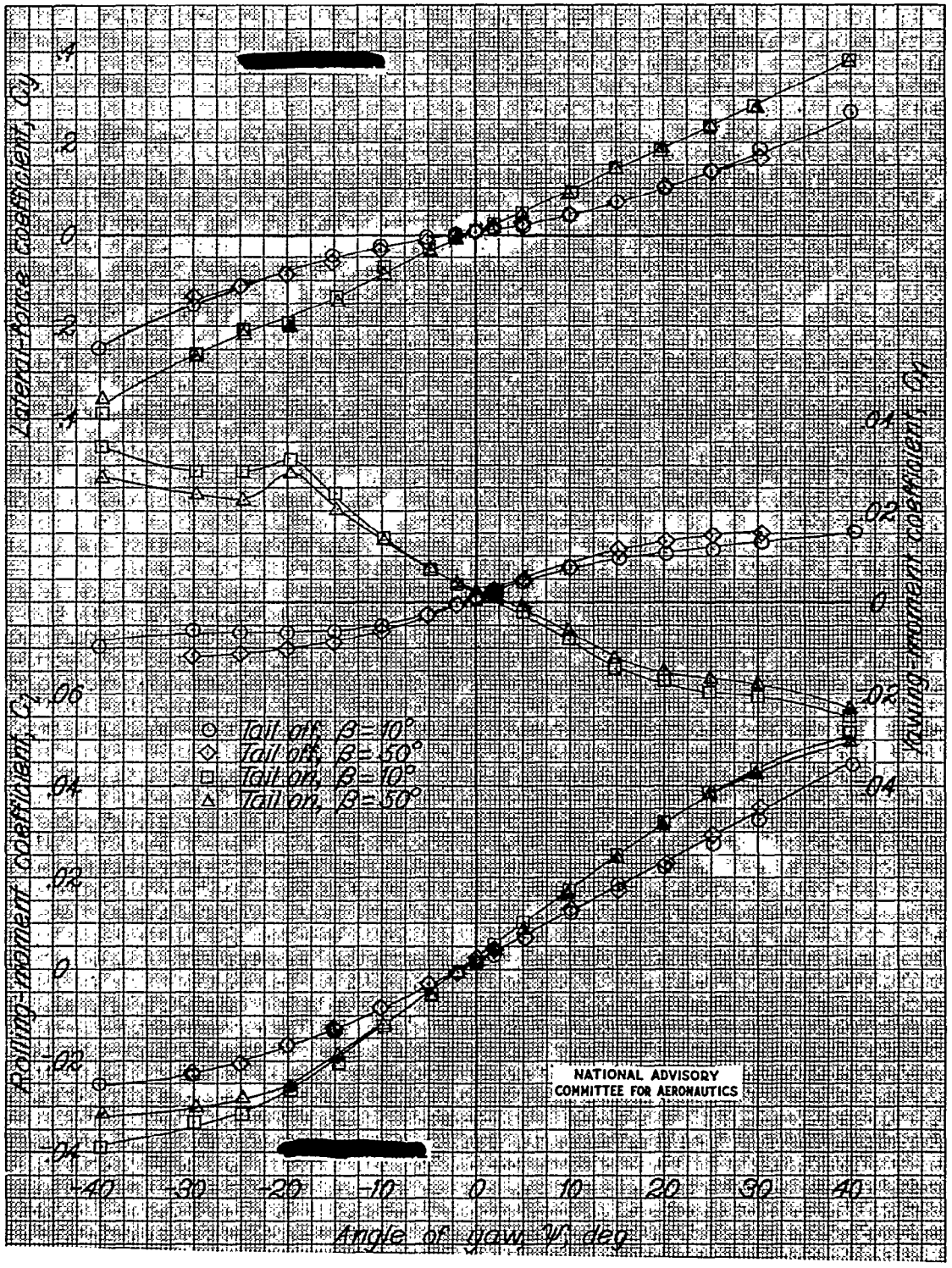

(a) $\alpha = .89°$.

Figure 34.- Effect of propeller blade angle on aerodynamic characteristics in yaw of a 1/8-scale model of the Grumman XTB3F-1 airplane. $T_c' = 0$; $\delta_f = 0°$; $q = 16.37$ pounds per square foot.

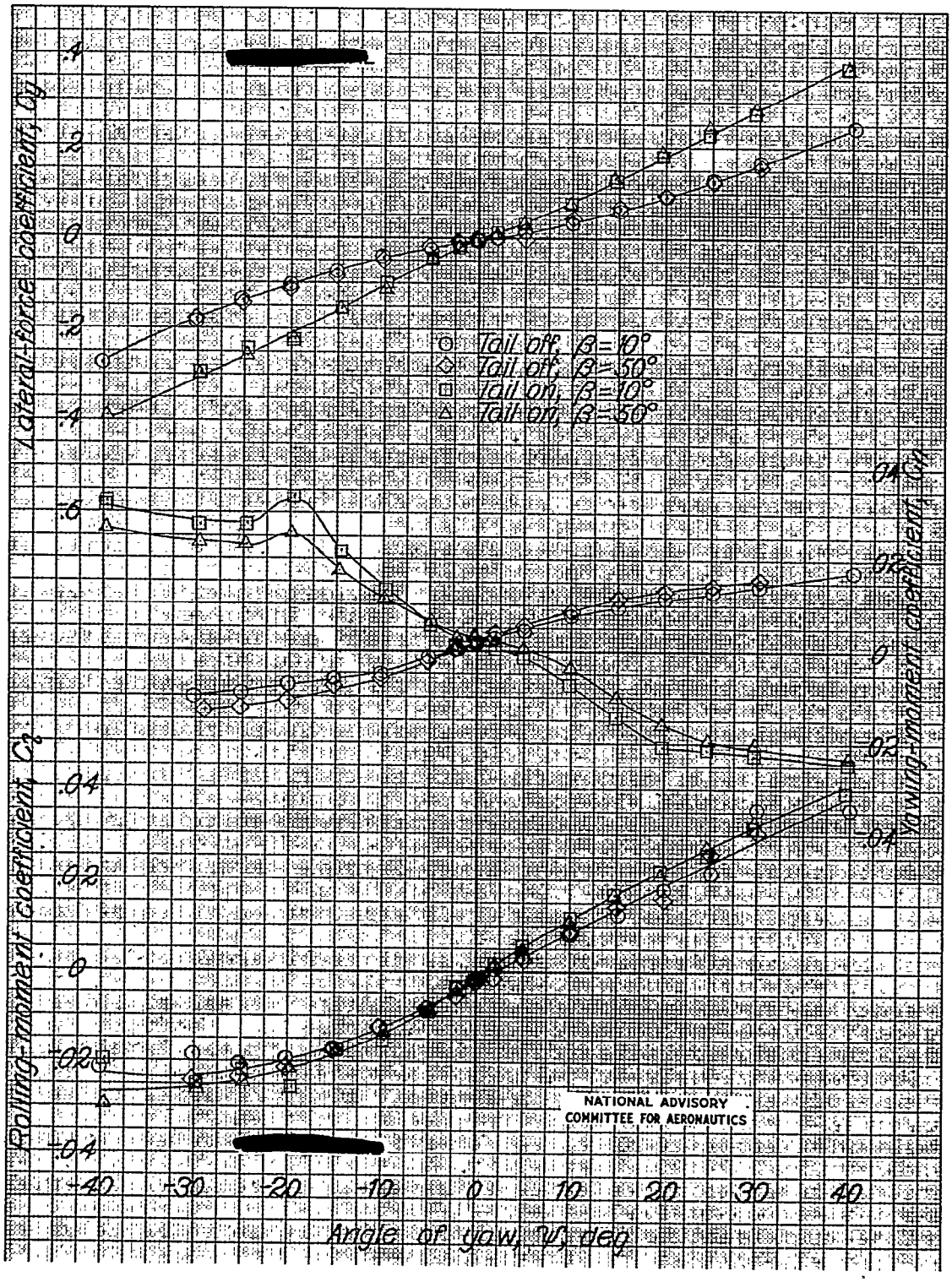

(b) $\alpha = 8.86°$.

Figure 34.- Concluded.

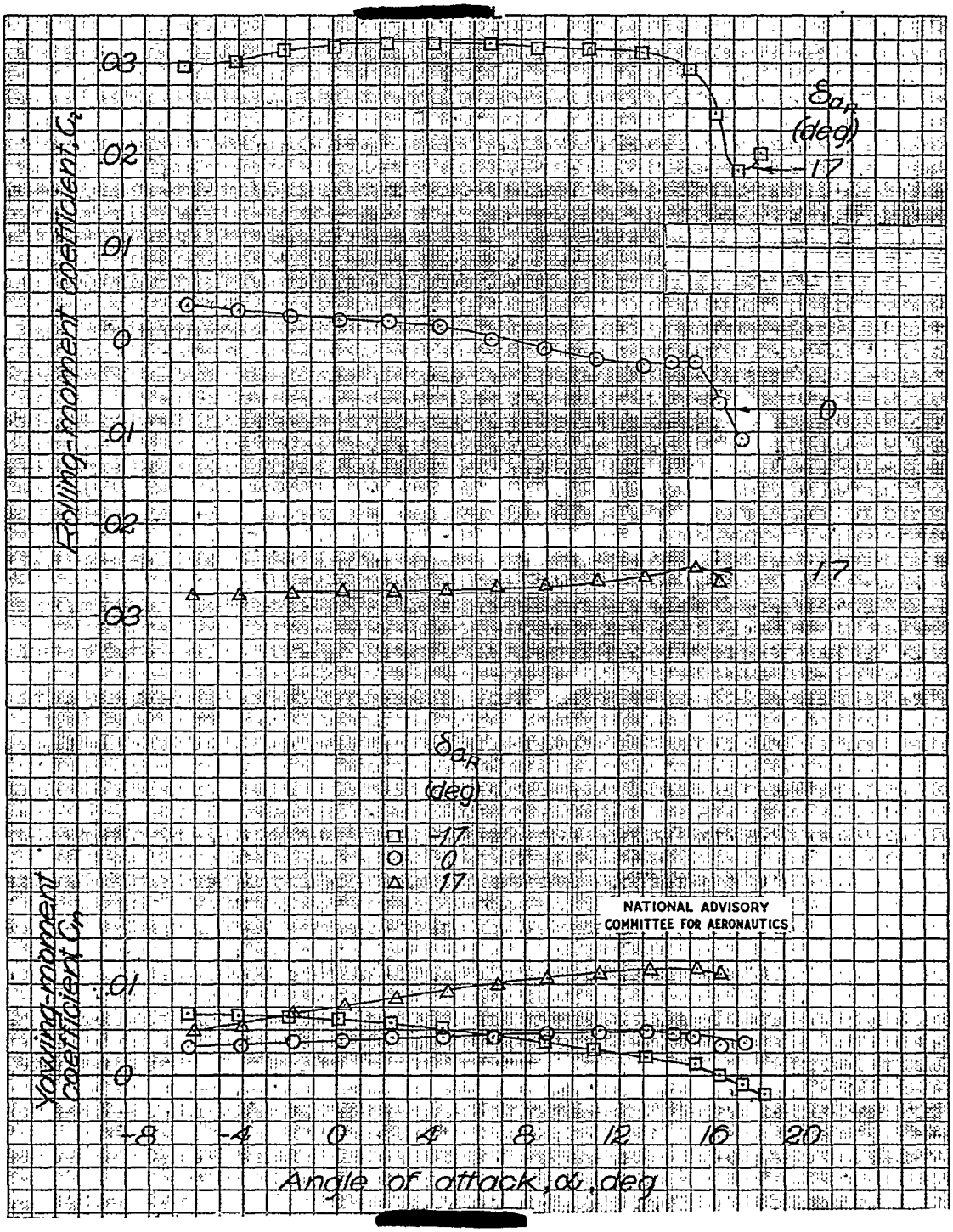

(a) Glide configuration.

Figure 35.- Aileron characteristics of a 1/8-scale model of the Grumman XTB3F-1 airplane. Windmilling propeller; $\delta_{a_L} = 0^\circ$.

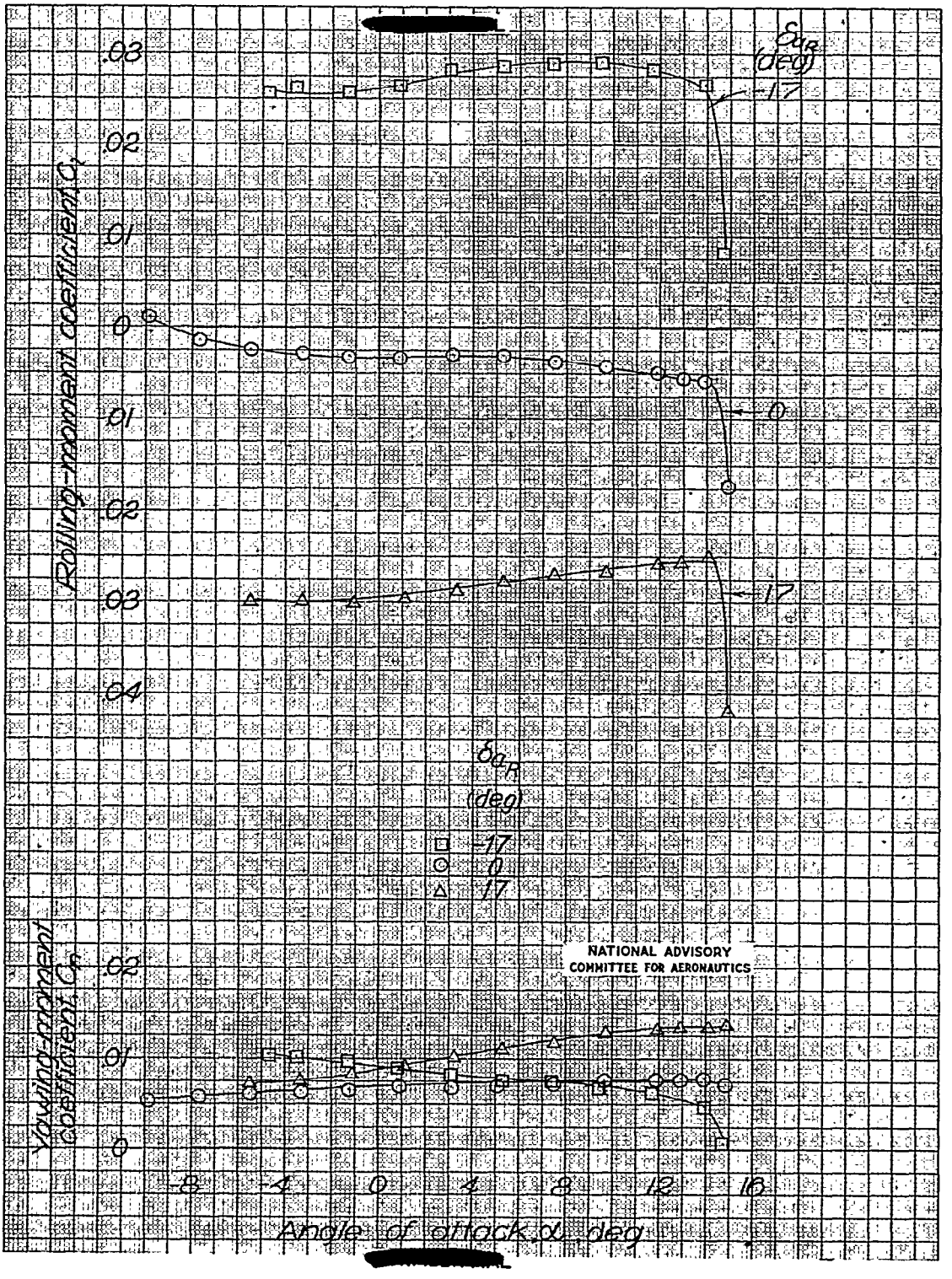

(b) Landing configuration.

Figure 35.- Concluded.

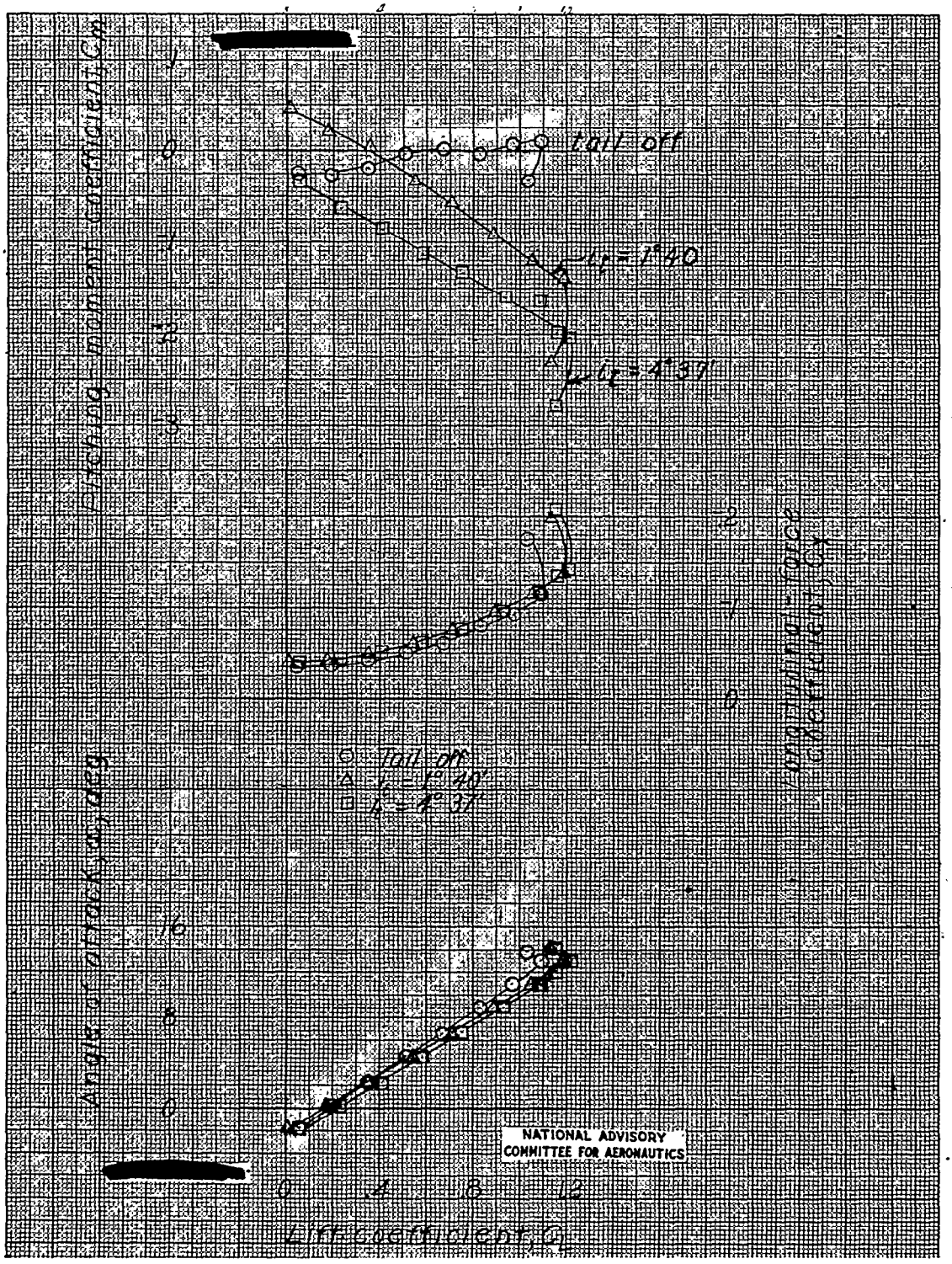

(a) Propeller off; flow condition "P".

Figure 36.- Effect of jet simulation on the aerodynamic characteristics in pitch of a 1/8-scale model of the Grumman XTB3F-1 airplane. $\delta_f = 0°$.

[redacted]

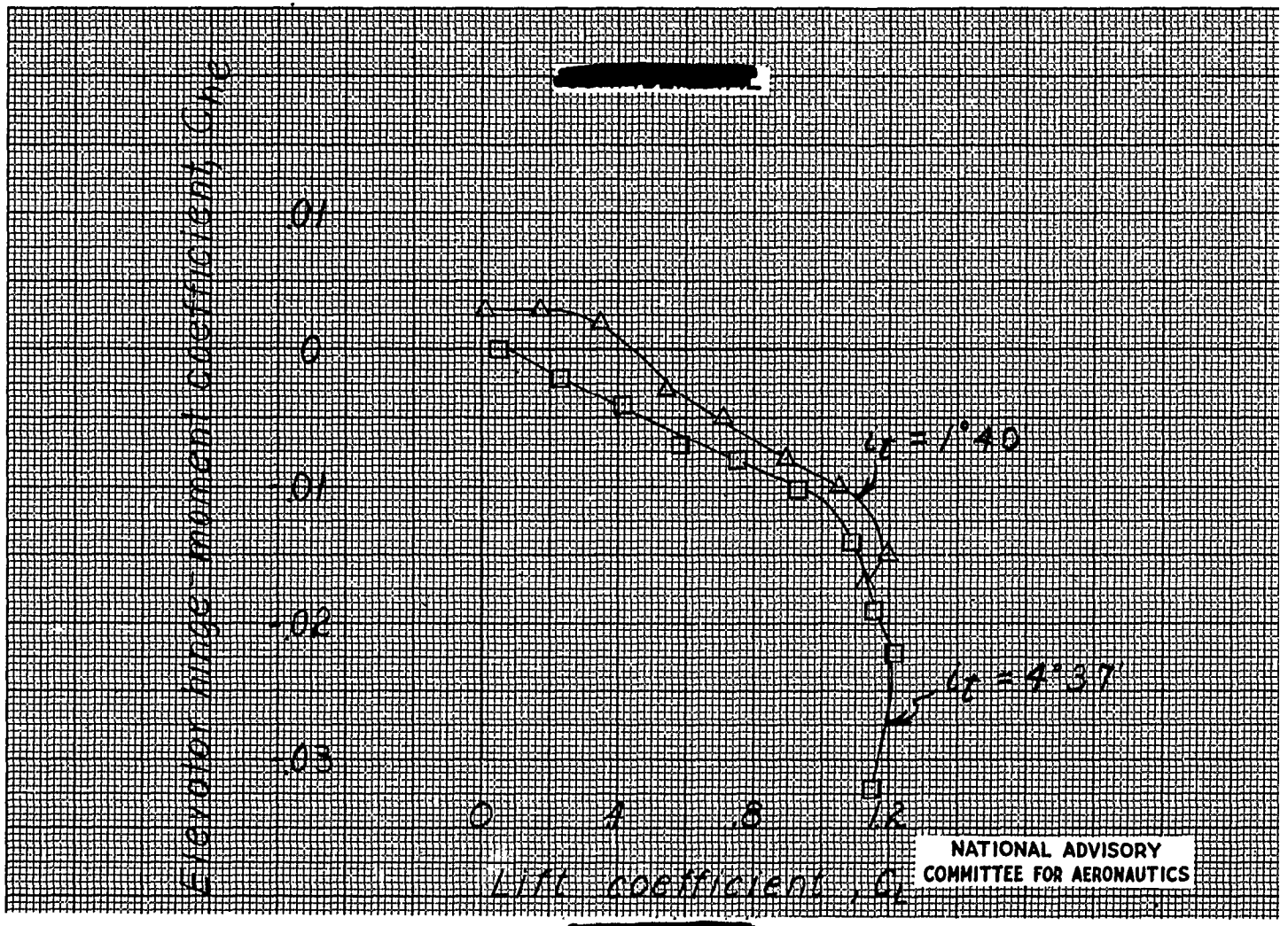

[redacted]

(a) Concluded.

Figure 36.- Continued.

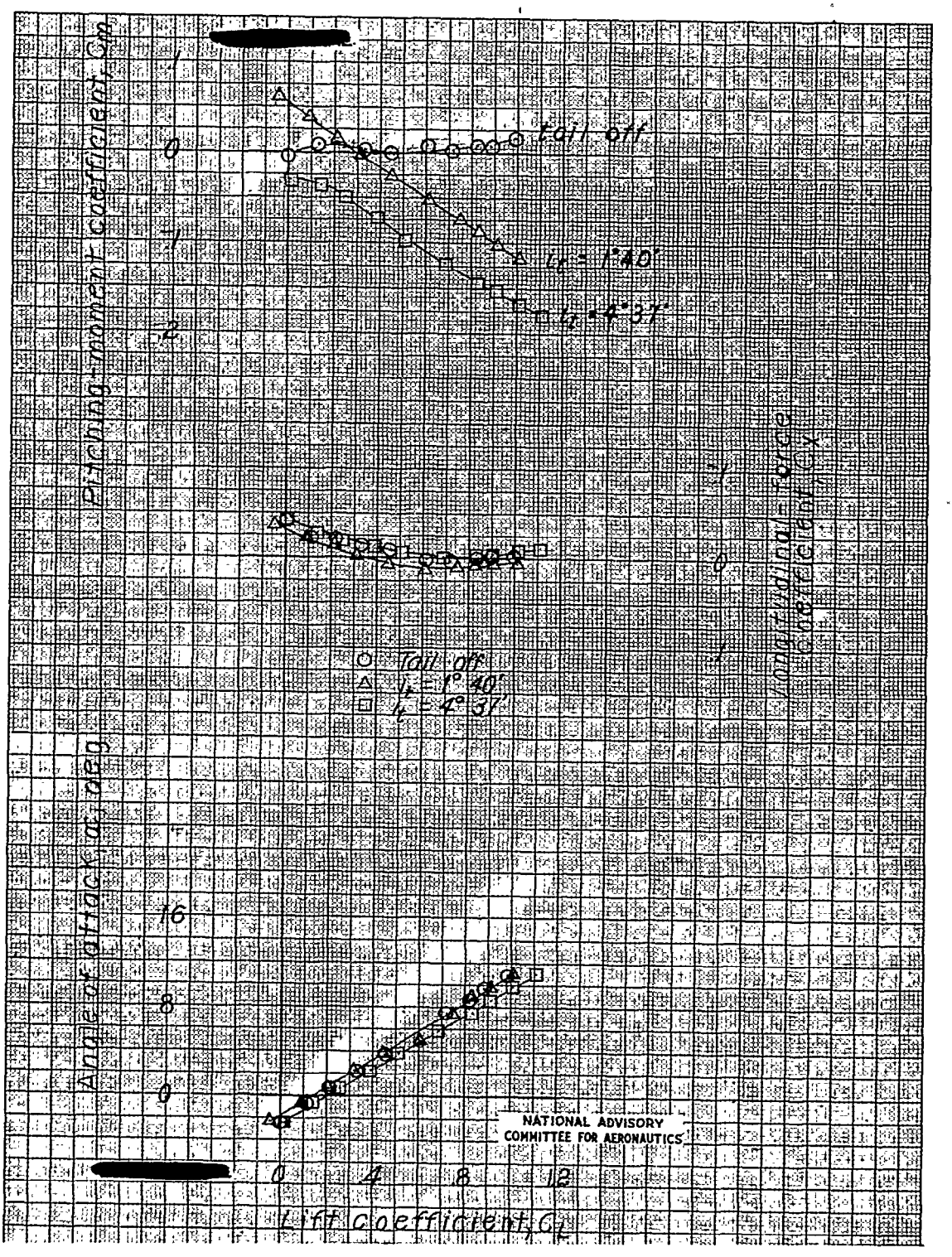

(b) Propeller off; flow condition "I".

Figure 36.- Continued.

[redacted]

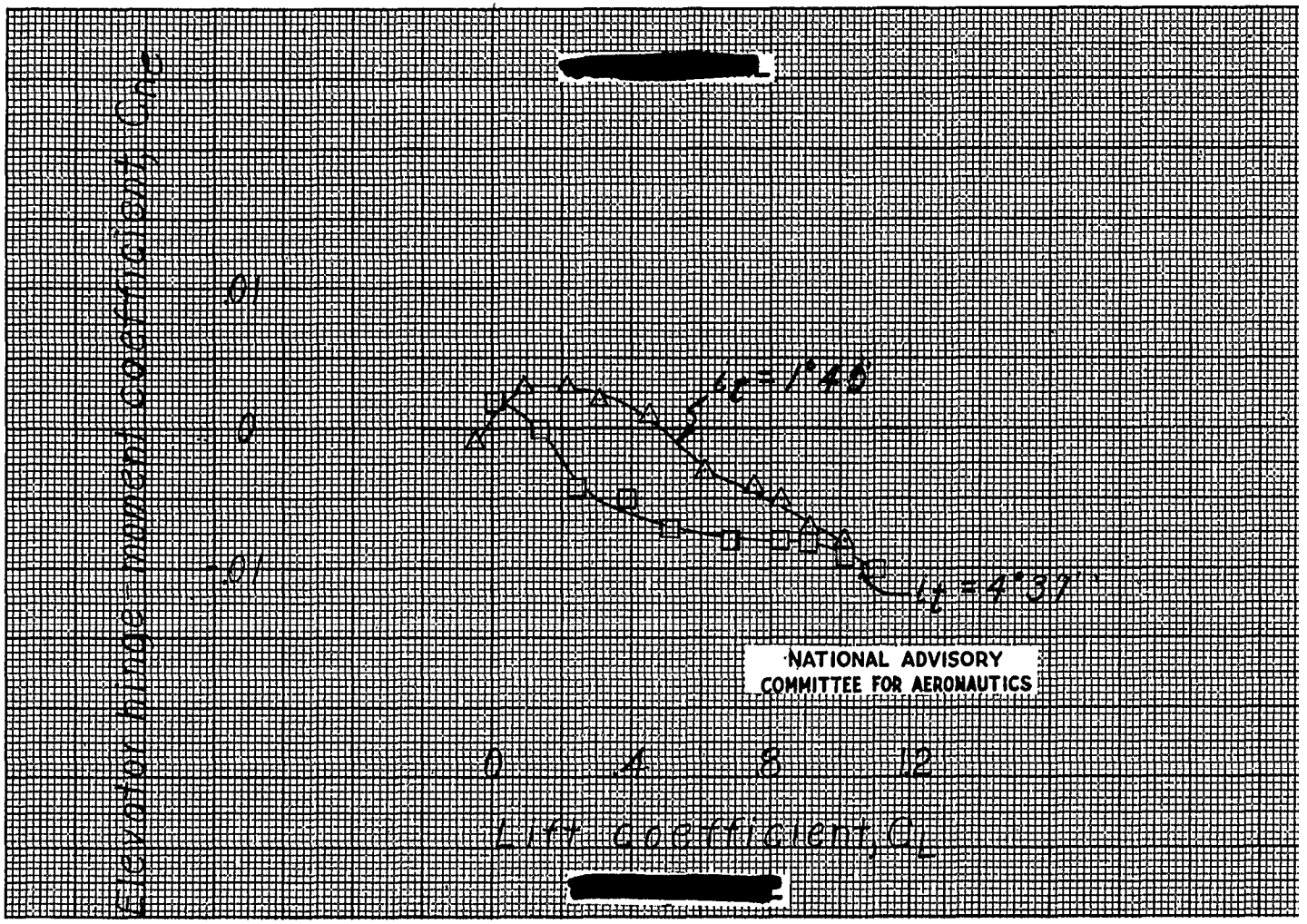

[redacted]

(b) Concluded.

Figure 36.- Continued.

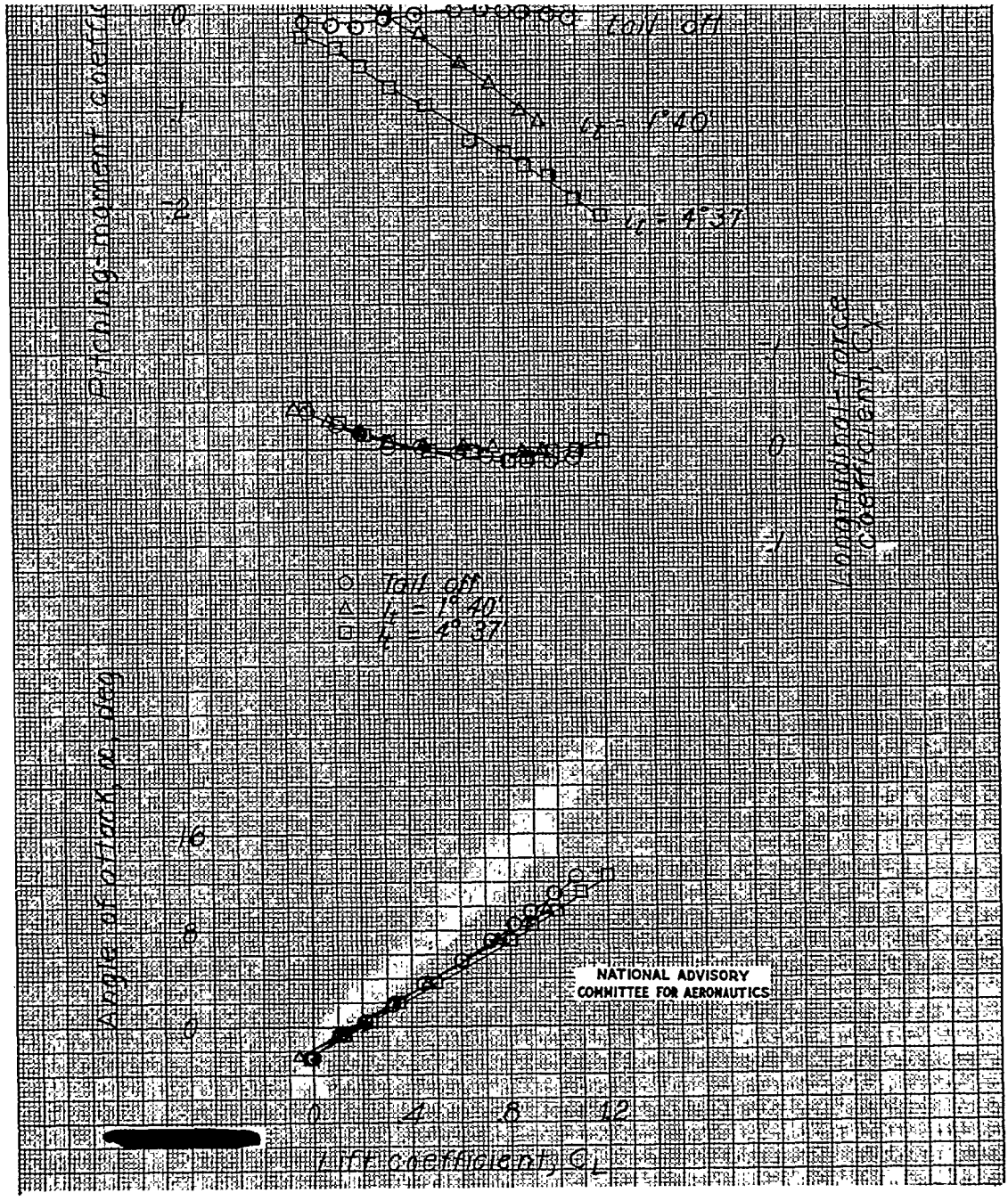

(c) Propeller off; flow condition "S".

Figure 36.- Continued.

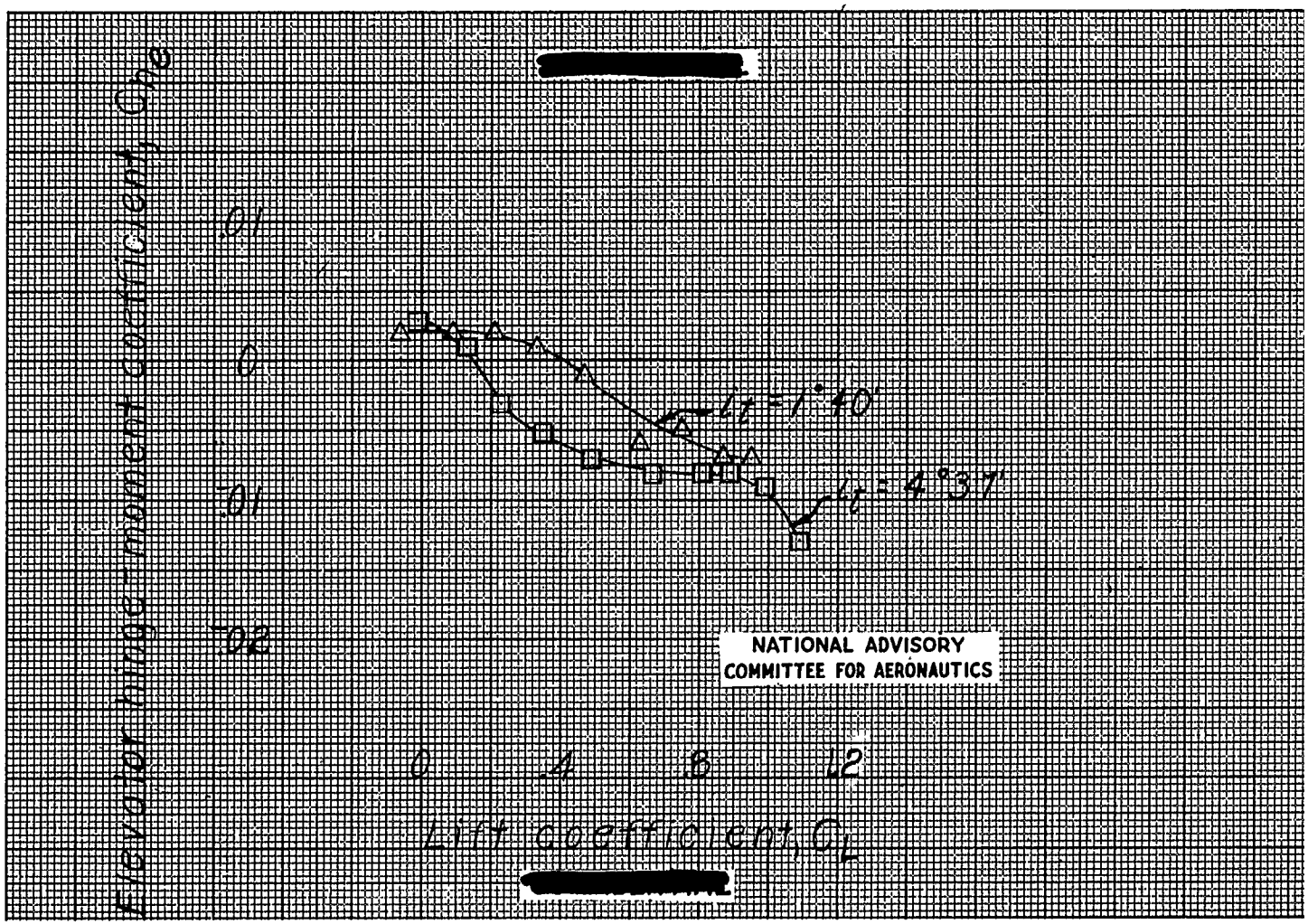

(c) Concluded.

Figure 36.- Continued.

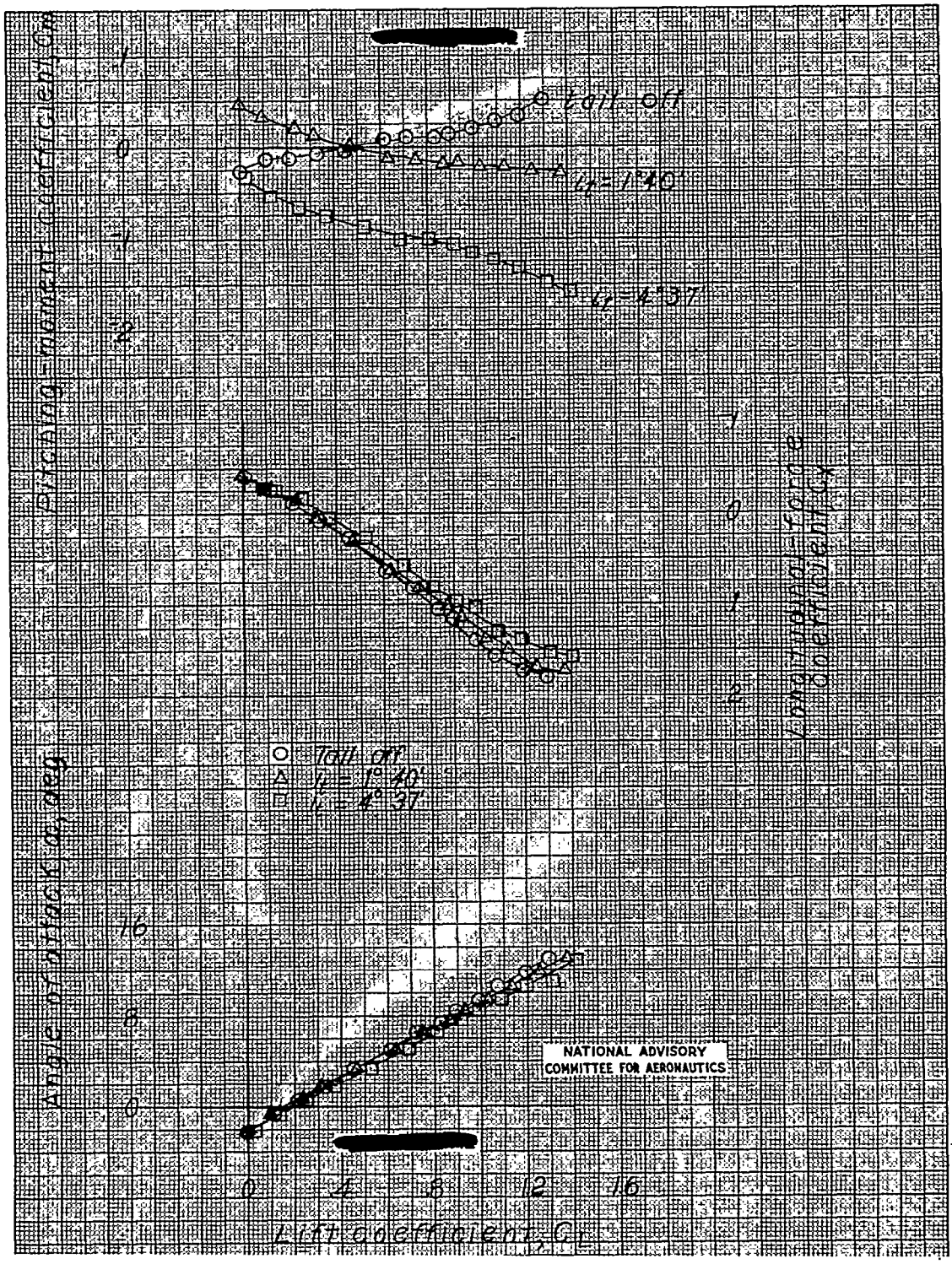

(d) Power-on clean; flow condition "P"

Figure 36.- Continued.

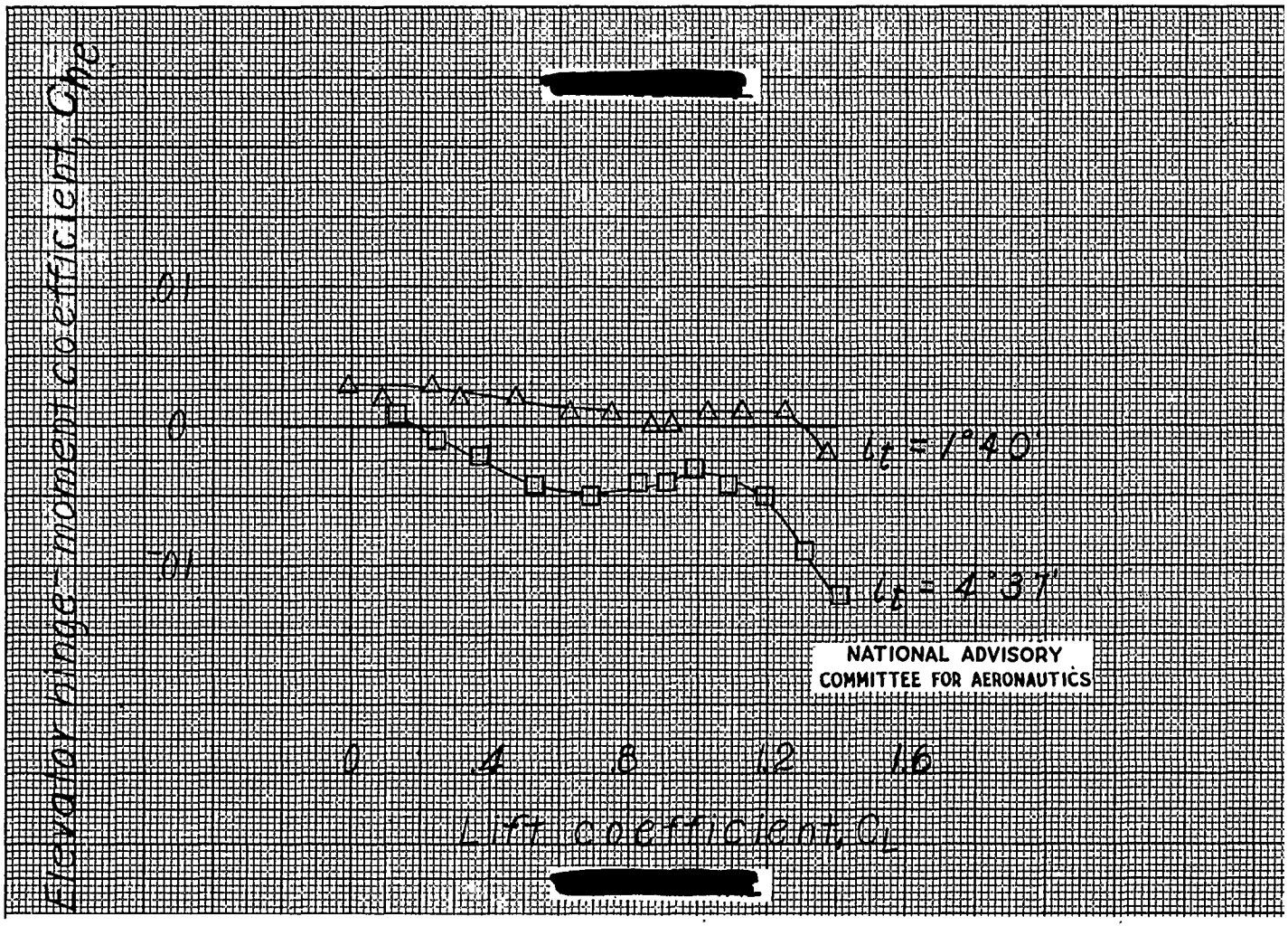

(d) Concluded.

Figure 36.- Continued.

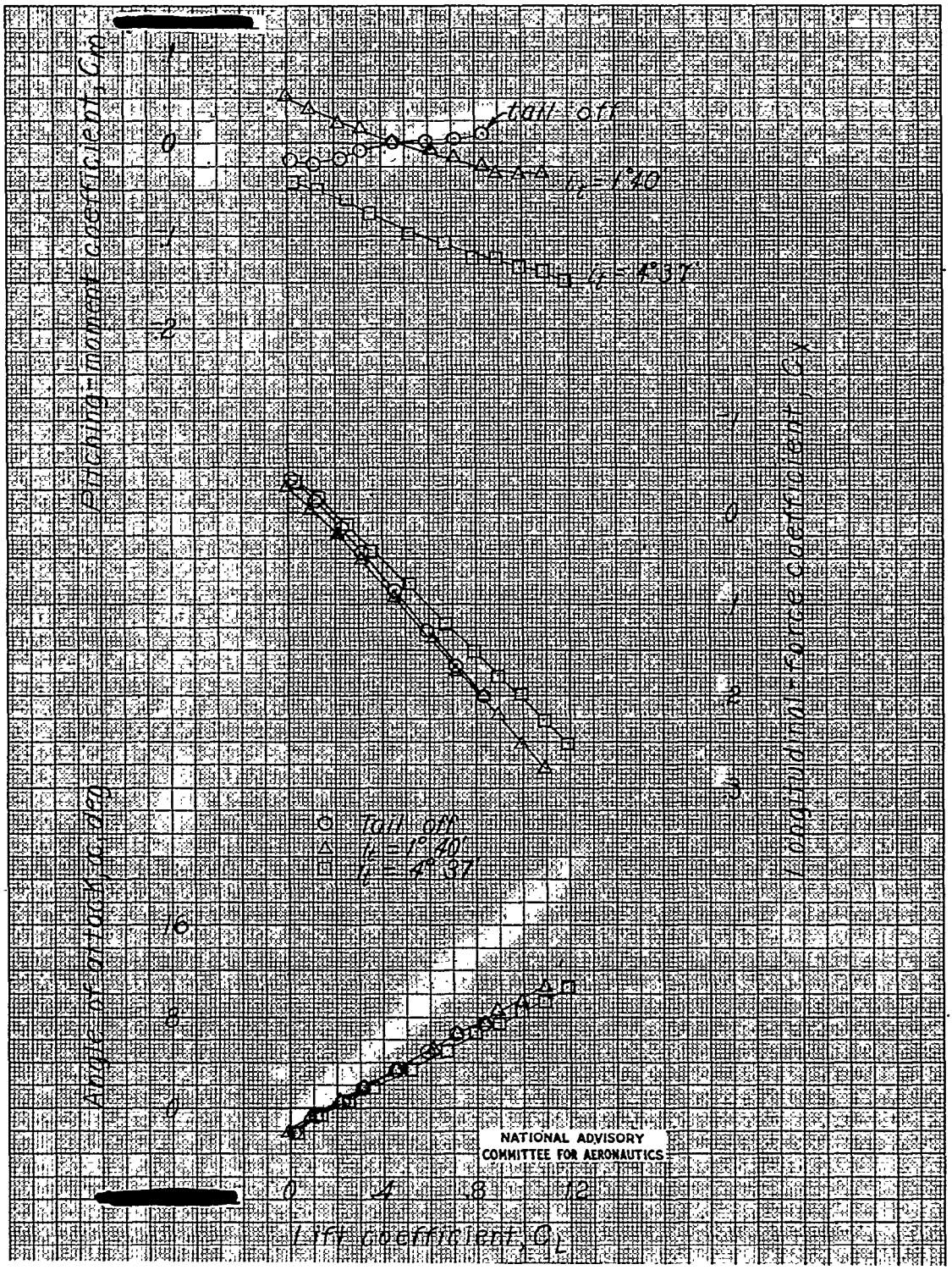

(e) Power-on clean; flow condition "I"

Figure 36.- Continued.

[redacted]

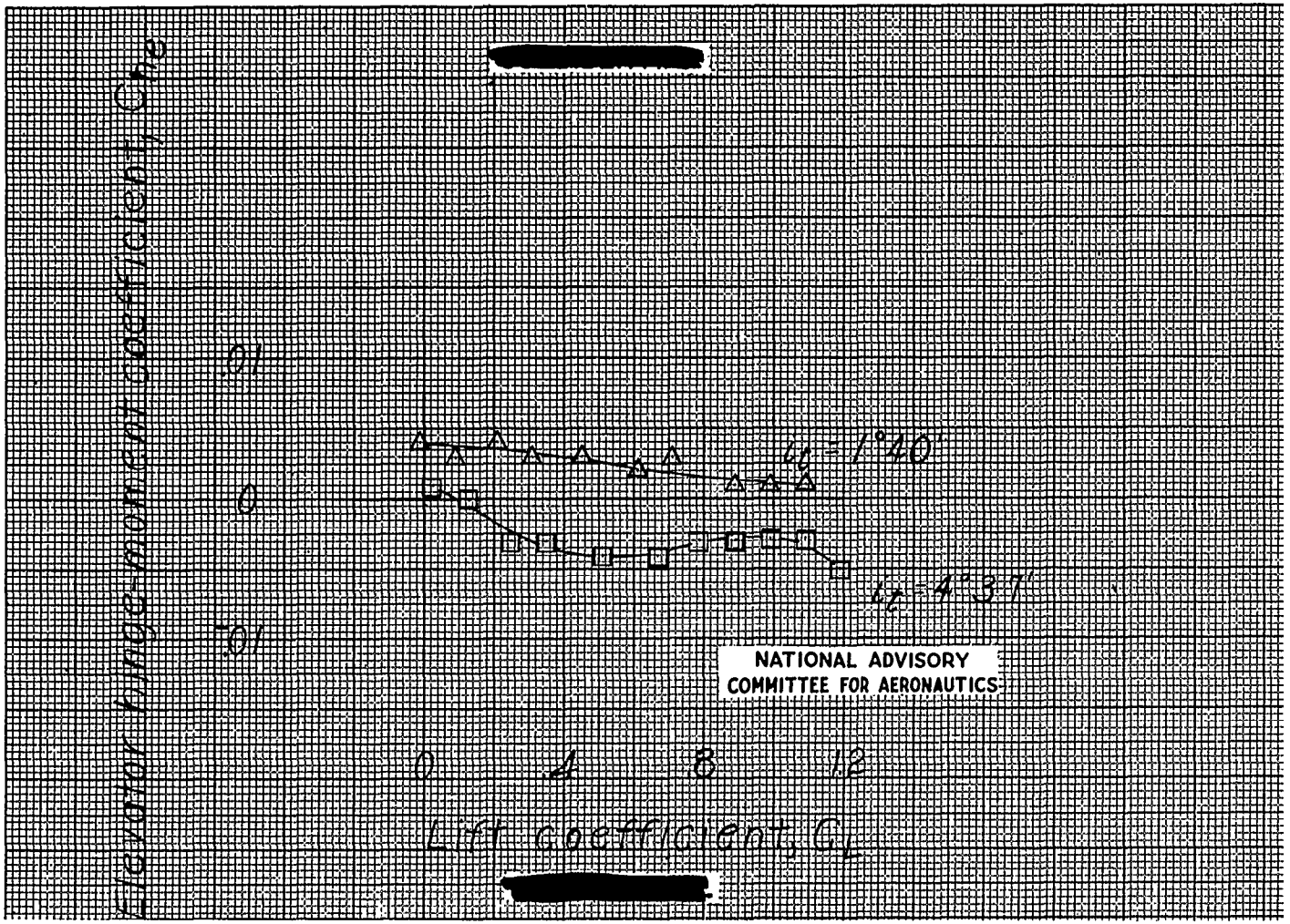

[redacted]

(e) Concluded

Figure 36.- Concluded.

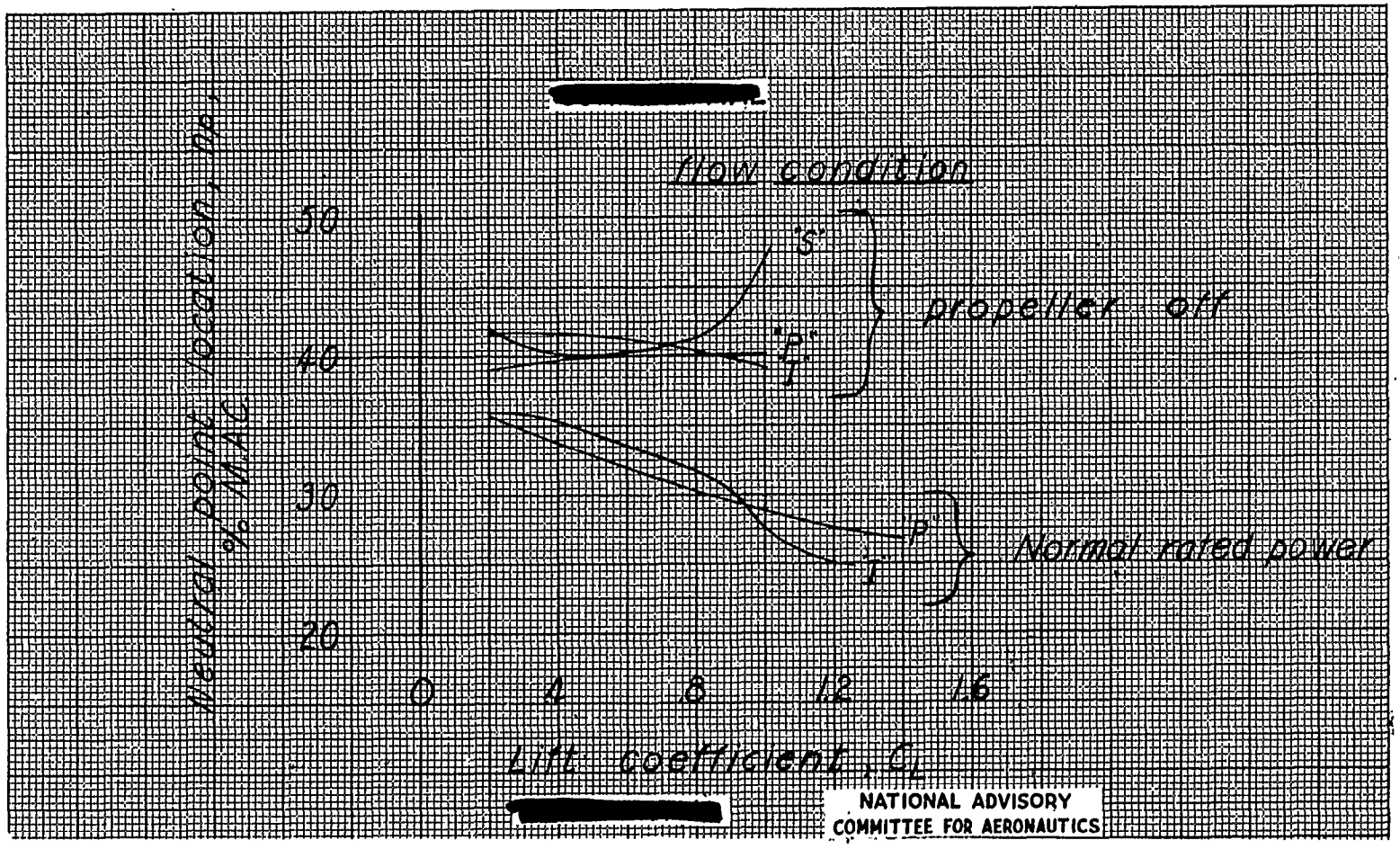

Figure 37.- Effect of jet simulation on neutral point location of the 1/8-scale model of the Grumman XTB3F-1 airplane. $\delta_f = 0^\circ$

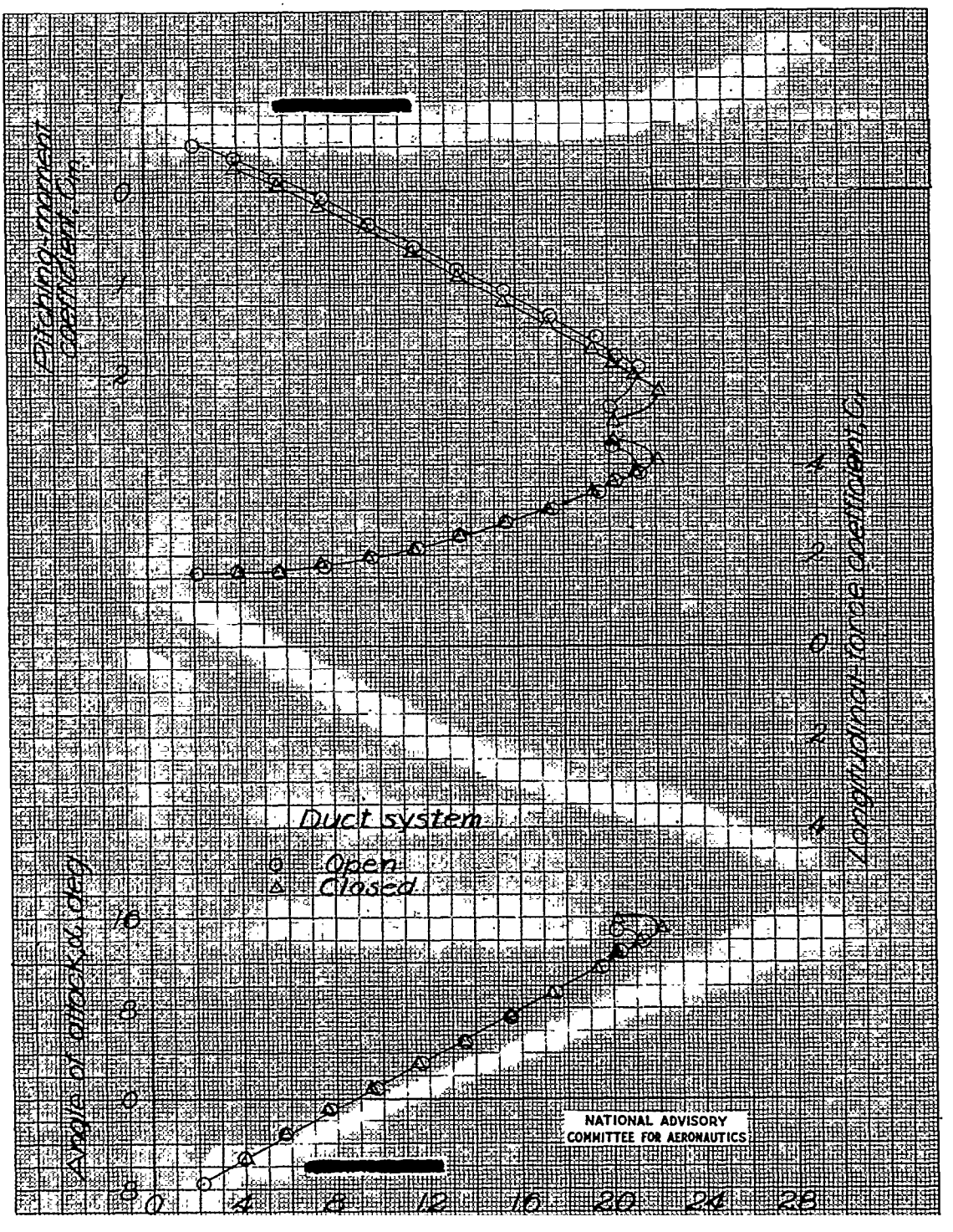
Pitching-moment coefficient, C_m
Longitudinal-force coefficient, C_x
Angle of attack, deg
Duct system
Open
Closed
NATIONAL ADVISORY COMMITTEE FOR AERONAUTICS

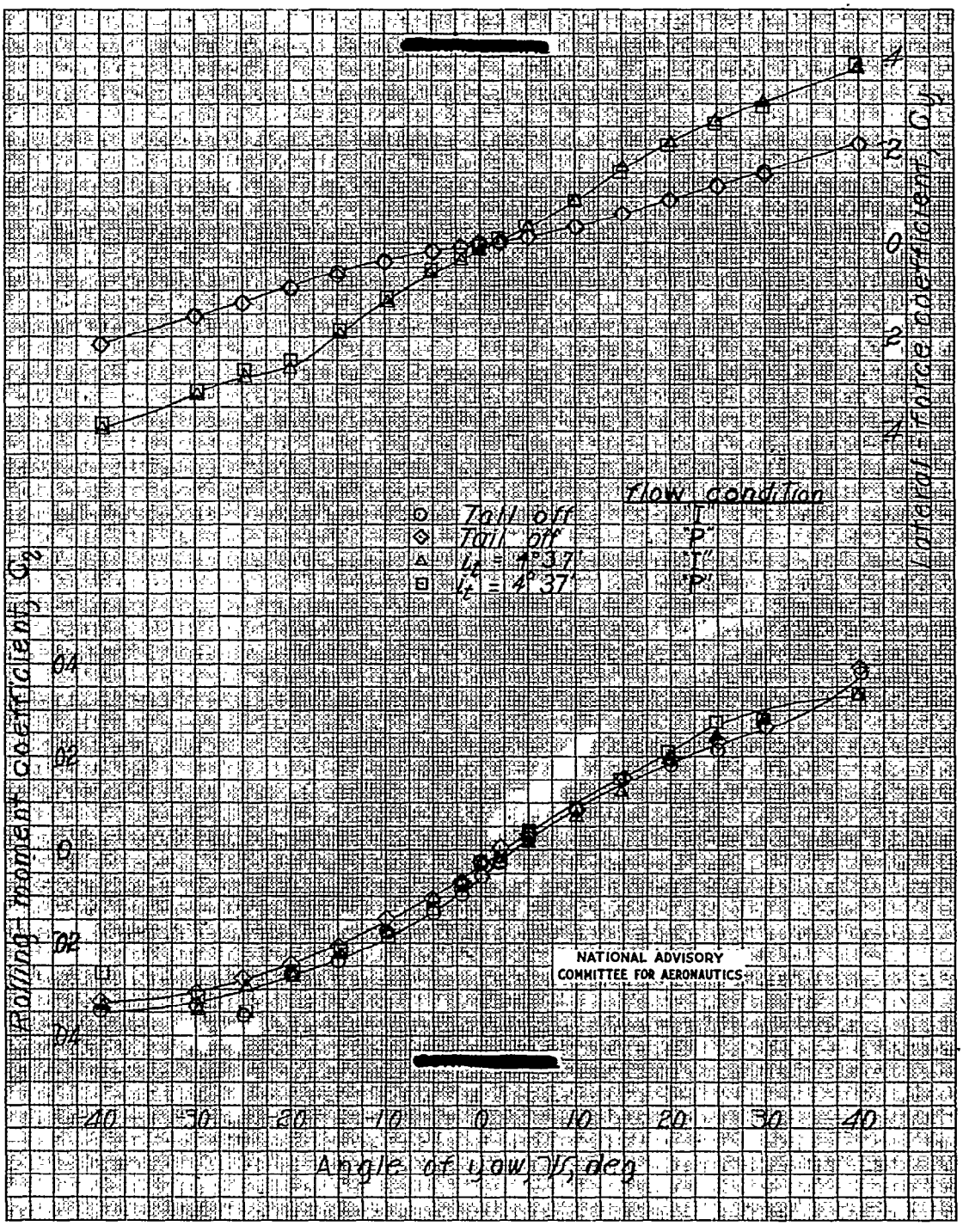
[redacted]
Tail off
Tail off
$i_t = 4°37'$
$i_t = 4°37'$
Flow condition
"T"
"P"
"T"
"P"
Rolling-moment coefficient, C_l
.04
.02
0
-.02
-.04
Lateral-force coefficient, C_Y
.4
.2
0
-.2
-.4
-40
-30
-20
-10
0
10
20
30
40
Angle of yaw, ψ, deg
NATIONAL ADVISORY
COMMITTEE FOR AERONAUTICS
[redacted]

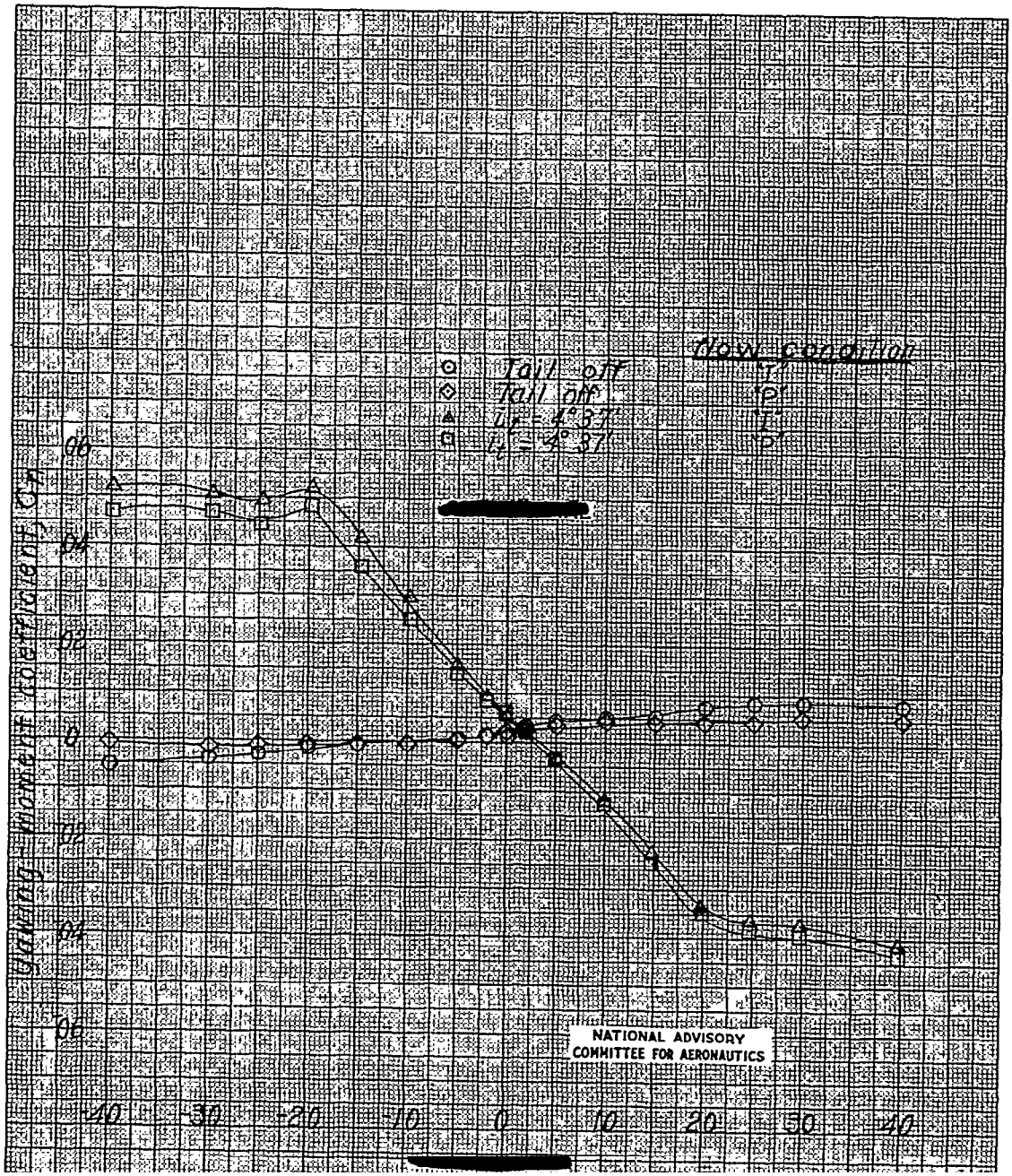
Tail off
Tail off
$i_t = 4°37'$
$i_t = 4°37'$
Flow condition
'T'
'P'
'T'
'P'
[redacted]
Yawing-moment coefficient, C_n
.06
.04
.02
0
.02
.04
.06
-40
-30
-20
-10
0
10
20
30
40
NATIONAL ADVISORY
COMMITTEE FOR AERONAUTICS
[redacted]

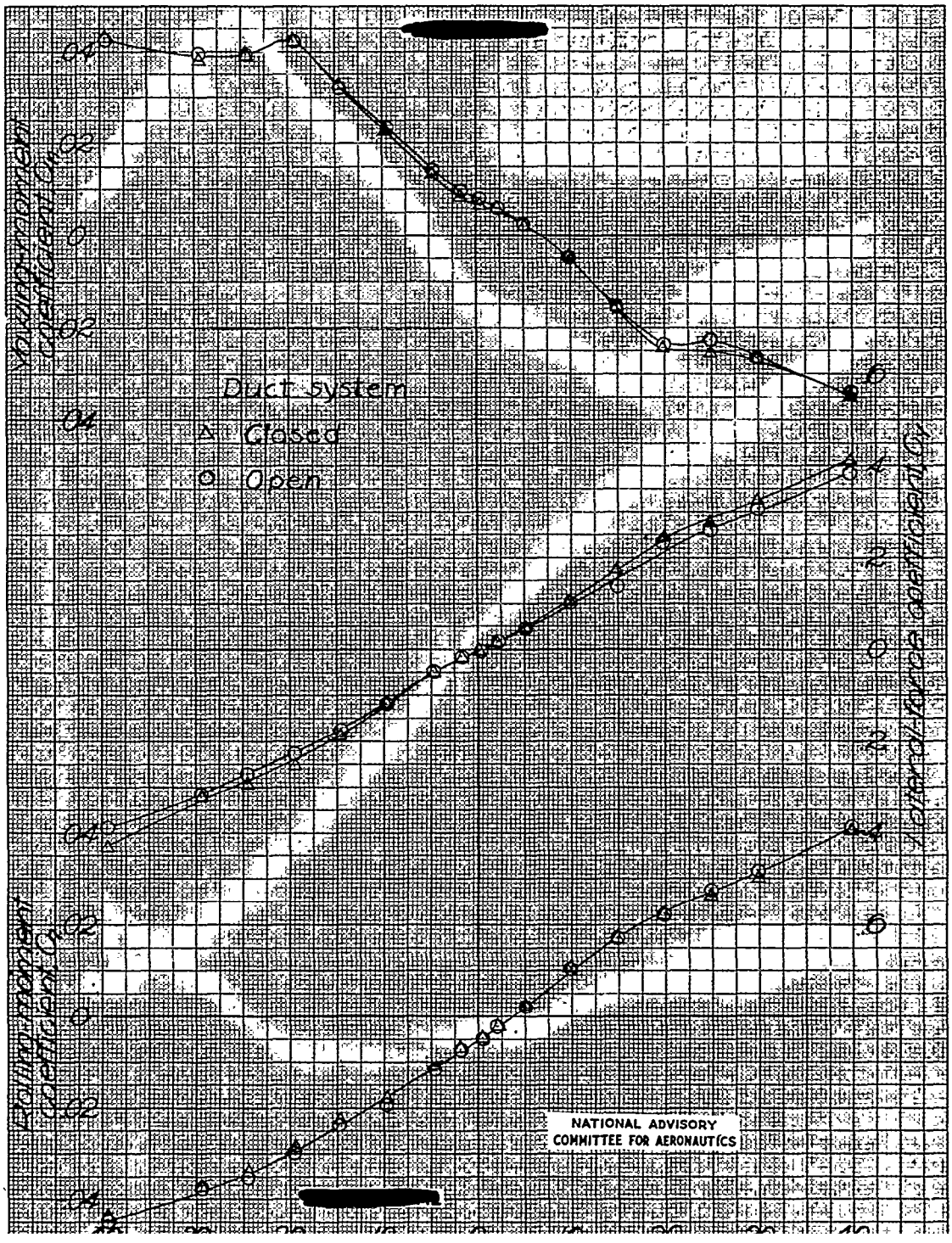
Duct system
Closed
Open
NATIONAL ADVISORY
COMMITTEE FOR AERONAUTICS

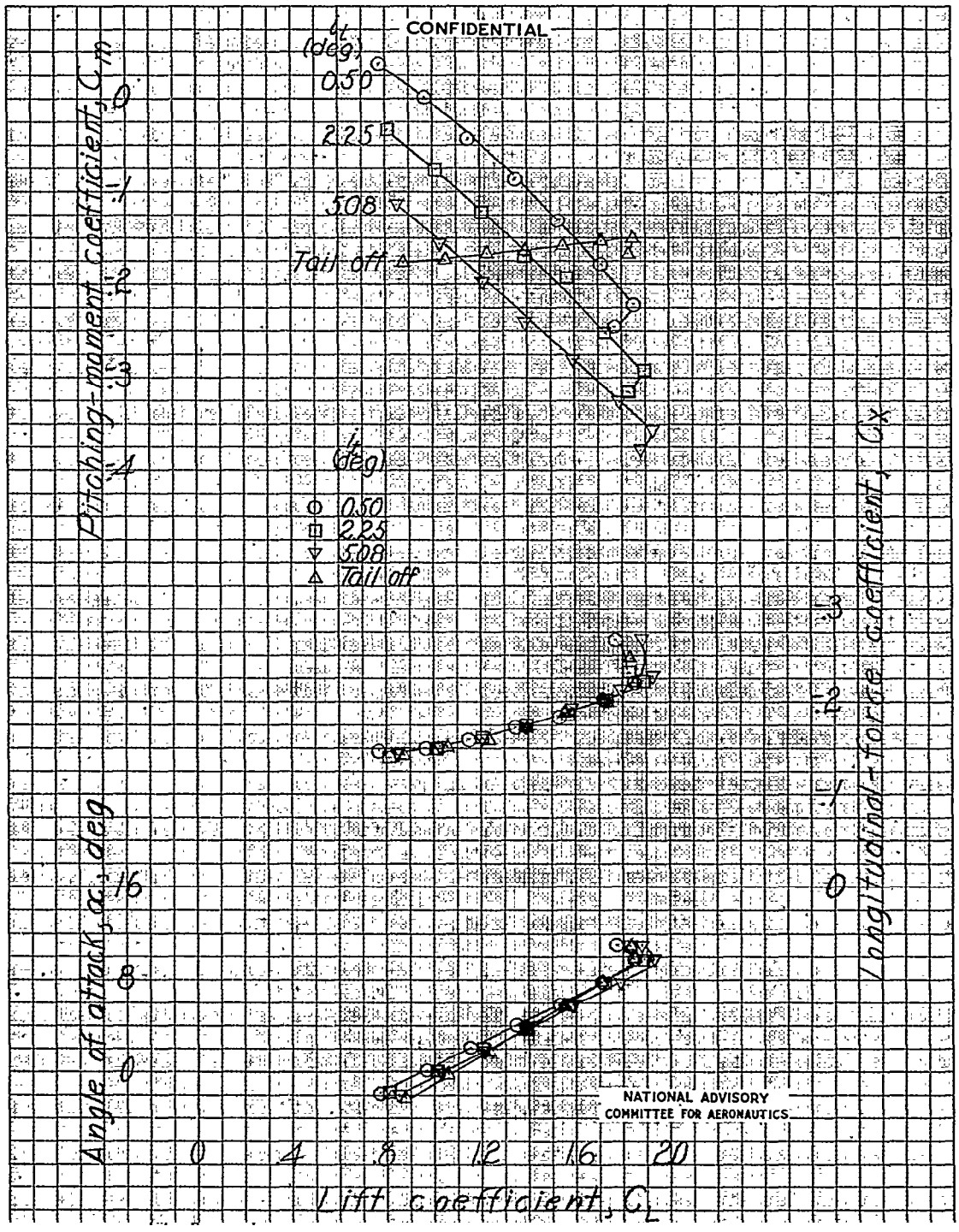
CONFIDENTIAL
i_t (deg)
0.50
2.25
5.08
Tail off
Pitching-moment coefficient, C_m
.1
0
-.1
-.2
-.3
-.4
i_t (deg)
0.50
2.25
5.08
Tail off
Longitudinal-force coefficient, C_X
.3
.2
.1
0
Angle of attack, α, deg
16
8
0
0
4
8
12
16
20
Lift coefficient, C_L
NATIONAL ADVISORY
COMMITTEE FOR AERONAUTICS

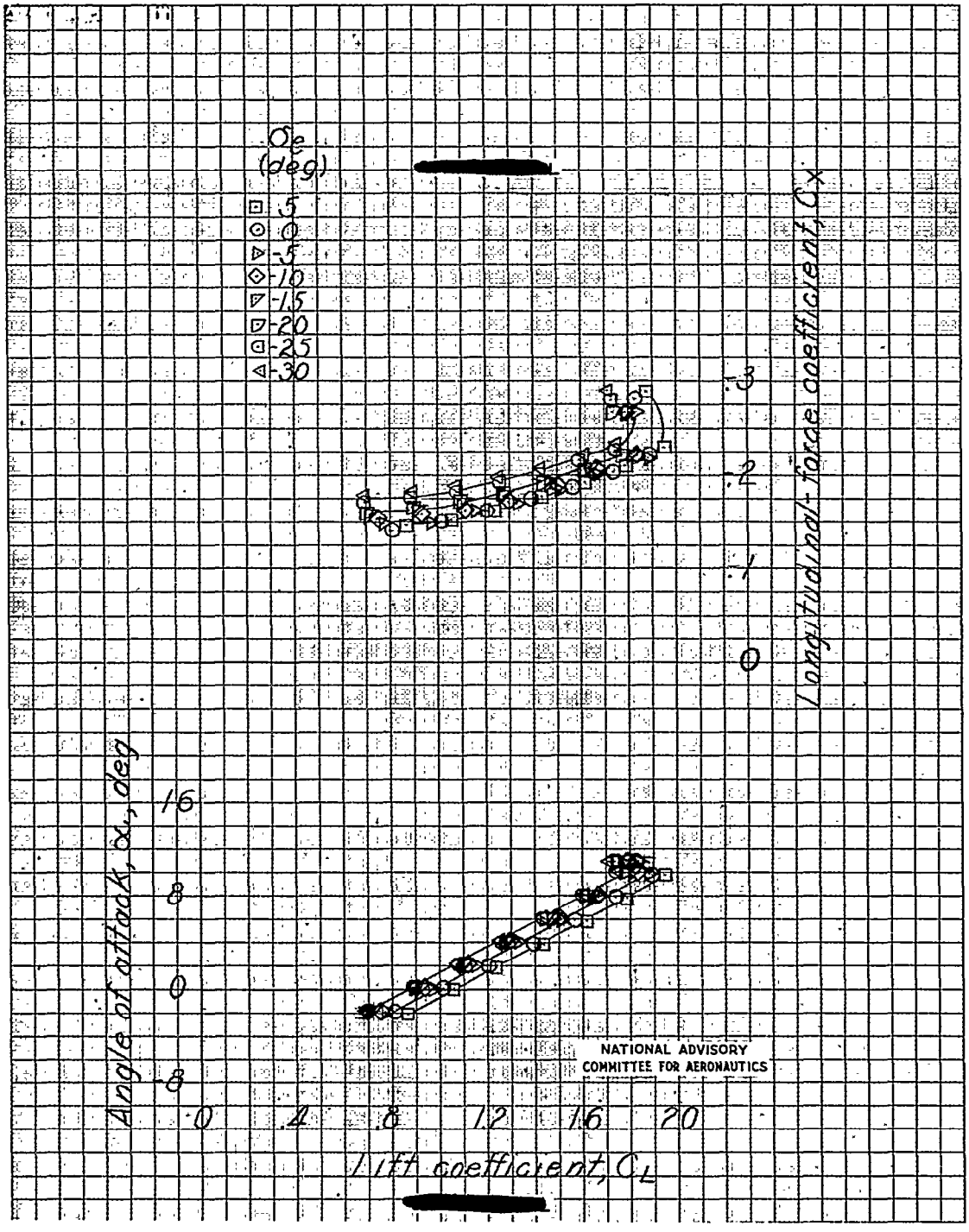
δ_e (deg)
.5
0
-.5
-1.0
-1.5
-2.0
-2.5
-3.0
Longitudinal-force coefficient, C_X
.3
.2
.1
0
Angle of attack, α_r, deg
16
8
0
-8
0
.4
.8
1.2
1.6
2.0
Lift coefficient, C_L
NATIONAL ADVISORY
COMMITTEE FOR AERONAUTICS

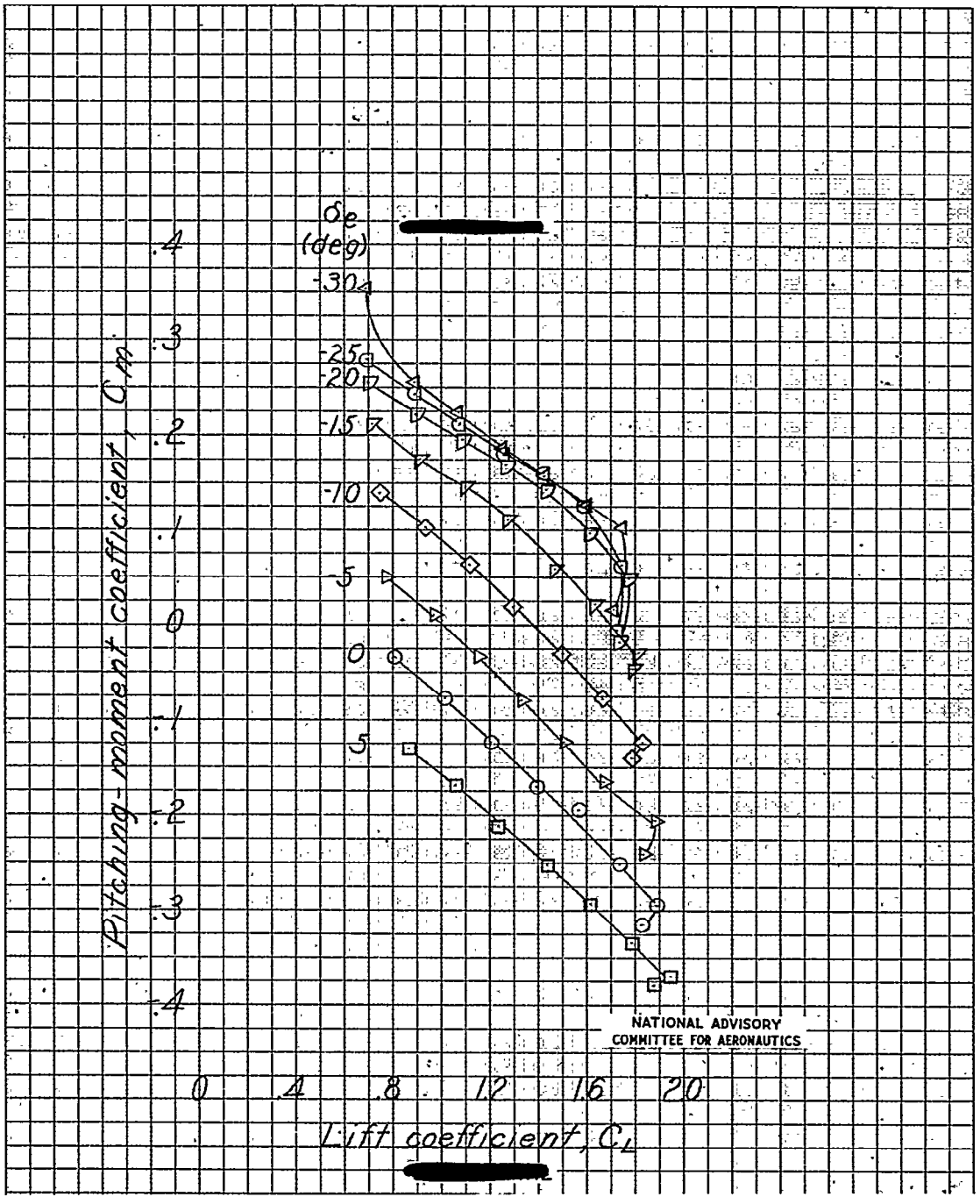
[redacted]
δ_e (deg)
-30
-25
-20
-15
-10
-5
0
5
.4
.3
.2
.1
0
-.1
-.2
-.3
-.4
Pitching-moment coefficient, C_m
0
.4
.8
1.2
1.6
2.0
Lift coefficient, C_L
[redacted]
NATIONAL ADVISORY COMMITTEE FOR AERONAUTICS

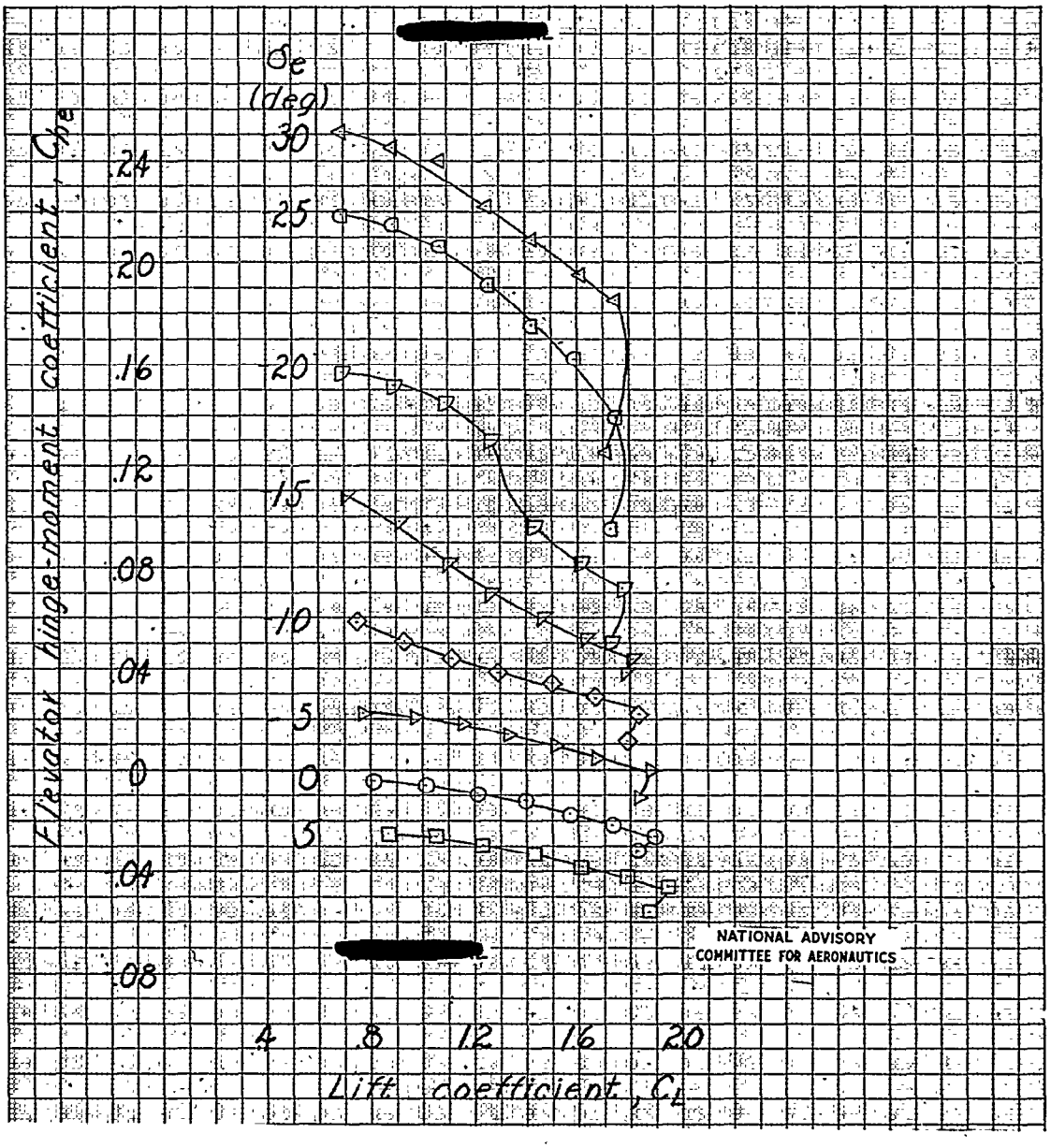

(b) Concluded.

Figure 41.- Concluded.

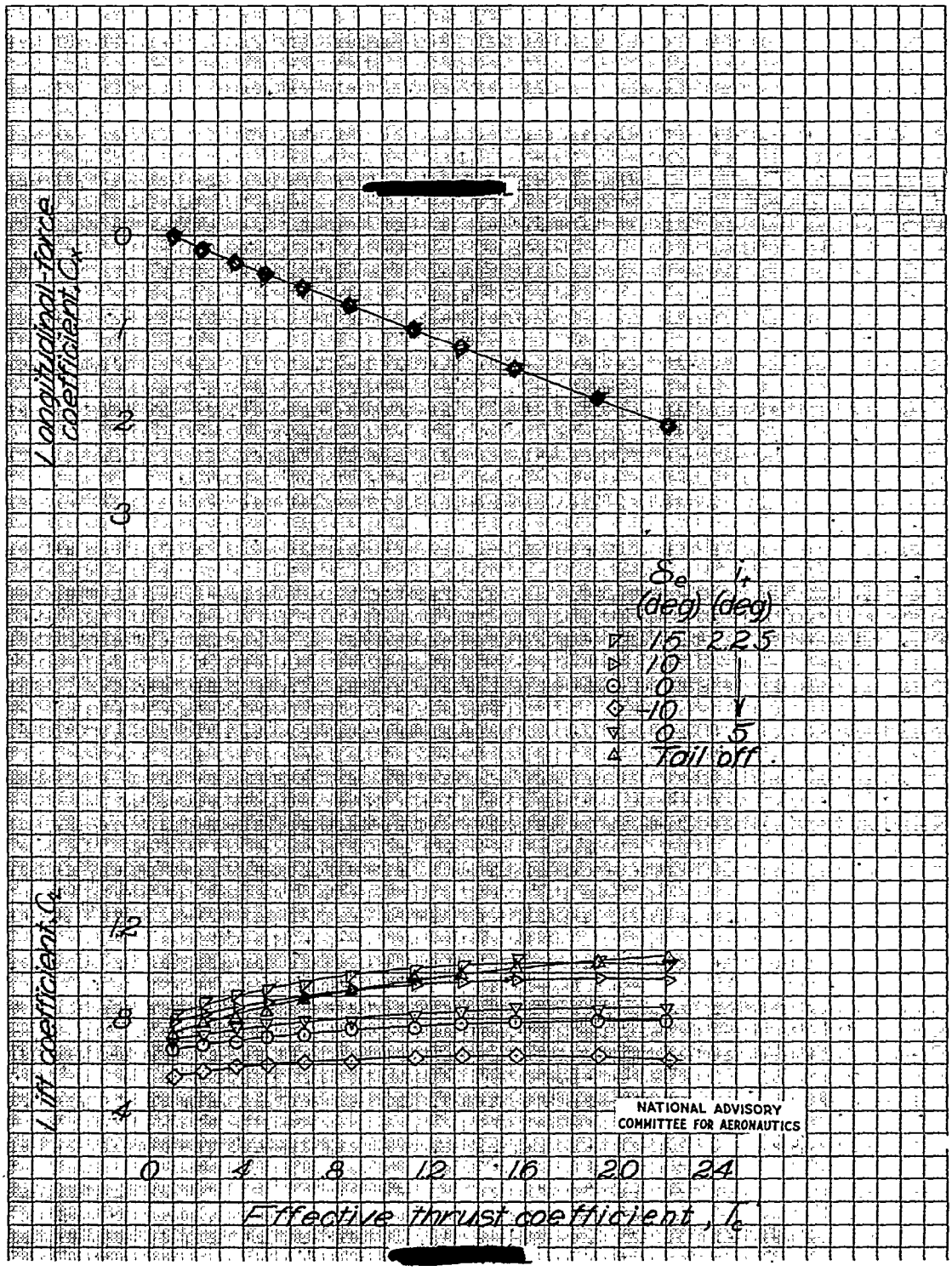

(a) $\alpha = 0^{\circ}$; original thrust line.

Figure 42.- Aerodynamic characteristics of a 1/8-scale model of the Grumman XTB3F-1 airplane with ground board in place. Take-off configuration; $\beta = 25^{\circ}$; $\psi = 0^{\circ}$

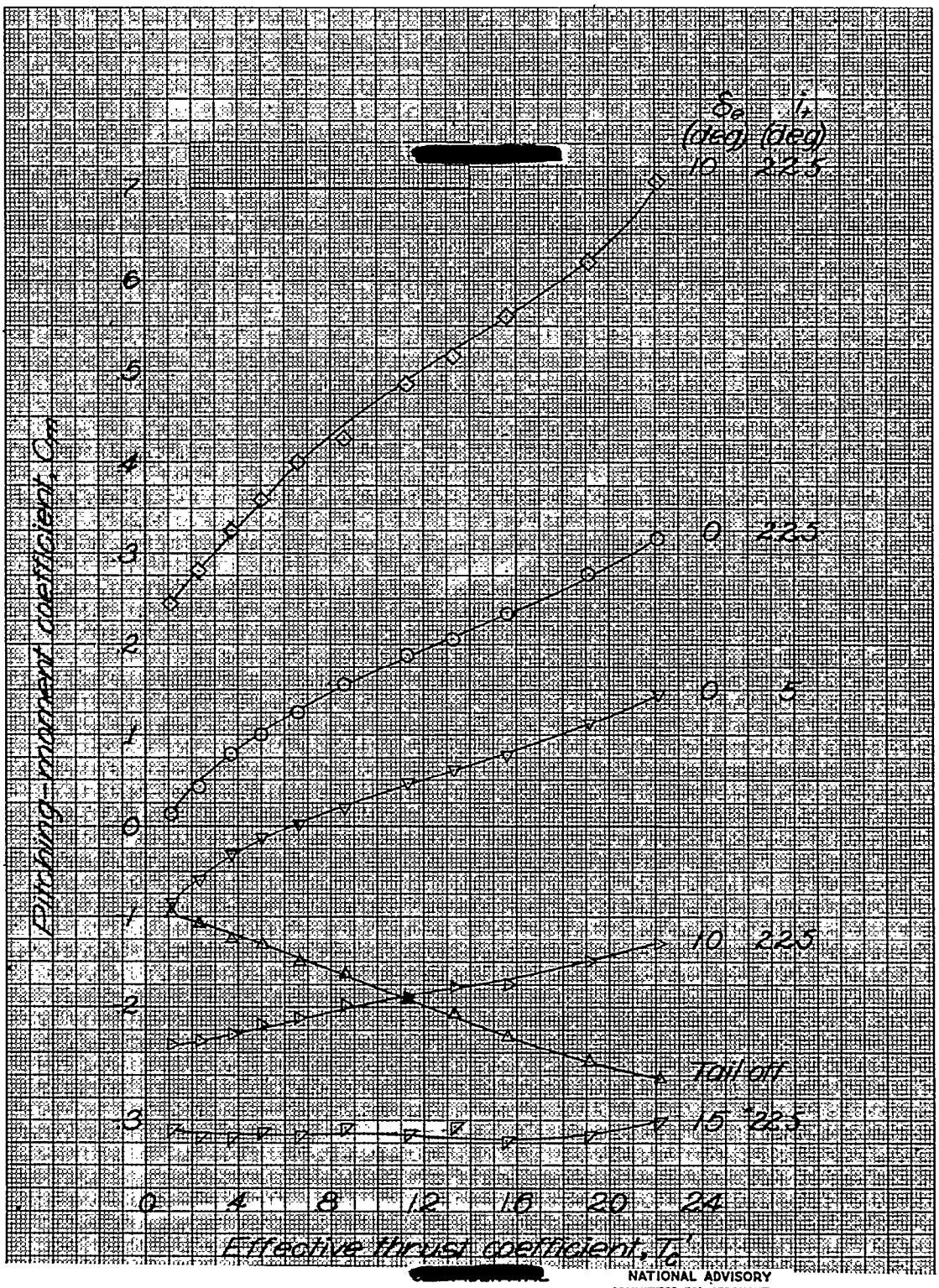

NATIONAL ADVISORY COMMITTEE FOR AERONAUTICS

(a) Continued.

Figure 42.- Continued.

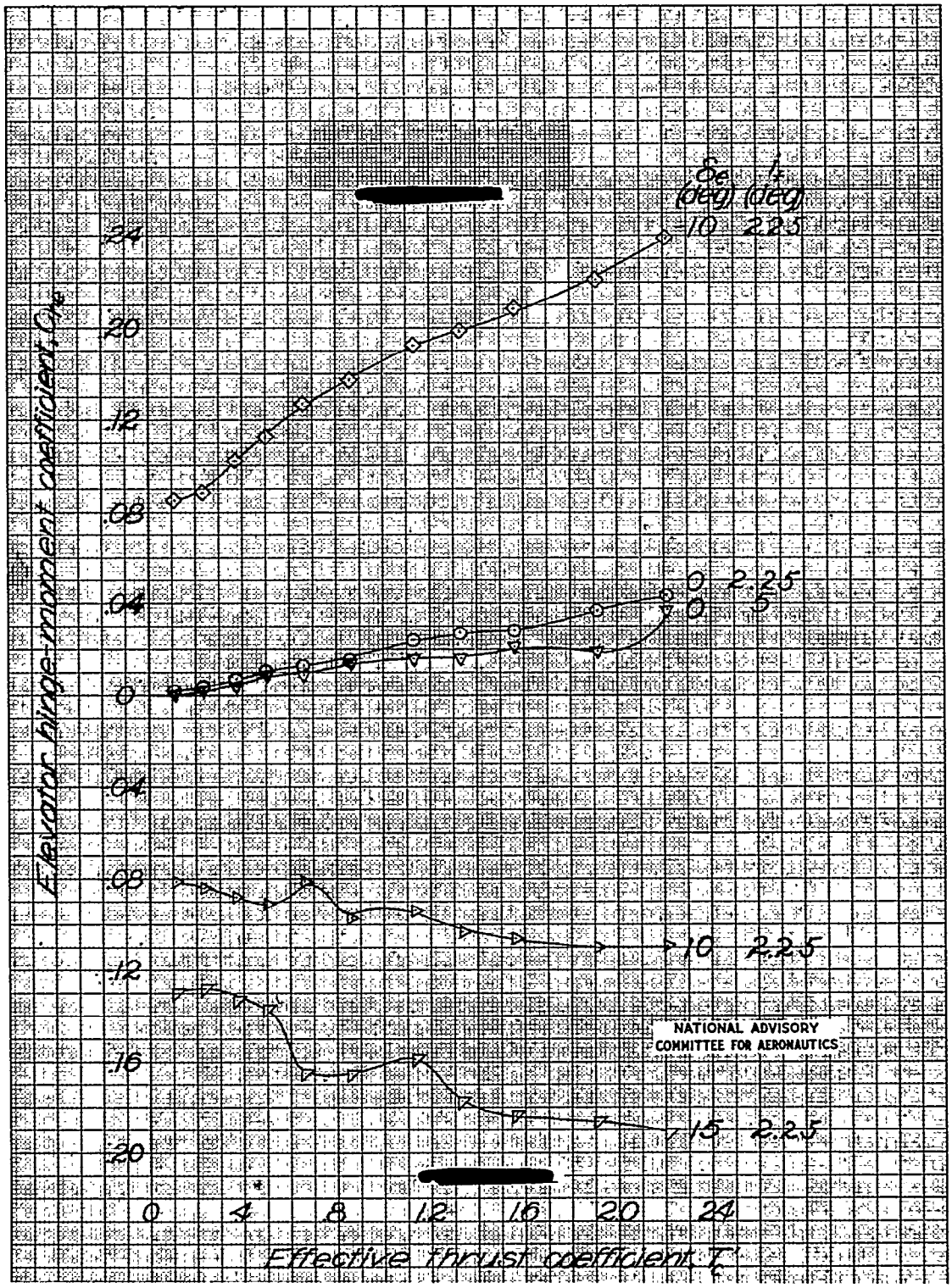

(a) Concluded.

Figure 42.- Continued.

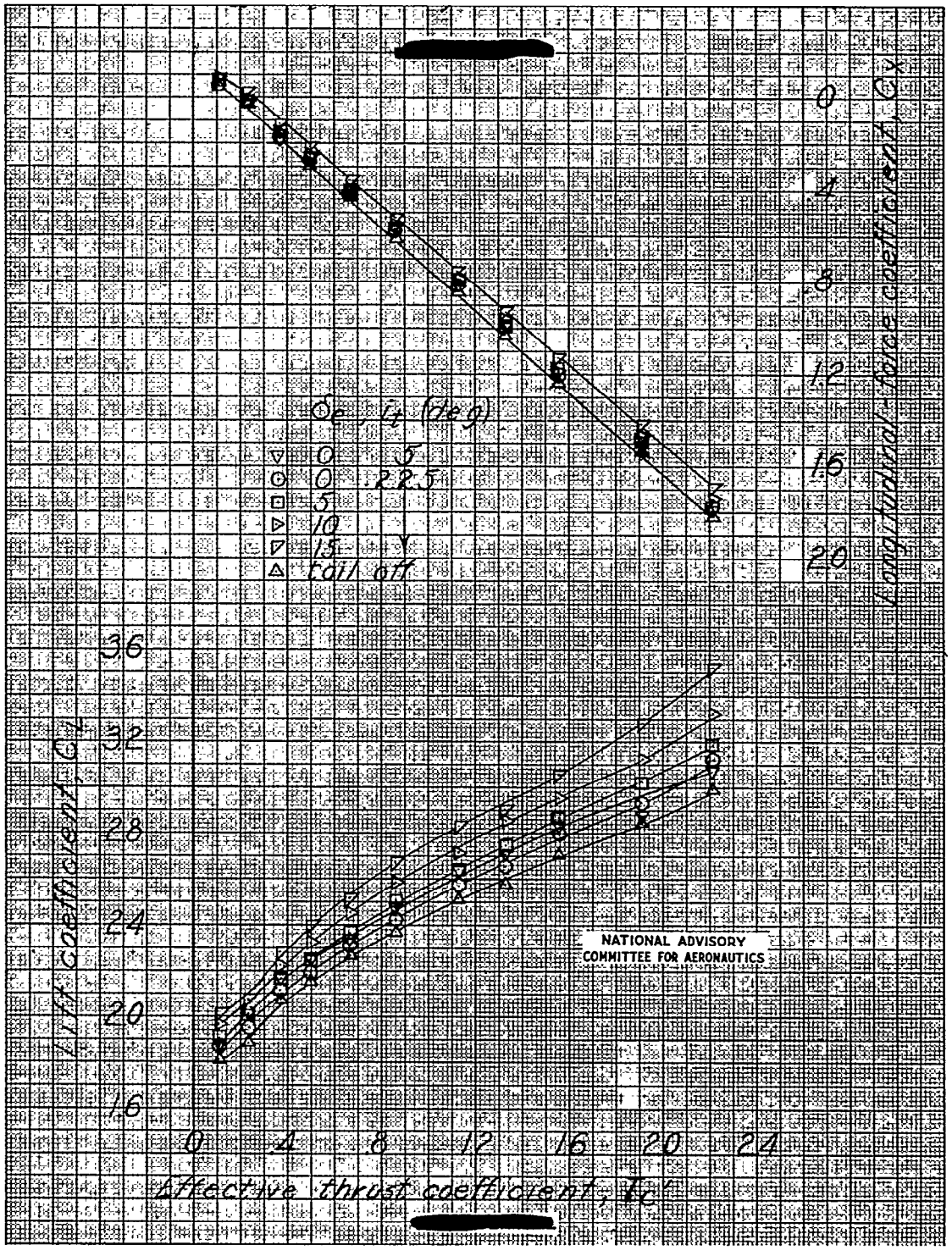

(b) $\alpha = 11.5^{\circ}$; original thrust line

Figure 42.- Continued

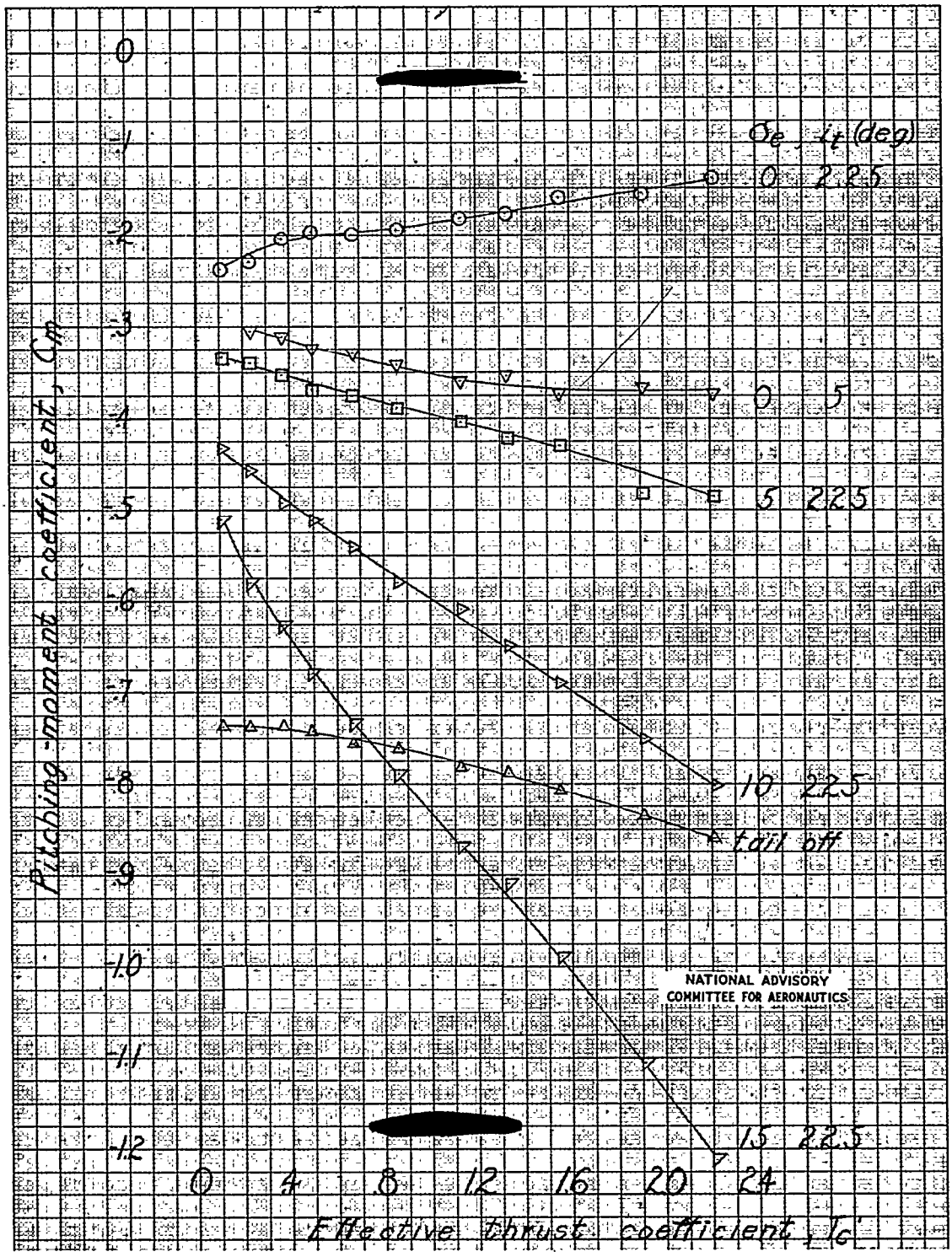

(b) Continued.

Figure 42.- Continued.

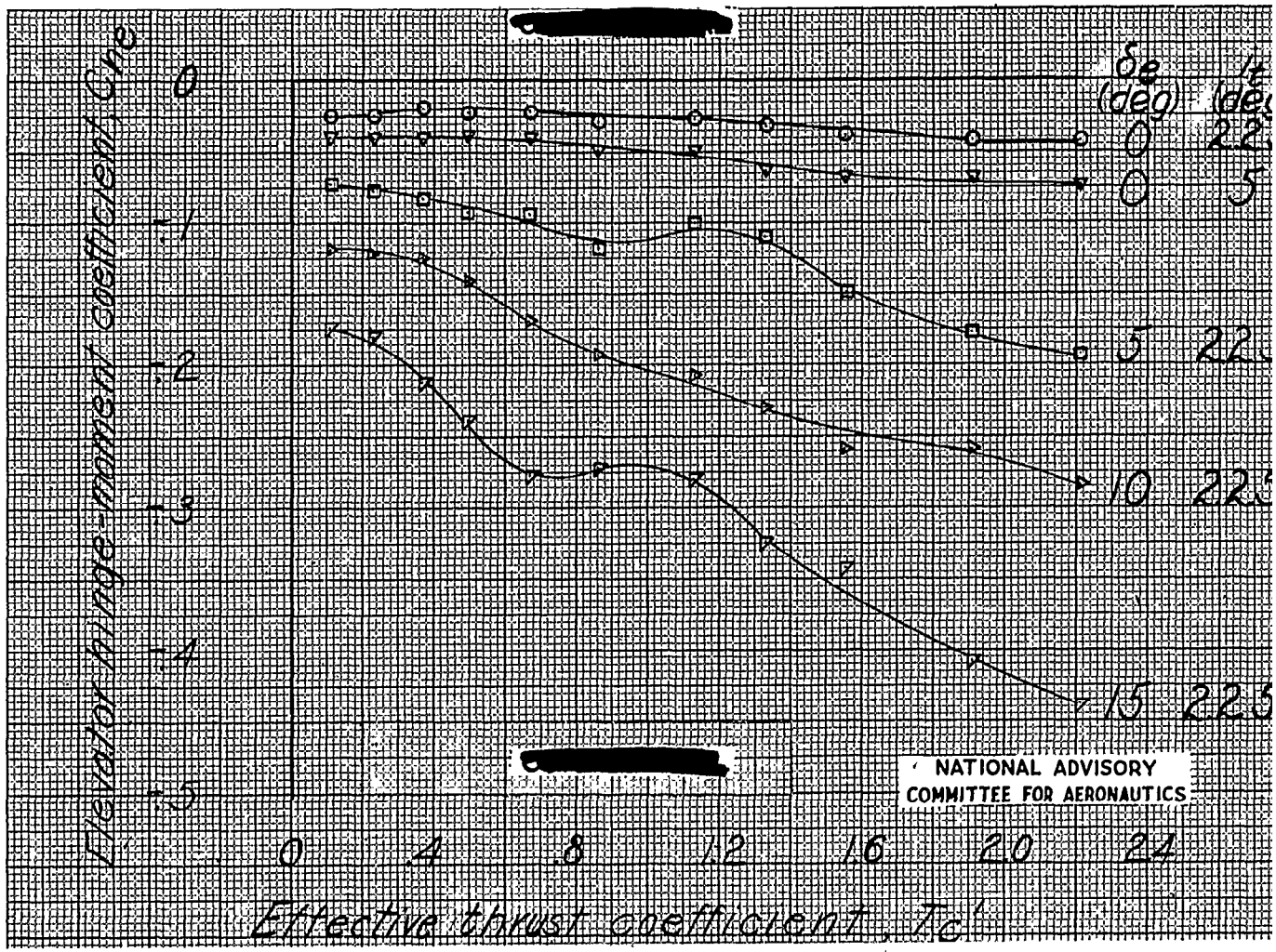

(b) Concluded.

Figure 42.- Continued.

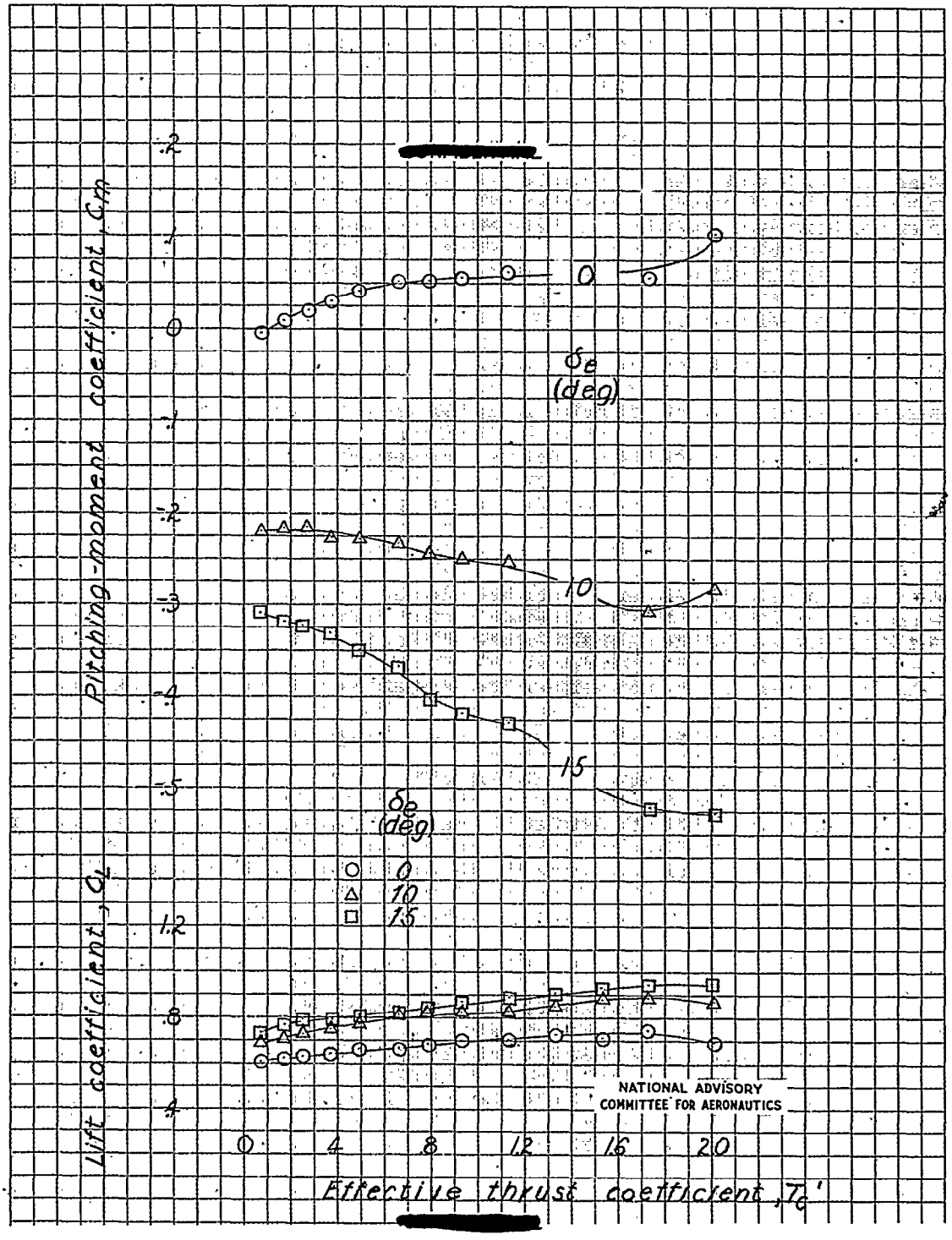

(c) $\alpha = -.1^\circ$; thrust line tilted down 3°.

Figure 42.- Continued.

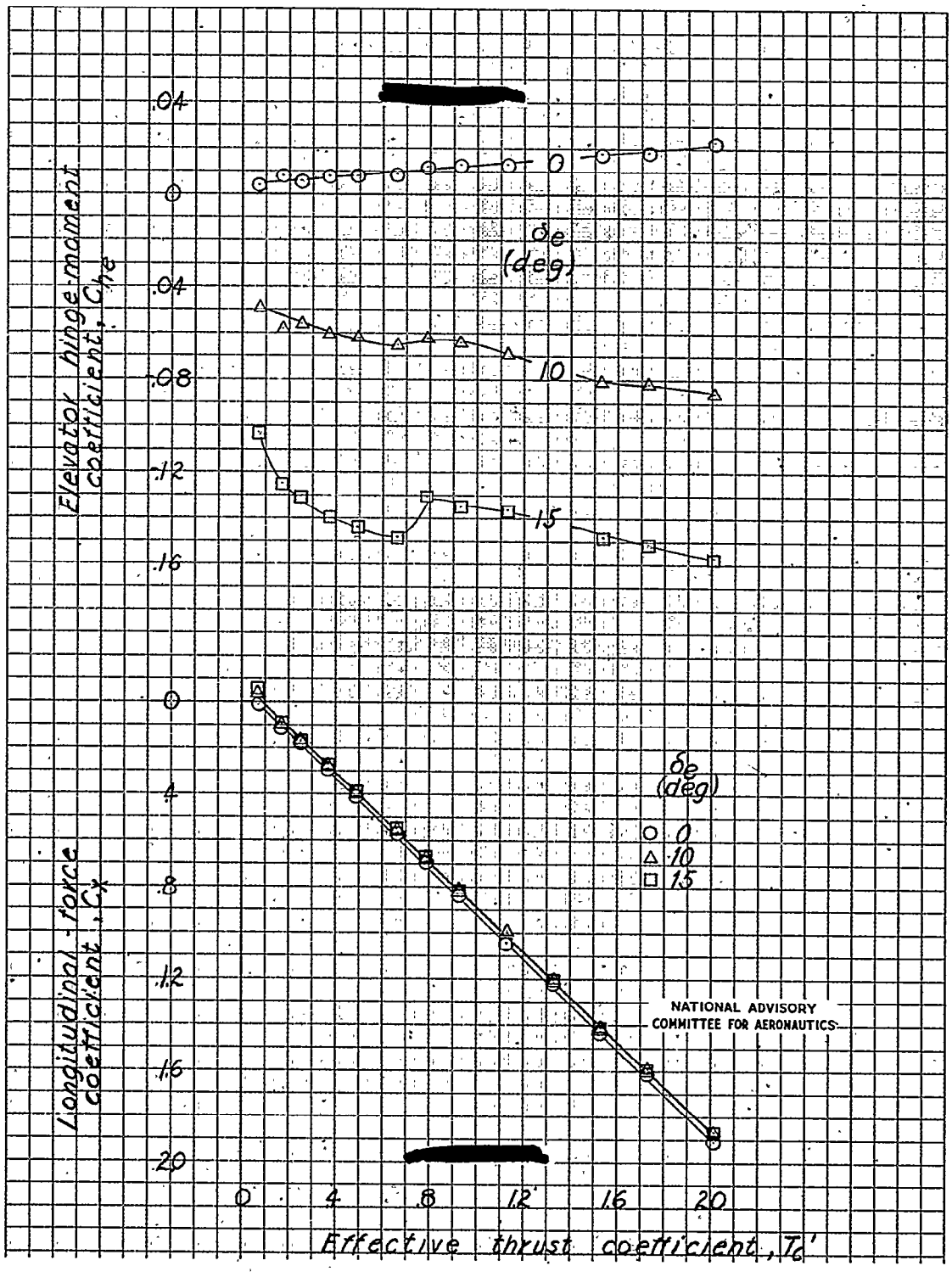

(c) Concluded.

Figure 42.- Continued.

[redacted]

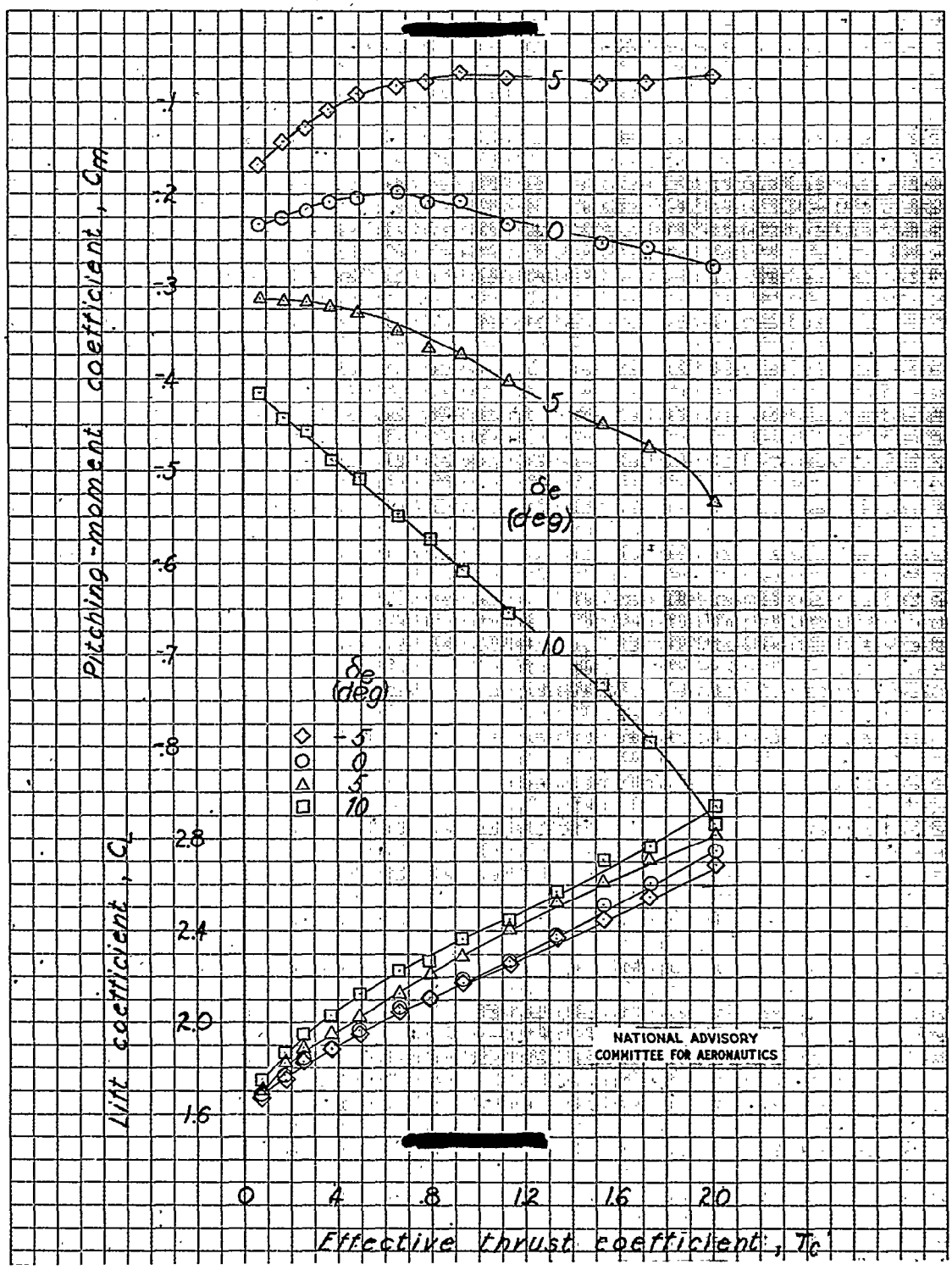

[redacted]

(d) $\alpha = 11.3^\circ$; thrust line tilted down 3°; $i_t = 2.25^\circ$.

Figure 42.- Continued.

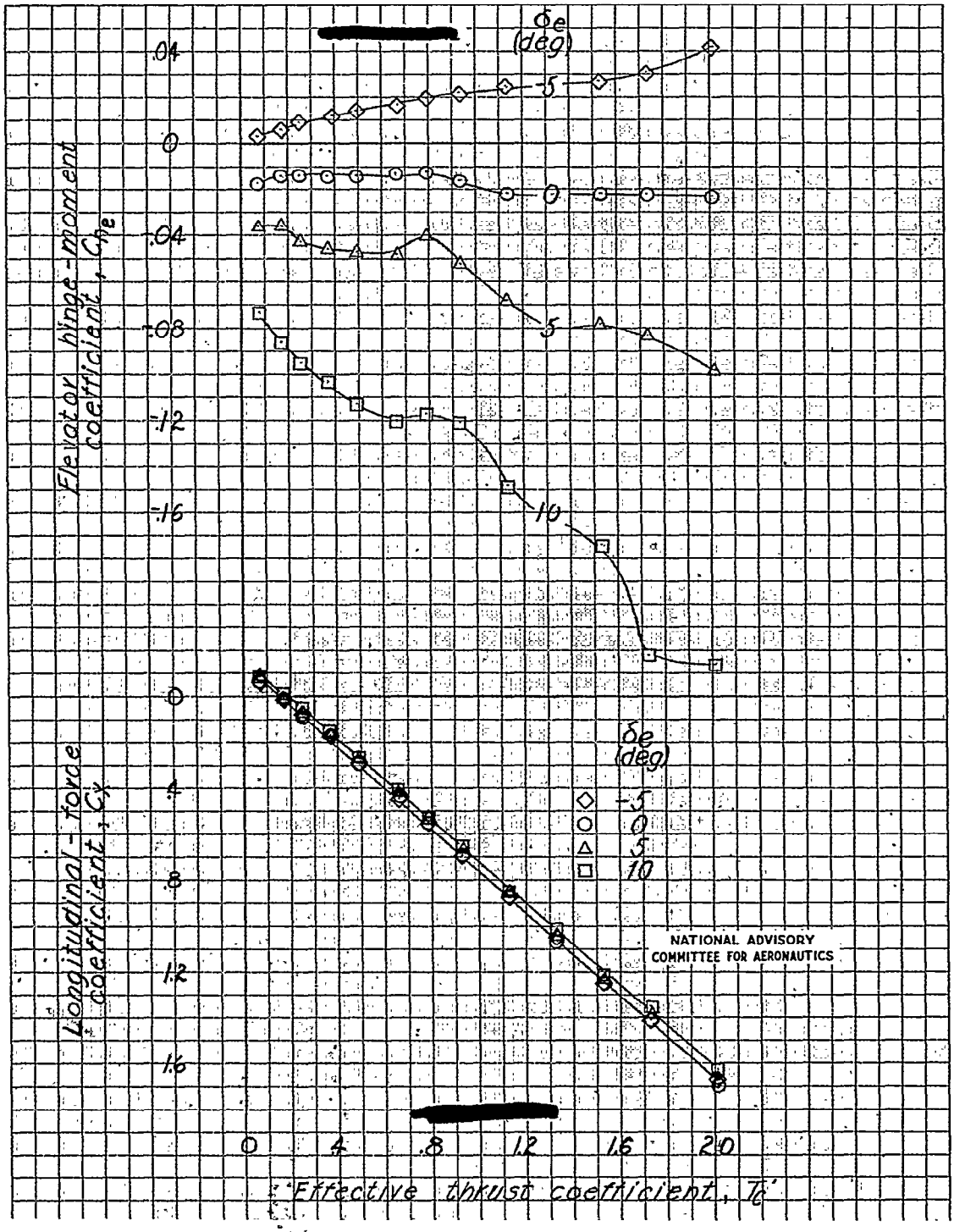

(d) Concluded.

Figure 42.- Concluded.

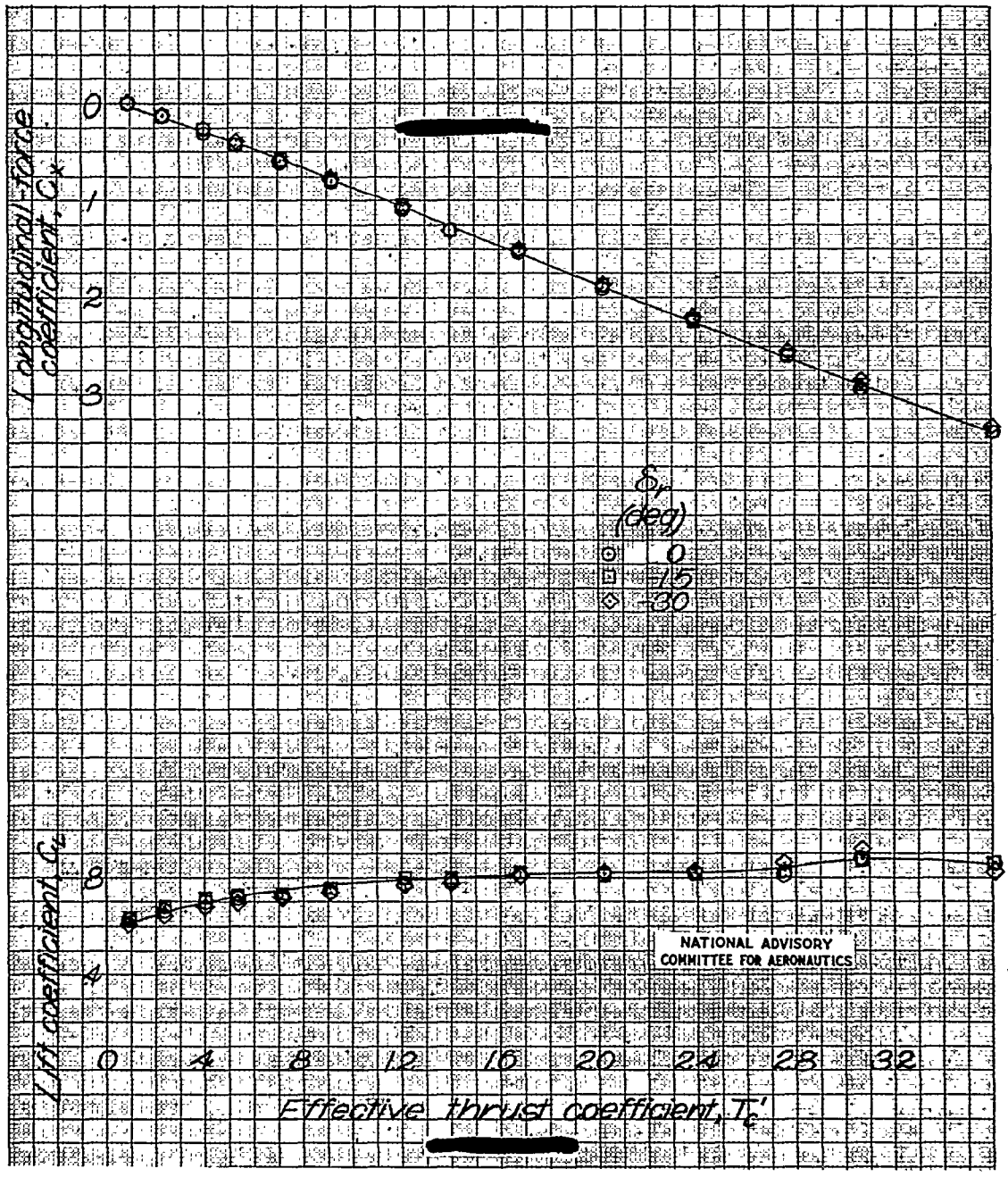

(a) $\alpha = 0^\circ$; original thrust line; original vertical tail.

Figure 43.- Effect of rudder deflection on the aerodynamic characteristics of a 1/8-scale model of the Grumman XTB3F-1 airplane with the ground board in place. Take-off configuration; $\beta = 15^\circ$; $\Psi = 0^\circ$; original dorsal fin; $i_{fin} = -2^\circ 15'$.

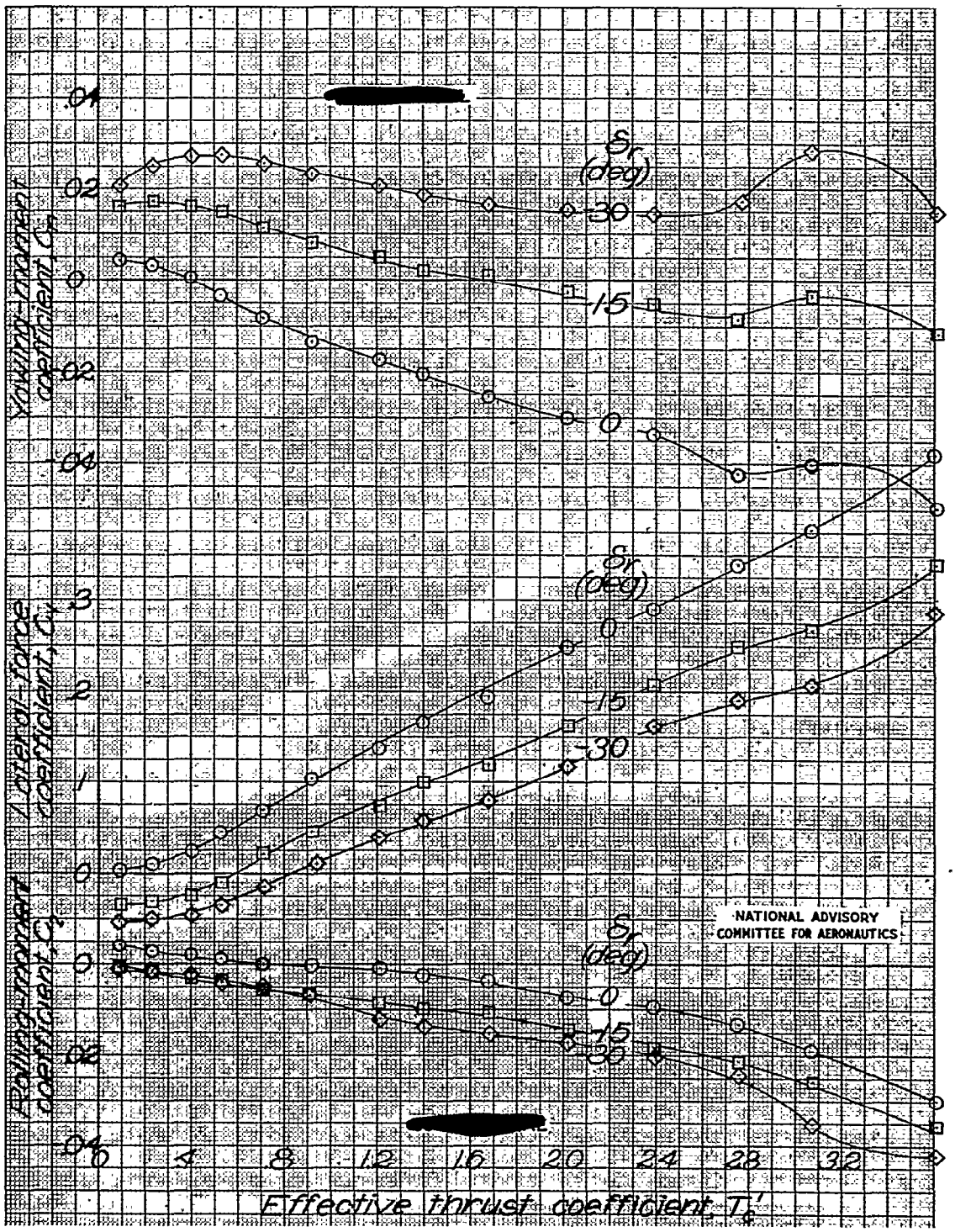

(a) Continued.

Figure 43.- Continued.

[redacted]

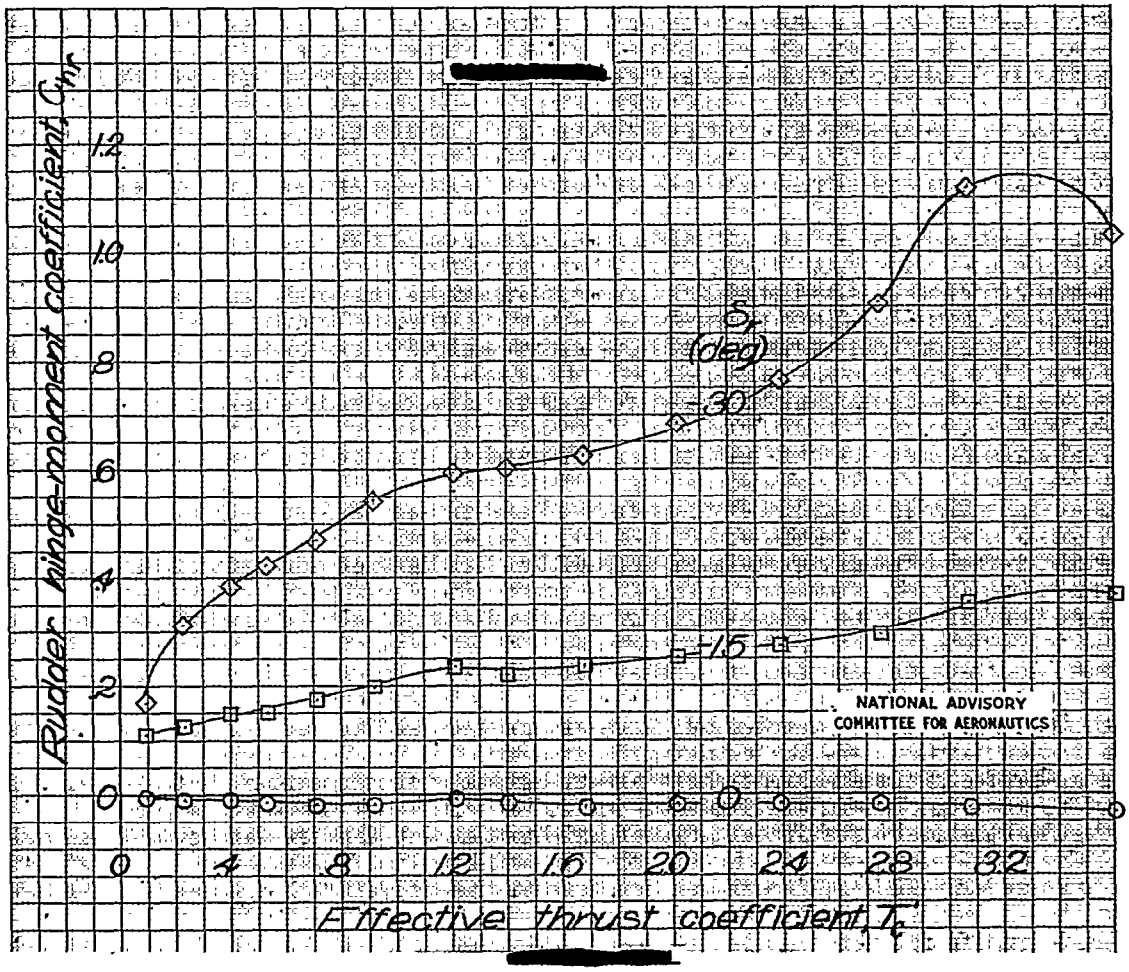

[redacted]

(a) Concluded.

Figure 43.- Continued.

[redacted]

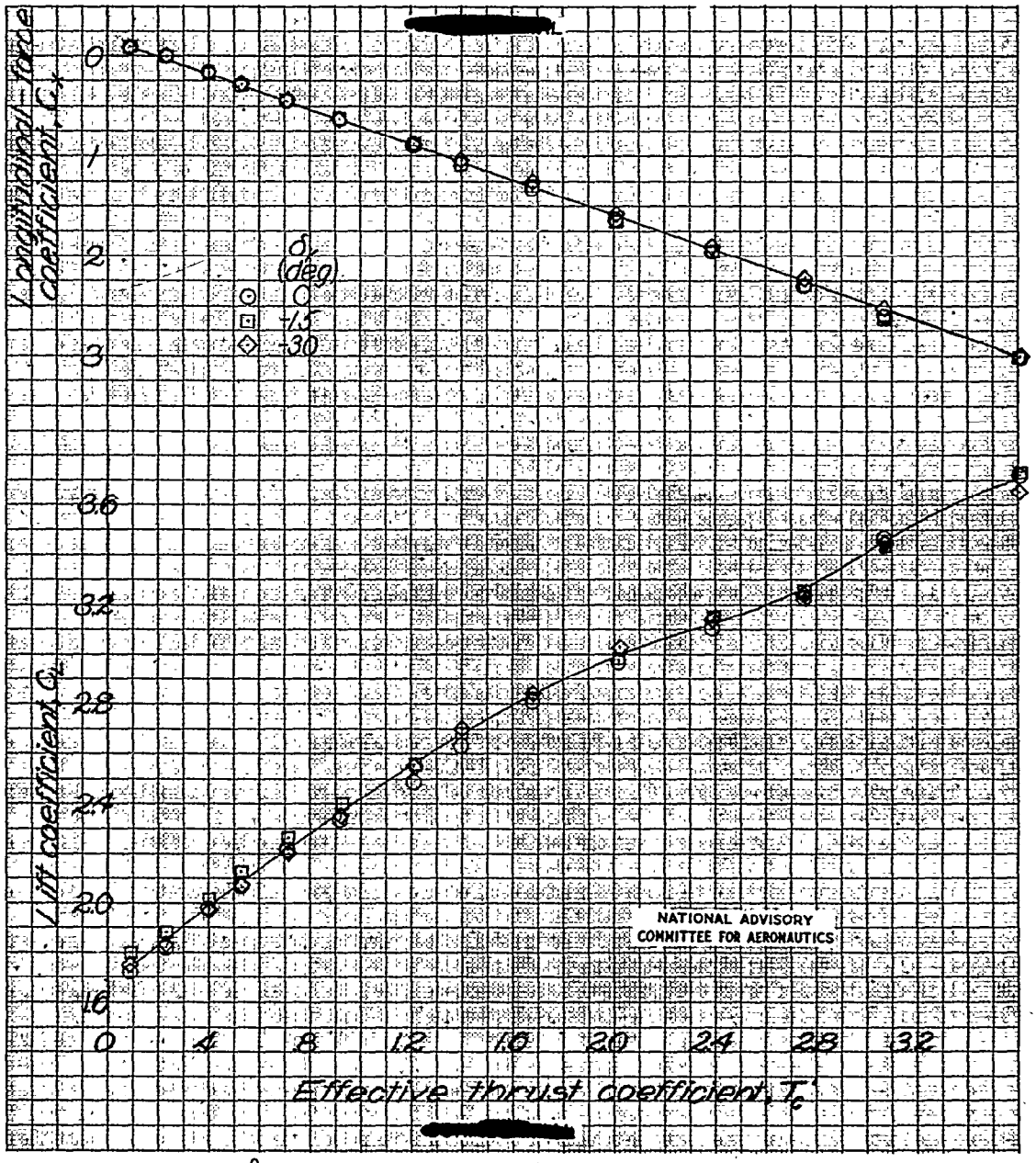

[redacted]

(b) $\alpha = 11.5^{\circ}$; original thrust line; original vertical tail.

Figure 43.- Continued.

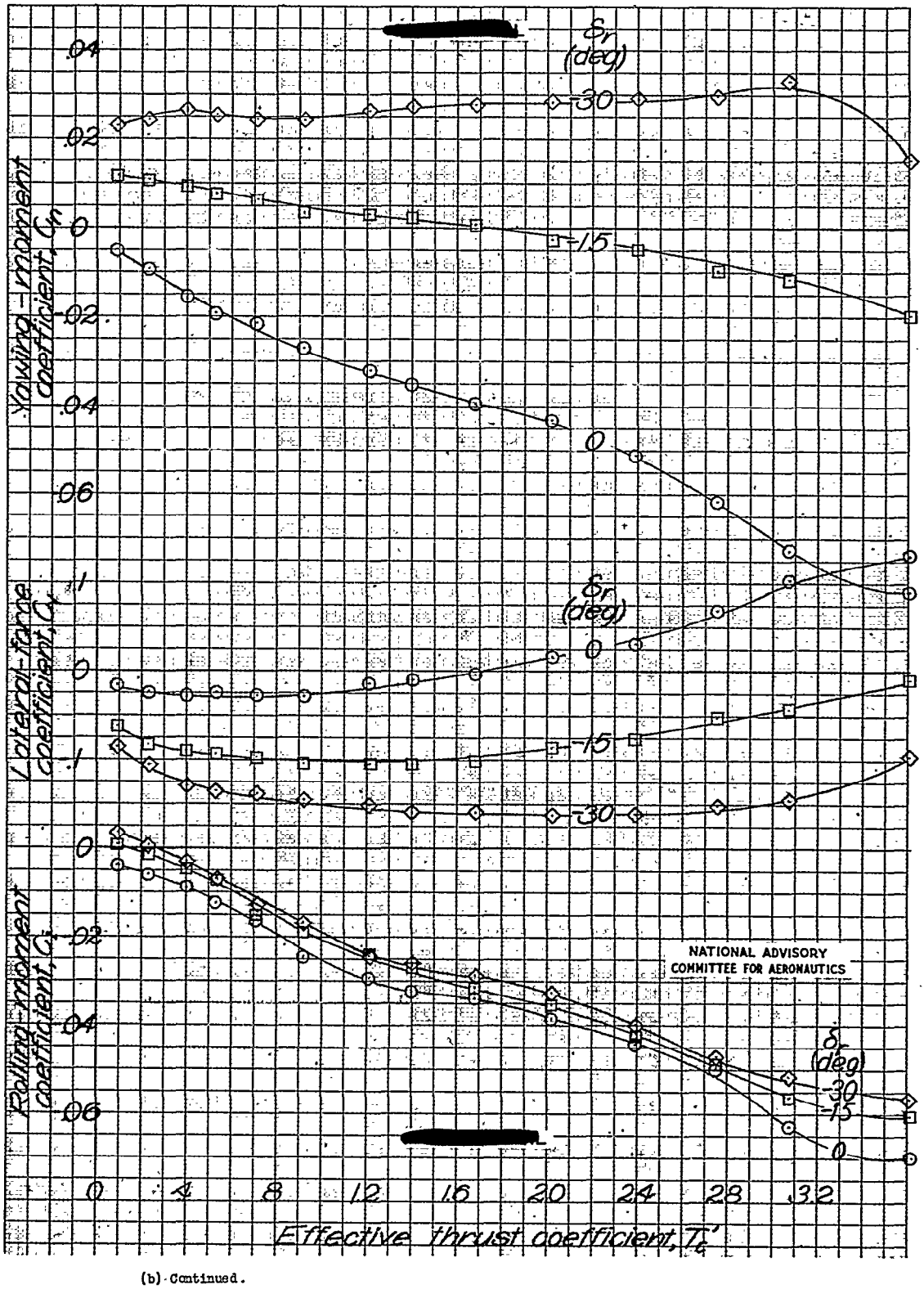

(b) Continued.

Figure 43.- Continued.

[redacted]

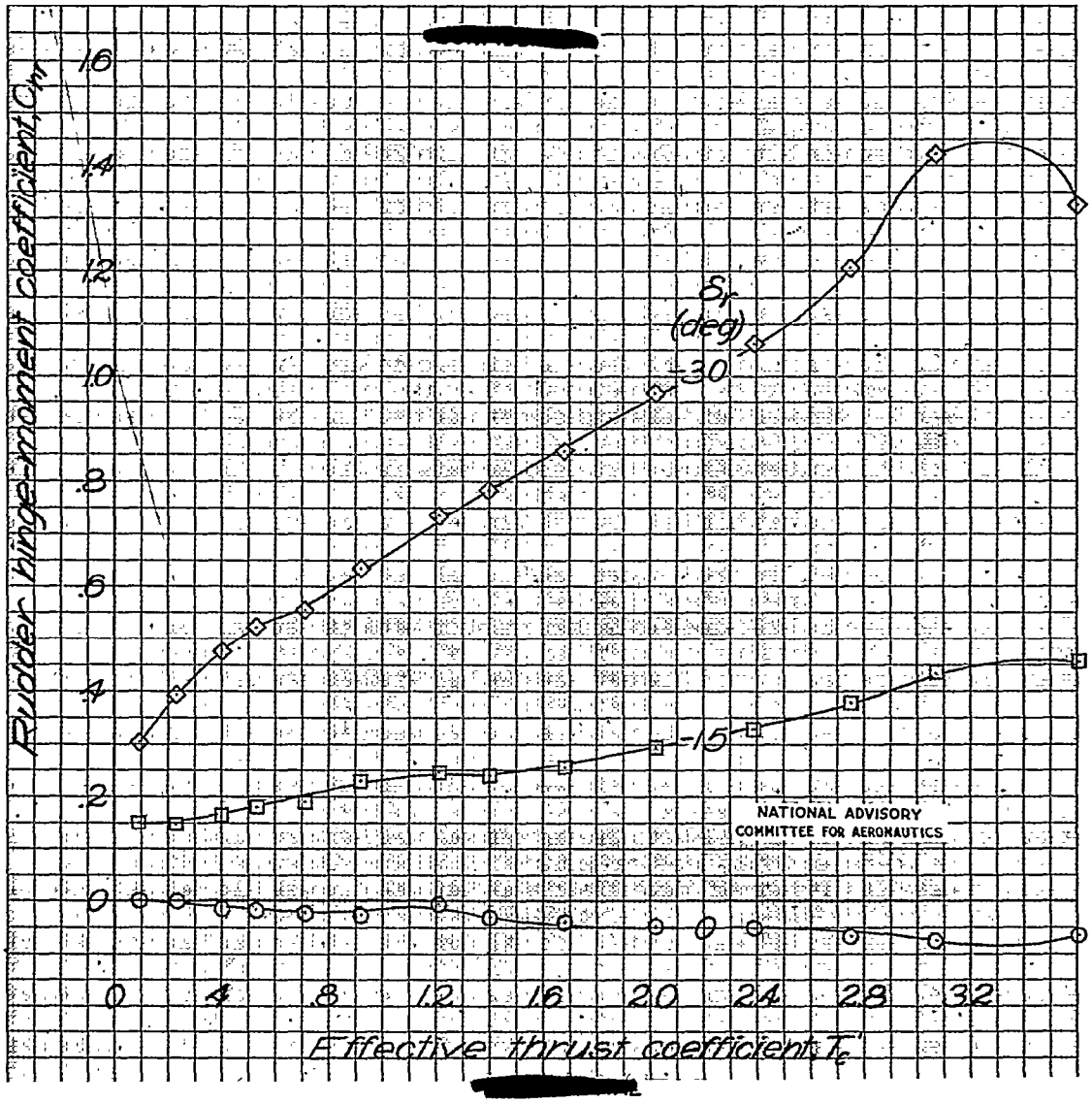

[redacted]

(b) Concluded.

Figure 43.- Continued.

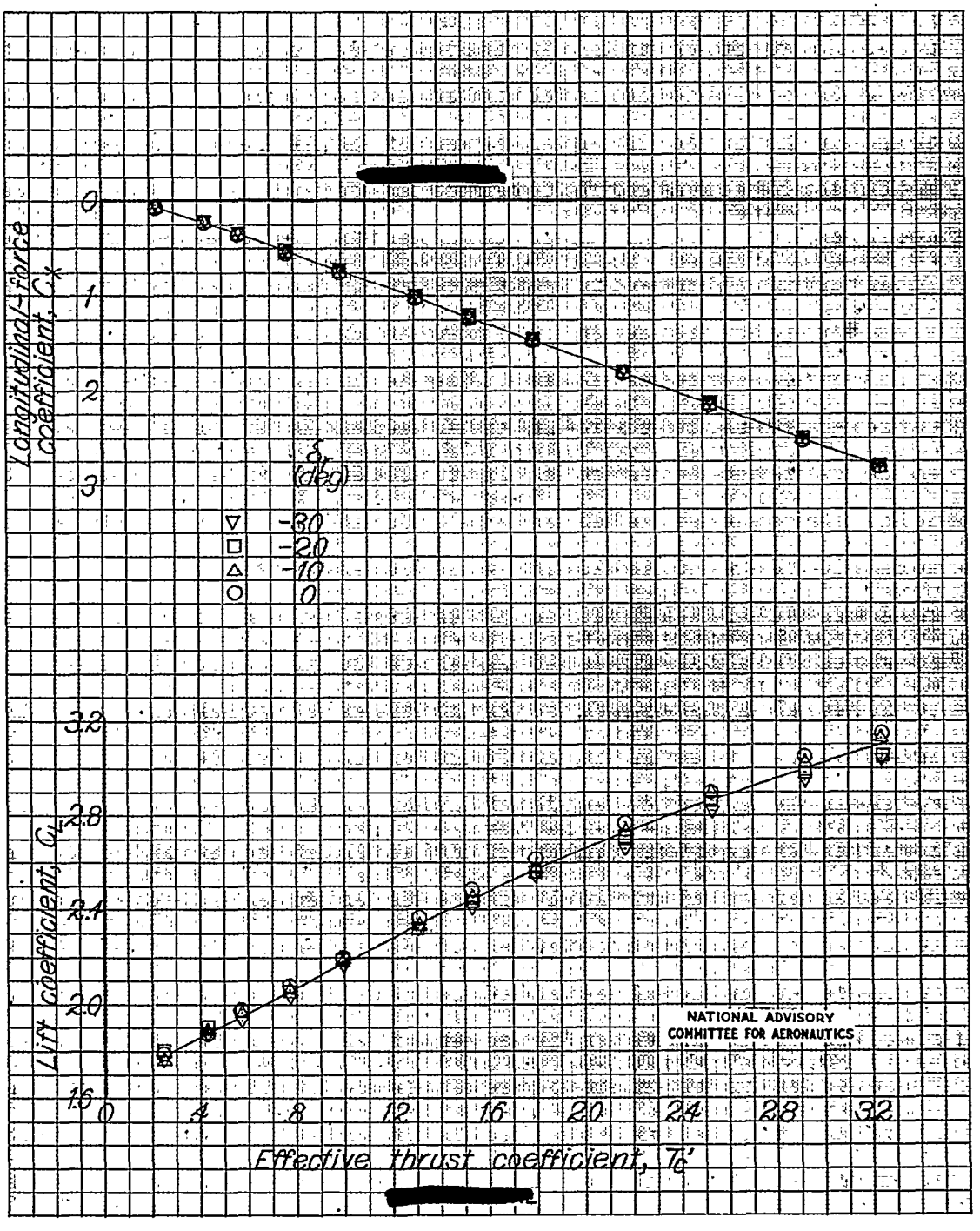

(c) $\alpha = 11.4^\circ$; 1.5-inch base extension on vertical tail; thrust line tilted down 3°.

Figure 43.- Continued.

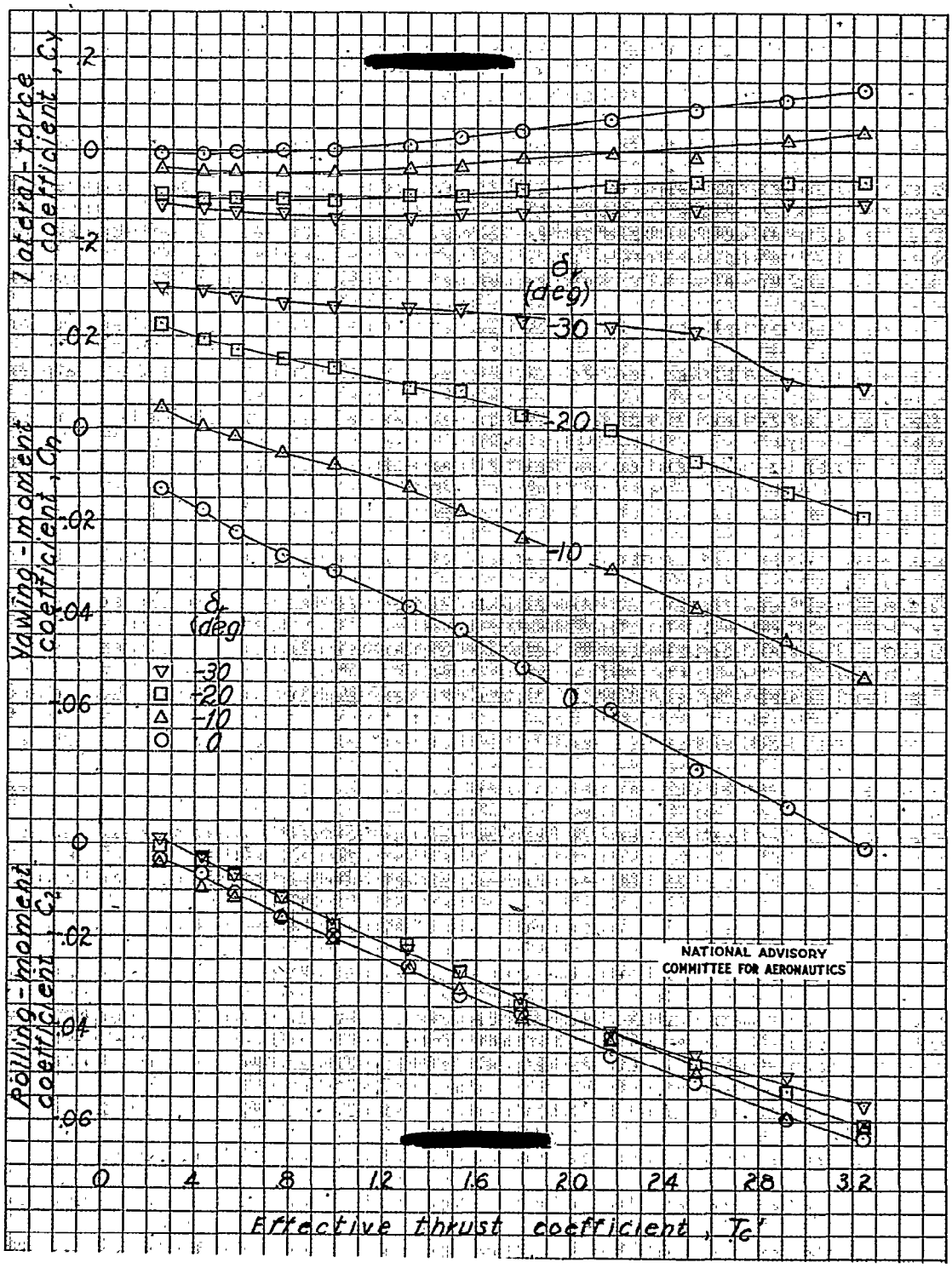

(c) Continued.

Figure 43.- Continued.

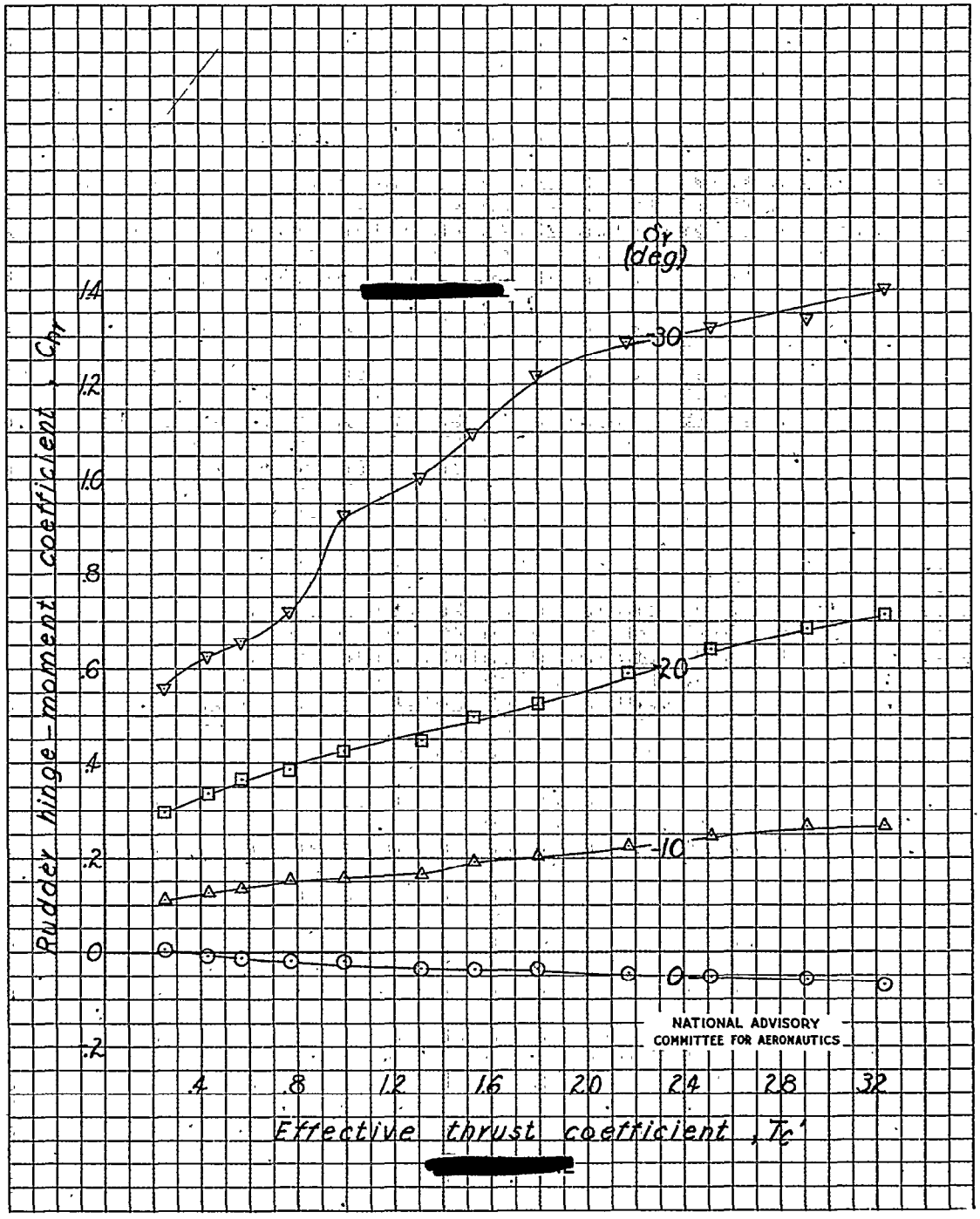

(c) Concluded.

Figure 43.- Concluded.

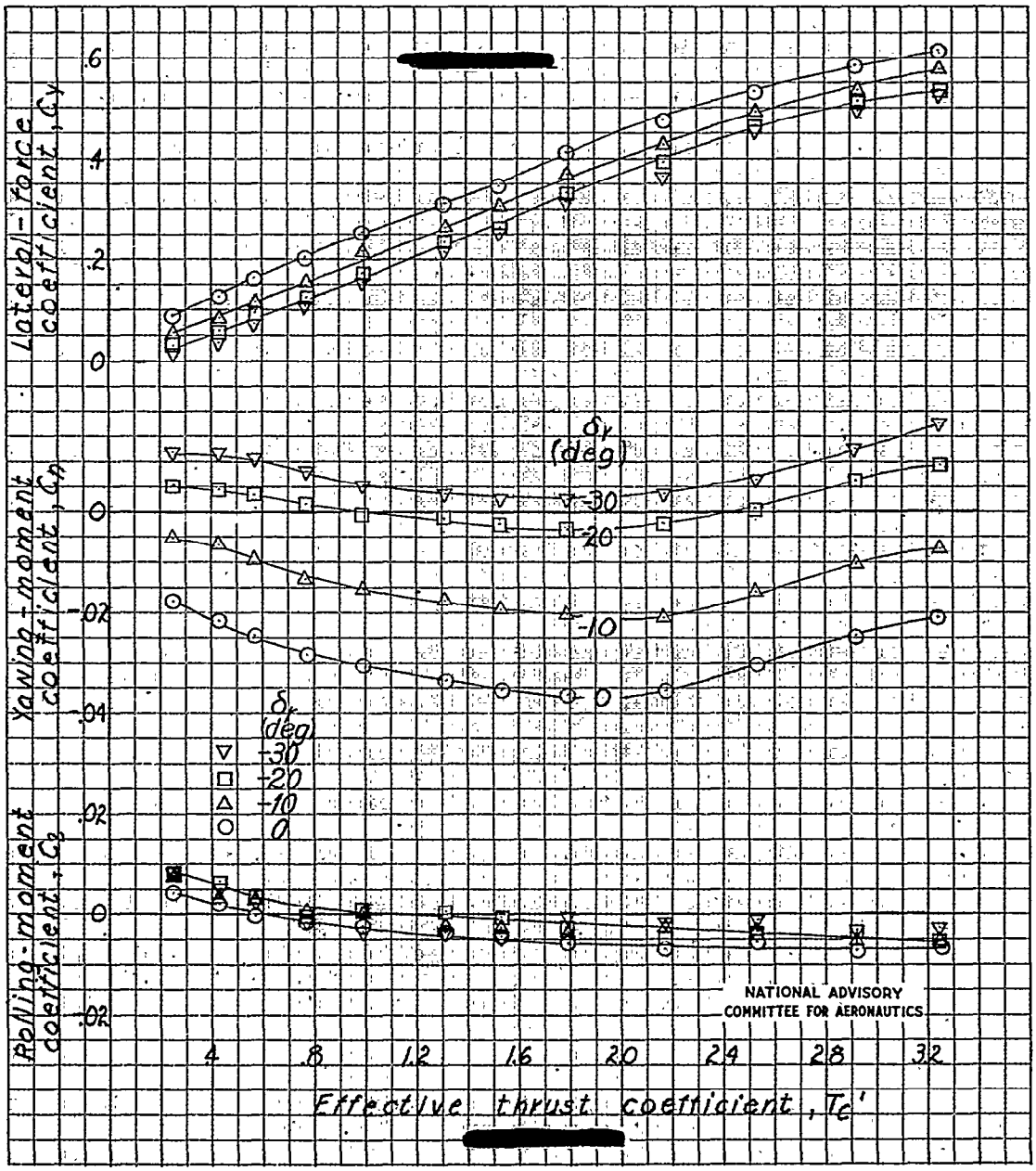

Figure 44.- Effect of rudder deflection on the aerodynamic characteristics of a 1/8-scale model of the Grumman XTB3F-1 airplane with the ground board in place. Simulated take-off in a 17.6 m.p.h. crosswind, from the left, at 90° to the flight path; take-off configuration; $\alpha = 11.4°$; $\beta = 15°$; 1.5 inch base extension on vertical tail; original dorsal fin; thrust line tilted down 3°; $i_{fin} = -2°15'$.

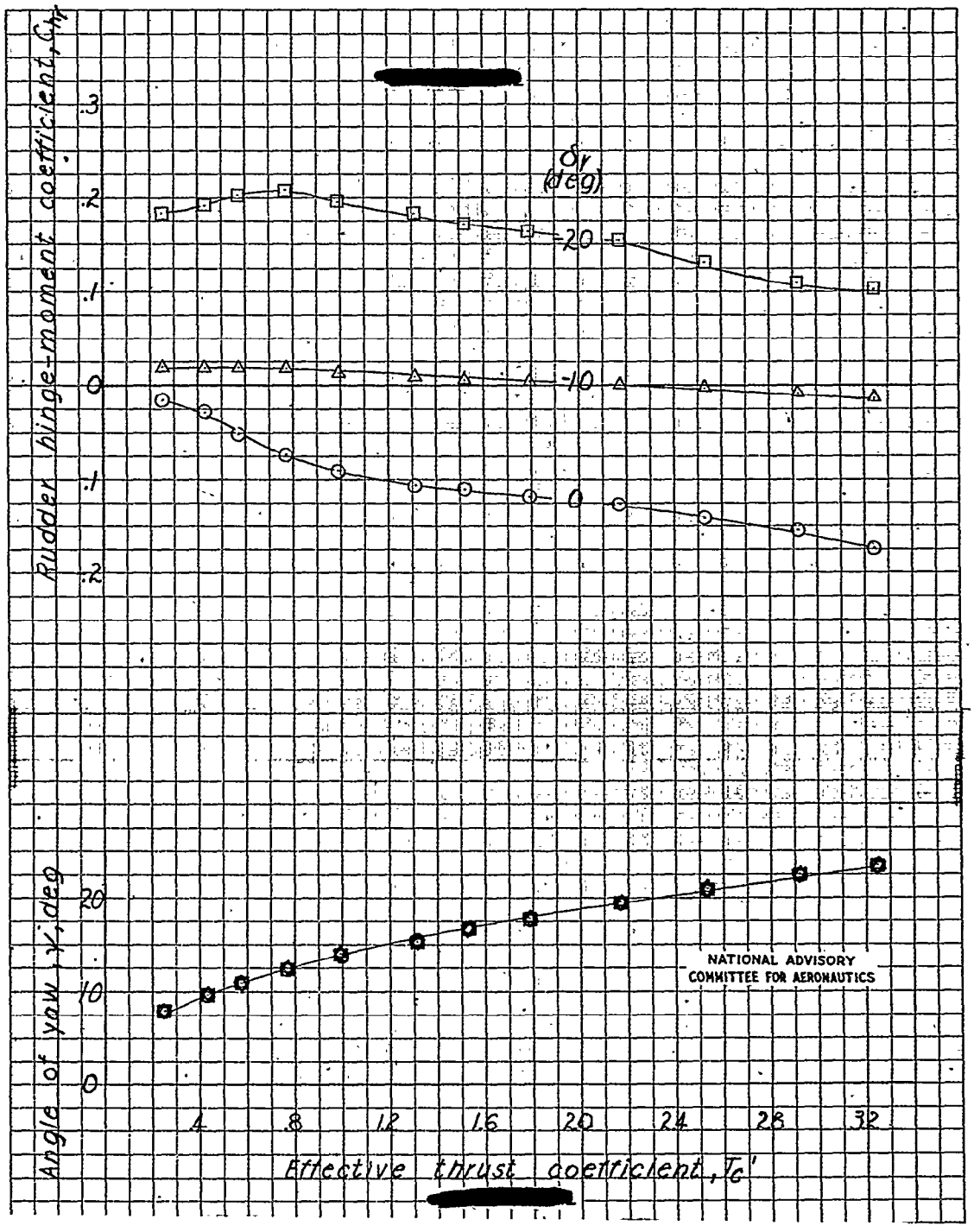

Figure 44.- Continued.

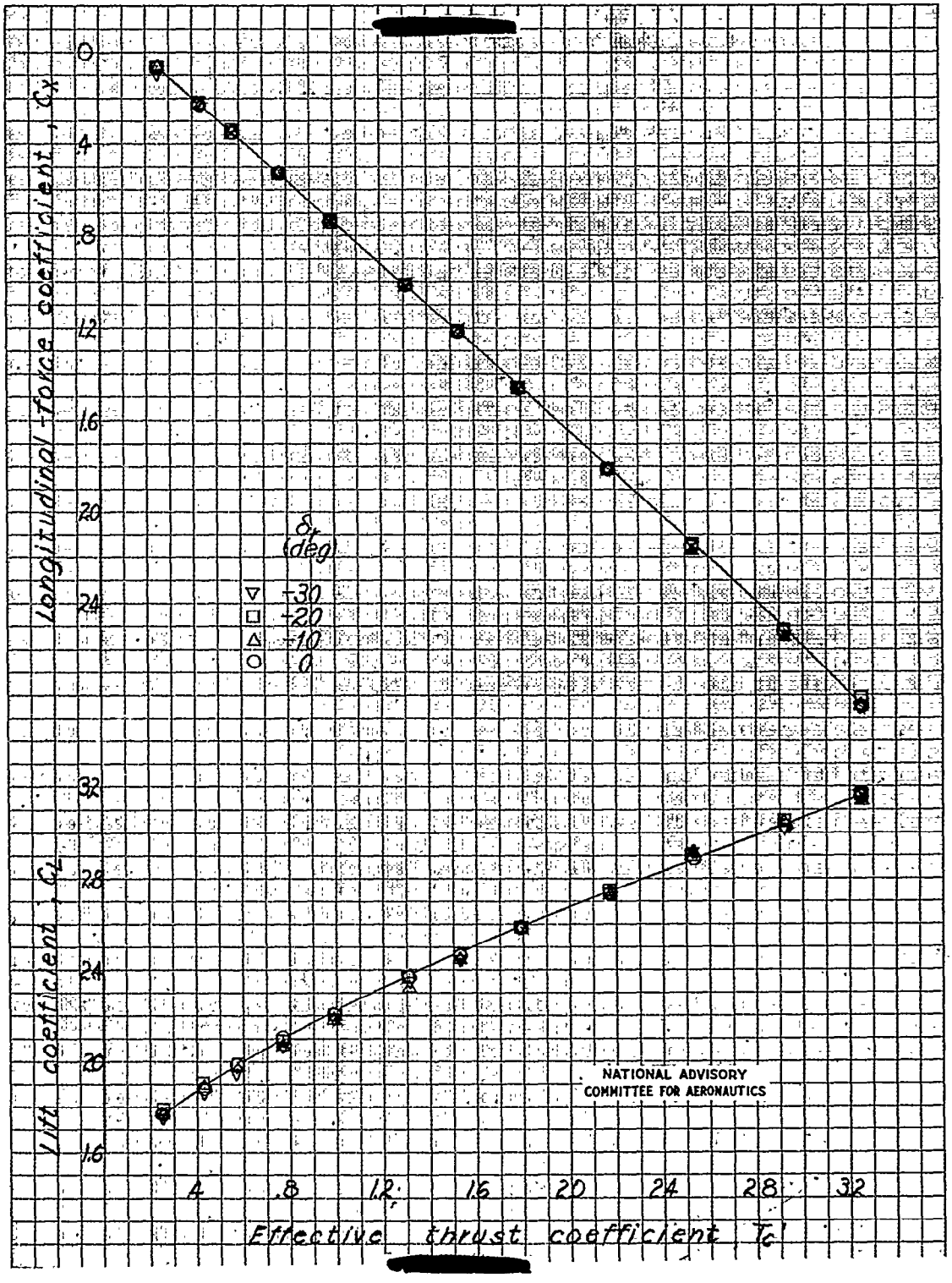

Figure 44.- Concluded.

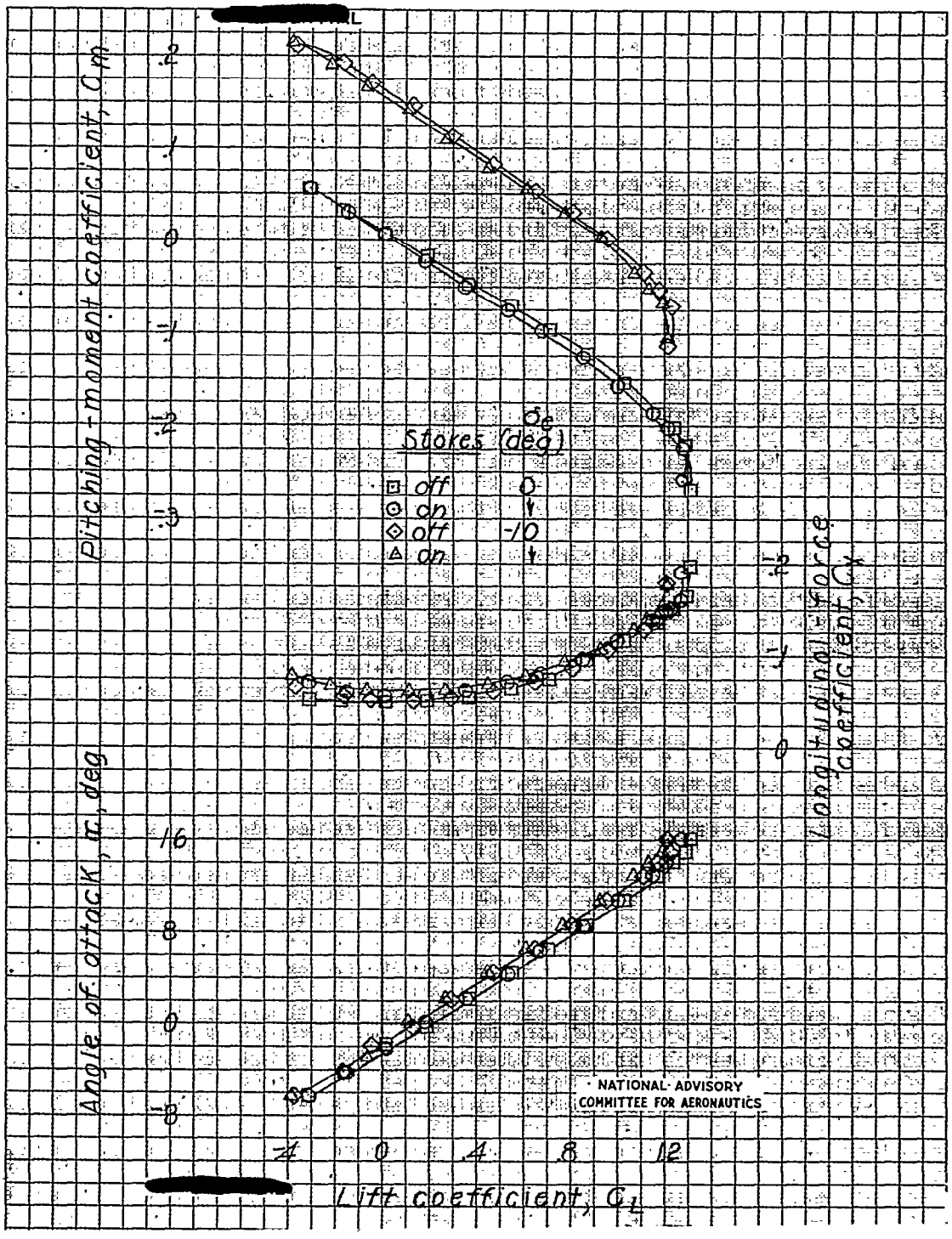

(a) Glide configuration.

Figure 45.- Effect of external stores on the aerodynamic characteristics in pitch of a 1/8-scale model of the Grumman XTB3F-1 airplane. Thrust line tilted down 3°.

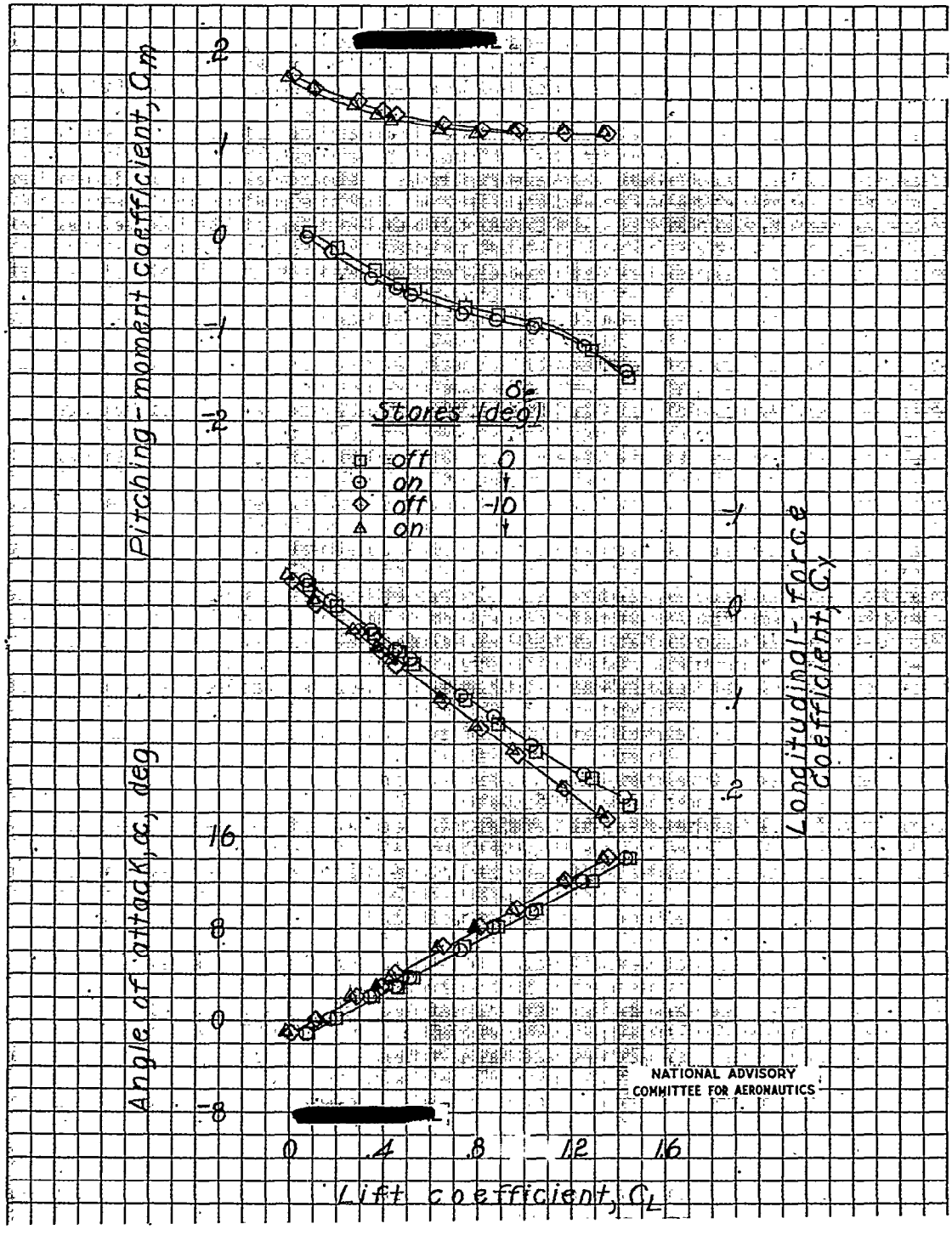

(b) Power-on clean configuration.

Figure 45.- Concluded.

[redacted]

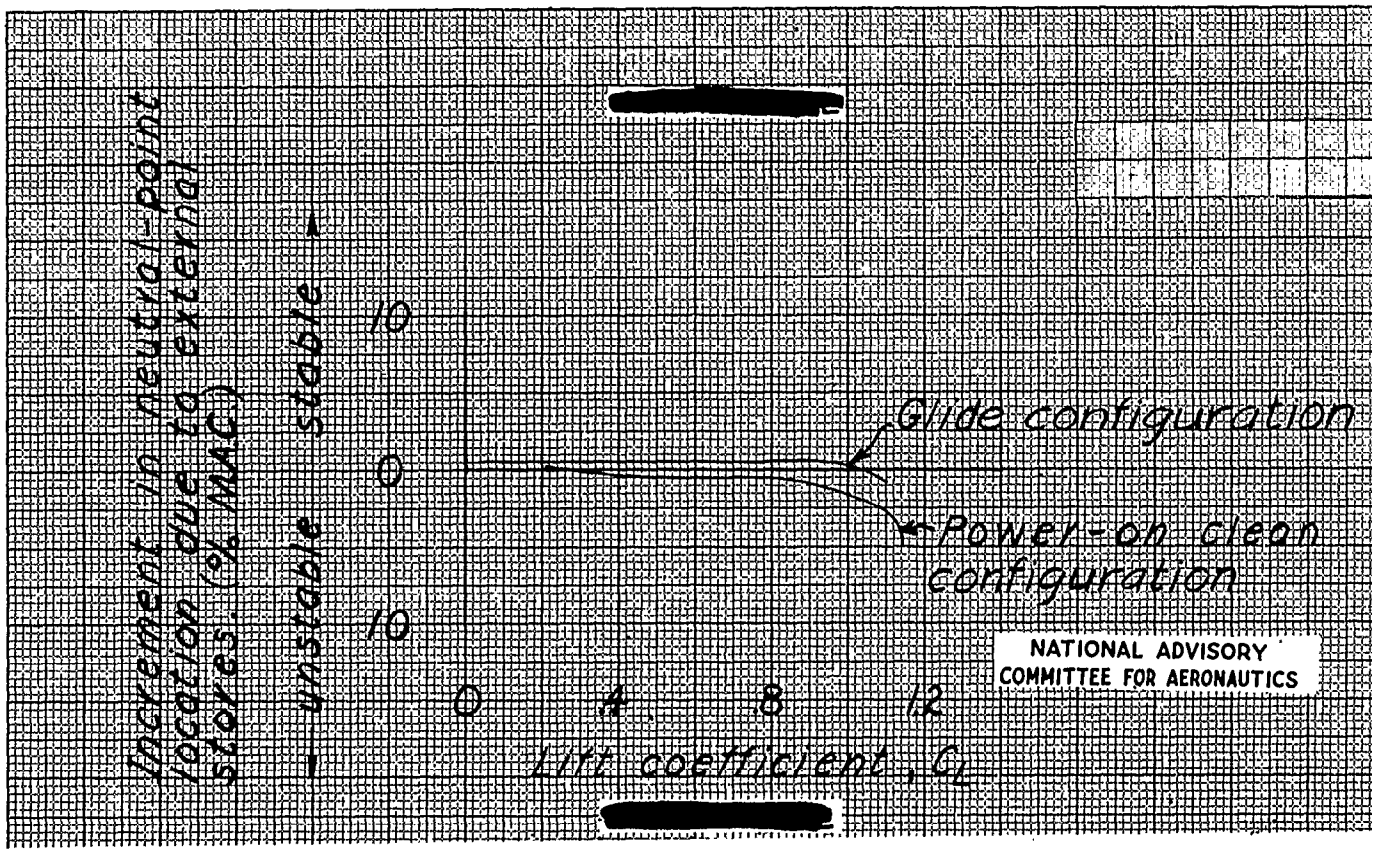

[redacted]

Figure 46.- Increment in neutral-point location due to external stores for a 1/8-scale model of the Grumman XTB3F-1 airplane.

[redacted]

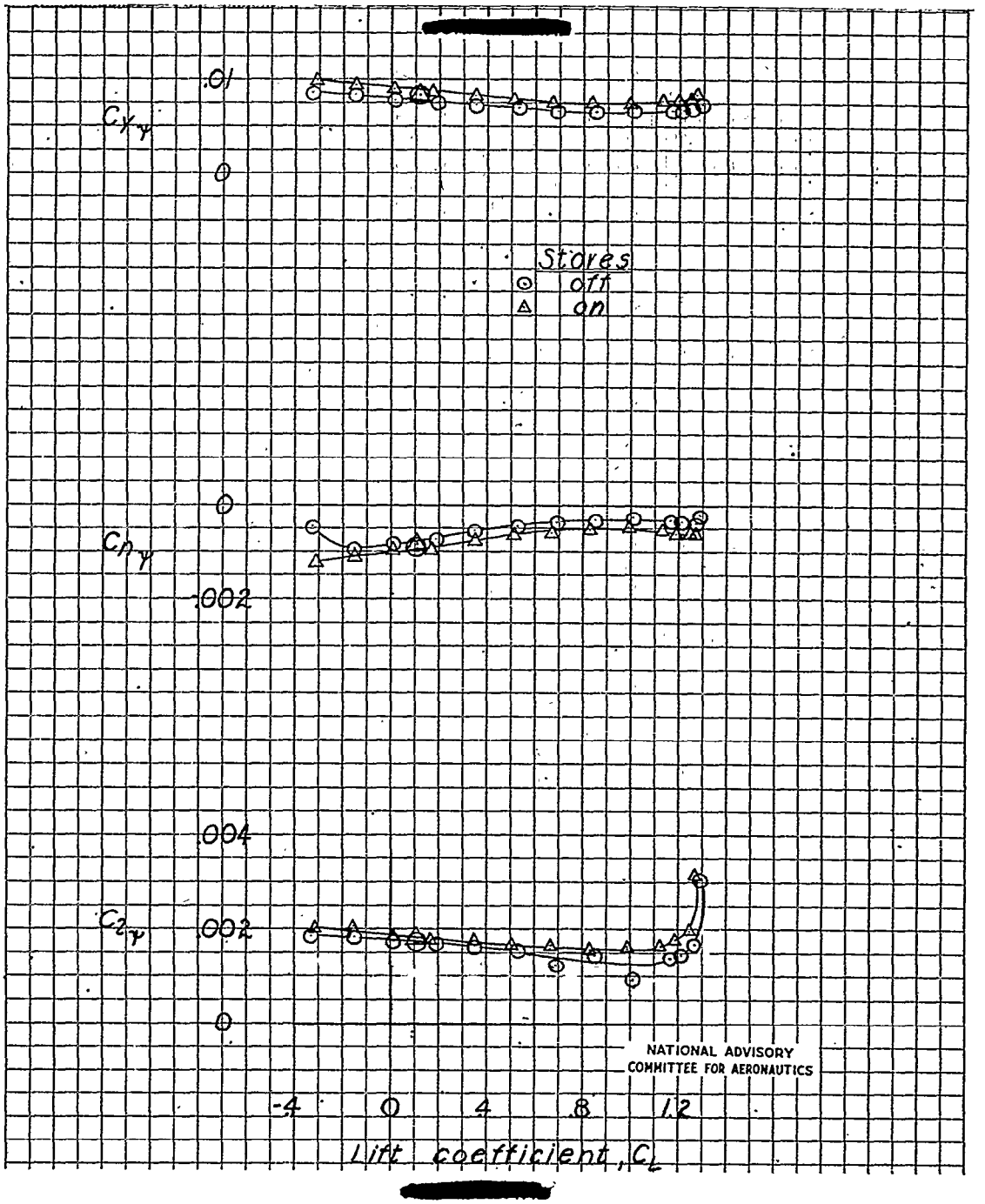

[redacted]

(a) Glide configuration.

Figure 47.- Effect of external stores on the lateral stability parameters of a 1/8-scale model of the Grumman XTB3F-1 airplane. Large dorsal fin; 1.5-inch base extension on vertical tail.

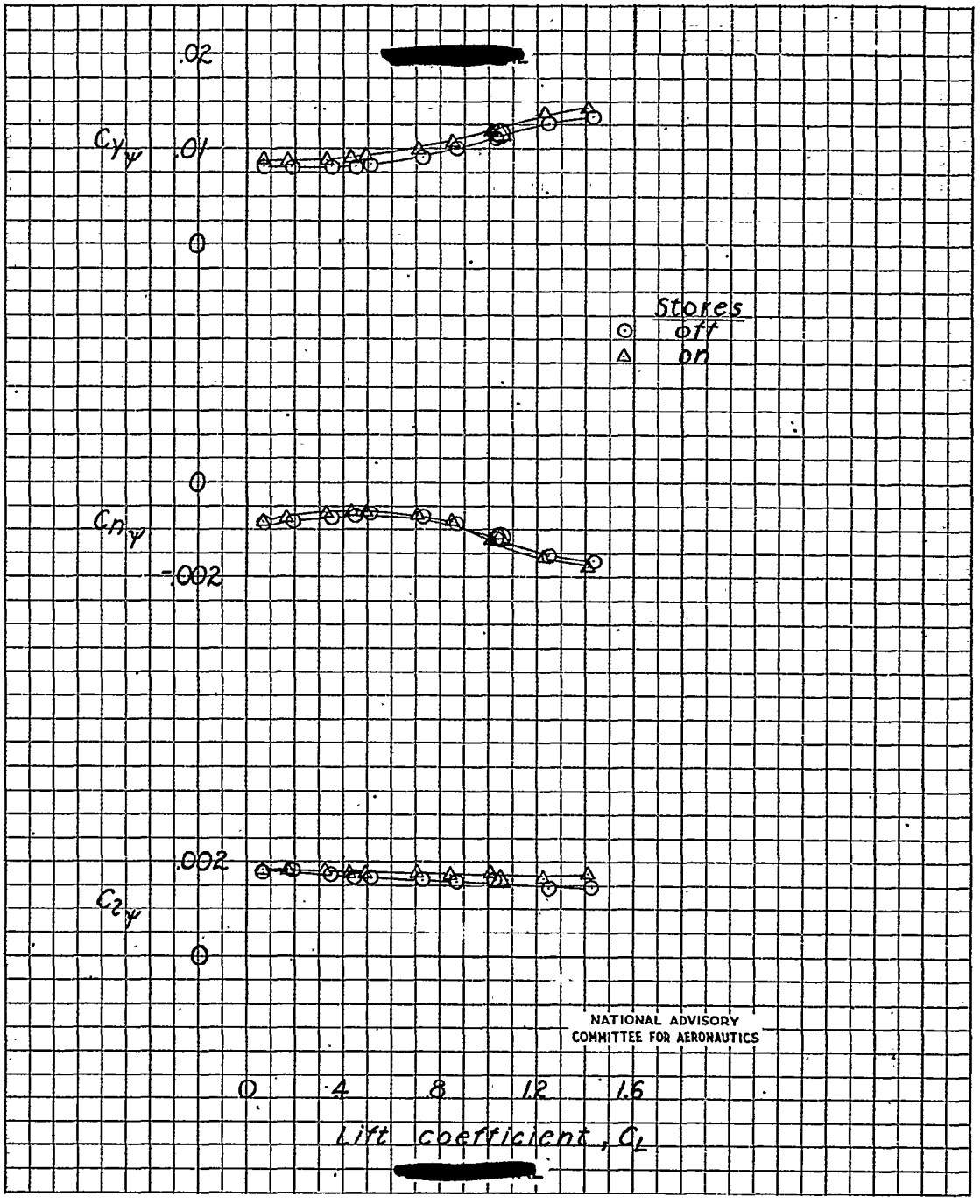

(b) Power-on clean configuration.

Figure 47.- Concluded.

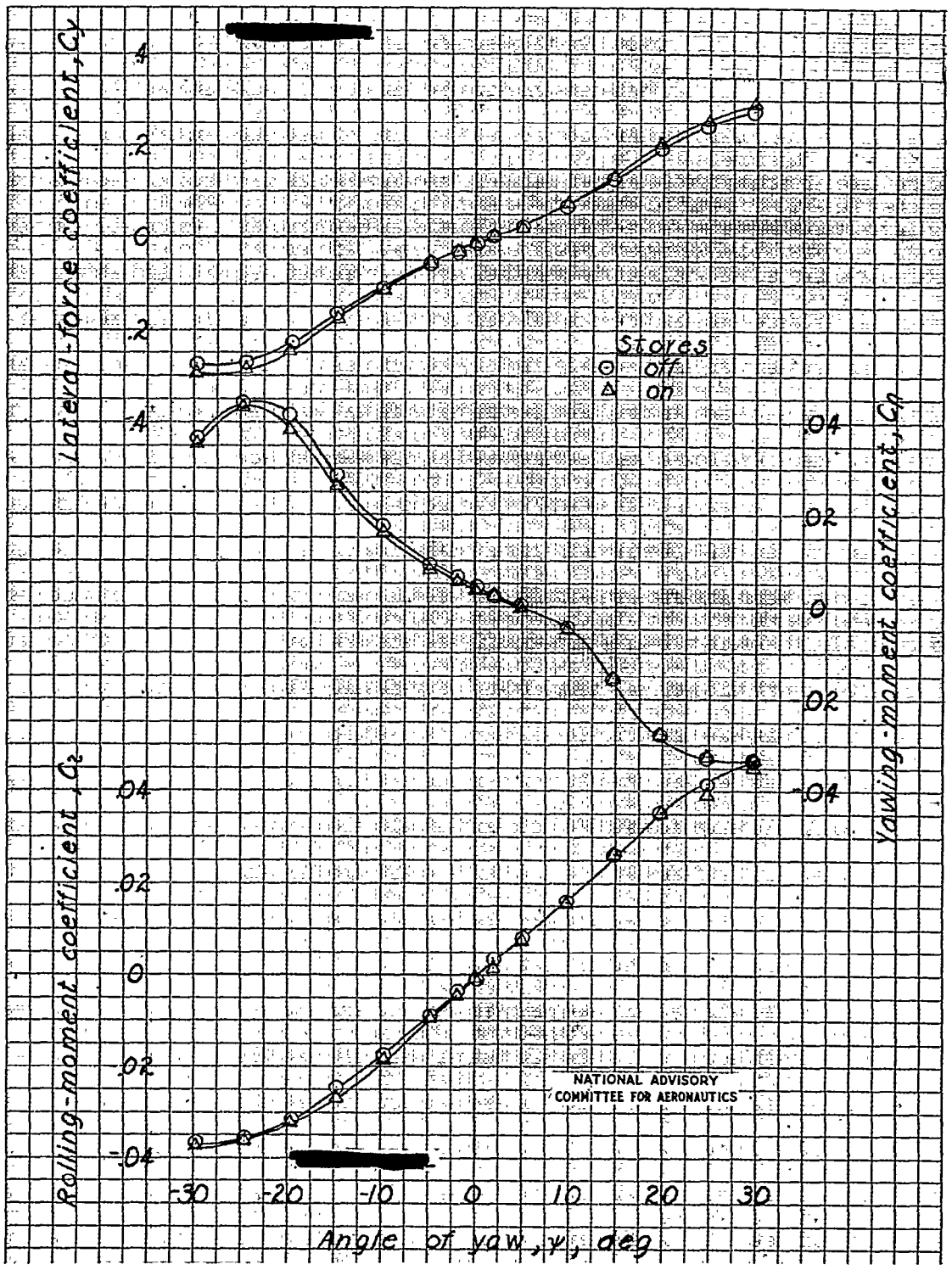

(a) Glide configuration; $\alpha = -1.1^{\circ}$, $C_L = 0.11$.

Figure 48.- Effect of external stores on the aerodynamic characteristics in yaw of a 1/8-scale model of the Grumman XTBF-1 airplane. Large dorsal fin; 1.5-inch base extension on vertical tail.

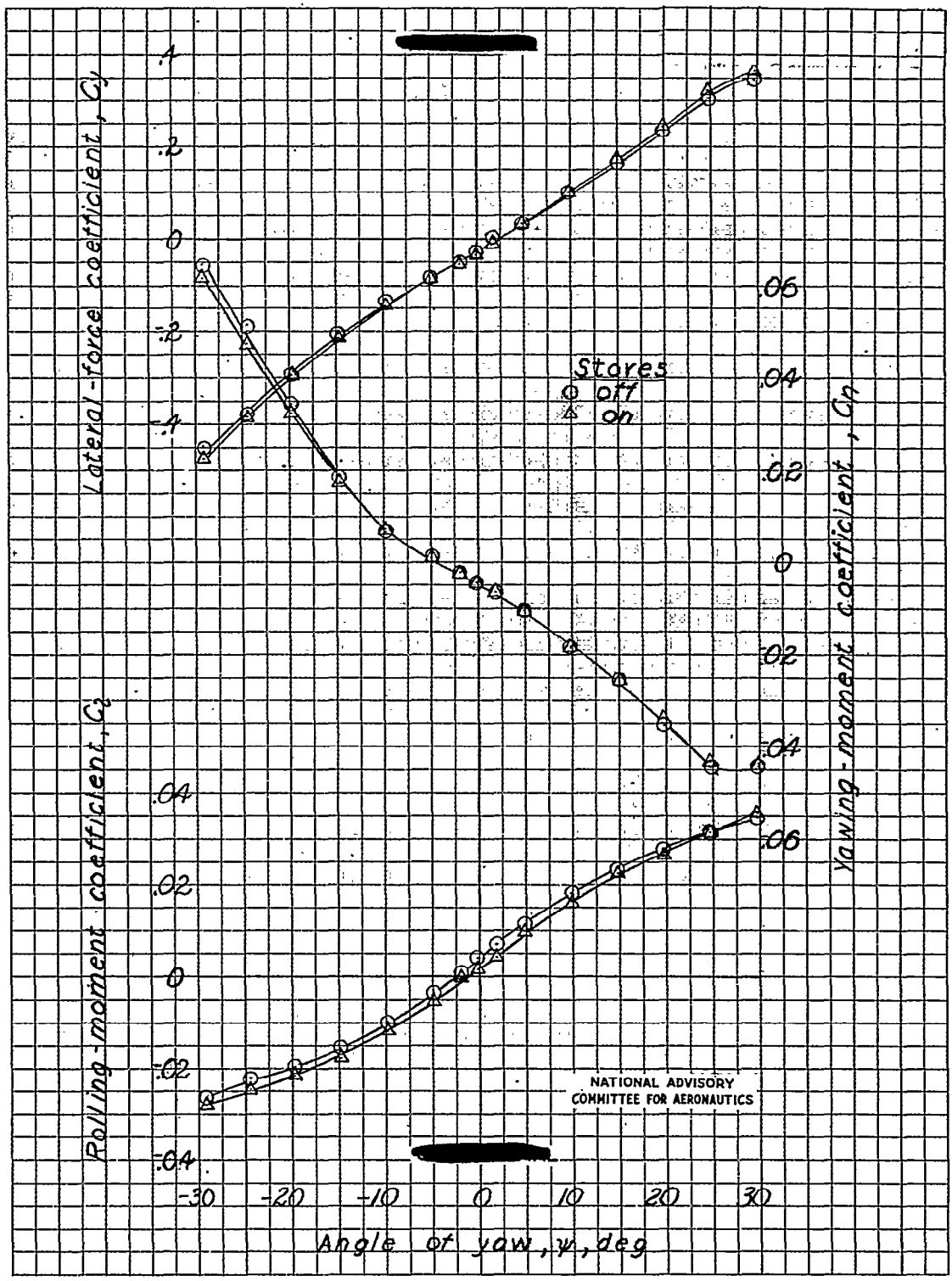

(b) Power-on clean configuration; $\alpha = 9.8^{\circ}$, $C_L = 1.05$.

Figure 48.- Concluded.

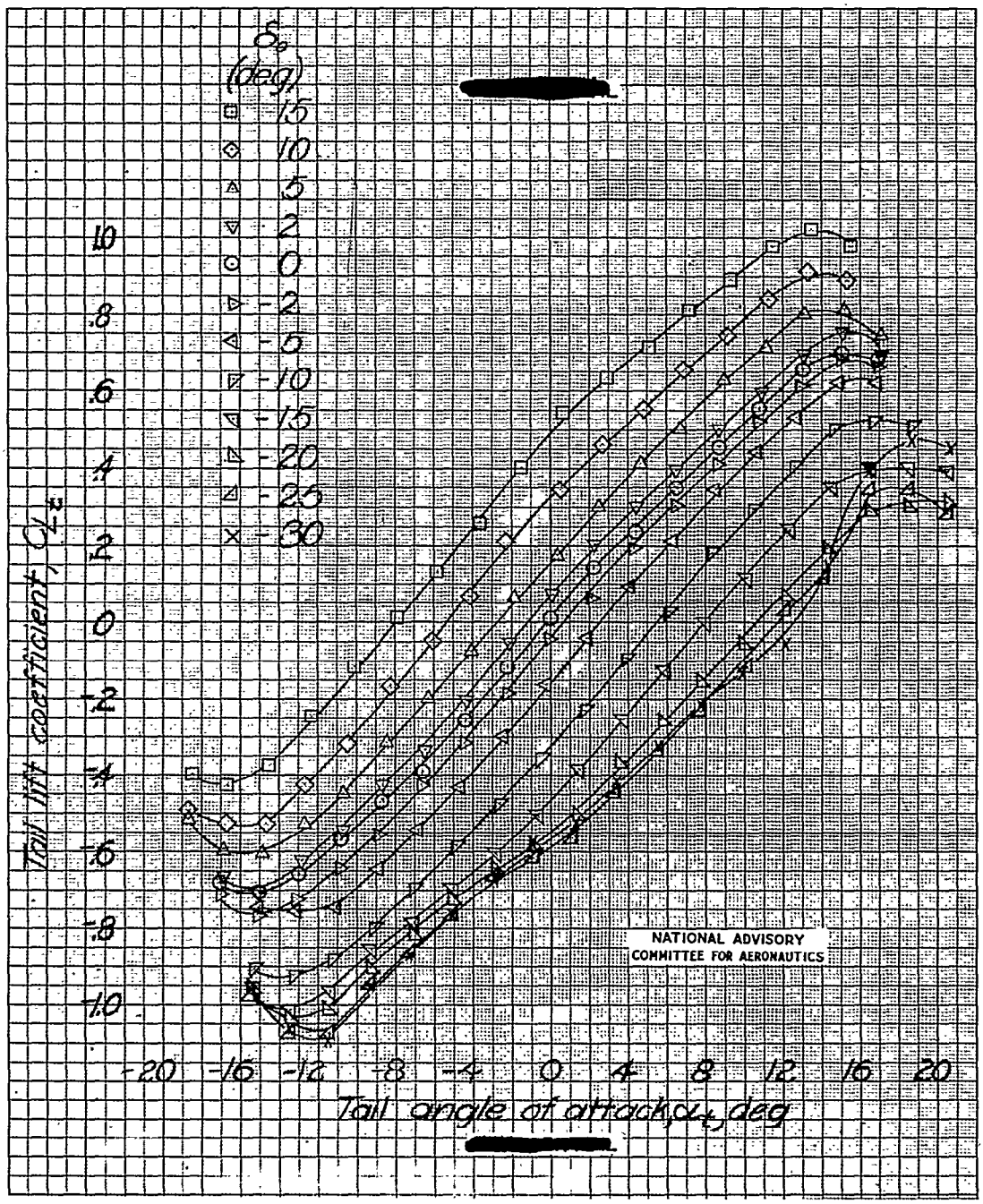

(a) $\delta_{e_t} = 0^\circ$, $\delta_{fantail} = 0^\circ$.

Figure 49.- Aerodynamic characteristics of the isolated horizontal tail of a 1/8-scale model of the Grumman XTB3F-1 airplane.

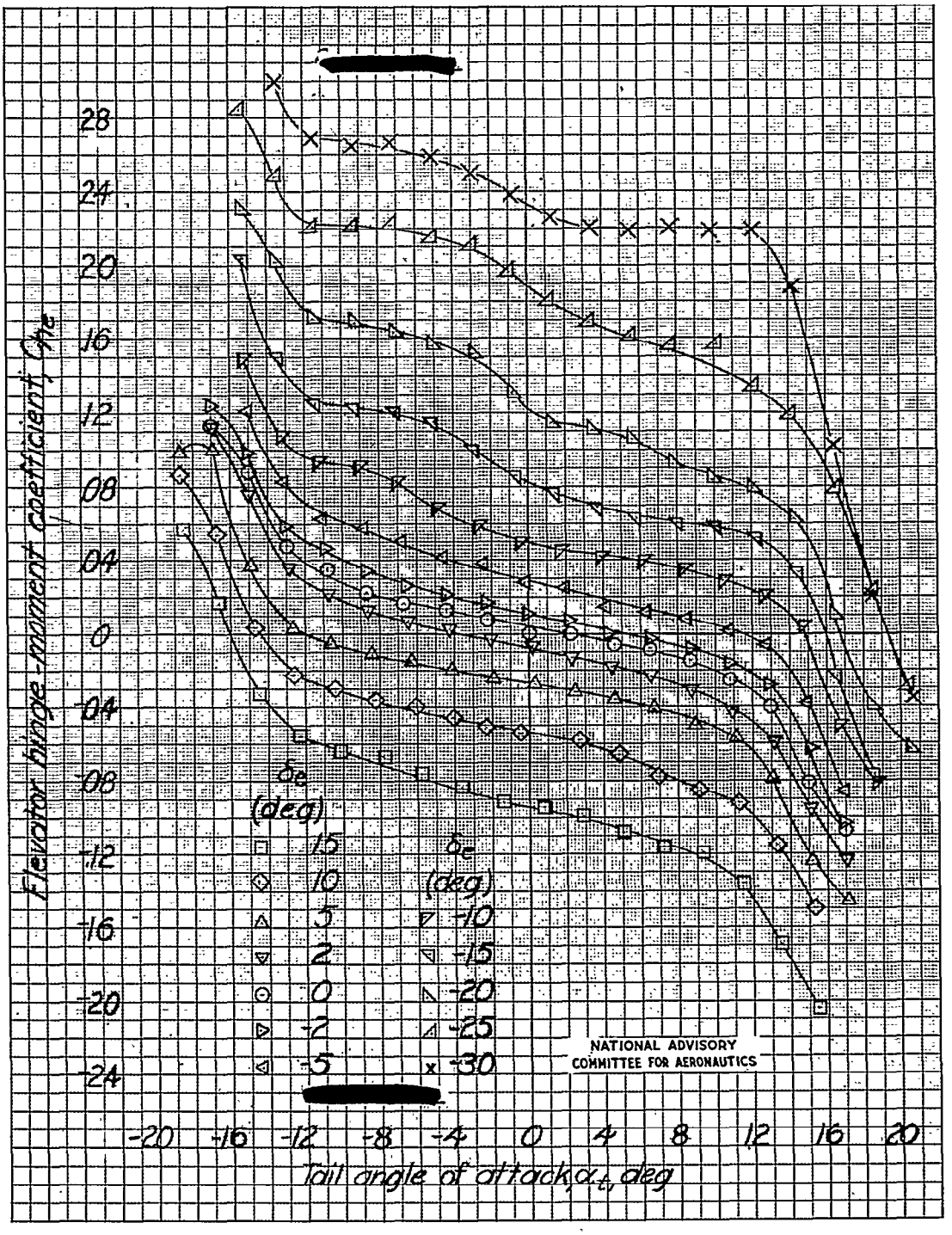

(a) Concluded.

Figure 49.- Continued.

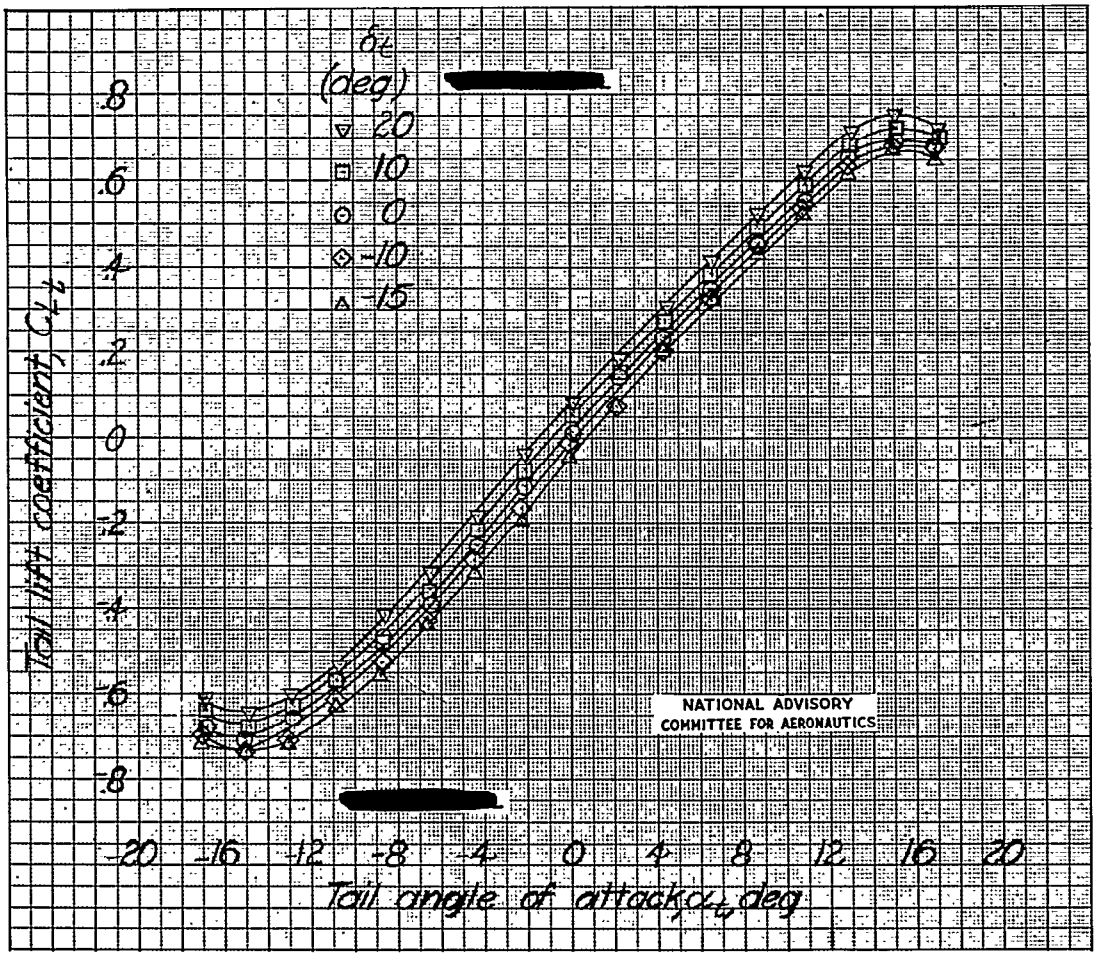

(b) $\delta_e = 0^\circ$; $\delta_{fantail} = 0^\circ$.

Figure 49.- Continued.

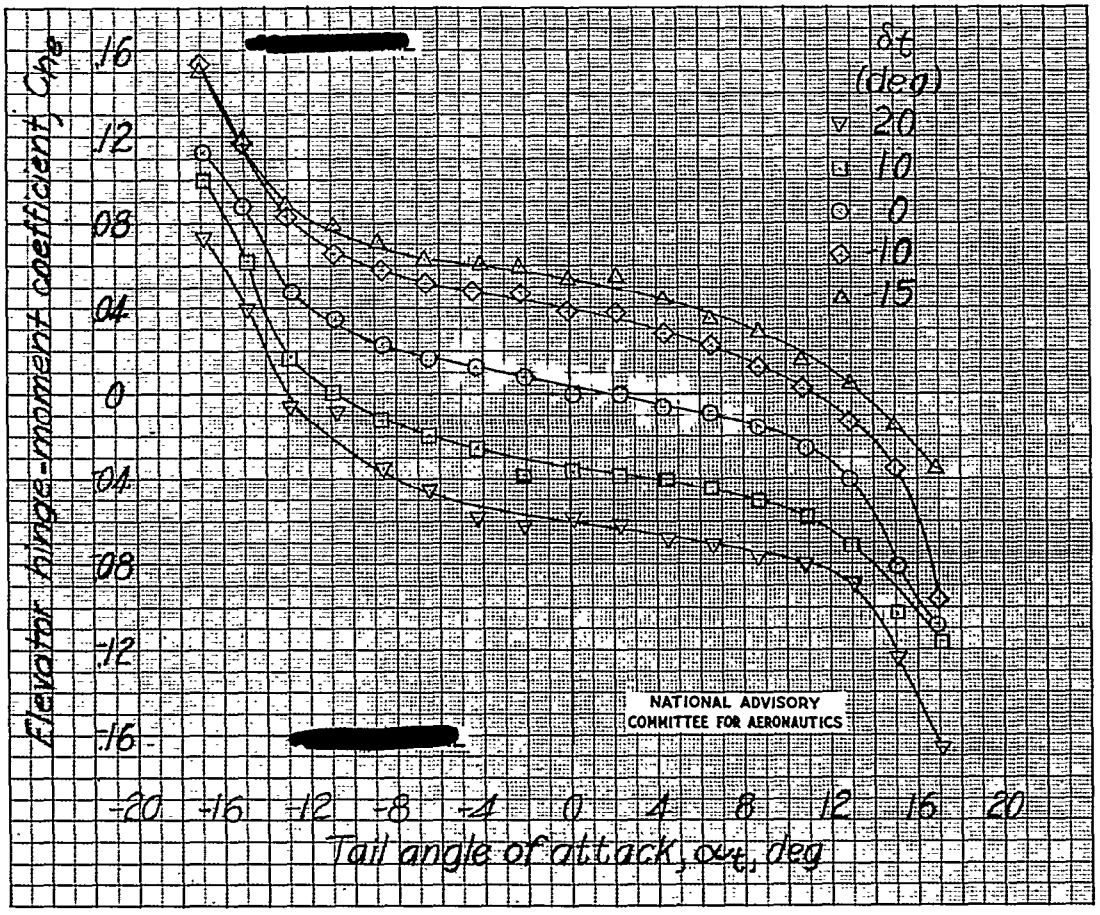

(b) Concluded.

Figure 49.- Continued.

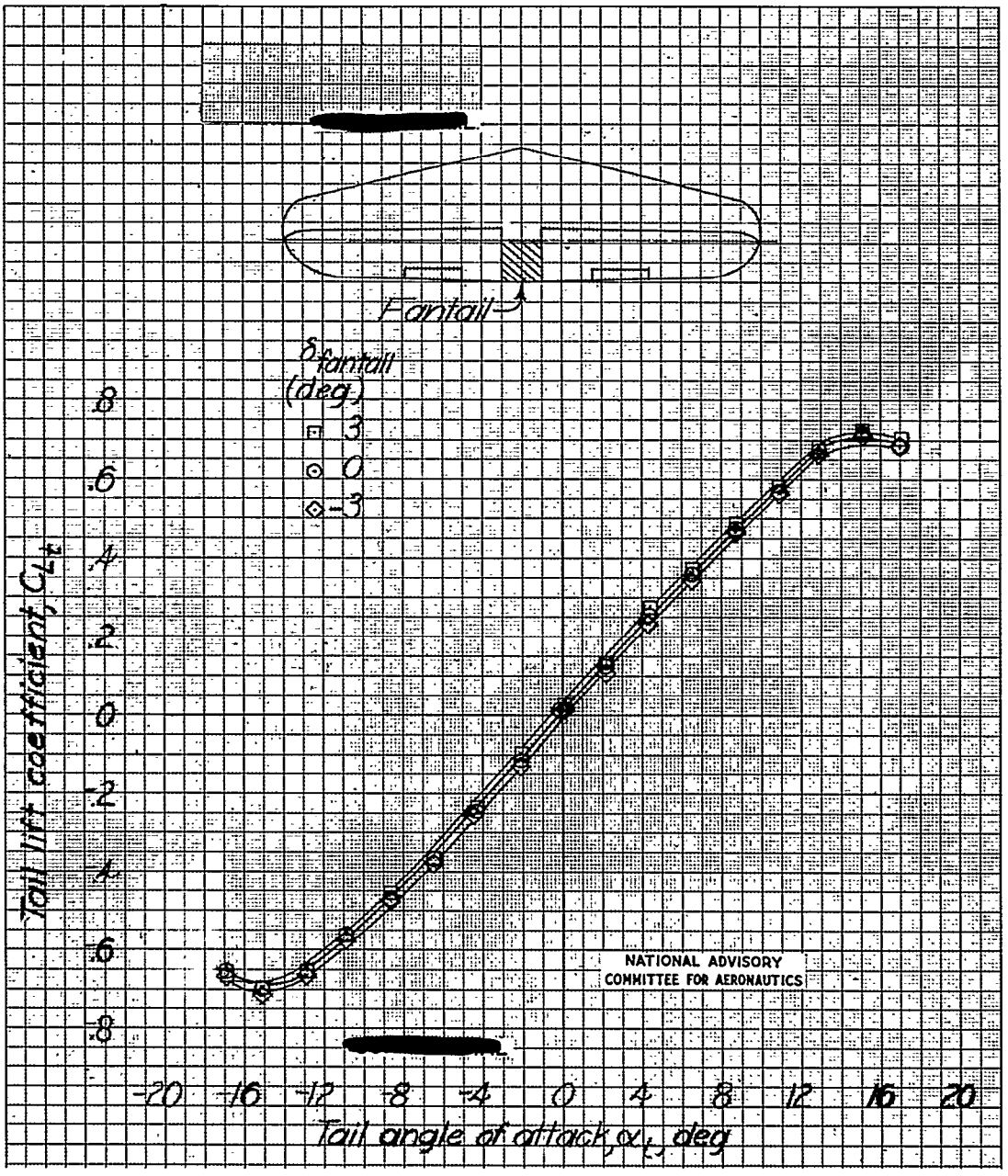

(c) $\delta_e = 0^\circ$; $\delta_{e_t} = 0^\circ$.

Figure 49.- Continued.

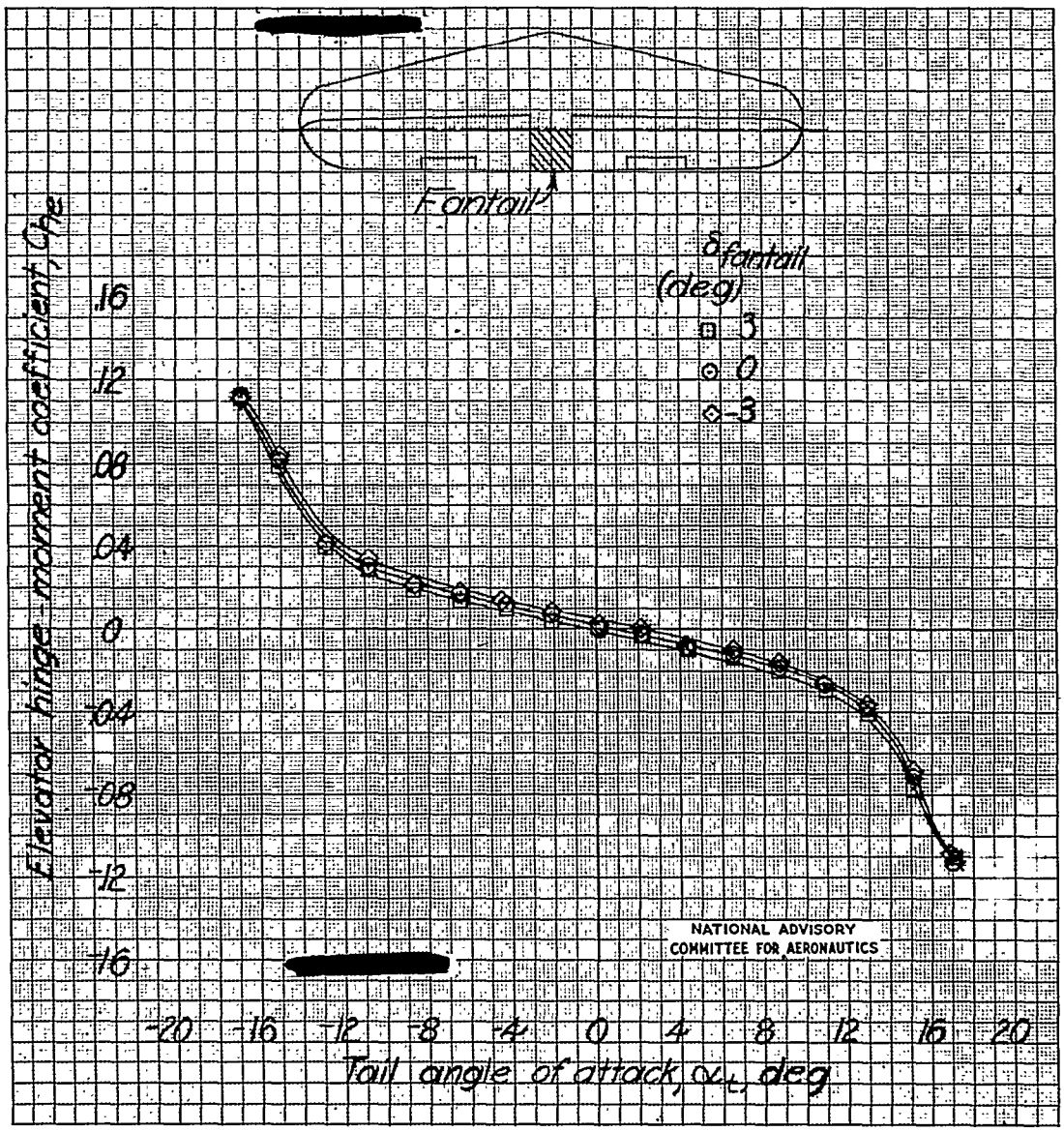

(c) Concluded.

Figure 49.- Concluded.

NASA Technical Library
3 1176 01437 5266